

Advances

in Clinical and Experimental Medicine

MONTHLY ISSN 1899-5276 (PRINT) ISSN 2451-2680 (ONLINE)

advances.umw.edu.pl

2023, Vol. 32, No. 7 (July)

Impact Factor (IF) – 2.1
Ministry of Science and Higher Education – 140 pts
Index Copernicus (ICV) – 168.52 pts



WROCLAW
MEDICAL UNIVERSITY

Advances
in Clinical and Experimental
Medicine



Advances in Clinical and Experimental Medicine

ISSN 1899-5276 (PRINT)

ISSN 2451-2680 (ONLINE)

advances.umw.edu.pl

MONTHLY 2023
Vol. 32, No. 7
(July)

Advances in Clinical and Experimental Medicine (*Adv Clin Exp Med*) publishes high-quality original articles, research-in-progress, research letters and systematic reviews and meta-analyses of recognized scientists that deal with all clinical and experimental medicine.

Editorial Office

ul. Marcinkowskiego 2–6
50-368 Wrocław, Poland
Tel.: +48 71 784 12 05
E-mail: redakcja@umw.edu.pl

Publisher

Wrocław Medical University
Wybrzeże L. Pasteura 1
50-367 Wrocław, Poland

Online edition is the original version
of the journal

Editor-in-Chief

Prof. Donata Kurpas

Deputy Editor

Prof. Wojciech Kosmala

Managing Editor

Marek Misiak, MA

Statistical Editors

Wojciech Bombała, MSc
Anna Kopszak, MSc
Dr. Krzysztof Kujawa

Manuscript editing

Marek Misiak, MA, Jolanta Prazeres, MA

Scientific Committee

Prof. Sabine Bährer-Kohler
Prof. Antonio Cano
Prof. Breno Diniz
Prof. Erwan Donal
Prof. Chris Fox
Prof. Naomi Hachiya
Prof. Carol Holland
Prof. Markku Kurkinen
Prof. Christos Lionis

Prof. Raimundo Mateos
Prof. Zbigniew W. Raś
Prof. Jerzy W. Rozenblit
Prof. Silvina Santana
Prof. James Sharman
Prof. Jamil Shibli
Prof. Michał Toborek
Prof. László Vécsei
Prof. Cristiana Vitale

Section Editors

Anesthesiology

Prof. Marzena Zielińska

Basic Sciences

Prof. Iwona Bil-Lula
Prof. Bartosz Kempisty
Dr. Wiesława Kranc
Dr. Anna Lebedeva
Dr. Maciej Sobczyński

Clinical Anatomy, Legal Medicine, Innovative Technologies

Prof. Rafael Boscolo-Berto

Dentistry

Prof. Marzena Dominiak
Prof. Tomasz Gedrange
Prof. Jamil Shibli

Laser Dentistry

Assoc. Prof. Kinga Grzech-Leśniak

Dermatology

Prof. Jacek Szepietowski

Emergency Medicine, Innovative Technologies

Prof. Jacek Smereka

Gynecology and Obstetrics

Prof. Olimpia Sipak-Szmigiel

Histology and Embryology

Dr. Mateusz Olbromski

Internal Medicine

Angiology

Dr. Angelika Chachaj

Cardiology

Prof. Wojciech Kosmala
Dr. Daniel Morris

Endocrinology

Prof. Marek Bolanowski

Gastroenterology

Assoc. Prof. Katarzyna Neubauer

Hematology

Prof. Andrzej Deptała

Prof. Dariusz Wołowicz

Nephrology and Transplantology

Assoc. Prof. Dorota Kamińska

Assoc. Prof. Krzysztof Letachowicz

Pulmonology

Prof. Anna Brzecka

Microbiology

Prof. Marzenna Bartoszewicz

Assoc. Prof. Adam Junka

Molecular Biology

Dr. Monika Bielecka

Prof. Jolanta Saczko

Neurology

Assoc. Prof. Magdalena Koszewicz

Assoc. Prof. Anna Pokryszko-Dragan

Dr. Masaru Tanaka

Neuroscience

Dr. Simone Battaglia

Dr. Francesco Di Gregorio

Oncology

Prof. Andrzej Deptała

Prof. Adam Maciejczyk

Dr. Marcin Jędryka

Gynecological Oncology

Dr. Marcin Jędryka

Orthopedics

Prof. Paweł Reichert

Otolaryngology

Assoc. Prof. Tomasz Zatoński

Pediatrics

Pediatrics, Metabolic Pediatrics, Clinical Genetics, Neonatology, Rare Disorders

Prof. Robert Śmigiel

Pediatric Nephrology

Prof. Katarzyna Kiliś-Pstrusińska

Pediatric Oncology and Hematology

Assoc. Prof. Marek Ussowicz

Pharmaceutical Sciences

Assoc. Prof. Marta Kepinska

Prof. Adam Matkowski

Pharmacoeconomics, Rheumatology

Dr. Sylwia Szafraniec-Buryło

Psychiatry

Prof. Jerzy Leszek

Assoc. Prof. Bartłomiej Stańczykiewicz

Public Health

Prof. Monika Sawhney

Prof. Izabella Uchmanowicz

Qualitative Studies, Quality of Care

Prof. Ludmiła Marcinowicz

Radiology

Prof. Marek Sądadek

Rehabilitation

Dr. Elżbieta Rajkowska-Labon

Surgery

Assoc. Prof. Mariusz Chabowski

Prof. Renata Taboła

Telemedicine, Geriatrics, Multimorbidity

Assoc. Prof. Maria Magdalena

Bujnowska-Fedak

Editorial Policy

Advances in Clinical and Experimental Medicine (Adv Clin Exp Med) is an independent multidisciplinary forum for exchange of scientific and clinical information, publishing original research and news encompassing all aspects of medicine, including molecular biology, biochemistry, genetics, biotechnology and other areas. During the review process, the Editorial Board conforms to the "Uniform Requirements for Manuscripts Submitted to Biomedical Journals: Writing and Editing for Biomedical Publication" approved by the International Committee of Medical Journal Editors (www.ICMJE.org). The journal publishes (in English only) original papers and reviews. Short works considered original, novel and significant are given priority. Experimental studies must include a statement that the experimental protocol and informed consent procedure were in compliance with the Helsinki Convention and were approved by an ethics committee.

For all subscription-related queries please contact our Editorial Office: redakcja@umw.edu.pl

For more information visit the journal's website: advances.umw.edu.pl

Pursuant to the ordinance of the Rector of Wrocław Medical University No. 12/XVI R/2023, from February 1, 2023, authors are required to pay a fee for each manuscript accepted for publication in the journal Advances in Clinical and Experimental Medicine. The fee amounts to 990 EUR for original papers and meta-analyses, 700 EUR for reviews, and 350 EUR for research-in-progress (RIP) papers and research letters.

Advances in Clinical and Experimental Medicine has received financial support from the resources of Ministry of Science and Higher Education within the "Social Responsibility of Science – Support for Academic Publishing" project based on agreement No. RCN/SP/0584/2021.



Ministry of Education and Science
Republic of Poland

Czasopismo Advances in Clinical and Experimental Medicine korzysta ze wsparcia finansowego ze środków Ministerstwa Edukacji i Nauki w ramach programu „Społeczna Odpowiedzialność Nauki – Rozwój Czasopism Naukowych” na podstawie umowy nr RCN/SP/0584/2021.



Ministerstwo
Edukacji i Nauki

Indexed in: MEDLINE, Science Citation Index Expanded, Journal Citation Reports/Science Edition, Scopus, EMBASE/Excerpta Medica, Ulrich's™ International Periodicals Directory, Index Copernicus

Typographic design: Piotr Gil, Monika Kołęda

DTP: Wydawnictwo UMW

Cover: Monika Kołęda

Printing and binding: Drukarnia I-BiS Bierońscy Sp.k.

Contents

Meta-analyses

- 723 Chunxiu Wang, Cuicui Zhang
Meta-analysis to assess the role of maternal characteristics and risk factors on postpartum hemorrhage

Original papers

- 733 Rui Chen, Hao Jiang, Wei Jiang, Kangjia Luo, Hao Zhang, Feng Gao
Effects of different inferior mesenteric artery ligation levels on the prognosis of patients with low rectal cancer
- 741 Hongwei Tang, Nan Zhang, Huan Li, Ying Chen, Xinlei Liu, Hongbo Xiao, Jianchuan Deng, Kang Zhou
TG-interacting factor 1 improves risk stratification in patients with NPM1-mutated acute myeloid leukemia
- 753 Fang Li, Fang-Jian Zhou, Tong-Wei Zhu, Hua-Li Qiu, Xiao-Ting Zhang, Bo-Wen Ruan, De-Yi Huang
Nomogram for predicting skip metastasis in cN0 papillary thyroid cancer patients at increased risk of lymph node metastasis
- 763 Haotian Shang, Aiguo Xu, Haicui Yan, Dandan Xu, Jingyu Zhang, Xinjian Fang
PIEZO2 promotes cell proliferation and metastasis in colon carcinoma through the SLIT2/ROBO1/VEGFC pathway
- 777 Anna Junkiert-Czarnecka, Maria Pilarska-Deltow, Aneta Bąk, Marta Heise, Olga Haus
A novel mutation in collagen transport protein, MIA3 gene, detected in a patient with clinical symptoms of Ehlers–Danlos hypermobile syndrome
- 783 Tomasz Mackiewicz, Jakub Włodarczyk, Marta Zielińska, Marcin Włodarczyk, Adam Durczyński, Piotr Hogendorf, Łukasz Dziki, Jakub Fichna
Increased GPR35 expression in human colorectal and pancreatic cancer samples: A preliminary clinical validation of a new biomarker
- 791 Zhijie Wei, Rui Wu, Li Zhang, Ping Xu
ATPIF1 alleviates oxygen glucose deprivation/reoxygenation-induced astrocyte injury in vitro: A rat model of ischemic brain injury
- 803 Xigang Wen, Wenling Han, Chao Liu
hsa_circ_0017842 acts as a competing endogenous RNA to enhance the malignancy of gastric cancer

Reviews

- 813 Niloufar Najar Nobari, Masoumeh Roohaninasab, Afsaneh Sadeghzadeh-Bazargan, Azadeh Goodarzi, Elham Behrangi, Farahnaz Nikkhal, Mohammadreza Ghassemi
A systematic review of clinical trials using single or combination therapy of oral or topical finasteride for women in reproductive age and postmenopausal women with hormonal and nonhormonal androgenetic alopecia

Meta-analysis to assess the role of maternal characteristics and risk factors on postpartum hemorrhage

Chunxiu Wang^{1,A–F}, Cuicui Zhang^{2,A–F}¹ Emergency Obstetrics and Gynecology Department, Northwest Women's and Children's Hospital, Xi'an, China² Emergency Department, The Second Affiliated Hospital of Air Force Military Medical University, Xi'an, China

A – research concept and design; B – collection and/or assembly of data; C – data analysis and interpretation; D – writing the article; E – critical revision of the article; F – final approval of the article

Advances in Clinical and Experimental Medicine, ISSN 1899–5276 (print), ISSN 2451–2680 (online)

Adv Clin Exp Med. 2023;32(7):723–731

Address for correspondence

Cuicui Zhang

E-mail: zhangcuicui_sci@outlook.com

Funding sources

None declared

Conflict of interest

None declared

Received on September 16, 2022

Reviewed on October 28, 2022

Accepted on December 22, 2022

Published online on February 8, 2023

Abstract

Background. Postpartum hemorrhage (PPH) is a serious condition that can lead to several complications. Many different factors precipitate PPH.

Objectives. To assess the role and impact of different factors such as body mass index (BMI), age, hypertension, parity, and embryo transfer on PPH.

Materials and methods. Thirty-one studies have been included in the current meta-analysis. The outcomes of these studies were analyzed using a random-effects model and it was used to calculate the mean difference (MD) with 95% confidence interval (95% CI) in order to quantify the impact of different risk factors on PPH.

Results. Regarding the maternal age, older subjects (≥ 35 years) showed a significantly higher incidence of PPH (MD = 1.15, 95% CI: 1.03–1.27, $p = 0.01$). On the other hand, BMI had no impact on the incidence of PPH (MD = 0.76, 95% CI: 0.26–2.24, $p = 0.62$). At the same time, primiparous subjects, those with hypertension and those in whom frozen–thawed embryo transfer (FTET) was performed showed a significantly higher PPH incidence (MD = 1.27, 95% CI: 1.02–1.56, $p = 0.03$; MD = 1.51, 95% CI: 1.42–1.61, $p < 0.001$; and MD = 1.43, 95% CI: 1.11–1.85, $p = 0.006$, respectively).

Conclusions. The weight of the subjects is not a risk factor for PPH. However, a higher incidence of the disease can be observed in older, hypertensive and primiparous subjects, as well as those in whom FTET performed.

Key words: BMI, postpartum hemorrhage, maternal, pregnancy, age

Cite as

Wang C, Zhang C. Meta-analysis to assess the role of maternal characteristics and risk factors on postpartum hemorrhage.

Adv Clin Exp Med. 2023;32(7):723–731.

doi:10.17219/acem/158474

DOI

10.17219/acem/158474

Copyright

Copyright by Author(s)

This is an article distributed under the terms of the Creative Commons Attribution 3.0 Unported (CC BY 3.0)

(https://creativecommons.org/licenses/by/3.0/)

Introduction

Postpartum hemorrhage (PPH) is a medical emergency, regardless of the type of delivery.¹ Postpartum hemorrhage is defined as blood loss after delivery greater than 500 mL and it occurs in 18% of births. About 3% of all vaginal births are accompanied by severe PPH,² and this condition is a leading cause of maternal mortality. Severe PPH is defined as blood loss of more than 1000 mL.¹

Each year, about 14 million of people lose their lives due to PPH.³ About half of all postpartum deaths occur during the first 24 h, and the majority (66%) happen within the first week. It is difficult to recognize the signs of a medical emergency during labor and the first 24 h after giving birth, which contributes to maternal mortality.⁴ The global prevalence of PPH is estimated at 6% and 10%.⁵ According to the previous systematic review of the epidemiology of PPH,⁶ the overall prevalence of PPH is between 6.09 and 10.55% (7.23% when objectively examined and 5.40% when evaluated subjectively). The evaluation of prevalence according to study design revealed a 5.95% prevalence in observational studies and a 13.94% prevalence in randomized controlled studies.⁷

Postpartum hemorrhage-related deaths are more prevalent in places with limited access to medical care. The consequences of PPH may be exacerbated in such settings by factors such as malnutrition, malaria and anemia. In places with suitable infrastructure and medical care, PPH-related deaths are quite uncommon.⁸ To reduce the occurrence of PPH, midwives should assess the expectant mother's risk factors during each prenatal appointment.⁹ Pregnant women should be included in the care plan design, and high-quality medical care should be made available to them.⁷ Midwives play an integral role in assessing risks, implementing safeguards and obtaining medical attention.¹⁰

According to the World Health Organization (WHO), postpartum care should cater to the individual requirements of both mothers and newborns, to avoid potential health problems and provide prompt medical attention in the event of any.¹¹ Over 2/3 of women with PPH have no identifiable risk factors.¹² No risk factors for PPH have been discovered, and the risk of PPH associated with high multiparity and many pregnancies has grown, according to the World Health Organization's Recommendations for the Prevention and Treatment of PPH.³ A history of PPH, being nulliparous, being multiparous (going into labor more than 5 times), having coagulopathy (congenital or acquired, use of drugs such as aspirin or heparin), abnormal placental attachment, being older than 30, anemia, excessive stretching of the uterus (multiple pregnancies, polyhydramnios), and fetal macrosomia are all risk factors for PPH in the antepartum period.^{1,13,14} The meta-analysis approach has been used to analyze some of the maternal characteristics in the antepartum period that either increase or decrease the risk of PPH, in order to identify risk factors that are directly associated with PPH.

Over 5 million babies have been born thanks to in vitro fertilization (IVF) as a therapy method of infertility.¹⁵ The use of frozen–thawed embryos has become commonplace ever since the first successful live birth was reported using a cryopreserved embryo transfer in 1984.^{16–18} Improved perinatal outcomes of frozen–thawed embryo transfer (FTET) due to the fast refining of embryo cryopreservation procedures have made FTET a competitive option for fresh embryo transfer (FET).^{19,20} In light of the mounting evidence showing that FET is superior to FET, “freeze-all” cycles are replacing FETs in clinical practice.^{15,21} The current data that support embryo cryopreservation are based on low-quality randomized controlled trials and individual observational studies,^{8,9} which lack the power to demonstrate statistically significant differences in some perinatal outcomes when low background risk of complications exists. There is still some debate as to whether FTET provides better clinical outcomes. Quantifying the risks of complications and bad birth outcomes calls for a meta-analysis.

Objectives

The study aims to assess the role and impact of different factors such as body mass index (BMI), age, hypertension, parity, and embryo transfer on the incidence of PPH.

Materials and methods

Study design

This systematic review and meta-analysis of clinical trials was included in the epidemiological declaration and had a set study protocol. For data collection and analysis, several of databases were searched.

Data pooling

Prospective and retrospective cohort studies focusing on the assessment of the impact of several risk factors on the incidence of PPH were chosen for this analysis. Human-related studies were included, regardless of language. There were no restrictions regarding the sample size. We did not include reviews, editorials or letters to the editor because they do not report a measure of association. The study procedure is depicted in Fig. 1.

Eligibility and inclusion

Analysis of the impact of different maternal characteristics and embryo transfer on the incidence of PPH was used to construct a summary.

The sensitivity analysis comprised only papers reporting the role of age, BMI, hypertension, parity, and embryo transfer on PPH. Several methods of analysis were

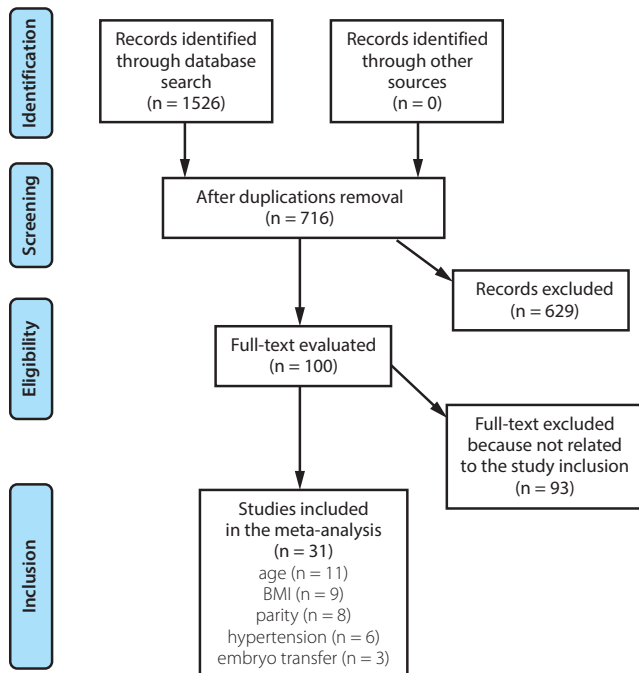


Fig. 1. Schematic diagram of the study procedure

BMI – body mass index.

employed to demonstrate the impact of different factors on PPH.

The inclusion criteria were as follows:

1. Retrospective, prospective or cohort studies;
2. The target population consisted of individuals with certain maternal characteristics related to age, BMI, parity, hypertension, and embryo transfer;
3. The intervention regimen of the included studies was based on comparing the incidence of PPH among subjects with different levels/scores for each analyzed outcome.

The exclusion criteria were as follows:

1. Studies that failed to identify the incidence rate (event number or percent) of PPH;
2. Review articles, letters, books, and book chapters;
3. Studies not focusing on the comparison between different groups regarding the outcomes of the study.

Identification

According to the PICOS principle, a protocol of search strategy was developed³² and defined as follows: P (population) – female subjects with a previous history of pregnancy; I (intervention/exposure) – PPH incidence; C (comparison) – age (<35 years and ≥35 years), BMI (<25 kg/m² and ≥25 kg/m²), blood pressure (hypertensive and nonhypertensive women), parity (primiparity and multiparity), and embryo transfer method (FTET and FET); O (outcome) – number or percent of occurrence for each parameter in different conditions; S (study design) – cohort studies.³³

Using the keywords and associated phrases listed in Table 1, we conducted a complete search of the PubMed,

Table 1. Search strategy for each database

Database	Search strategy
PubMed	#1 "postpartum hemorrhage"[MeSH terms] OR "maternal"[all fields] #2 "age"[MeSH terms] OR "risk factors"[all fields] #3 #1 AND #2
OVID	#1 "postpartum hemorrhage"[all fields] OR "maternal"[all fields] #2 "age"[all fields] OR "risk factors"[all fields] #3 #1 AND #2
Google Scholar	#1 "postpartum hemorrhage" OR "maternal" #2 "age" OR "risk factors" #3 #1 AND #2
Embase	#1 "postpartum hemorrhage"/exp OR "maternal" #2 "age"/exp OR "risk factors" #3 #1 AND #2
Cochrane Library	#1 "postpartum hemorrhage": ti,ab,kw OR "maternal": ti,ab,kw (word variations have been searched) #2 "age": ti,ab,kw OR "risk factors": ti,ab,kw (word variations have been searched) #3 #1 AND #2

ti,ab,kw – terms in either title or abstract or keyword fields;
exp – exploded indexing term.

OVID, Cochrane Library, Embase, and Google Scholar databases concerning studies published between January 2000 and August 2022. The titles and abstracts of all the publications that had been collated into reference managing software have been reviewed. The 2 authors (CZ and CW) identified suitable studies.

Screening

According to the following criteria, data were compiled to include: study- and subject-related features in a standard format, the surname of the first author, the period of the study, the year of publication, the country of the study, the design of the study, the population type recruited in the study, the total number of subjects, qualitative and quantitative evaluation method, demographic data, clinical and treatment characteristics, information source, outcome evaluation, and statistical analysis results.³⁴ Each study was assessed for bias, and the methodological quality of the chosen studies was evaluated by 2 abovementioned authors in a blinded fashion.

The Newcastle–Ottawa Scale (NOS), a quality and bias assessment tool developed specifically for observational research, was used to evaluate the quality and bias of the study. The NOS examines the sample, the comparability of cases and controls, and the exposure in observational studies, and the results is expressed by assigning values between 0 and 9. Studies with a rating of 7–9 are of the highest quality and have the lowest risk of bias compared to those with a rating of 4. Studies with a rating of 4–6 are considered to be of moderate quality. Each study underwent a methodological evaluation by the 2 abovementioned authors (CW and CZ).

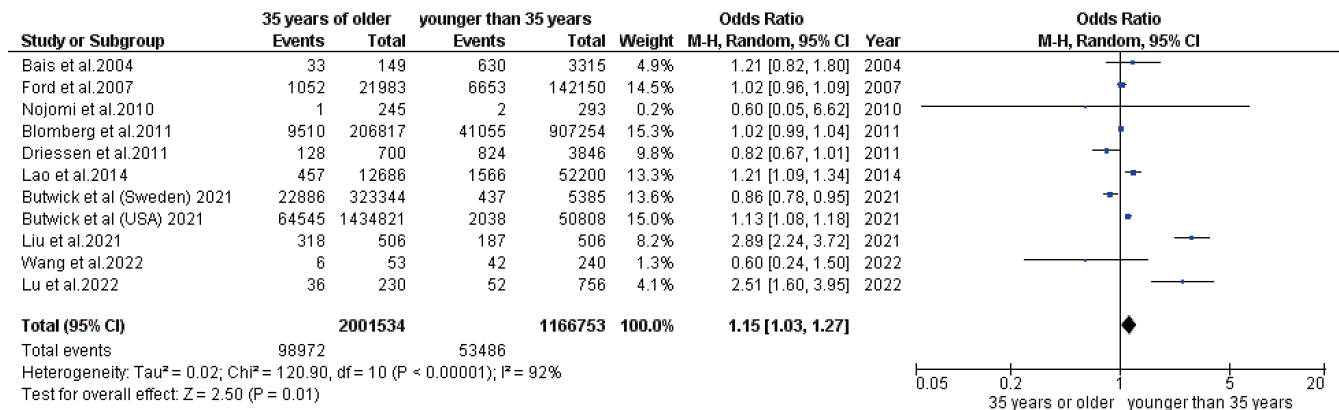


Fig. 2. Forest plot showing the impact of age (<35 years and ≥35 years) on postpartum hemorrhage (PPH)

95% CI – 95% confidence interval; df – degrees of freedom.

Statistical analyses

In the current meta-analysis, the mean difference (MD) with a 95% confidence interval (95% CI) was calculated using a random-effects model. Since using the fixed-effects model requires a high similarity between included studies and low heterogeneity (I^2) level, all groups were analyzed using the random-effects model due to high heterogeneity in some groups and inconsistent methodology in other groups. The I^2 index (determined using Reviewer Manager v. 5.3 (The Nordic Cochrane Centre, The Cochrane Collaboration, Copenhagen, Denmark) and expressed in the form of forest plots), in a form of a numeric value ranging from 0% to 100%, was calculated. Values ranging from 0% to 25%, 50% and 75% indicated no, low, moderate, and high heterogeneity, respectively. As previously stated, the subcategory analysis was performed by stratifying the initial evaluation into result categories. Publication bias was investigated quantitatively using the Begg's test and publication bias was considered present if $p > 0.05$.³⁷ To obtain the p-values, a two-tailed test was used. The statistical analysis and graphs were presented with Reviewer Manager v. 5.3 and jamovi software v. 2.3 (<https://www.jamovi.org/>) using the dichotomous model.

Results

After a review of 1526 relevant articles, a total of 31 studies published between January 2000 and August 2022 were included in the meta-analysis because they fit the inclusion criteria.^{22–52} Table 2 summarizes the findings of these investigations.

Age

Ten studies (the study by Butwock et al. was presented twice in the same analysis, one for American subjects and the other for Swedish subjects) including 3,168,287

subjects reported data stratified according to age (subjects ≥35 years compared subjects <35 years; Fig. 2). Older subjects had a higher incidence of PPH compared with subjects younger than 35 years (MD = 1.15, 95% CI: 1.03–1.27, $p = 0.01$, $I^2 = 92\%$).

BMI

Nine studies including 791,597 subjects reported data stratified according to BMI (BMI ≥ 25 kg/m² compared to BMI < 25 kg/m²; Fig. 3). The weight of included subjects had no impact on the incidence rate of PPH, as both groups showed nonsignificant rates (MD = 0.76, 95% CI: 0.26–2.24, $p = 0.62$, $I^2 = 100\%$).

Parity

Eight studies including 1,120,995 subjects reported data stratified according to parity (primiparous compared to multiparous subjects; Fig. 4). Multiparous subjects were associated with a lower incidence of PPH compared to primiparous subjects (MD = 1.27, 95% CI: 1.02–1.56, $p = 0.03$, $I^2 = 39\%$).

Hypertension

Six studies including 365,354 subjects reported data stratified according to the presence of hypertension during pregnancy (hypertensive compared to nonhypertensive subjects; Fig. 5). Hypertensive subjects had a higher PPH incidence compared with nonhypertensive pregnant subjects (MD = 1.51, 95% CI: 1.42–1.61, $p < 0.00001$, $I^2 = 0\%$).

Embryo transfer

Three studies including 8610 subjects analyzed the impact of embryo transfer method (FTET compared to FET; Fig. 6). Frozen–thawed embryo transfer showed a significantly higher incidence of PPH compared with FET (MD = 1.43, 95% CI: 1.11–1.85, $p = 0.006$, $I^2 = 48\%$).

Table 2. Characteristics of the studies selected for the meta-analysis

Study	Year	Country	Total, n	Group 1, n	Group 2, n	Group 1 characteristics	Group 2 characteristics	NOS
Bais et al. ²²	2004	Netherlands	3464	149	3315	≥35 years	<35 years	9
Baker and Haeri ²³	2012	USA	730	65	665	hypertensive	not hypertensive	7
Basak et al. ²⁴	2022	Bangladesh	104	53	51	primiparous	multiparous	6
Biguzzi et al. ²⁵	2012	Italy	2699	2074	625	primiparous	multiparous	8
Blomberg ²⁶	2011	Sweden	1,114,071	494,162	619,909	primiparous	multiparous	9
	2011	Sweden	206,817	206,817	206,817	≥35 years	<35 years	
Bujold et al. ²⁷	2005	Germany	8217	5916	66	BMI ≥ 25 kg/m ²	BMI < 25 kg/m ²	7
Butwick et al. ²⁸	2021	USA	1,485,629	1,434,821	50,808	≥35 years	<35 years	9
	2021	Sweden	328,729	323,344	5385	≥35 years	<35 years	
Driessen et al. ²⁹	2011	France	4546	700	3846	≥35 years	<35 years	9
Ford et al. ³⁰	2007	Australia	164,133	21,983	142,150	≥35 years	<35 years	9
	2007	Australia	164,043	15,343	148,700	hypertensive	not hypertensive	
Gofton et al. ³¹	2001	Canada	12,765	1331	11,434	hypertensive	not hypertensive	9
Guo et al. ³²	2016	China	1516	587	929	FTET	FTET	6
Halloran et al. ³³	2012	USA	160,362	7912	1346	BMI ≥ 25 kg/m ²	BMI < 25 kg/m ²	9
Healy et al. ³⁴	2010	Australia	6730	2503	4227	FTET	FTET	8
Lao et al. ³⁵	2014	China	64,886	12,686	52,200	≥35 years	<35 years	8
Liu et al. ³⁶	2021	China	1012	506	506	≥35 years	<35 years	8
	2021	China	506	506	395	BMI ≥ 25 kg/m ²	BMI < 25 kg/m ²	
	2021	China	33,334	506	32,828	hypertensive	not hypertensive	
Lu et al. ³⁷	2022	China	986	230	756	≥35 years	<35 years	6
Magann et al. ³⁸	2011	USA	27,563	2256	412	BMI ≥ 25 kg/m ² or more	BMI < 25 kg/m ²	8
Marzieh et al. ³⁹	2010	Iran	538	245	293	≥35 years	<35 years	6
Miller et al. ⁴⁰	2017	USA	159	159	132	BMI ≥ 25 kg/m ²	BMI < 25 kg/m ²	6
Nove et al. ⁴¹	2012	UK	481,171	121,422	20,247	BMI ≥ 25 kg/m ²	BMI < 25 kg/m ²	8
Otigbah et al. ⁴²	2000	UK	602	266	336	primiparous	multiparous	6
Puri et al. ⁴³	2011	India	38	18	20	primiparous	multiparous	6
Sebire et al. ⁴⁴	2001	UK	111,092	110,290	6	BMI ≥ 25 kg/m ²	BMI < 25 kg/m ²	7
Shabbir et al. ⁴⁵	2014	Pakistan	2401	682	1719	primiparous	multiparous	6
Sharma et al. ⁴⁶	2005	India	958	320	638	primiparous	multiparous	7
Sheiner et al. ⁴⁷	2005	Israel	154,311	9591	144,720	hypertensive	not hypertensive	8
Suzuki et al. ⁴⁸	2007	Japan	171	14	157	hypertensive	not hypertensive	7
Tixier et al. ⁴⁹	2011	France	122	52	70	primiparous	multiparous	6
Tsakamoto et al. ⁵⁰	2007	Japan	2243	277	52	BMI ≥ 25 kg/m ²	BMI < 25 kg/m ²	8
Wang et al. ⁵¹	2022	China	293	53	240	≥35 years	<35 years	6
	2022	China	284	50	37	BMI ≥ 25 kg/m ²	BMI < 25 kg/m ²	
Wikland et al. ⁵²	2010	Sweden	364	214	150	FTET	FTET	7

NOS – Newcastle–Ottawa Scale; BMI – body mass index; FTET – frozen–thawed embryo transfer; ET – fresh embryo transfer.

It was not possible to assess the impact of individual characteristics such as ethnicity on the comparison results because no data on these variables had been analyzed in the study. In addition, publication bias was assessed using the Begg’s test and it showed a nonsignificant bias for all included groups with a value of $p > 0.05$. The obtained p-values for age, BMI, parity, hypertension,

and embryo transfer method analysis were $p = 0.65$, $p = 0.61$, $p = 0.4$, $p = 0.47$, and $p = 0.99$, respectively.

The risk of bias assessment was evaluated using NOS (Table 2). Twenty-one studies had a score between 7 and 9, which reflect a low risk of bias and high methodological quality. Ten studies showed a moderate risk of bias, achieving a score ranging from 4 to 6 points.

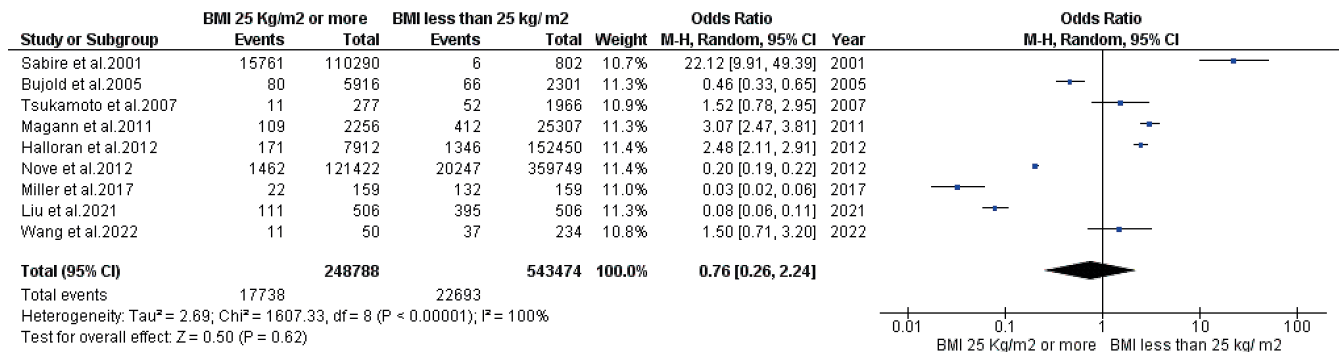


Fig. 3. Forest plot showing the impact of body mass index (BMI) (<25 kg/m² and ≥25 kg/m²) on postpartum hemorrhage (PPH)

95% CI – 95% confidence interval; df – degrees of freedom.

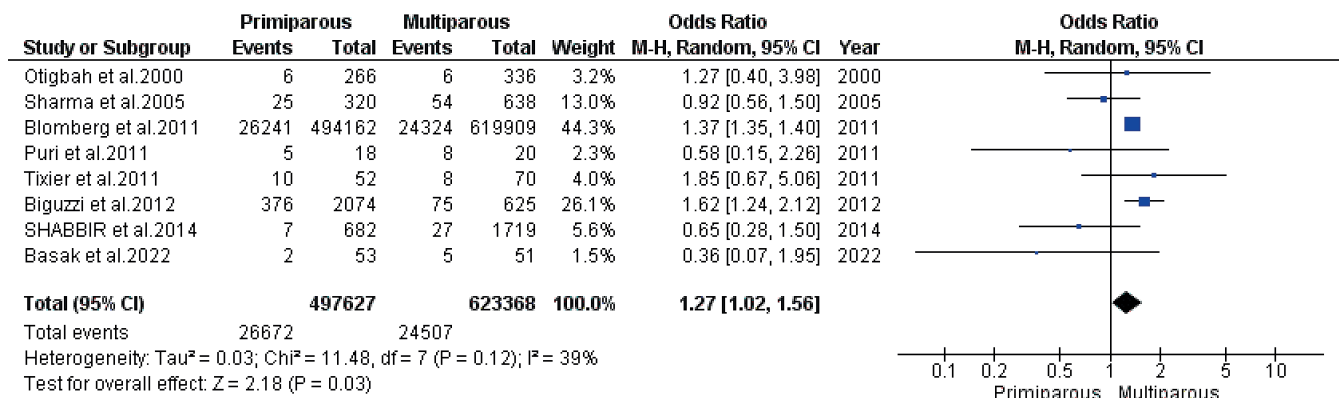


Fig. 4. Forest plot showing the impact of parity (primiparity and multiparity) on postpartum hemorrhage (PPH)

95% CI – 95% confidence interval; df – degrees of freedom.

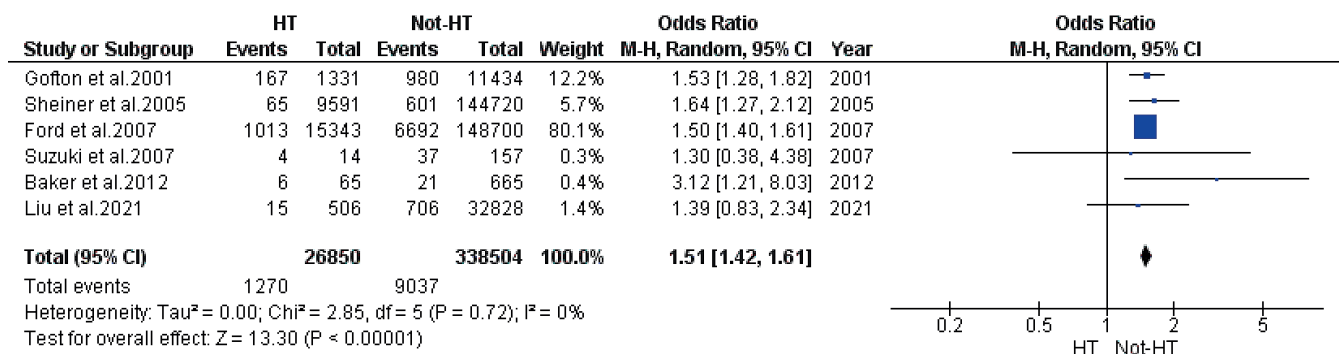


Fig. 5. Forest plot showing the impact of hypertension (hypertensive and nonhypertensive women) on postpartum hemorrhage (PPH)

95% CI – 95% confidence interval; df – degrees of freedom.

Discussion

A total of 5,454,843 subjects from different countries examined in 31 cohort studies were included in the current meta-analysis.

Every successful PPH treatment must begin with a prompt diagnosis. Learning about the potential causes of PPH is crucial. According to the National Institute for Health and Care Excellence (NICE), women with PPH risk factors should give birth in a unit equipped to handle emergencies.⁵³ This meta-analysis found that a BMI

of 25 kg/m² or higher has no impact on the PPH incidence rate. Regarding maternal age, older subjects (≥35 years) showed a significantly higher incidence of PPH (MD = 1.15, 95% CI: 1.03–1.27, p = 0.01). On the other hand, BMI had no impact on the incidence of PPH (MD = 0.76, 95% CI: 0.26–2.24, p = 0.62). At the same time, primiparous subjects, those with hypertension, and those with FTET showed a significantly higher PPH incidence (MD = 1.27, 95% CI: 1.02–1.56, p = 0.03; MD = 1.51, 95% CI: 1.42–1.61, p < 0.001; and MD = 1.43, 95% CI: 1.11–1.85, p = 0.006, respectively).

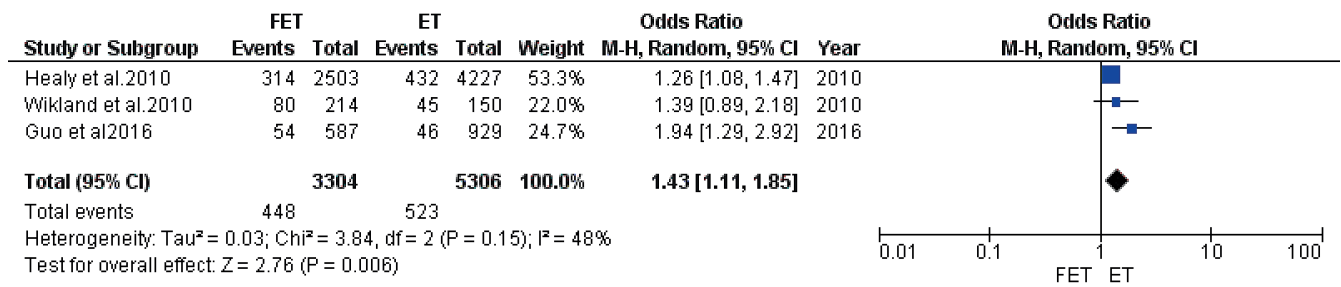


Fig. 6. Forest plot showing the impact of embryo transfer (frozen–thawed embryo transfer (FTET) and fresh embryo transfer (FET)) on postpartum hemorrhage (PPH)

95% CI – 95% confidence interval; df – degrees of freedom.

According to the Society of Obstetricians and Gynaecologists of Canada, women older than 35 are more likely to have adverse birth outcomes, such as miscarriage, complications during pregnancy, premature delivery, or to bear more than 2 babies in 1 delivery (i.e., twins or more).⁵⁴ Maternal age ≥ 40 years increases the risk of PPH, according to both the NICE⁵³ and the Royal College of Obstetricians and Gynecologists (RCOG) clinical guidelines⁵⁵ for the prevention and management of PPH. Pregnant women aged ≥ 35 years had a higher risk of adverse pregnancy and delivery outcome.⁵⁶ After conducting a meta-analysis, Walker et al. found that inducing labor did not increase the incidence of cesarean section for women aged ≥ 35 years.⁵⁷ In their meta-analysis, Wood et al. found that inducing labor had no effect on cesarean section rates among women aged ≥ 45 years in a subgroup analysis.⁵⁸ The current meta-analysis indicated that older age is related to adverse events such as PPH, which is consistent with the recommendations of RCOG.⁵⁵ The studies included in the meta-analysis covered study populations different countries. Maternal age is a significant risk factor for PPH in many nations because of the low quality of care provided to mothers aged ≥ 35 years throughout pregnancy, delivery and the postpartum period.

According to the WHO, having a BMI ≥ 25 kg/m² is associated with an increased chance of comorbidities, and the risk of complications increases with increasing obesity. According to NICE guidelines, an increased risk was associated with a BMI ≥ 35 kg/m².⁵³ According to RCOG (2011), having a BMI ≥ 35 kg/m² is associated with an increased risk of PPH. Obese pregnant women have a higher risk of perinatal problems and interventionist delivery, according to research by Bogaerts et al.⁵⁹ The current meta-analysis found no significant difference between the ideal body weight and obese subjects regarding the PPH rate. In addition, the current study included obese subjects with a BMI ≥ 25 kg/m², and the studies that showed a significantly lower impact of obesity stated that a BMI ≥ 35 kg/m² is related to such adverse events. Hence, we cannot make a general conclusion indicating that obesity is related to PPH.

Post-term birth is more common in first-time mothers, as indicated by the American College of Obstetricians and Gynecologists in their clinical management guide for obstetricians/gynecologists (OB/GYNs).⁶⁰ According to a comprehensive review and meta-analysis by McDonald et al.,⁶¹ parity increased the risk of premature delivery in IVF and twin pregnancies; however, this association was not statistically significant. A comprehensive review conducted by Wang et al. found that primiparity is a risk factor in perineal lacerations.⁶² According to the results of the present research, first-time mothers are at a higher risk of developing PPH.

According to research published in 2013, hypertension rates increase in pregnancy, and preeclampsia rates are 4 times greater than the mean in 5% of pregnant women worldwide. The risk of PPH is increased by prenatal hypertension, preeclampsia and eclampsia, according to the RCOG clinical guidelines for the prevention and management of PPH.⁵⁵ In this way, the current results are consistent with the clinical standards. Postpartum hemorrhage is a potential complication of maternal hypertension.

Postpartum hemorrhage was more common in the FTET group, as shown in the current study. Whether or not the embryo cryopreservation process had a negative impact on the increased risk ratios of these events is unknown. The risk of hypertension problems was found to be greater in a FTET compared to FET in observational cohort research comparing outcomes in sibling pregnancies in women.⁶³ Somewhat inconclusive results came from a short study conducted in China that compared FET with vitrified and slow-frozen embryo transfer.⁶⁴

Limitations

This study may have been skewed by the exclusion of many trials from the meta-analysis. However, our meta-analysis excluded studies that did not meet the inclusion criteria. In addition, some of the included studies have not evaluated the impact of race on the represented outcomes. Thus, it was not possible to assess the impact of ethnicity on the results. Some of the included studies have moderate methodology quality, as evaluated using the NOS score.


Variables such as nutritional status were not considered in the included studies, which may have skewed the results. Study results could be biased if there are unpublished articles and uncollected data.

Conclusions

The weight of the subjects is not a risk factor for PPH. However, a higher incidence of the disease can be observed in older (≥ 35 years), hypertensive and primiparous subjects, as well as those in whom FTET was performed. Hence, controlling the blood pressure and using the optimum embryo transfer method could result in beneficial outcomes regarding PPH. Nevertheless, future clinical multicenter studies are needed to reach a more sensible conclusion.

ORCID iDs

Chunxiu Wang  <https://orcid.org/0000-0002-3130-6534>

Cuicui Zhang  <https://orcid.org/0000-0003-4534-4678>

References

- Su CW. Postpartum hemorrhage. *Prim Care*. 2012;39(1):167–187. doi:10.1016/j.pop.2011.11.009
- Anderson JM, Etches D. Prevention and management of postpartum hemorrhage. *Am Fam Physician*. 2007;75(6):875–882. PMID:17390600.
- World Health Organization. WHO postpartum haemorrhage (PPH) summit. HRP Project Brief. World Health Organization. September 29, 2022. https://cdn.who.int/media/docs/default-source/hrp/projects/mph/project-brief-pph-summit.pdf?sfvrsn=3b0e505a_6&download=true.
- Nour NM. An introduction to maternal mortality. *Rev Obstet Gynecol*. 2008;1(2):77–81. PMID:18769668.
- Burke C. Active versus expectant management of the third stage of labor and implementation of a protocol. *J Perinatal Pediatr Neonatal Nurs*. 2010;24(3):215–228. doi:10.1097/JPN.0b013e3181e8ce90
- Carroli G, Cuesta C, Abalos E, Gulmezoglu AM. Epidemiology of postpartum haemorrhage: A systematic review. *Best Pract Res Clin Obstet Gynaecol*. 2008;22(6):999–1012. doi:10.1016/j.bpobgyn.2008.08.004
- Ward A. The midwife confronts postpartum hemorrhage. In: Arulkumar S, Karoshi M, Keith L, Lalonde A, Lynch C, eds. *A Comprehensive Textbook of Postpartum Hemorrhage: An Essential Clinical Reference for Effective Management*. 2nd ed. The Global Library of Women's Medicine. London, UK: Sapiens Publishing; 2012:549–554. https://www.glowm.com/pdf/PPH_2nd_edn_Chap-66.pdf. ISBN:978-0-9552282-7-8.
- Hofmeyr GJ, Abdel-Aleem H, Abdel-Aleem MA. Uterine massage for preventing postpartum haemorrhage. *Cochrane Database Syst Rev*. 2013;2014(7):CD006431. doi:10.1002/14651858.CD006431.pub3
- Haftu A, Hagos H, Mehari MA, G/Her B. Pregnant women adherence level to antenatal care visit and its effect on perinatal outcome among mothers in Tigray public health institutions, 2017: Cohort study. *BMC Res Notes*. 2018;11(1):872. doi:10.1186/s13104-018-3987-0
- Royal College of Midwifery. High quality midwifery care. 2014. <https://www.rcm.org.uk/media/2354/high-quality-midwifery-care.pdf>. Accessed October 9, 2022.
- World Health Organization. Postpartum care of the mother and newborn: A practical guide. 1998. http://apps.who.int/iris/bitstream/10665/66439/1/WHO_RHT_MSM_98.3.pdf. Accessed October 9, 2022.
- Buzaglo N, Harlev A, Sergienko R, Sheiner E. Risk factors for early postpartum hemorrhage (PPH) in the first vaginal delivery, and obstetrical outcomes in subsequent pregnancy. *J Matern Fetal Neonatal Med*. 2015;28(8):932–937. doi:10.3109/14767058.2014.937698
- Fukami T, Koga H, Goto M, et al. Incidence and risk factors for postpartum hemorrhage among transvaginal deliveries at a tertiary perinatal medical facility in Japan. *PLoS One*. 2019;14(1):e0208873. doi:10.1371/journal.pone.0208873
- Ononge S, Mirembe F, Wandabwa J, Campbell OMR. Incidence and risk factors for postpartum hemorrhage in Uganda. *Reprod Health*. 2016;13(1):38. doi:10.1186/s12978-016-0154-8
- Evans J, Hannan NJ, Edgell TA, et al. Fresh versus frozen embryo transfer: Backing clinical decisions with scientific and clinical evidence. *Hum Reprod Update*. 2014;20(6):808–821. doi:10.1093/humupd/dmu027
- Zeilmaker GH, Alberda AT, van Gent I, Rijkmans CMPM, Drogendijk AC. Two pregnancies following transfer of intact frozen-thawed embryos. *Fertil Steril*. 1984;42(2):293–296. doi:10.1016/S0015-0282(16)48029-5
- Pereira N, Rosenwaks Z. A fresh(er) perspective on frozen embryo transfers. *Fertil Steril*. 2016;106(2):257–258. doi:10.1016/j.fertnstert.2016.06.028
- Kushnir VA, Barad DH, Albertini DF, Darmon SK, Gleicher N. Systematic review of worldwide trends in assisted reproductive technology 2004–2013. *Reprod Biol Endocrinol*. 2017;15(1):6. doi:10.1186/s12958-016-0225-2
- Shapiro BS, Daneshmand ST, Garner FC, Aguirre M, Hudson C. Clinical rationale for cryopreservation of entire embryo cohorts in lieu of fresh transfer. *Fertil Steril*. 2014;102(1):3–9. doi:10.1016/j.fertnstert.2014.04.018
- Özgür K, Berkkanoglu M, Bulut H, Isikli A, Coetzee K. Higher clinical pregnancy rates from frozen-thawed blastocyst transfers compared to fresh blastocyst transfers: A retrospective matched-cohort study. *J Assist Reprod Genet*. 2015;32(10):1483–1490. doi:10.1007/s10815-015-0576-1
- Shapiro BS, Daneshmand ST, Garner FC, Aguirre M, Hudson C, Thomas S. Evidence of impaired endometrial receptivity after ovarian stimulation for in vitro fertilization: A prospective randomized trial comparing fresh and frozen-thawed embryo transfer in normal responders. *Fertil Steril*. 2011;96(2):344–348. doi:10.1016/j.fertnstert.2011.05.050
- Bais JMJ, Eskes M, Pel M, Bonsel GJ, Bleker OP. Postpartum haemorrhage in nulliparous women: Incidence and risk factors in low and high risk women. *Eur J Obstet Gynecol Reprod Biol*. 2004;115(2):166–172. doi:10.1016/j.ejogrb.2003.12.008
- Baker AM, Haeri S. Estimating risk factors for development of pre-eclampsia in teen mothers. *Arch Gynecol Obstet*. 2012;286(5):1093–1096. doi:10.1007/s00404-012-2418-z
- Basak R, Sarker A, Roy N, et al. Comparative study on breech deliveries among the primiparous and multiparous women in a tertiary care hospital. *Sch Int J Obstet Gynecol*. 2022;5(3):95–100. doi:10.36348/sijog.2022.v05i03.006
- Biguzzi E, Franchi F, Ambrogi F, et al. Risk factors for postpartum hemorrhage in a cohort of 6011 Italian women. *Thromb Res*. 2012;129(4):e1–e7. doi:10.1016/j.thromres.2011.09.010
- Blomberg M. Maternal obesity and risk of postpartum hemorrhage. *Obstet Gynecol*. 2011;118(3):561–568. doi:10.1097/AOG.0b013e31822a6c59
- Bujold E, Hammoud A, Schild C, Krapp M, Baumann P. The role of maternal body mass index in outcomes of vaginal births after cesarean. *Am J Obstet Gynecol*. 2005;193(4):1517–1521. doi:10.1016/j.ajog.2005.03.041
- Butwick AJ, Liu C, Guo N, et al. Association of gestational age with postpartum hemorrhage: An international cohort study. *Anesthesiology*. 2021;134(6):874–886. doi:10.1097/ALN.0000000000003730
- Driessen M, Bouvier-Colle MH, Dupont C, Khoshnood B, Rudigoz RC, Deneux-Tharaux C. Postpartum hemorrhage resulting from uterine atony after vaginal delivery: Factors associated with severity. *Obstet Gynecol*. 2011;117(1):21–31. doi:10.1097/AOG.0b013e318202c845
- Ford JB, Roberts CL, Simpson JM, Vaughan J, Cameron CA. Increased postpartum hemorrhage rates in Australia. *Int J Gynaecol Obstet*. 2007;98(3):237–243. doi:10.1016/j.ijgo.2007.03.011
- Gofton EN, Capewell V, Natale R, Gratton RJ. Obstetrical intervention rates and maternal and neonatal outcomes of women with gestational hypertension. *Am J Obstet Gynecol*. 2001;185(4):798–803. doi:10.1067/mob.2001.117314
- Guo Y, Yin Y, Tian L. The pregnancy outcomes of fresh embryo transfer and frozen embryo transfer [in Chinese]. *Chin J Clin Obstet Gynecol*. 2015;17:526–529.
- Halloran DR, Marshall NE, Kunovich RM, Caughey AB. Obesity trends and perinatal outcomes in black and white teenagers. *Am J Obstet Gynecol*. 2012;207(6):492.e1–492.e7. doi:10.1016/j.ajog.2012.09.023

34. Healy DL, Breheny S, Halliday J, et al. Prevalence and risk factors for obstetric haemorrhage in 6730 singleton births after assisted reproductive technology in Victoria, Australia. *Hum Reprod.* 2010;25(1):265–274. doi:10.1093/humrep/dep376
35. Lao TT, Sahota DS, Cheng YKY, Law LW, Leung TY. Advanced maternal age and postpartum hemorrhage: Risk factor or red herring? *J Matern Fetal Neonatal Med.* 2014;27(3):243–246. doi:10.3109/14767058.2013.807240
36. Liu CN, Yu FB, Xu YZ, et al. Prevalence and risk factors of severe postpartum hemorrhage: A retrospective cohort study. *BMC Pregnancy Childbirth.* 2021;21(1):332. doi:10.1186/s12884-021-03818-1
37. Lu L, Li JH, Dai XF, Wei JB, Chen LH, Hu JF. Impact of advanced maternal age on maternal and neonatal outcomes in preterm birth. *Ginekol Pol.* 2022;93(2):134–141. doi:10.5603/GP.a2021.0224
38. Magann EF, Doherty DA, Chauhan SP, Klimpel JM, Huff SD, Morrison JC. Pregnancy, obesity, gestational weight gain, and parity as predictors of peripartum complications. *Arch Gynecol Obstet.* 2011;284(4):827–836. doi:10.1007/s00404-010-1754-0
39. Nojomi M, Haghighi L, Bijari B, Rezvani L, Tabatabaee S. Delayed childbearing: Pregnancy and maternal outcomes. *Iran J Reprod Med.* 2010;8(2):80–85. <http://ijrm.ir/article-1-178-fa.pdf>. Accessed October 10, 2022.
40. Miller CM, Cohn S, Akdagli S, Carvalho B, Blumenfeld YJ, Butwick AJ. Postpartum hemorrhage following vaginal delivery: Risk factors and maternal outcomes. *J Perinatol.* 2017;37(3):243–248. doi:10.1038/jp.2016.225
41. Nove A, Berrington A, Matthews Z. Comparing the odds of postpartum haemorrhage in planned home birth against planned hospital birth: Results of an observational study of over 500,000 maternities in the UK. *BMC Pregnancy Childbirth.* 2012;12(1):130. doi:10.1186/1471-2393-12-130
42. Otigbah CM, Dhanjal MK, Harmsworth G, Chard T. A retrospective comparison of water births and conventional vaginal deliveries. *Eur J Obstet Gynecol Reprod Biol.* 2000;91(1):15–20. doi:10.1016/S0301-2115(99)00238-9
43. Puri M, Patra S, Singh P, et al. Factors influencing occurrence of postpartum haemorrhage in pregnant women with hepatitis E infection and deranged coagulation profile. *Obstet Med.* 2011;4(3):108–112. doi:10.1258/om.2011.110031
44. Sebire N, Jolly M, Harris J, et al. Maternal obesity and pregnancy outcome: A study of 287 213 pregnancies in London. *Int J Obes.* 2001;25(8):1175–1182. doi:10.1038/sj.ijo.0801670
45. Shabbir S, Zahid M, Qazi A. To detect outcome of pregnancy in advanced maternal age among Pakistani women. *Pak J Med Sci.* 2018;8(3):709–712. https://www.pjmhsonline.com/2014/july_sep/pdf/709%20%20To%20Detect%20Outcome%20of%20Pregnancy%20in%20Advanced%20Maternal%20Age%20among%20Pakistani%20Women.pdf. Accessed October 9, 2022.
46. Sharma JB, Pundir P, Malhotra M, Arora R. Evaluation of placental drainage as a method of placental delivery in vaginal deliveries. *Arch Gynecol Obstet.* 2005;271(4):343–345. doi:10.1007/s00404-004-0619-9
47. Sheiner E, Sarid L, Levy A, Seidman DS, Hallak M. Obstetric risk factors and outcome of pregnancies complicated with early postpartum hemorrhage: A population-based study. *J Matern Fetal Neonatal Med.* 2005;18(3):149–154. doi:10.1080/14767050500170088
48. Suzuki S, Kikuchi F, Ouchi N, et al. Risk factors for postpartum hemorrhage after vaginal delivery of twins. *J Nippon Med Sch.* 2007;74(6):414–417. doi:10.1272/jnms.74.414
49. Tixier H, Boucard C, Ferdynus C, Douvier S, Sagot P. Interest of using an underbuttocks drape with collection pouch for early diagnosis of postpartum hemorrhage. *Arch Gynecol Obstet.* 2011;283(1):25–29. doi:10.1007/s00404-009-1265-z
50. Tsukamoto H, Fukuoka H, Inoue K, Koyasu M, Nagai Y, Takimoto H. Restricting weight gain during pregnancy in Japan: A controversial factor in reducing perinatal complications. *Eur J Obstet Gynecol Reprod Biol.* 2007;133(1):53–59. doi:10.1016/j.ejogrb.2006.07.031
51. Wang K, Qiu J, Meng L, Lai X, Yao Z, Peng S. Postpartum hemorrhage and postpartum depressive symptoms: A retrospective cohort study. *Depress Anxiety.* 2022;39(3):246–253. doi:10.1002/da.23245
52. Wikland M, Hardarson T, Hillensjö T, et al. Obstetric outcomes after transfer of vitrified blastocysts. *Hum Reprod.* 2010;25(7):1699–1707. doi:10.1093/humrep/deq117
53. National Collaborating Centre for Women's and Children's Health. *Intrapartum Care. Care of Healthy Women and Their Babies During Childbirth. Clinical Guideline 190 Methods, Evidence and Recommendations. December 2014, Updated February 2017.* London, UK: National Institute for Health and Care Excellence; 2017. <https://www.nice.org.uk/guidance/cg190/evidence/full-guideline-pdf-248734770>
54. Johnson JA, Tough S, Wilson RD, et al. Delayed child-bearing. *J Obstet Gynaecol Can.* 2012;34(1):80–93. doi:10.1016/S1701-2163(16)35138-6
55. Royal College of Obstetricians and Gynaecologists. Prevention and management of postpartum haemorrhage: Green-top guideline No. 52. 2014. <https://www.rcog.org.uk/guidance/browse-all-guidance/green-top-guidelines/prevention-and-management-of-postpartum-haemorrhage-green-top-guideline-no-52/>. Accessed October 10, 2022.
56. Grotegut CA, Chisholm CA, Johnson LNC, Brown HL, Heine RP, James AH. Medical and obstetric complications among pregnant women aged 45 and older. *PLoS One.* 2014;9(4):e96237. doi:10.1371/journal.pone.0096237
57. Walker KF, Malin G, Wilson P, Thornton JG. Induction of labour versus expectant management at term by subgroups of maternal age: An individual patient data meta-analysis. *Eur J Obstet Gynecol Reprod Biol.* 2016;197:1–5. doi:10.1016/j.ejogrb.2015.11.004
58. Wood S, Cooper S, Ross S. Does induction of labour increase the risk of caesarean section? A systematic review and meta-analysis of trials in women with intact membranes. *BJOG.* 2014;121(6):674–685. doi:10.1111/1471-0528.12328
59. Bogaerts A, Witters I, Van den Bergh BRH, Jans G, Devlieger R. Obesity in pregnancy: Altered onset and progression of labour. *Midwifery.* 2013;29(12):1303–1313. doi:10.1016/j.midw.2012.12.013
60. Doi L, Williams AJ, Marrayat L, Frank J. Cohort study of high maternal body mass index and the risk of adverse pregnancy and delivery outcomes in Scotland. *BMJ Open.* 2020;10(2):e026168. doi:10.1136/bmjopen-2018-026168
61. McDonald S, Murphy K, Beyene J, Ohlsson A. Perinatal outcomes of in vitro fertilization twins: A systematic review and meta-analyses. *Am J Obstet Gynecol.* 2005;193(1):141–152. doi:10.1016/j.ajog.2004.11.064
62. Wang H, Jayasekara R, Warland J. The effect of “hands on” techniques on obstetric perineal laceration: A structured review of the literature. *Women Birth.* 2015;28(3):194–198. doi:10.1016/j.wombi.2015.02.006
63. Opdahl S, Henningsen AA, Tiitinen A, et al. Risk of hypertensive disorders in pregnancies following assisted reproductive technology: A cohort study from the CoNARTaS group. *Hum Reprod.* 2015;30(7):1724–1731. doi:10.1093/humrep/dev090
64. Liu SY, Teng B, Fu J, Li X, Zheng Y, Sun XX. Obstetric and neonatal outcomes after transfer of vitrified early cleavage embryos. *Hum Reprod.* 2013;28(8):2093–2100. doi:10.1093/humrep/det104

Effects of different inferior mesenteric artery ligation levels on the prognosis of patients with low rectal cancer

*Rui Chen^{1,D}, *Hao Jiang^{2,3,C}, Wei Jiang^{1,B}, Kangjia Luo^{1,C}, Hao Zhang^{1,E}, Feng Gao^{2,3,A,F}

¹ The First Hospital of Ningbo University, China

² Institute of Digestive Disease of Ningbo University, China

³ Department of Colorectal Surgery, The Second Affiliated Hospital of Harbin Medical University, China

A – research concept and design; B – collection and/or assembly of data; C – data analysis and interpretation;

D – writing the article; E – critical revision of the article; F – final approval of the article

Advances in Clinical and Experimental Medicine, ISSN 1899–5276 (print), ISSN 2451–2680 (online)

Adv Clin Exp Med. 2023;32(7):733–739

Address for correspondence

Rui Chen

E-mail: 1056331162@qq.com

Funding sources

The study was funded by Wu Jieping Medical Foundation (grant No. 320.6750.18492) and Research on Higher Education Teaching Reform in Heilongjiang Province (grant No. SJGY20200448).

Conflict of interest

None declared

*Rui Chen and Hao Jiang contributed equally to this work.

Received on April 13, 2022

Reviewed on August 11, 2022

Accepted on December 16, 2022

Published online on June 15, 2023

Abstract

Background. Regarding low rectal cancer (RC) low anterior resection (LAR), a specific consensus regarding the optimal level of inferior mesenteric artery (IMA) ligation does not exist.

Objectives. To systematically evaluate the effects of different IMA ligation methods on the prognosis of patients with low RC, so as to further guide clinical treatment.

Materials and methods. Between January 2013 and December 2018, 158 patients with low RC underwent LAR. According to the IMA ligation method used, the cases were divided into the low-ligation group (LL group; n = 66) and the high-ligation group (HL group; n = 92). The basic information, operation indicators, postoperative data, and long-term survival in the 2 groups were compared.

Results. Sixty cases in the HL group and 60 cases in the LL group were successfully matched using propensity score matching (PSM). There were no statistically significant differences in intraoperative bleeding, intraoperative time, postoperative hospital stay, harvested lymph nodes (LNs), postoperative complications (including urinary retention, urinary incontinence, anastomotic leaks, bowel obstruction, incisional infection, and anal function 3 months after surgery), overall survival (OS), disease-free survival (DFS), local recurrence, and distant metastasis between the 2 groups ($p > 0.05$). Compared with the HL group, the time to first flatus and the time to fluid intake were shorter in the LL group ($p < 0.05$).

Conclusions. In general, the different IMA ligation methods have no significantly different effects on the prognosis of patients with low RC, but the LL group showed restored intestinal motility earlier.

Key words: prognosis, propensity score matching, low rectal cancer, ligation of inferior mesenteric artery

Cite as

Chen R, Jiang H, Jiang W, Luo K, Zhang H, Gao F. Effects of different inferior mesenteric artery ligation levels on the prognosis of patients with low rectal cancer.

Adv Clin Exp Med. 2023;32(7):733–739.

doi:10.17219/acem/157565

DOI

10.17219/acem/157565

Copyright

Copyright by Author(s)

This is an article distributed under the terms of the Creative Commons Attribution 3.0 Unported (CC BY 3.0) (<https://creativecommons.org/licenses/by/3.0/>)

Background

Only 200 years have passed since the industrial revolution, when rectal cancer (RC) patients were first treated surgically and the basic principle of total mesorectal excision (TME) was widely accepted by surgeons.¹ Although RC surgical techniques flourished during this period, the management of the left colonic artery (LCA) in RC surgery has not been systematically defined. In the early 20th century, Miles² and Moynihan³ proposed 2 different approaches to the inferior mesenteric artery (IMA): low ligation (LL) and high ligation (HL). Low ligation involves ligation of the IMA immediately distal to the origin of the LCA, and a complete removal of the mesenteric vessels and lymph nodes (LNs) within its limits in order to provide rich blood flow to the anastomosis. High ligation involves dissection of the vessels at the root of the IMA from the abdominal aorta to allow complete clearance of the LNs at the root of the IMA.

The question of whether the LCA needs to be preserved has been widely discussed by clinical scholars.^{4–7} However, in previous studies, RC or colorectal cancer (CRC) has always been analyzed as a whole, with little distinction made between the different segments and locations of tumors in the colorectum. Low RC has a unique anatomy compared to mid-RC, high RC or colon cancer. In particular, it is located lower, in the narrow pelvis. Because of its location, the anastomosis is likely to receive less blood flow after low RC surgery, as it is further from the proximal vessels, thus contributing to the development of anastomotic leakage (AL). In recent years, the use of anal-saving operations has become more widespread as the demands for quality of life have increased. Therefore, the proper choice of IMA management for low RC is crucial. This study examines the effects of different IMA treatments on low RC.

Objectives

Although there have been many studies comparing the safety and feasibility of different IMA ligation methods in patients with CRC, few studies have investigated low RC separately. Thus, the purpose of this study is to systematically assess the impact of different ICA management techniques on the prognosis of patients with low RC.

Materials and methods

Study design

Patients diagnosed with low RC and undergoing low anterior resection (LAR) performed by the same surgical team at the Second Affiliated Hospital of Harbin Medical University, China, between January 2013 and December 2018 were included in the study. Depending on the intraoperative

LCA treatment method used, patients were divided into 2 groups: high ligation of the IMA (HL group; $n = 92$) and low ligation of the IMA (LL group; $n = 66$).

Inclusion and exclusion criteria

Patients were considered eligible for the study if: 1) they were diagnosed with RC during pathological examination and the distance from the lower edge of the tumor lesion to the dentate line was ≤ 5 cm; 2) had stage I–III disease; and 3) had complete clinical records. The exclusion criteria were: 1) patients who received neoadjuvant radiotherapy or chemotherapy; 2) RC patients who underwent emergency surgery due to obstruction, massive bleeding, perforation, or other emergencies; 3) patients who underwent abdominoperineal resection or diverting ileostomy; and 4) patients with American Society of Anesthesiologists (ASA) grade IV who were considered by anesthesiologists to be unfit to undergo surgery.

Surgery

Surgical methods included laparotomy and laparoscopy. For all of the enrolled patients, the TME principle was followed during radical resection, and complete resection of the diseased bowel segment and the corresponding mesentery was performed, including complete dissection of the vessels, nerves, lymphatic vessels, and LNs, followed by anastomosis of the bowel. The HL was performed when preoperative computed tomography (CT) showed suspicious metastatic LNs at the root of the IMA or when metastatic LNs were diagnosed using frozen biopsy at the root of IMA. In the other cases, LL was performed. For the LL group, the vessels were severed below the LCA emanating from IMA, and lymph nodes were dissected. For the HL group, the vessels were severed about 1 cm below the IMA root, and LN dissection was performed at the IMA root. All arteries and veins were skeletonized, and LNs larger than 0.5 cm were dissected.

Observation indicators

The intraoperative variables included intraoperative blood loss and operation time. Postoperative data included pathological information, the postoperative recovery index, postoperative complications, postoperative LN detection, lymphatic invasion, vascular invasion, perineural invasion, postoperative tumor differentiation, pathological type, time to first flatus, time to fluid intake, postoperative hospitalization days, postoperative intestinal obstruction, urinary retention, urinary incontinence, AL, and anal function 3 months after surgery. The postoperative long-term survival variables included overall survival (OS), disease-free survival (DFS), local recurrence, and distant metastasis. All patients with stage II (including high-risk factors) and stage III according to the tumor–nodule–metastasis (TNM) staging

system were routinely treated with the standard XELOX protocol (8 cycles of capecitabine and 8 cycles of oxaliplatin) for chemotherapy. The patients were followed up to December 2021 for at least 36 months or until death.

Statistical analyses

The IBM Statistical Package for Social Sciences (SPSS) v. 26.0 software (IBM Corp., Armonk, USA) was used for data analysis. The baseline information in the 2 groups were matched using propensity score matching (PSM), and variables including gender, age, tumor size, body mass index (BMI), pathological tumor (pT) stage, pathological lymph node (pN) stage, carcinoembryonic antigen (CEA) level, and ASA grade were considered covariates in the performance of 1:1 PSM (caliper value = 0.1). All calculated data are expressed in terms of frequency and percentage. The Kolmogorov–Smirnov test was used to test the normality of the subgroups and the Levene’s test was used to evaluate the homogeneity of variance. Mean and standard deviation (M ±SD) were used to present the measurement data conforming to a normal distribution, and Student’s t-test or Mann–Whitney U test were used for further comparisons. The χ^2 test or Fisher’s exact test were used for comparisons of counted data. Survival curves were drawn using the Kaplan–Meier method and analyzed with the log-rank test using GraphPad Prism v. 8.0 software (GraphPad Software, San Diego, USA). The value of $p \leq 0.05$ was considered statistically significant.

Results

Baseline data in the LL and HL groups

According to the inclusion and exclusion criteria, 158 patients with low RC were included in this retrospective study, and were divided into the LL (n = 66) and HL (n = 92) groups, according to whether LCA was retained during operation. The basic patient characteristics in the LL and HL groups were analyzed. Before matching, BMI ($p = 0.004$) and tumor size ($p = 0.025$) were significantly different between the 2 groups. After PSM, the characteristics of the 2 groups tended to be balanced, and 60 pairs of cases were successfully matched. There were no statistical differences in the baseline data of these 2 groups ($p > 0.05$; Table 1). Normality and homogeneity of variance tests were performed before the analysis of data.

Postoperative pathological information

In terms of the postoperative pathological data, there were no significant differences in differentiation degree ($p = 0.114$), number of LNs harvested ($p = 0.973$), vascular invasion ($p = 0.699$), perineural invasion ($p = 0.350$), lymphatic invasion ($p = 0.079$), or pathological type ($p = 0.810$) between the 2 groups (Table 2).

Table 1. Baseline characteristics of patients

Variable	Before matching			After matching			
	HL (n = 92)	LL (n = 66)	p-value	HL (n = 60)	LL (n = 60)	p-value	
Gender, n (%)	male	54 (58.7)	41 (62.1)	0.665 ^b	35 (58.3)	38 (63.3)	0.575 ^b
	female	38 (41.3)	25 (37.9)		25 (41.7)	22 (36.7)	
Age [years], M ±SD	60.0 ±11.1	58.2 ±10.9	0.339 ^c	59.7 ±11.9	58.5 ±10.7	0.551 ^c	
BMI [kg/m ²], M±SD	22.3 ±2.9	23.8 ±3.7	0.004^c	22.9 ±2.7	23.4 ±3.4	0.362 ^c	
Size, n (%)	<5	71 (77.2)	40 (60.6)	0.025^b	45 (75.0)	39 (65.0)	0.232 ^b
	≥5	21 (22.8)	26 (39.4)		15 (25.0)	21 (35.0)	
pT staging, n (%)	T1/2	16 (17.4)	8 (12.1)	0.363 ^b	7 (11.7)	8 (13.3)	0.783 ^b
	T3/4a	76 (82.6)	58 (87.9)		53 (88.3)	52 (86.7)	
pN staging, n (%)	N0	58 (63.0)	41 (62.1)	0.906 ^b	38 (63.3)	39 (65.0)	0.849 ^b
	N1/2	34 (37.0)	25 (37.9)		22 (36.7)	21 (35.0)	
CEA, n (%)	<5	68 (73.9)	51 (77.3)	0.629 ^b	47 (78.3)	46 (76.7)	0.827 ^b
	≥5	24 (26.1)	15 (22.7)		13 (21.7)	14 (23.3)	
ASA score, n (%)	I	6 (6.5)	2 (3.0)	0.198 ^a	3 (5.0)	2 (3.3)	0.514 ^a
	II	71 (77.2)	50 (75.8)		44 (73.3)	46 (76.7)	
	III	15 (16.3)	11 (16.7)		13 (21.7)	10 (16.7)	
	IV	0 (0.0)	3 (4.5)		0 (0.0)	2 (3.3)	

Values in bold indicate variables with $p < 0.05$. ^a Fisher’s exact test; ^b χ^2 test; ^c Student’s t-test. Values are expressed as number, median and range (min, max), and percentages. HL – high-ligation group; LL – low-ligation group; BMI – body mass index; M ±SD – mean ± standard deviation; CEA – carcinoembryonic antigen; ASA – American Society of Anesthesiology; pT staging – pathological tumor staging; pN staging – pathological lymph node staging.

Table 2. Postoperative pathological characteristics of patients

Variable		HL (n = 60)	LL (n = 60)	t/ χ^2 /F/Z	p-value
Differentiation, n (%)	high	6 (10.0)	2 (3.3)	4.568	0.114 ^a
	moderate	45 (75.0)	54 (90.0)		
	low	9 (15.0)	4 (6.7)		
	lymph nodes harvested	14 (11–22)	14 (3–27)	–0.034	0.973 ^c
Vascular invasion, n (%)	no	41 (68.3)	39 (65.0)	0.150	0.699 ^b
	yes	19 (31.7)	21 (35.0)		
Perineural invasion, n (%)	no	26 (43.3)	21 (35.0)	0.874	0.350 ^b
	yes	34 (56.7)	39 (65.0)		
Lymphatic invasion, n (%)	no	45 (75.0)	36 (60.0)	3.077	0.079 ^b
	yes	15 (25.0)	24 (40.0)		
Histology, n (%)	adenocarcinoma	50 (83.3)	49 (81.7)	0.058	0.810 ^b
	mucinous adenocarcinoma/signet ring cell carcinoma	10 (16.7)	11 (18.3)		

^a Fisher's exact test; ^b χ^2 test; ^c Mann–Whitney U test. Values are expressed as number, median and range (min, max), and percentages. HL – high-ligation group; LL – low-ligation group.

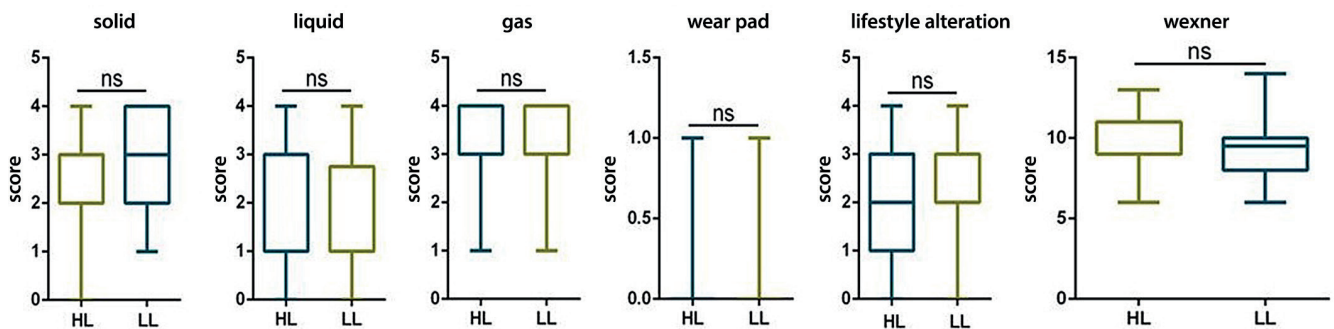


Fig. 1. Comparison of anal function

ns – no significant difference; HL – high-ligation group; LL – low-ligation group.

Surgical operation indicators, postoperative recovery indicators and postoperative complications

In the analysis of intraoperative indicators, there were no significant differences in operative duration ($p = 0.720$), intraoperative blood loss ($p = 0.143$) or the time of first postoperative feeding ($p = 0.151$) between the 2 groups. In the postoperative information analysis, the first postoperative flatus time in the LL group (48 h, range: 10–96 h) was earlier than that in the HL group (50 h, range: 14–110 h; $p = 0.022$). There were no statistical differences between the 2 groups in the length of postoperative hospital stay ($p = 0.261$), AL ($p = 0.186$), postoperative intestinal obstruction ($p = 1.000$), postoperative urinary retention ($p = 1.000$), urinary incontinence ($p = 0.752$), or incision infection ($p = 1.000$). Anal function was evaluated using the Wexner scale 3 months after surgery, and no significant difference was found between the HL (9.58 ± 1.52) and LL (9.77 ± 1.52) groups (Table 3, Fig. 1).

Survival analysis

The median postoperative follow-up time was 75.5 months in the HL group and 80 months in the LL group. At the end of follow-up, there were 10 deaths in the LL group and 12 deaths in the HL group due to recurrence or metastasis of RC. Survival curves showed that the HL and LL groups had no obvious differences in OS ($p = 0.573$), DFS ($p = 0.925$), local recurrence ($p = 0.952$) or distant metastasis ($p = 0.852$; Fig. 2).

Discussion

For the same surgical team, the length of the operation and the amount of intraoperative blood loss can reflect the difficulty of surgery.⁸ In the HL and LL comparisons, the increased difficulty and time of the LL operation was mainly due to the dissection of the LNs. In HL, the IMA is severed within 2 cm from the abdominal aorta, and then

Table 3. Intraoperative and postoperative characteristics of patients

Variable		HL (n = 60)	LL (n = 60)	t/ χ^2 /Z	p-value
Surgical approach, n (%)	laparotomy	38 (63.3)	35 (58.3)	0.315	0.575 ^b
	laparoscopy	22 (36.7)	25 (41.7)		
Operation time [min]		180 (125–265)	180 (105–260)	-0.358	0.720 ^d
Operative bleeding [mL]		50 (20–600)	100 (15–500)	-1.432	0.143 ^d
Postoperative hospital days [days]		14 (8–44)	13 (14–39)	-1.124	0.261 ^d
Time to first flatus [h]		50 (14–110)	48 (10–96)	-2.292	0.022^d
Time to fluid intake [h]		72.5 (40–162)	72 (34–120)	-1.436	0.151 ^d
Anastomotic leakage, n (%)		7 (11.7)	3 (5.0)	1.745	0.186 ^b
Bowel obstruction, n (%)		2 (3.3)	3 (5.0)	–	1.000 ^a
Urinary retention, n (%)		3 (5.0)	2 (3.3)	–	1.000 ^a
Urinary incontinence, n (%)		5 (8.3)	6 (10.0)	0.100	0.752 ^b
Incision infection, n (%)		4 (6.7)	4 (6.7)	–	1.000 ^a
Wexner score, M \pm SD		9.77 \pm 1.52	9.58 \pm 1.52	0.660	0.511 ^c

Values in bold indicate variables with $p < 0.05$. ^a Fisher’s exact test; ^b χ^2 test; ^c Student’s t-test; ^d Mann–Whitney U test. Values are expressed as number, median and range (min, max), and percentages. M \pm SD – mean \pm standard deviation; HL – high-ligation group; LL – low-ligation group.

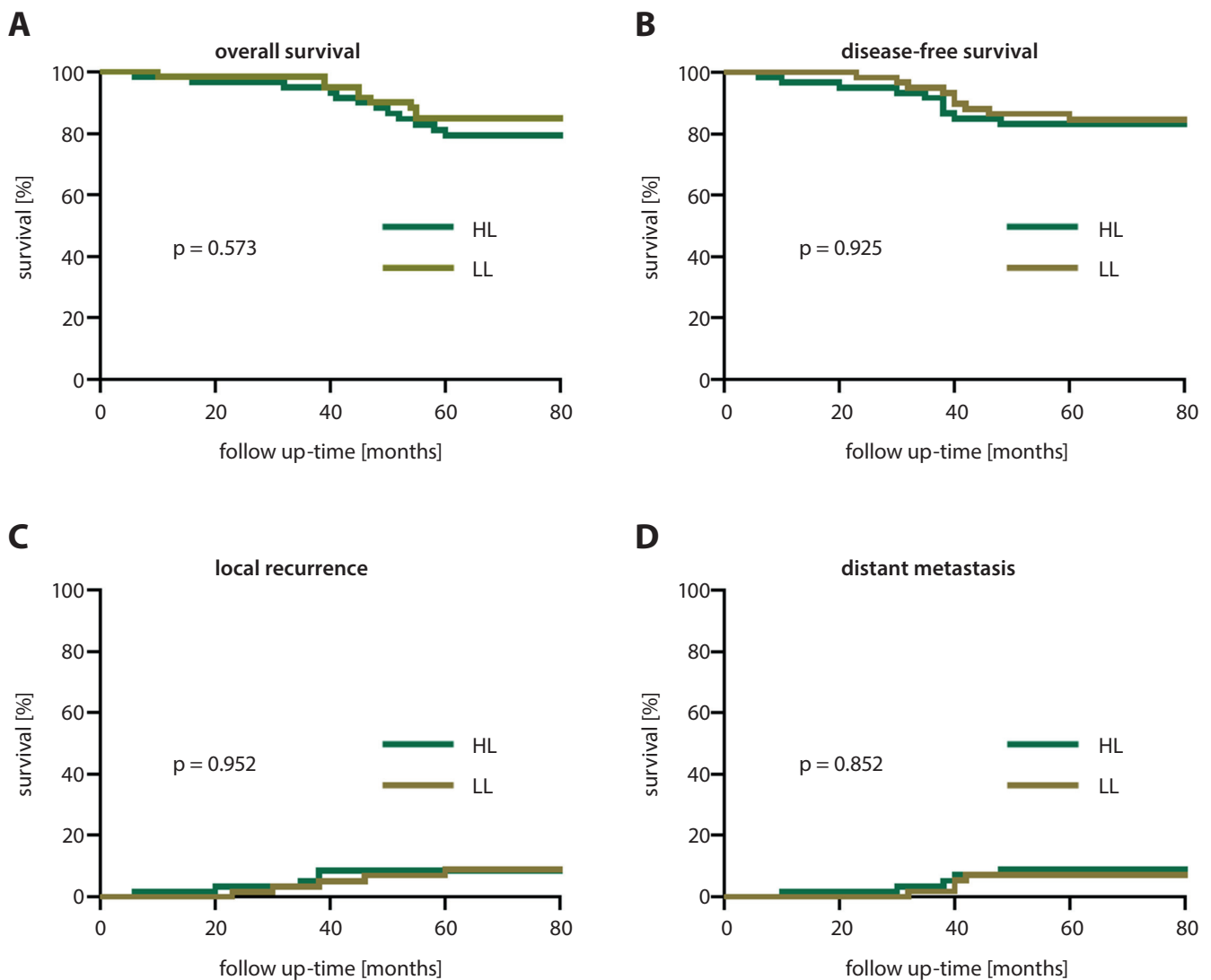


Fig. 2. Survival comparison. A. Overall survival ($p = 0.573$); B. Disease-free survival ($p = 0.925$); C. Local recurrence ($p = 0.952$); D. Distant metastasis ($p = 0.852$) HL – high-ligation group; LL – low-ligation group.

the LNs at the root of the IMA are dissected together. However, in LL, the IMA is dissected from below where the LCA emanates, and then cleared along the area of the IMA root where LNs are enclosed by the IMA, LCA, inferior mesenteric vein (IMV), etc. The technical difficulties in identifying anatomical variants of the IMA and LCA, protection of nerves, performing vascular skeletonization, and dissection of peripheral and dorsal LNs are significantly higher in LL. In addition, LL involves preservation of the LCA. According to previous reports, preserving the LCA has the potential to increase anastomotic tension, and the surgeon tends to free more of the bowel and even the splenic flexure of the colon to provide a longer, movable bowel for anastomosis in order to reduce anastomotic tension. In this study, there were no significant differences in intraoperative blood loss or operation time between the HL and LL groups ($p > 0.05$). This is likely due to the fact that, in the actual operation process, in order to ensure adequate blood supply of anastomotic stoma, the surgeon often excises more intestinal loops during HL surgery, thus increasing the possibility of having to mobilize the splenic flexure. Furthermore, in our view, in a mature surgical team that completed the surgeon's learning curve and developed minimally invasive laparoscopic techniques, the different ligation methods will not have an evident impact on the course of the procedure, even if they do have some impact on its difficulty.

The influence on postoperative complications, among which AL is a complication that clinicians pay more attention to, has been analyzed. Once AL occurs, it will not only aggravate the pain and stress of patients, but also increase hospitalization costs and length of stay, and can endanger patients' lives. There are 2 main factors that affect AL: anastomotic tension and anastomotic blood supply. Low ligation is more likely to increase intraoperative anastomotic tension compared to HL, due to the retention of the LCA. However, surgeons often use various methods during surgery (freeing more intestinal loops or the splenic flexure, diverting ileostomy, minimally invasive liver surgery (MILS), etc.) to ensure patient safety. Other reports⁹ have indicated that IMA LL can make the anastomosis tension-free in 80% of patients; thus, anastomotic tension is not unavoidable in LL. With regard to the anastomotic blood supply, in HL of the IMA, the supply mainly comes from the left branch of MCA, reaches the left colon through the Riolan's arch, and finally reaches the anastomotic site. In LL of the IMA, apart from MCA, the retained LCA also provides part of the blood supply. It has been reported that Riolan's arch is present in less than 50% of the population, and it is more likely to cause vascular stenosis, occlusion or blood flow through longer intestinal canals in elderly men, patients with cardiovascular and cerebrovascular diseases, diabetics, and patients with a lower tumor location.¹⁰ For these patients, the risk of insufficient blood supply to the intestinal canal and anastomotic stoma may increase.^{11,12} In a study

using a Doppler flow analyzer to measure anastomotic blood supply at different IMA ligation levels, it was found that the anastomotic blood supply in the LL group was significantly higher than in the HL group.¹³ In another study, Park et al. reported similar results.¹⁴ In the current paper, there was no statistical difference in AL between the 2 groups ($p = 0.186$). There were 7 AL patients in the HL group (11.7%) and 3 in the LL group (5.0%). The reason for this result may be that, although IMA HL can cause a decreased anastomotic blood supply, the decreased blood flow is not enough to cause AL. Therefore, the different ligation methods produce no significant differences in low RC AL.

There were statistically significant differences between HL and LL groups in terms of first postoperative flatus ($p < 0.05$), which is consistent with the fact that a retained LCA can provide more blood supply to the early postoperative bowel and promote the recovery of peristalsis. No significant difference could be found in anal function scores between the 2 groups 3 months after surgery ($p > 0.05$), indicating that there was no significant difference in intraoperative pelvic floor and anal muscle injury and related nerve injury between the 2 ligation methods. In the 2 groups, we achieved similar results in terms of postoperative urinary retention and urinary incontinence ($p > 0.05$), which is consistent with an earlier retrospective cohort study.¹⁵ Thus, the different ligation levels have no significant effects on urinary function injuries and postoperative recovery.

In RC, LN metastasis notably affects the long-term survival of patients. Complete LN dissection can more accurately determine the stage and prognosis of RC, and can aid in guiding treatment after surgery.^{16,17} Therefore, the number of dissected LNs can be used to evaluate the outcome of RC surgery. In this study, there were no statistically significant differences in the number of postoperative LN examinations, OS, DFS, local recurrence, or distant metastasis between the HL and LL groups ($p > 0.05$). Thus, IMA ligation level has no evident impact on LN dissection and long-term oncology prognosis, and both methods can ensure a good therapeutic effect. These results are consistent with previous studies.^{18,19} Although the 2 different ligation methods entail different dissection methods for IMA root LNs, as long as the TME principle is strictly followed and the mesorectum is completely removed, the radical cure in oncology can be achieved.

Although neoadjuvant therapy is considered a vital treatment method for locally advanced RC, patients receiving neoadjuvant therapy were excluded from the current study. According to previous work, neoadjuvant therapy can significantly influence the extent of LN examination, and treatment impact cannot be analyzed reliably. As the number of harvested LNs in the HL and LL groups was a crucial point that needed to be taken into account in this study in order to objectively compare the oncology outcomes of the 2 different approaches, patients receiving neoadjuvant therapy were excluded from the study. In our

paper, a notable number of patients who were characterized by a high risk of recurrence did not receive neoadjuvant therapy. This was due to the fact that the patients' conditions, such as the presence of serious comorbidities, significant bleeding or obstruction, did not allow them to receive standard therapy.

Limitations

The current study has some important limitations. First, as it is a retrospective study, there is inevitably a selection bias, which may reduce the persuasiveness of the findings. To minimize selection bias, we performed PSM on patient baseline information and discussed the results objectively and adequately. Second, the sample size is relatively small and a larger sample size is needed to confirm our results. Third, since most of the patients in this study were elderly, there was no systematic study of the effects on sexual life and reproductive functions. Moreover, as the center was not able to routinely send the third station LN (station 253 LN) separately for examination, a deeper understanding of the root LNs of the IMA was not possible. Therefore, further research on the issue of IMA root LN metastasis is needed.

Conclusions

In conclusion, in low RC LAR, IMA LL not only achieves the same oncological prognosis as HL, but also shows no significant differences in intraoperative and postoperative complications, and is superior to HL in terms of the recovery of early bowel function.

ORCID iDs

Rui Chen  <https://orcid.org/0009-005-1952-7974>
 Hao Jiang  <https://orcid.org/0000-0003-2742-3698>
 Wei Jiang  <https://orcid.org/0009-0001-6934-4456>
 Kangjia Luo  <https://orcid.org/0000-0003-0419-8512>
 Hao Zhang  <https://orcid.org/0000-0002-1437-9918>
 Feng Gao  <https://orcid.org/0000-0002-8701-1911>

References

- MacFarlane JK, Ryall RDH, Heald RJ. Mesorectal excision for rectal cancer. *Lancet*. 1993;341(8843):457–460. doi:10.1016/0140-6736(93)90207-W
- Miles WE. A method of performing abdomino-perineal excision for carcinoma of the rectum and of the terminal portion of the pelvic colon (1908). *CA Cancer J Clin*. 1971;21(6):361–364. doi:10.3322/canjclin.21.6.361
- Moynihan B. The surgical treatment of cancer of the sigmoid flexure and rectum. *Surg Gynecol Obstet*. 1908;6:463.
- Hida JI, Okuno K. High ligation of the inferior mesenteric artery in rectal cancer surgery. *Surg Today*. 2013;43(1):8–19. doi:10.1007/s00595-012-0359-6
- Dimitriou N, Felekouras E, Karavokyros I, et al. High versus low ligation of inferior mesenteric vessels in rectal cancer surgery: A retrospective cohort study. *JBUON*. 2018;23(5):1350–1361. PMID:30570858.
- Akagi T, Inomata M, Hara T, et al. Clinical impact of D3 lymph node dissection with left colic artery (LCA) preservation compared to D3 without LCA preservation: Exploratory subgroup analysis of data from JCOG0404. *Ann Gastroenterol Surg*. 2020;4(2):163–169. doi:10.1002/ags3.12318
- AlSuhaimi MA, Yang SY, Kang JH, AlSabilah JF, Hur H, Kim NK. Operative safety and oncologic outcomes in rectal cancer based on the level of inferior mesenteric artery ligation: A stratified analysis of a large Korean cohort. *Ann Surg Treat Res*. 2019;97(5):254–260. doi:10.4174/astr.2019.97.5.254
- Zeng J, Su G. High ligation of the inferior mesenteric artery during sigmoid colon and rectal cancer surgery increases the risk of anastomotic leakage: A meta-analysis. *World J Surg Onc*. 2018;16(1):157. doi:10.1186/s12957-018-1458-7
- Buunen M, Lange MM, Ditzel M, Kleinrensink GJ, van de Velde CJH, Lange JF. Level of arterial ligation in total mesorectal excision (TME): An anatomical study. *Int J Colorectal Dis*. 2009;24(11):1317–1320. doi:10.1007/s00384-009-0761-8
- Hinoi T, Okajima M, Shimomura M, et al. Effect of left colonic artery preservation on anastomotic leakage in laparoscopic anterior resection for middle and low rectal cancer. *World J Surg*. 2013;37(12):2935–2943. doi:10.1007/s00268-013-2194-3
- Sörelilius K, Svensson J, Matthiessen P, Rutegård J, Rutegård M. A nationwide study on the incidence of mesenteric ischaemia after surgery for rectal cancer demonstrates an association with high arterial ligation. *Colorectal Dis*. 2019;21(8):925–931. doi:10.1111/codi.14674
- You X, Liu Q, Wu J, et al. High versus low ligation of inferior mesenteric artery during laparoscopic radical resection of rectal cancer: A retrospective cohort study. *Medicine (Baltimore)*. 2020;99(12):e19437. doi:10.1097/MD.00000000000019437
- Komen N, Sliker J, de Kort P, et al. High tie versus low tie in rectal surgery: Comparison of anastomotic perfusion. *Int J Colorectal Dis*. 2011;26(8):1075–1078. doi:10.1007/s00384-011-1188-6
- Park H, Piozzi GN, Lee TH, Kim JS, Choi HB, Kim SH. Arc of Rioldominant colonic perfusion identified by indocyanine green after high ligation of inferior mesenteric artery: Critical in preventing anastomotic ischemia. *Dis Colon Rectum*. 2021;64(4):e64. doi:10.1097/DCR.0000000000001864
- Kverneng Hultberg D, Afshar AA, Rutegård J, et al. Level of vascular tie and its effect on functional outcome 2 years after anterior resection for rectal cancer. *Colorectal Dis*. 2017;19(11):987–995. doi:10.1111/codi.13745
- Shiomi A, Ito M, Maeda K, et al. Effects of a diverting stoma on symptomatic anastomotic leakage after low anterior resection for rectal cancer: A propensity score matching analysis of 1,014 consecutive patients. *J Am Coll Surg*. 2015;220(2):186–194. doi:10.1016/j.jamcollsurg.2014.10.017
- Nash GM. Lymph node yield and oncologic outcome after colorectal cancer resection. *Ann Surg Oncol*. 2012;19(7):2084–2085. doi:10.1245/s10434-012-2340-4
- Sekimoto M, Takemasa I, Mizushima T, et al. Laparoscopic lymph node dissection around the inferior mesenteric artery with preservation of the left colic artery. *Surg Endosc*. 2011;25(3):861–866. doi:10.1007/s00464-010-1284-7
- Yang Y, Wang G, He J, Zhang J, Xi J, Wang F. High tie versus low tie of the inferior mesenteric artery in colorectal cancer: A meta-analysis. *Int J Surg*. 2018;52:20–24. doi:10.1016/j.ijsu.2017.12.030

TG-interacting factor 1 improves risk stratification in patients with NPM1-mutated acute myeloid leukemia

Hongwei Tang^{A–D}, Nan Zhang^{A–C}, Huan Li^{B,C}, Ying Chen^{B,C}, Xinlei Liu^B, Hongbo Xiao^B, Jianchuan Deng^{A,F}, Kang Zhou^{E,F}

Department of Hematology, The Second Affiliated Hospital of Chongqing Medical University, China

A – research concept and design; B – collection and/or assembly of data; C – data analysis and interpretation; D – writing the article; E – critical revision of the article; F – final approval of the article

Advances in Clinical and Experimental Medicine, ISSN 1899–5276 (print), ISSN 2451–2680 (online)

Adv Clin Exp Med. 2023;32(7):741–751

Address for correspondence

Kang Zhou

E-mail: zhoukang@hospital.cqmu.edu.cn

Funding sources

This study was sponsored by the Natural Science Foundation of Chongqing, China (grant No. 2021jcyj-msxmX0064).

Conflict of interest

None declared

Received on August 11, 2022

Reviewed on November 14, 2022

Accepted on December 14, 2022

Published online on February 8, 2023

Abstract

Background. Acute myeloid leukemia (AML) is a heterogeneous disease characterized by diverse genetic abnormalities. The *NPM1* is the most commonly mutated gene in newly diagnosed patients. Optimizing risk stratification in this population could facilitate more rational clinical decision-making.

Objectives. To identify biomarkers that optimize risk stratification in AML patients with *NPM1* mutations.

Materials and methods. Acute myeloid leukemia patients from multiple centers were included in this study. Univariate, multivariate and Kaplan–Meier survival analyses were used to assess risk factors and clinical outcomes. The gene set enrichment analysis (GSEA) was conducted to identify the related enrichment of biological function.

Results. TG-interacting factor 1 (TGIF1) is a good prognostic indicator of disease progression in AML patients. It is closely related to *NPM1* mutation, in which age and TGIF1 expression are independent prognostic factors. Multicenter data sources have shown that high expression of TGIF1 is beneficial for AML, regardless of whether patients received bone marrow transplantation. In the *NPM1*-mutated AML group, age, *FLT3-ITD* and TGIF1 were independent prognostic factors. Moreover, the *NPM1*-mutated subgroup could be well dichotomized into 2 groups with distinct prognoses through TGIF1 combined with European LeukemiaNet (ELN) 2017 risk stratification.

Conclusions. The TGIF1 has an important value in the prognosis of AML. The *NPM1*-mutated patients were further subdivided into risk stratification groups based on TGIF1 expression, which could optimize the ELN 2017 to achieve individualized treatment.

Key words: risk stratification, NPM1, acute myeloid leukemia, TG-interacting factor 1

Cite as

Tang H, Zhang N, Li H, et al. TG-interacting factor 1 improves risk stratification in patients with NPM1-mutated acute myeloid leukemia. *Adv Clin Exp Med.* 2023;32(7):741–751. doi:10.17219/acem/157478

DOI

10.17219/acem/157478

Copyright

Copyright by Author(s)

This is an article distributed under the terms of the Creative Commons Attribution 3.0 Unported (CC BY 3.0) (<https://creativecommons.org/licenses/by/3.0/>)

Background

Acute myeloid leukemia (AML) is a highly aggressive hematologic malignancy of the myeloid lineage characterized by extramedullary malignant infiltration of various organs, portending a poor prognosis.¹ For patients with AML who underwent conventional chemotherapy, the 5-year overall survival (OS) rate was 40–45% compared with 10–20% OS rate of the elder ones.^{2,3} Although the efficacy of the intensive frontline therapy is encouraging, 30% of those patients still relapse after treatment.⁴ Furthermore, the pathophysiology of AML is tightly linked with distinct genetic and molecular abnormalities, and clinicians obtain prognostic information and classification due to the molecular changes occurring in AML. Despite the recent advances in the understanding of pathogenesis and therapeutic methods of AML, it is still intractable and its risk stratification and targeted therapy are complicated due to the cytogenetical, molecular and clinical heterogeneities. Since more and more abnormalities in gene expression have been reported in the occurrence and development of AML, it is apparent that finding more specific biomarkers for AML patients is conducive to patient classification, and serves as an essential prerequisite for individualized treatment.^{5,6}

The *NPM1*-mutated AML is one of the monocytic subtypes of AML, which acts by translocating the *NPM1* mutation gene to partner genes such as anaplastic lymphoma kinase gene (*NPM-ALK*) and normal karyotype gene (*NPM-NK*), rendering heterodimers, producing fusion proteins and promoting cytoplasmic delocalization and cellular transformation.^{7–9} About 30% of heterozygous *NPM1*-mutated AML cases occur in adults and 50–60% of them involve normal karyotype AML (*NK-AML*).¹⁰ However, the complex interactions of this mutation with some prognosis-related accompanying mutations including *FLT3-ITD*, *NPM1/N-RAS* and *NPM1-RAD21*, as well as their joint effect on the clinical outcome remain unclear.^{11–14} Novel molecular information is needed to identify subsets of patients and improve the diagnosis and outcome prediction.

The TG-interacting factor 1 (TGIF1) is a member of the three-amino-acid loop extension (TALE) family of atypical homeodomain-containing transcription factors.¹⁵ It is known as a transcriptional repressor, which participates in various biological signaling pathways including TGF- β , retinoic acid signaling and others, in order to exert its suppressive effects by recruiting and interacting with other co-repressor complexes, such as mSin3/HDAC and CtBP.^{16,17} As a critical suppressive factor of the important signaling pathway, the function of TGIF1 in tumorigenesis and tumor development has attracted considerable research attention. Therefore, in our study, we evaluated the expression of TGIF1 in patients with an initial diagnosis of AML, as well as explored the clinical and potential therapeutic value of TGIF1 in AML.

Objectives

Although several preclinical studies have confirmed that TGIF1 plays a key role in regulating hematopoietic stem cell self-renewal, and that a loss of TGIF1 can lead to the occurrence of AML, there is little evidence of clinical application of TGIF1 in guiding healthcare decisions. Therefore, in our study, we evaluated the expression of TGIF1 in patients with an initial AML diagnosis and demonstrated that TGIF1 plays an independent role in AML and *NPM1*-mutated AML in terms of the prediction of clinical outcomes, as well as provides useful insight for risk stratification and clinical individualized diagnosis and treatment.

Materials and methods

Data acquisition

The expression of TGIF1 was analyzed in the publicly available mRNA sequencing cohort from the Oregon Health and Science University (OHSU)-AML project (405 patients) that included detailed clinical data.¹⁸ Another source of clinical data and gene expression for validation was The Cancer Genome Atlas (TCGA)-AML (151 patients).¹⁹ Validation data analyses for survival outcomes were also obtained from the Therapeutically Applicable Research to Generate Effective Treatment (TARGET)-AML project (296 patients), and Gene Expression Omnibus (GEO) data that are accessible under accession No. GSE37642. We have downloaded the published data until April 28, 2022.

The patients were classified according to the French–American–British classification systems and the risk group stratification was as per the National Comprehensive Cancer Network (NCCN) guidelines. Patients included in the study were evaluated for somatic mutations as well as fusion genes that are common in AML. The datasets generated in this study are available as the Supplementary material. The patient data were obtained from publicly available datasets and did not require further ethical approval.

Gene set enrichment analysis

Gene set enrichment analysis (GSEA, v. 4.0.1; <http://www.gsea-msigdb.org/>) is a widely used bioinformatics analysis tool that determines concordant differences between biological processes. The GSEA was used to verify the differences in molecular pathways between high-expression and low-expression TGIF1 groups. The input data matrix was derived from the OHSU cohort. The 'c2.cp.kegg.v7.1.symbols.gmt' were examined and 1000 permutations were run.

Statistical analyses

The univariate and multivariate Cox regression analyses were performed using the 'survival' R package, and

the main code was provided in Supplementary material. The Kaplan–Meier survival analysis with log-rank test was used to evaluate the prognostic role of TGIF1 cutoff value, and AML patients were grouped according to the optimal difference in OS. Results are expressed as hazard ratio (HR) and 95% confidence interval (95% CI). Statistical analysis and graphing were performed using GraphPad Prism v. 8.02 (GraphPad Software, San Diego, USA) and

R software v. 3.5.2 (R Foundation for Statistical Computing, Vienna, Austria). The Mann–Whitney test and χ^2 test were used to clarify the association between gene expression and clinicopathological characteristics, and when expected counts produced by IBM SPSS v. 26.0 software (IBM Corp., Armonk, USA) were less than 1, the Fisher’s exact test was performed (Table 1).²⁰ The value of $p < 0.05$ was considered statistically significant.

Table 1. Relationship between clinical and molecular characteristics and TGIF1 expression in patients with AML

Characteristics		Total	TGIF1-low (n = 214)	TGIF1-high (n = 191)	p-value
Age [years] [#]			62 (46.25–71)	61 (45–71)	0.6380*
Age group (n (%))	<60 years	186	95 (51.1)	91 (48.9)	0.5122 [§]
	≥60 years	219	119 (54.3)	100 (45.7)	
Gender (n (%))	male	228	119 (52.2)	109 (47.8)	0.7674 [§]
	female	177	95 (53.7)	82 (46.3)	
WBC [$\times 10^9/L$] [#]			20.8 (6.22–49.37)	16.66 (5.6–48.03)	0.0770*
PLT [$\times 10^9/L$] [#]			39.5 (22–74.75)	36 (23–73.5)	0.6480*
BM [blast/%] [#]			66 (33–86)	70 (33.75–85)	0.4660*
PB [blast/%] [#]			40.2 (12–77.6)	48.6 (12–77)	0.2130*
SCR [mg/dL] [#]			0.85 (0.66–1.03)	0.83 (0.66–1.04)	0.1170*
Gene fusions (n (%))					
Normal		298	161 (54)	137 (46)	0.4244 [§]
Complex karyotype		2	2 (100)	0 (0)	0.1805 [§]
<i>CBFB-MYH11</i>		22	5 (22.7)	17 (77.3)	0.0036[§]
<i>DEK-NUP214</i>		3	2 (66.7)	1 (33.3)	0.6301 [§]
<i>GATA2-MECOM</i>		7	6 (85.7)	1 (14.3)	0.0788 [§]
<i>MLLT3-KMT2A</i>		11	9 (81.8)	2 (18.2)	0.0509 [§]
<i>PML-RARA</i>		12	2 (16.7)	10 (83.3)	0.0108[§]
<i>RUNX1-RUNX1T1</i>		11	3 (27.3)	8 (72.7)	0.0850 [§]
Others		39	24 (61.5)	15 (38.5)	0.2523 [§]
<i>FLT3-ITD</i> mutation (n (%))					
Positive		94	52 (55.3)	42 (44.7)	0.5826 [§]
Negative		310	161 (51.9)	149 (48.1)	0.5103 [§]
Others		1	1 (100)	0 (0)	0.3442 [§]
<i>NPM1</i> mutation (n (%))					
Positive		100	46 (46)	54 (54)	0.1144 [§]
Negative		302	166 (55)	136 (45)	0.142 [§]
Others		3	2 (66.7)	1 (33.3)	0.6301 [§]
Risk_Cyto (n (%))					
Favorable		117	41 (35)	76 (65)	0.0000[§]
Intermediate		135	67 (49.6)	68 (50.4)	0.3602 [§]
Adverse		152	105 (69.1)	47 (30.9)	0.0000[§]
Others		1	1 (100)	0 (0)	0.3442 [§]
Response to treatment (n (%))					
Complete response		186	90 (48.4)	96 (51.6)	0.0981 [§]
Refractory		115	69 (60)	46 (40)	0.0691 [§]
Others		104	55 (52.9)	59 (56.7)	0.2464 [§]

AML – acute myeloid leukemia; WBC – white blood cells; PLT – platelets; BM – bone marrow; PB – peripheral blood; SCR – serum creatinine; Risk_Cyto – cytogenetic risk stratification. Values in bold denote a statistically significant difference ($p < 0.05$). [#] continuous variable data shown as median (25th, 75th percentile) values; * Mann–Whitney U test; [§] χ^2 test. Complex karyotype is defined as more than or equal to 3 chromosomal abnormalities.

Results

Patient characteristics

A total of 405 AML cases were taken from the OHSU dataset and divided into 2 groups according to the expression level of TGIF1, for a further determination of the relevance between TGIF1 expression and other various clinical and molecular characteristics. The baseline characteristics of the patients are listed in Table 1. A considerable difference between TGIF1 high- and low-expression groups could be observed in cytogenetic risk stratification: the results showed that patients with high expression of TGIF1 tended to be allocated to favorable cytogenetic risk groups ($p < 0.0001$), whereas low TGIF1 expression was associated with adverse cytogenetic risk stratification ($p < 0.0001$). In addition, the TGIF1 high-expression group had a higher frequency of gene fusions *CBFB-MYH11* ($p = 0.0009$) and

PML-RARA ($p = 0.0108$) when compared with the TGIF1 low-expression group. There was no statistical association between TGIF1 and age, gender, white blood cell (WBC) count, platelet (PLT) count, serum creatinine (SCr), peripheral blast (PB) count, complex karyotype, *DEK-NUP214*, *GATA2-MECOM*, *MLLT3-KMT2A*, *RUNX1-RUNX1T1*, *FLT3-ITD*, or *NPM1* mutations.

TGIF1 is a good indicator of AML disease progression

Due to the baseline association between TGIF1 and established prognosis-related cytogenetic risk stratification, it was important to analyze the clinical outcomes of patients with AML with different TGIF1 expression levels. Four databases were analyzed including OHSU, TCGA, TARGET, and GSE37642. The Kaplan–Meier survival analysis of OHSU cohort demonstrated that patients

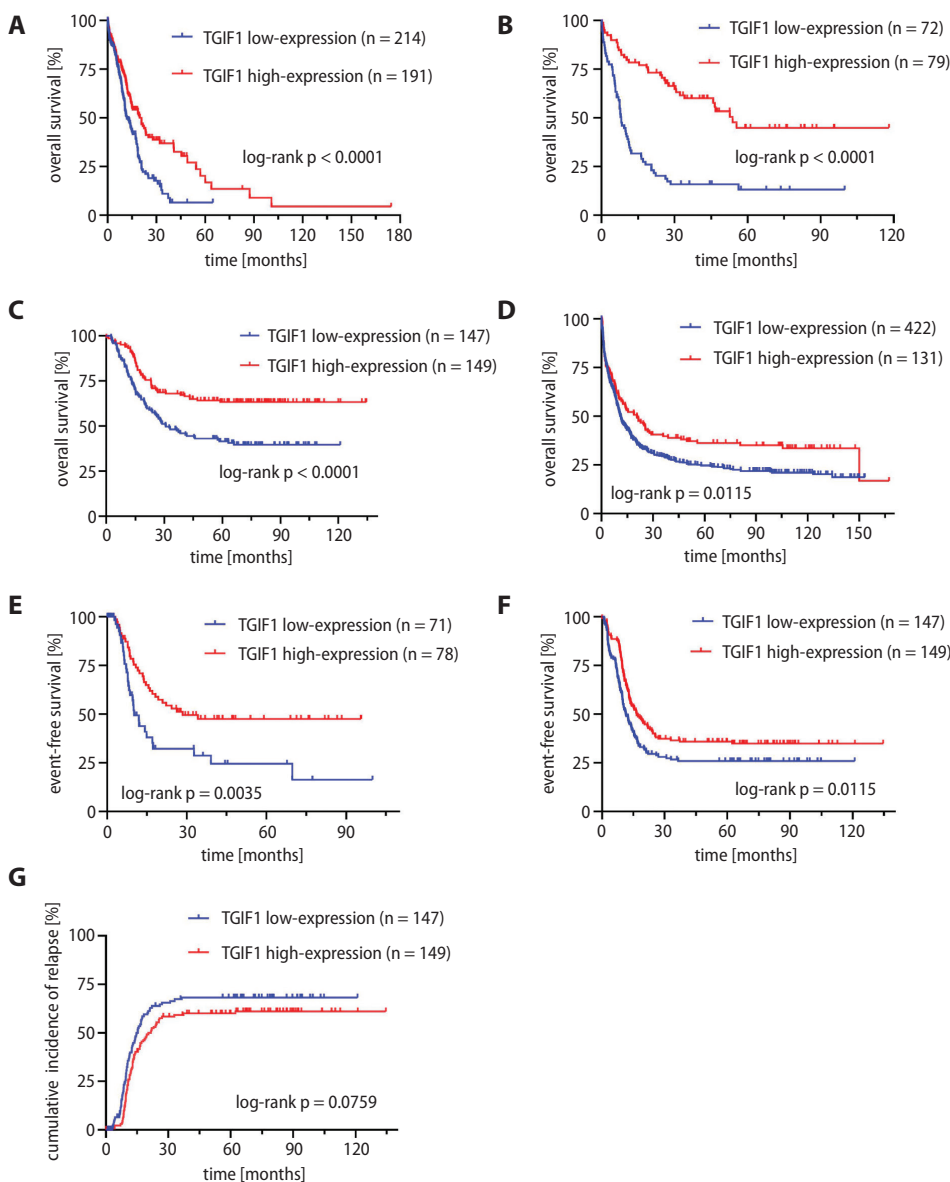


Fig. 1. TGIF1 expression level is a reliable prognostic indicator of disease progression in acute myeloid leukemia (AML) patients. A. Cumulative overall survival (OS) curves of 405 patients with the Oregon Health and Science University (OHSU)-AML divided into low-expression and high-expression subgroups ($p < 0.0001$); B. Cumulative OS curves of 151 patients with the Cancer Genome Atlas (TCGA)-AML divided into low-expression and high-expression subgroups ($p < 0.0001$); C. Cumulative OS curves of 296 patients with Therapeutically Applicable Research to Generate Effective Treatment (TARGET)-AML divided into low-expression and high-expression subgroups ($p < 0.0001$); D. Cumulative OS curves of 553 patients with GSE37642-AML divided into low-expression and high-expression subgroups ($p = 0.0115$); E, F. High TGIF1 expression was strongly associated with favorable event-free survival (TCGA-AML: $p = 0.0035$; TARGET-AML: $p = 0.0115$); G. The cumulative incidence of relapse with high TGIF1 expression was slightly lower (TARGET-AML: $p = 0.0759$).

with high TGIF1 levels had longer OS than those with low TGIF1 expression ($p < 0.0001$, Fig. 1A). Similar results were obtained from mutual validations over 3 other independent datasets ($p < 0.0001$ compared to $p < 0.0001$ compared to $p = 0.0115$; Fig. 1B–D). On the other hand, more favorable event-free survival (EFS) could be observed in the high TGIF1 expression group when compared to the patients with low TGIF1 expression (TCGA-AML cohort: HR = 0.5015, 95% CI: 0.2994–0.8399, $p = 0.0035$; TARGET-AML cohort: HR = 0.6997, 95% CI: 0.5304–0.9231, $p = 0.0115$; Fig. 1E,F). Figure 1G presents a slightly lower cumulative incidence of relapse in the high TGIF1 expression group (TARGET cohort: HR = 0.7576, 95% CI: 0.5551–0.1034, $p = 0.0759$; Fig. 1G).

Univariate and multivariate analyses for prognostic factors

Since the described results suggested the expression level of TGIF1 is closely correlated to a favorable AML prognosis, univariate and multivariate analyses were performed for further analysis. We evaluated clinical and molecular genetic factors of AML patients from the OHSU cohort, including age (≥ 60 years compared to < 60 years), gender (male compared to female), *FLT3-ITD* (positive compared to negative), *NPM1* (mutated compared to wild-type), *CBFB-MYH11* (positive compared to negative), *RUNX1-RUNX1T1* (positive compared to negative), *MLL3-KMT2A* (positive compared to negative), *PML-RARA* (positive compared to negative), cytogenetic risk stratification (adverse compared to intermediate/favorable), and expression levels of TGIF1 (high compared to low). After multivariable analyses, age < 60 years (HR = 1.94, 95% CI: 1.48–2.55, $p < 0.0001$) and high expression level of TGIF1 (HR = 0.65, 95% CI: 0.50–0.86, $p = 0.0020$) remained significant independent predictors of a good prognosis in AML patients (Table 2).

Effect of TGIF1 expression on disease progression in AML patients with and without bone marrow transplantation

Currently, the standard treatment protocol for most AML patients is intensive induction chemotherapy, and once a complete remission is achieved, appropriate post-remission therapies are necessary, such as conventional chemotherapy and hematopoietic cell transplantation.²¹ To verify the role of TGIF1 in different treatment groups, we compared Kaplan–Meier curves for the survival of the patients with and without bone marrow transplantation. The results presented in Fig. 2A,D (data from OHSU and TCGA cohort, respectively) show that bone marrow transplants can improve the OS rate by mutual validation. However, survival distribution curves of bone transplantation demonstrated a trend for shorter EFS than those of the standard chemotherapy group ($p = 0.0825$; Fig. 2G). Considering post-transplant complications such as graft-versus-host disease, the results were acceptable. In the chemotherapy group, the high-TGIF1-expression subgroup showed better OS (both $p < 0.0001$ in OHSU and TCGA cohorts) and EFS ($p = 0.0044$) than the low-expression subgroup (Fig. 2B,E,H). In the transplantation subgroup, high TGIF1 expression level was associated with better OS ($p = 0.0357$; Fig. 2C, and $p = 0.0051$; Fig. 2F), but no difference was found regarding EFS ($p = 0.2394$; Fig. 2I). The findings indicate that high TGIF1 might be a beneficial factor in AML patients undergoing conventional chemotherapy or bone marrow transplantation.

Risk stratification optimization based on AML cohort analysis

Patients from the OHSU cohort were classified according to the European LeukemiaNet (ELN) 2017 risk stratification systems²² into favorable ($n = 117$), intermediate

Table 2. Influence of TGIF1 expression on overall survival (OS) analyzed with univariate and multivariate analysis in AML patients

Variable	Univariate analysis			Multivariate analysis		
	HR	95% CI	p-value	HR	95% CI	p-value
Age (≥ 60 years compared to < 60 years)	2.23	1.71–2.92	< 0.0001	1.94	1.48–2.55	< 0.0001
Gender (male compared to female)	1.23	0.95–1.6	0.1116	–	–	–
<i>FLT3-ITD</i> (positive compared to negative)	1.27	0.95–1.71	0.1023	–	–	–
<i>NPM1</i> (positive compared to negative)	0.99	0.74–1.34	0.9636	–	–	–
<i>CBFB-MYH11</i> (positive compared to negative)	0.39	0.17–0.88	0.0232	0.63	0.27–1.48	0.2913
<i>RUNX1-RUNX1T1</i> (positive compared to negative)	0.13	0.02–0.95	0.0439	0.23	0.03–1.63	0.1398
<i>MLL3-KMT2A</i> (positive compared to negative)	0.66	0.27–1.6	0.3541	–	–	–
<i>PML-RARA</i> (positive compared to negative)	0.12	0.02–0.85	0.0340	0.17	0.02–1.28	0.0863
Risk_Cyto (adverse compared to intermediate/favorable)	2.07	1.48–2.91	< 0.0001	1.37	0.96–1.97	0.0862
TGIF1 expression (high compared to low)	0.59	0.45–0.77	0.0001	0.65	0.50–0.86	0.0020

AML – acute myeloid leukemia; HR – hazard ratio; 95% CI – 95% confidence interval; Risk_Cyto – cytogenetic risk stratification. Values in bold denote a statistically significant difference ($p < 0.05$).

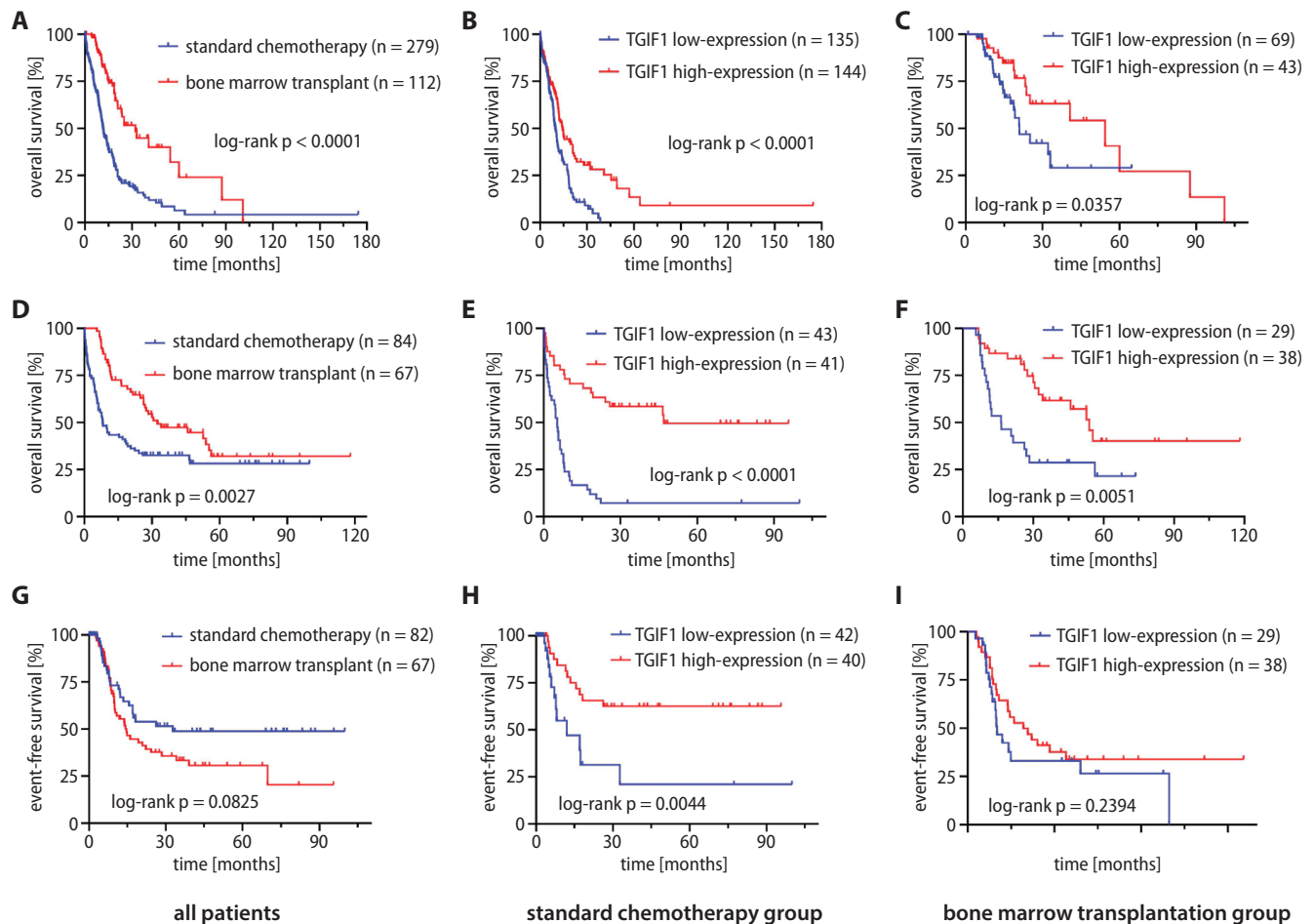


Fig. 2. Effect of TGIF1 expression on disease progression in acute myeloid leukemia (AML) patients with and without bone marrow transplantation. A–C. The Oregon Health and Science University (OHSU)-AML data suggest that bone marrow transplantation can improve the overall survival (OS) rate of AML patients ($p < 0.0001$), and high expression of TGIF1 is beneficial in both the standard chemotherapy group ($p < 0.0001$) and the bone marrow transplantation group ($p = 0.0357$); D–F. The Cancer Genome Atlas (TCGA)-AML data suggest that bone marrow transplantation can improve the OS rate of AML patients ($p = 0.0027$), and high expression of TGIF1 is beneficial in both the standard chemotherapy group ($p < 0.0001$) and the bone marrow transplantation group ($p = 0.0051$); G. TCGA data showed an increased incidence of events in AML patients who underwent bone marrow transplantation ($p = 0.0825$); H, I. TCGA data showed that low expression of TGIF1 was related to low event-free survival in the standard chemotherapy group ($p = 0.0044$), but not in the bone marrow transplantation group ($p = 0.2394$).

Table 3. Influence of TGIF1 expression on overall survival (OS) analyzed with univariate and multivariate analysis in *NPM1*-mutated AML patients

Variable	Univariate analysis			Multivariate analysis		
	HR	95% CI	p-value	HR	95% CI	p-value
Age (≥ 60 years compared to < 60 years)	1.72	1.01–2.93	0.0460	2.05	1.19–3.52	0.0094
Gender (male compared to female)	1.30	0.77–2.21	0.3240	–	–	–
<i>FLT3-ITD</i> (positive compared to negative)	2.24	1.30–3.86	0.0037	2.35	1.13–4.89	0.0229
Risk_Cyto (adverse/intermediate compared to favorable)	1.79	1.05–3.05	0.0327	1.21	0.59–2.49	0.6041
TGIF1 expression (high compared to low)	0.44	0.26–0.76	0.0034	0.38	0.21–0.67	0.0008

AML – acute myeloid leukemia; HR – hazard ratio; 95% CI – 95% confidence interval; Risk_Cyto – cytogenetic risk stratification. Variables with $p < 0.1$ in the univariate analysis were included in the multivariate analysis. Values in bold denote a statistically significant difference ($p < 0.05$).

($n = 135$) and adverse ($n = 152$) risk groups (Fig. 3A). Previous studies have suggested that there was a significant interaction effect between mutant *NPM1* and *FLT3-ITD*, leading to different treatment responses and survival prognoses.^{23,24} Figure 3B demonstrates the effect on OS according to the interrelations between *NPM1* and *FLT3-ITD* mutations as per the survival curve, which was consistent

with the current guidelines.^{25,26} However, mutant/wild-type *NPM1* alone cannot independently predict OS in AML patients ($p = 0.9253$; Fig. 3C). Interestingly, TGIF1 was proved to be independently associated with favorable clinical outcomes in the *NPM1*-mutated subgroup of AML (Table 3). Therefore, attempts were made to reanalyze the role of TGIF1 played in the *NPM1*-mutated subgroup

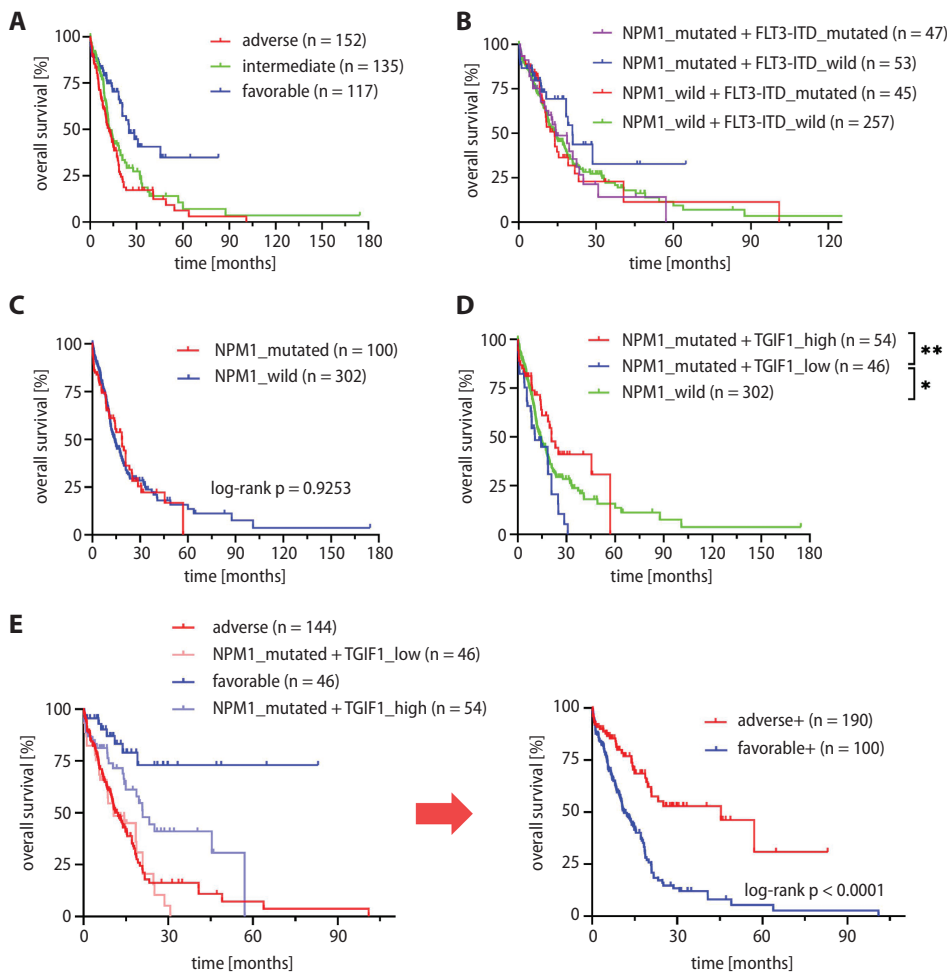


Fig. 3. Risk stratification of acute myeloid leukemia (AML) patients from the Oregon Health and Science University (OHSU)-AML data analysis. A. Prognostic impact of the European LeukemiaNet (ELN) 2017 risk classification in patients with AML; B. Frequent associations between *NPM1* and *FLT3* mutations are known markers for predicting overall survival in AML; C. *NPM1* mutations and wild-type *NPM1* cannot independently predict overall survival in AML patients ($p = 0.9253$); D. Survival differences in *NPM1*-mutated AML patients were influenced by *TGIF1* expression and distinguished from wild-type *NPM1*; E. The information on *NPM1* mutation combined with *TGIF1* was integrated into the ELN classification schema to optimize the favorable and adverse group

from the OHSU cohort. The *NPM1*-mutated group with low *TGIF1* levels had a shorter OS when compared with the *NPM1* wild-type group ($p < 0.05$; Fig. 3D). Besides, patients with high *TGIF1* level had a longer OS than those with low *TGIF1* in the *NPM1*-mutated subgroup ($p < 0.01$; Fig. 3D). These results prove the prognostic role *TGIF1* plays in AML, especially in the *NPM1*-mutated subgroup. Furthermore, by integrating the information on AML prognosis relevant to *NPM1* mutation and *TGIF1* expression level, improved risk stratification may be revealed ($p < 0.0001$; Fig. 3E), providing a theoretical basis and new ideas for treatment. For further validation, the same analyses were conducted with another TCGA dataset, and the results confirmed that *TGIF1* expression significantly affected the prognosis of the *NPM1*-mutated group and supported risk stratification optimization (Fig. 4). Likewise, the *TGIF1* expression remained a significant predictor of EFS in *NPM1*-mutated AML patients, which is consistent with our previous findings (Supplementary material).

GSEA delineates biological pathways correlated with *TGIF1* expression

The GSEA is an important approach to identifying gene expression-related pathways. We performed GSEA

between high and low *TGIF1* levels data sets to elucidate biological pathways correlated with *TGIF1*. Some enrichment results showed that there was a significant correlation between high- and low-expression groups: multiple pathways, including galactose metabolism, biosynthesis of unsaturated fatty acids, glycolysis gluconeogenesis, peroxisome proliferator-activated receptor (PPAR) signaling pathway, and several others displayed the enrichment of low expression of *TGIF1* and ribosome in the high-*TGIF1*-expression group (Fig. 5). The gene set pathways were listed in order of significance in Table 4. These results may provide a mechanistic explanation for the scientific value and clinical significance of *TGIF1*.

Discussion

Besides commonly reported cytogenetic changes and recurrent gene mutations mentioned in ELN risk classification,²² numerous novel biomarkers also are related to AML leukemogenesis and were used to predict clinical outcomes,^{26–28} providing insights to further disease mechanisms and therapeutic directions. The *TGIF1* belongs to the family of TALE homeodomain, which regulates diverse cellular processes including proliferation, apoptosis and differentiation as a transcriptional repressor.

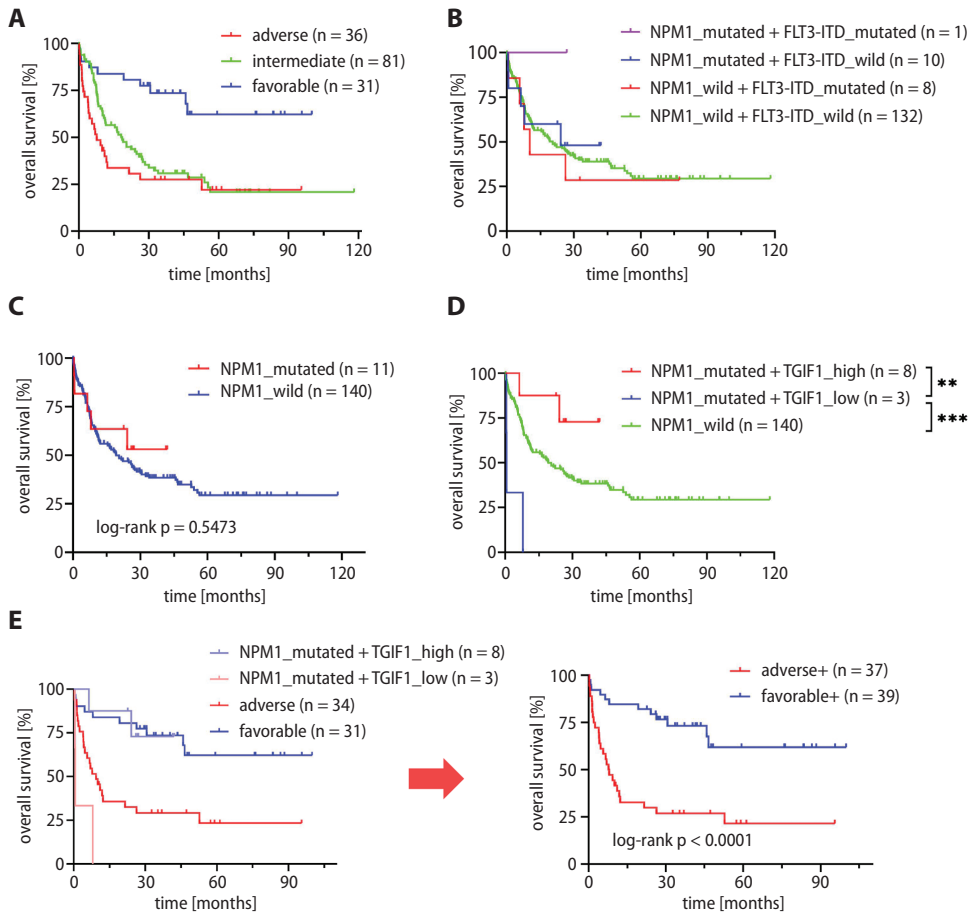


Fig. 4. The risk stratification of acute myeloid leukemia (AML) patients was analyzed using the Cancer Genome Atlas (TCGA)-AML data for validation. A. Overall survival (OS) probability over time based on the European LeukemiaNet (ELN) 2017 risk group; B. Effect of *NPM1* and FLT3 on the prognosis of patients with AML; C. *NPM1* mutations and wild-type *NPM1* cannot independently predict OS in AML patients (p = 0.5473); D. High expression of TGIF1 is beneficial to the OS of AML patients with *NPM1* mutation; E. *NPM1* mutation combined with TGIF1 can optimize ELN 2017 risk stratification

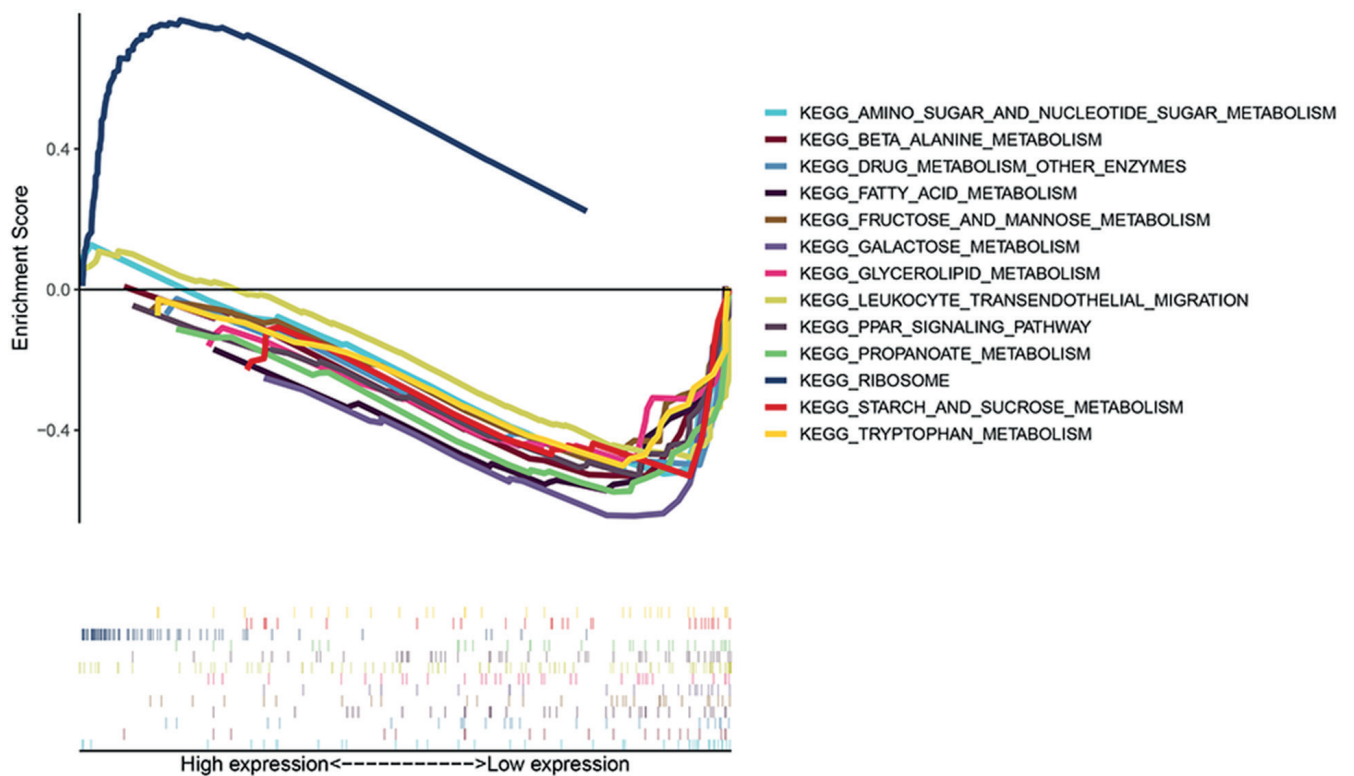


Fig. 5. Gene set enrichment analysis (GSEA) delineates biological pathways correlated with TGIF1 expression. Some enrichment results showed that there was a significant correlation between high and low TGIF1 expression groups

Table 4. Gene set enrichment analysis (GSEA) demonstrated the correlation between TGIF1_{high} and TGIF1_{low} phenotypes

Name	ES	NES	NOM p-value	FDR q-value	Leading edge
Ribosome	0.7657	1.6477	0.0393	0.7182	tags = 81%, list = 16%, signal = 96%
Galactose metabolism	-0.6884	-1.9013	0.0032	0.2882	tags = 45%, list = 10%, signal = 51%
Biosynthesis of unsaturated fatty acids	-0.6983	-1.8904	0.0051	0.1622	tags = 67%, list = 19%, signal = 83%
Glycolysis gluconeogenesis	-0.6352	-1.8743	0.0062	0.1319	tags = 51%, list = 15%, signal = 60%
PPAR signaling pathway	-0.5521	-1.8445	0.0021	0.1366	tags = 35%, list = 14%, signal = 40%
Pentose phosphate pathway	-0.6633	-1.8314	0.0071	0.123	tags = 54%, list = 18%, signal = 66%
Leukocyte transendothelial migration	-0.4905	-1.8007	0.0058	0.132	tags = 28%, list = 6%, signal = 30%
Fc-gamma R-mediated phagocytosis	-0.5348	-1.797	0.0091	0.1175	tags = 39%, list = 10%, signal = 43%
Starch and sucrose metabolism	-0.5857	-1.7804	0.0141	0.1213	tags = 32%, list = 6%, signal = 34%
Amino sugar and nucleotide sugar metabolism	-0.5479	-1.7695	0.0102	0.1207	tags = 43%, list = 10%, signal = 47%
Lysosome	-0.5317	-1.7287	0.0326	0.1558	tags = 43%, list = 14%, signal = 50%
Drug metabolism other enzymes	-0.5791	-1.7214	0.0104	0.1505	tags = 26%, list = 5%, signal = 27%
Pathogenic <i>Escherichia coli</i> infection	-0.5274	-1.7129	0.0192	0.1473	tags = 30%, list = 6%, signal = 32%
Glycerolipid metabolism	-0.514	-1.7017	0.0135	0.1494	tags = 35%, list = 17%, signal = 42%
Fatty acid metabolism	-0.5976	-1.6919	0.0315	0.1497	tags = 45%, list = 19%, signal = 56%
Pantothenate and coa biosynthesis	-0.6258	-1.6918	0.0185	0.1399	tags = 53%, list = 14%, signal = 62%
Fructose and mannose metabolism	-0.5324	-1.6871	0.0235	0.1354	tags = 52%, list = 18%, signal = 63%
Systemic lupus erythematosus	-0.5401	-1.6828	0.0424	0.1324	tags = 50%, list = 24%, signal = 66%
Propanoate metabolism	-0.6005	-1.6664	0.0254	0.1426	tags = 45%, list = 16%, signal = 53%
β-alanine metabolism	-0.5775	-1.6543	0.0224	0.1475	tags = 45%, list = 13%, signal = 52%
Vibrio cholerae infection	-0.4992	-1.6506	0.0252	0.1444	tags = 36%, list = 10%, signal = 40%
Long-term potentiation	-0.4729	-1.6401	0.0292	0.1490	tags = 35%, list = 11%, signal = 39%
Alzheimer's disease	-0.4444	-1.633	0.0352	0.1487	tags = 38%, list = 16%, signal = 45%
Tryptophan metabolism	-0.5296	-1.6317	0.0262	0.1434	tags = 42%, list = 17%, signal = 50%
Regulation of actin cytoskeleton	-0.4169	-1.6314	0.0206	0.1379	tags = 22%, list = 6%, signal = 23%
Vascular smooth muscle contraction	-0.4232	-1.6191	0.0171	0.1437	tags = 26%, list = 11%, signal = 30%

ES – enrichment score; FDR – false discovery rate; NES – normalized enrichment score; NOM – nominal.

According to recent studies, TGIF1 functions as a tumor suppressor in pancreatic ductal adenocarcinoma by inhibiting Twist1 expression and activity.^{29,30} The deletion of TGIF1 can induce the activation of the HAS2-CD44 signaling pathway and the upregulation of PD-L1, resulting in promoting the development of pancreatic ductal adenocarcinoma (PDAC). Given the essential role TGF-β and retinoic acid (RA) signaling play in hematopoiesis, some studies have been extended in recent years, attempting to find out the connections between TGIF1 and hematological diseases.³¹ In myeloid lineage leukemias, TGIF1 seems to function as a vital regulator in normal and malignant hematopoiesis.^{15,30} Hamid and Brandt³¹ proposed that TGIF1 may regulate the balance between proliferation and differentiation during the myelopoiesis of human myeloid leukemia cells. Yan et al. showed that TGIF1 acts as a novel regulator of normal hematopoietic stem cell (HSC) function by suppressing HSC maintenance, self-renewal and quiescence in mice, resulting in the reduction of malignant transformation risk and leukemic stem cell or progenitor cell survival with chemotherapy.¹⁵ Moreover,

further exploration analyzed the specific role TGIF1 plays in leukemia initiation and progression.^{32,33} For example, TGIF1 exerts antileukemic contributions by affecting TGF-β- and RA-driven functions.³¹ Willer et al. showed that TGIF1 interferes with MLL-rearranged AML maintenance by competing with MEIS1 for chromatin-binding regions.³⁰ Collectively, these findings demonstrated that TGIF1 plays an important role in stem cell function regulation by maintaining the balance between proliferation and differentiation, and might possess potential prognostic value.

In the present study, clinical and molecular characteristics data of AML patients from the OHSU study cohort were analyzed to explore the relevance between TGIF1 expression and AML clinical features. A strong relationship between TGIF1 and cytogenetic risk stratification was confirmed. Considering the tight association between cytogenetics and the prognosis of the disease,⁵ we examined TGIF1 expression compared to AML outcome, including OS, EFS and cumulative incidence of relapse (CIR) to assess the prognostic effects of TGIF1. Following

the identification of the relevance between higher TGIF1 expression and better prognosis, the same analyses were expanded on other independent datasets for confirmation, while univariate and multivariate analyses were performed for prognostic independence. Therefore, TGIF1 expression was regarded as the independent factor predicting better survival in patients with AML. Further analyses on TGIF1 should be performed to ensure the association between its expression and AML subtypes. For the OHSU cohort, Fig. 3D shows that AML patients with high TGIF1 level had a longer OS than those with low TGIF1 in the *NPM1*-mutated subgroup. We performed the Kaplan–Meier curve survival analysis, and the curve revealed a significant difference in survival between different expression levels of TGIF1 in the *NPM1*-mutated subgroup. This conclusion was congruent to TCGA cohort, which indicated that the favorable impact on prognosis that TGIF1 provided also applied for AML with *NPM1* mutations.

The *NPM1* and *FLT3-ITD* collectively determined AML prognosis when referring to the risk stratification systems by ELN 2017.²² Therefore, based on the information above, we successfully constructed a more practical stratification system by integrating prognostic information of different TGIF1 expressions and *NPM1*-mutant AML into the original one. The reliability of this improvement was corroborated by a comprehensive analysis of a separate study cohort.

Limitations

The study was based on information obtained from mutual validation of publicly available data. The strengths of the trial include its strong eligibility criteria and a uniform treatment regimen according to standard guidelines. Despite the fact that our results provide a novel risk stratification option for *NPM1*-mutant AML, there are still certain limitations. Our analysis has a retrospective study design, and thus the accuracy rate may be lower in small sample cases. This work is based on the results of an RNA-sequencing dataset, and morphological insights remain to be explored. Further verification of the reliability is needed for the multivariate analysis to identify predictors after univariate analysis in statistical descriptions, similarly to previous studies.^{33,34}

Conclusions

Our study proved that the upregulation of TGIF1 is closely associated with favorable prognosis in AML, and adding the expression level of TGIF1 examination can optimize risk stratification with *NPM1*-mutant AML, enhancing sensitivity and specificity in patient classification as well as providing reliable evidence for clinical decision-making. Further research is needed for new biomarkers and their combinations for personalized treatment.

Supplementary material

The supplementary files are available at <https://doi.org/10.5281/zenodo.7414416>. The package consists of the following files:

Supplementary Information 1. The difference analysis results of 2 groups of continuous variables involved in this study, including age, WBC, PLT, bone marrow (BM) blasts count, PB, and SCr.

Supplementary Information 2. Cox regression based on Schoenfeld residuals for testing proportional hazards assumptions.

Supplementary Information 3. The R code used in the proportional hazards assumption in this study.

Supplementary Information 4. The R code used in the univariate analysis in this study.

Supplementary Information 5. The R code used in the multivariate analysis in this study.

Supplementary Information 6. The R code used in the OS analysis in this study.

Supplementary Information 7. Event-free survival of AML patients was analyzed using TCGA-AML data.

ORCID iDs

Hongwei Tang  <https://orcid.org/0000-0002-5639-8981>
 Nan Zhang  <https://orcid.org/0000-0002-5877-1786>
 Huan Li  <https://orcid.org/0000-0001-9913-0937>
 Ying Chen  <https://orcid.org/0000-0001-5670-9965>
 Xinlei Liu  <https://orcid.org/0000-0003-1510-6222>
 Hongbo Xiao  <https://orcid.org/0000-0002-4628-1763>
 Jianchuan Deng  <https://orcid.org/0000-0001-9927-579X>
 Kang Zhou  <https://orcid.org/0000-0002-0260-409X>

References

- Papayannidis C, Sartor C, Marconi G, et al. Acute myeloid leukemia mutations: Therapeutic implications. *Int J Mol Sci.* 2019;20(11):2721. doi:10.3390/ijms20112721
- Bose P, Vachhani P, Cortes JE. Treatment of relapsed/refractory acute myeloid leukemia. *Curr Treat Options Oncol.* 2017;18(3):17. doi:10.1007/s11864-017-0456-2
- Edwards H, Ge Y. ONC201 shows promise in AML treatment. *Cell Cycle.* 2018;17(3):277–277. doi:10.1080/15384101.2017.1421035
- Angenendt L, Wöste M, Mikesch JH, et al. Calcitonin receptor-like (CAL-CRL) is a marker of stemness and an independent predictor of outcome in pediatric AML. *Blood Adv.* 2021;5(21):4413–4421. doi:10.1182/bloodadvances.2021005236
- Padmakumar D, Chandraprabha VR, Gopinath P, et al. A concise review on the molecular genetics of acute myeloid leukemia. *Leuk Res.* 2021;111:106727. doi:10.1016/j.leukres.2021.106727
- Kantarjian HM, Short NJ, Fathi AT, et al. Acute myeloid leukemia: Historical perspective and progress in research and therapy over 5 decades. *Clin Lymphoma Myeloma Leuk.* 2021;21(9):580–597. doi:10.1016/j.clml.2021.05.016
- Kumar D, Mehta A, Panigrahi MK, Nath S, Saikia KK. *NPM1* mutation analysis in acute myeloid leukemia. Comparison of three techniques: Sanger sequencing, pyrosequencing, and real-time polymerase chain reaction. *Turk J Hematol.* 2018;35(1):49–53. doi:10.4274/tjh.2017.0095
- Kelemen K. The role of nucleophosmin 1 (*NPM1*) mutation in the diagnosis and management of myeloid neoplasms. *Life.* 2022;12(1):109. doi:10.3390/life12010109
- Balusu R, Fiskus W, Rao R, et al. Targeting levels or oligomerization of nucleophosmin 1 induces differentiation and loss of survival of human AML cells with mutant *NPM1*. *Blood.* 2011;118(11):3096–3106. doi:10.1182/blood-2010-09-309674

10. Falini B, Mecucci C, Tiacci E, et al. Cytoplasmic nucleophosmin in acute myelogenous leukemia with a normal karyotype. *N Engl J Med*. 2005;352(3):254–266. doi:10.1056/NEJMoa041974
11. Falini B, Brunetti L, Sportoletti P, Martelli MP. *NPM1*-mutated acute myeloid leukemia: From bench to bedside. *Blood*. 2020;136(15):1707–1721. doi:10.1182/blood.2019004226
12. Falini B, Martelli MP, Bolli N, et al. Acute myeloid leukemia with mutated nucleophosmin (*NPM1*): Is it a distinct entity? *Blood*. 2011;117(4):1109–1120. doi:10.1182/blood-2010-08-299990
13. Eckardt JN, Middeke JM, Riechert S, et al. Deep learning detects acute myeloid leukemia and predicts *NPM1* mutation status from bone marrow smears. *Leukemia*. 2022;36(1):111–118. doi:10.1038/s41375-021-01408-w
14. Fu W, Huang A, Xu L, et al. Cytogenetic abnormalities in *NPM1*-mutated acute myeloid leukemia. *Leuk Lymphoma*. 2022;63(8):1956–1963. doi:10.1080/10428194.2022.2045600
15. Yan L, Womack B, Wotton D, et al. *Tgif1* regulates quiescence and self-renewal of hematopoietic stem cells. *Mol Cell Biol*. 2013;33(24):4824–4833. doi:10.1128/MCB.01076-13
16. Anderson AE, Taniguchi K, Hao Y, et al. *Tgif1* and *Tgif2* repress expression of the RabGAP Evi5l. *Mol Cell Biol*. 2017;37(5):e00527-16. doi:10.1128/MCB.00527-16
17. Kong L, Yu Y, Guan H, et al. TGIF1 plays a carcinogenic role in esophageal squamous cell carcinoma through the Wnt/ β -catenin and Akt/mTOR signaling pathways. *Int J Mol Med*. 2021;47(5):77. doi:10.3892/ijmm.2021.4910
18. Tyner JW, Tognon CE, Bottomly D, et al. Functional genomic landscape of acute myeloid leukaemia. *Nature*. 2018;562(7728):526–531. doi:10.1038/s41586-018-0623-z
19. The Cancer Genome Atlas Research Network. Genomic and epigenomic landscapes of adult de novo acute myeloid leukemia. *N Engl J Med*. 2013;368(22):2059–2074. doi:10.1056/NEJMoa1301689
20. Hess AS, Hess JR. Understanding tests of the association of categorical variables: The Pearson chi-square test and Fisher's exact test. *Transfusion*. 2017;57(4):877–879. doi:10.1111/trf.14057
21. Kadia TM, Wei AH. Evolution of therapy for older patients with acute myeloid leukemia: How should we use currently available agents? *Cancer J*. 2022;28(1):67–72. doi:10.1097/PPO.0000000000000574
22. Döhner H, Estey E, Grimwade D, et al. Diagnosis and management of AML in adults: 2017 ELN recommendations from an international expert panel. *Blood*. 2017;129(4):424–447. doi:10.1182/blood-2016-08-733196
23. Döhner K, Schlenk RF, Habdank M, et al. Mutant nucleophosmin (*NPM1*) predicts favorable prognosis in younger adults with acute myeloid leukemia and normal cytogenetics: Interaction with other gene mutations. *Blood*. 2005;106(12):3740–3746. doi:10.1182/blood-2005-05-2164
24. Verhaak RGW, Goudswaard CS, van Putten W, et al. Mutations in nucleophosmin (*NPM1*) in acute myeloid leukemia (AML): Association with other gene abnormalities and previously established gene expression signatures and their favorable prognostic significance. *Blood*. 2005;106(12):3747–3754. doi:10.1182/blood-2005-05-2168
25. Ostronoff F, Othus M, Lazenby M, et al. Prognostic significance of *NPM1* mutations in the absence of *FLT3*-internal tandem duplication in older patients with acute myeloid leukemia: A SWOG and UK National Cancer Research Institute/Medical Research Council Report. *J Clin Oncol*. 2015;33(10):1157–1164. doi:10.1200/JCO.2014.58.0571
26. Pastore F, Dufour A, Benthaus T, et al. Combined molecular and clinical prognostic index for relapse and survival in cytogenetically normal acute myeloid leukemia. *J Clin Oncol*. 2014;32(15):1586–1594. doi:10.1200/JCO.2013.52.3480
27. Yi J, Zhou LY, Yi YY, et al. Low expression of pseudogene POU5F1B affects diagnosis and prognosis in acute myeloid leukemia (AML). *Med Sci Monit*. 2019;25:4952–4959. doi:10.12659/MSM.914352
28. Wu G, Ma Z, Hu W, et al. Molecular insights of Gas6/TAM in cancer development and therapy. *Cell Death Dis*. 2017;8(3):e2700. doi:10.1038/cddis.2017.113
29. Onishi-Seebacher M, Erikson G, Sawitzki Z, et al. Repeat to gene expression ratios in leukemic blast cells can stratify risk prediction in acute myeloid leukemia. *BMC Med Genomics*. 2021;14(1):166. doi:10.1186/s12920-021-01003-z
30. Willer A, Jakobsen JS, Ohlsson E, et al. TGIF1 is a negative regulator of MLL-rearranged acute myeloid leukemia. *Leukemia*. 2015;29(5):1018–1031. doi:10.1038/leu.2014.307
31. Hamid R, Brandt SJ. Transforming growth-interacting factor (*TGIF*) regulates proliferation and differentiation of human myeloid leukemia cells. *Mol Oncol*. 2009;3(5–6):451–463. doi:10.1016/j.molonc.2009.07.004
32. Wang H, Peng J, Wang B, et al. Inconsistency between univariate and multiple logistic regressions. *Shanghai Arch Psychiatry*. 2017;29(2):124–128. doi:10.11919/j.issn.1002-0829.217031
33. Lo SK, Li IT, Tsou TS, See L. Non-significant in univariate but significant in multivariate analysis: A discussion with examples [in Chinese]. *Changcheng Yi Xue Za Zhi*. 1995;18(2):95–101. PMID:7641117.
34. Yan L, Davé UP, Engel M, Brandt SJ, Hamid R. Loss of TG-interacting factor 1 decreases survival in mouse models of myeloid leukaemia. *J Cell Mol Med*. 2020;24(22):13472–13480. doi:10.1111/jcmm.15977

Nomogram for predicting skip metastasis in cN0 papillary thyroid cancer patients at increased risk of lymph node metastasis

Fang Li^{1,A,D,E}, Fang-Jian Zhou^{2,B,D}, Tong-Wei Zhu^{3,B,D}, Hua-Li Qiu^{1,C,D}, Xiao-Ting Zhang^{1,C,D}, Bo-Wen Ruan^{1,C,D}, De-Yi Huang^{1,A,F}

¹ Department of Ultrasound, The People's Hospital of Yuhuan, China

² The Second Department of General Surgery, The People's Hospital of Yuhuan, China

³ Department of Ultrasound, Taizhou Hospital of Zhejiang Province, China

A – research concept and design; B – collection and/or assembly of data; C – data analysis and interpretation;

D – writing the article; E – critical revision of the article; F – final approval of the article

Advances in Clinical and Experimental Medicine, ISSN 1899–5276 (print), ISSN 2451–2680 (online)

Adv Clin Exp Med. 2023;32(7):753–761

Address for correspondence

De-Yi Huang

E-mail: huangdy18958676710@163.com

Funding sources

None declared

Conflict of interest

None declared

Received on August 8, 2022

Reviewed on October 19, 2022

Accepted on December 7, 2022

Published online on January 5, 2023

Abstract

Background. Skip lymph node metastasis (SLNM) refers to lateral lymph node metastasis (LLNM) without involving central lymph node (CLN). Some microscopic nodal positivity may be difficult to detect before surgery due to atypical imaging characteristics. These patients are misdiagnosed as having clinically node-negative (cN0) papillary thyroid cancer (PTC) even after central lymph node dissection, leading to a high risk of developing LNM after surgery. Current prediction models have limited clinical utility, as they are only applicable to predict SLNM from clinically node-positive (cN+) PTC, not cN0 PTC, and this has little impact on treatment strategies.

Objectives. This study aimed to establish a nomogram for preoperatively assessing the likelihood of SLNM in cN0 PTC patients with increased risk of LNM, thus optimizing their therapeutic options.

Materials and methods. The records of 780 PTC patients undergoing thyroidectomy along with bilateral central lymph node dissection were retrospectively reviewed. The cN0 patients with postoperative LLNM (occult SLNM) and cN+ patients without central lymph node metastasis (CLNM) (typical SLNM) were included in the SLNM group (n = 82). The CLNM-negative cN0 patients without postoperative LLNM were assigned to the non-SLNM group (n = 698). The independent correlates of SLNM constituted the nomogram for determining the likelihood of SLNM in high-risk cN0 PTC patients.

Results. The independent correlates of SLNM were age (hazard ratio (HR) = 1.016), tumor location (HR = 1.801), tumor size (HR = 1.528), and capsular invasion (HR = 2.941). They served as components in the development of the nomogram. This model was verified to present acceptable discrimination. It showed good calibration and a decent net benefit when the predicted probability was <60%.

Conclusions. We developed a nomogram incorporating preoperative clinical data to predict the probability of SLNM development in high-risk cN0 PTC patients, which contributed to their optimized treatment options.

Key words: papillary thyroid cancer, nomogram, central lymph node metastasis, clinically node-negative (cN0), skip lymph node metastasis

Cite as

Li F, Zhou FJ, Zhu TW, et al. Nomogram for predicting skip metastasis in cN0 papillary thyroid cancer patients at increased risk of lymph node metastasis.

Adv Clin Exp Med. 2023;32(7):753–761.

doi:10.17219/acem/157240

DOI

10.17219/acem/157240

Copyright

Copyright by Author(s)

This is an article distributed under the terms of the Creative Commons Attribution 3.0 Unported (CC BY 3.0) (<https://creativecommons.org/licenses/by/3.0/>)

Background

The metastasis of lymph node (LN) impacts surgical regimens and recurrence risk stratification in papillary thyroid cancer (PTC).^{1,2} The dissemination of PTC cells through the lymphatic system occurs in a sequential pattern, involving the central compartment first, continuing to the ipsilateral lateral compartment, and finally metastasizing to the contralateral, lateral or mediastinal compartments.³ Skip lymph node metastasis (SLNM), on the other hand, is a rare form of lymph node metastasis (LNM). It metastasizes to the lateral lymph node (LLN) without involving the central lymph node (CLN).⁴ Some microscopic nodal positivity may be difficult to detect with ultrasonography prior to surgery due to atypical imaging characteristics. These patients are misdiagnosed as clinically node-negative (cN0) even though they received central lymph node dissection (CLND) due to the presence of significant LNM risk factors. As a result, their metastatic risk will be defined as low, thus affecting the treatment plans. Lymph node metastasis is probable in these individuals following surgery, resulting in an unfavorable prognosis such as additional surgery, radiotherapy, etc.^{5–7}

Previous studies have found the independent correlates of SLNM, such as tumor in the upper pole of the thyroid gland and older age, and developed several prediction models for discerning patients with SLNM from those with typical LNM.^{8–10} However, the clinical utility of these models is limited because they are only applicable to assess the likelihood of SLNM in clinically node-positive (cN+) PTC, not cN0 PTC. In the abovementioned studies, surgical procedures and treatment strategies were identical for cN+ patients with or without SLNM. Although discerning SLNM from cN0 PTC may provide more individualized treatment strategies, including prophylactic lymph node dissection or closer nodal follow-up, we are currently unable to accurately determine the likelihood of SLNM in these high-risk cN0 PTC patients.

Objectives

The goal of this study was to establish a nomogram to preoperatively predict the likelihood of SLNM development in cN0 PTC patients who are at an increased risk of LNM, thereby optimizing their therapeutic options.

Materials and methods

The present study complied with the principles stated in the declaration of Helsinki. The institutional review board of the People's Hospital of Yuhuan approved this study (approval No. YYLS2018(015)), and informed consent was obtained from all patients.

Study population

This study retrospectively analyzed medical records of 1836 newly diagnosed primary PTC patients undergoing thyroidectomy along with bilateral CLND, including cN+ patients and cN0 patients with an increased risk of metastasis and recurrence (e.g., larger tumor size, multifocal disease, extrathyroidal extension, family history of thyroid cancer, etc.). These medical records were obtained for patients admitted from January 2015 to May 2020. The tumor stage (tumor–node–metastasis (TNM)) in all patients was T_{1–4}N_{0–1b}M₀ according to the 2015 American Joint Committee on Cancer (AJCC) guidelines.² Patients with cN+ stage and central lymph node metastasis (CLNM), cN0 stage and CLNM, poorly differentiated papillary cancer, history of neck surgery, and history of radiotherapy were excluded.

All included patients had complete pathology reports and were regularly followed up for at least 2 years (until they were diagnosed with lateral lymph node metastases (LLNM) after surgery (endpoint event) or lost to follow-up). The follow-up deadline was June 30, 2022. Ultimately, 780 patients were included in this study (median follow-up 42 months, with 28 patients lost to follow-up (3.5%)). Based on the postoperative pathology reports and follow-up outcomes, cN+ patients without CLNM and cN0 patients with postoperative LLNM were assigned to the SLNM group (n = 82), and the CLNM-negative cN0 patients without postoperative LLNM into the non-SLNM group (n = 698) (Fig. 1).

Data collection

The preoperative clinical data encompassing age, gender, body mass index (BMI), tumor (T) stage classified according to the tumor–node–metastasis (TNM) system, history of Hashimoto's thyroiditis, and family history of thyroid cancer were obtained through the hospital information system. Tumor location, size, number of lesions, lesion distribution, hypoechoic mass, capsular invasion, extraglandular invasion, calcified foci, and Doppler blood flow were all examined and recorded with MyLab Class C ultrasonography (Esaote, Genoa, Italy).

Nomogram establishment

By investigating the differences in clinical indicators between the SLNM and non-SLNM groups, the variables with statistically significant differences between the 2 groups – that is, those with false discovery rate (FDR)-adjusted p-values <0.05 calculated using Benjamini–Hochberg correction – underwent univariate and multivariate Cox regression analyses to screen for the independent correlates of SLNM. A nomogram model was established based on these independent factors to predict the likelihood of SLNM in high-risk cN0 PTC patients before surgery.

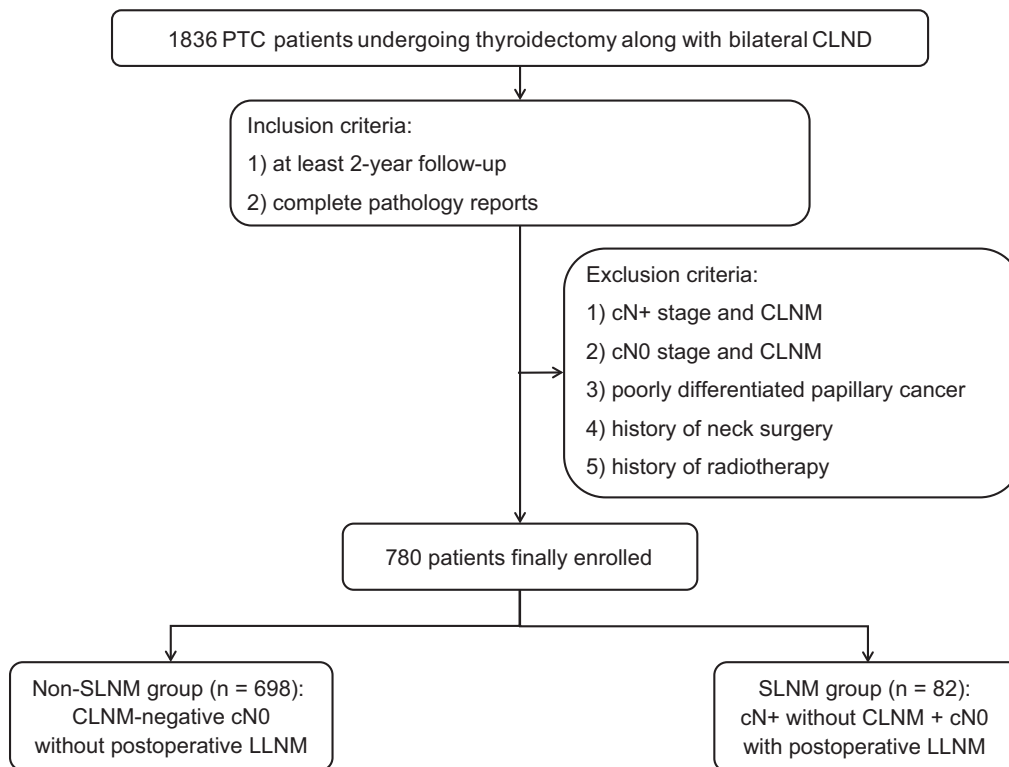


Fig. 1. Flowchart of patient selection and grouping

PTC – papillary thyroid cancer; CLND – central lymph node dissection; CLNM – central lymph node metastasis; SLNM – skip lymph node metastasis; cN0 – clinically node-negative; cN+ – clinically node-positive.

Statistical analyses

Independent-sample t-test or Mann–Whitney U test were employed to compare the continuous variables, depending on whether the distribution was normal or not (Shapiro–Wilk test). The homogeneity of variance was verified using Levene’s test prior to the t-tests. Categorical variables were compared using χ^2 tests, and if the expected count in any table cell was less than 5, Fisher’s exact test was applied. For ranked data, Mann–Whitney U test was used. Multivariate Cox regression was used to obtain the hazard ratio (HR) and 95% confidence interval (95% CI) of each independent predictor utilized to develop the nomogram. For the Cox proportional hazards regression model, we assessed the validity of the proportional hazards assumption using Schoenfeld residuals and the linearity assumption using Martingale residuals for each continuous variable against survival time. Bootstrap resampling was used to adjust the overfitting deviation (1000 times). The concordance index (C-index) and Hosmer–Lemeshow (H–L) test were used to evaluate the discrimination and calibration of the model. The area under the receiver operating characteristic (ROC) curve (AUC) and the calibration curve were used to show the distribution of the discrimination and calibration. Decision curve analysis (DCA) was applied to assess the clinical applicability of the model. IBM SPSS v. 22.0 (IBM Corp., Armonk, USA), MedCalc v. 22.0.22 (MedCalc Software Ltd, Ostend, Belgium) and R package v. 3.6.2 (R Foundation for Statistical Computing, Vienna, Austria) were used for statistical analyses.

Results

Clinical characteristics in the SLNM and non-SLNM groups

Table 1 presents the clinical data comparisons between the SLNM and non-SLNM groups. Only BMI was compared using a t-test because it satisfied both normal distribution and variance homogeneity ($p = 0.309$ and 0.320 , Shapiro–Wilk test; $p = 0.533$, Levene’s test). Regarding the comparison of categorical variables, χ^2 tests were applied since no expected count in any table cell was less than 5 (Table 2).

Compared with the non-SLNM group, patients in the SLNM group were older and had a larger tumor size (both FDR-adjusted p -values <0.05). The proportions of tumor in the upper pole, single lesion, capsular invasion, and extraglandular invasion in the SLNM group were 46.34%, 71.95%, 67.07%, and 42.68%, respectively, and were all significantly higher than in the non-SLNM group (all FDR-adjusted p -values <0.05). There were no significant differences in gender, BMI, family history of thyroid cancer, history of Hashimoto’s thyroiditis, tumor T stage, lesion distribution, calcified foci, Doppler blood flow, and hypoechoic mass between the 2 groups (all FDR-adjusted p -values >0.05).

Univariate and multivariate analyses for SLNM in PTC patients

Age, tumor location, number of lesions, tumor size, capsular invasion, and extraglandular invasion were

Table 1. Comparison of clinical characteristics of PTC patients between the SLNM and non-SLNM group

Variable		Non-SLNM group (n = 698)	SLNM group (n = 82)	t/Z/ χ^2 value	p-value	FDR-adjusted p-value
Age [years]		43 (29–60)	47 (31–65)	2.390*	0.017	0.043
Gender, n (%)	male	228 (32.66)	26 (31.71)	0.031	0.861	0.871
	female	470 (67.34)	56 (68.29)			
BMI [kg/m ²]		24.32 ±3.79	23.51 ±3.53	1.072	0.301	0.452
Family history of thyroid cancer, n (%)	yes	78 (11.2)	7 (8.5)	0.526	0.468	0.636
	no	620 (88.8)	75 (91.5)			
History of Hashimoto's thyroiditis, n (%)	yes	138 (19.8)	11 (13.4)	1.918	0.166	0.277
	no	560 (80.2)	71 (86.6)			
T stage of tumor, n (%)	T1	24 (3.4)	7 (8.5)	0.360*	0.719	0.830
	T2	378 (54.2)	41 (50.0)			
	T3	237 (34.0)	24 (29.3)			
	T4	59 (8.5)	10 (12.2)			
Tumor location, n (%)	upper pole	204 (29.2)	38 (46.3)	10.123	0.006	0.030
	middle	246 (35.2)	23 (28.0)			
	lower pole	248 (35.5)	21 (25.6)			
Number of lesions, n (%)	single	402 (57.6)	59 (72.0)	6.258	0.012	0.036
	multiple	296 (42.4)	23 (28.0)			
Distribution of lesions, n (%)	unilateral	448 (64.2)	60 (73.2)	2.610	0.106	0.227
	bilateral	250 (35.8)	22 (26.8)			
Tumor size [cm]		1.62 (1.27–2.30)	2.13 (1.50–2.93)	4.733*	<0.001	0.002
Capsular invasion, n (%)	yes	280 (40.1)	55 (67.1)	21.765	<0.001	0.002
	no	418 (59.9)	27 (32.9)			
Extraglandular invasion, n (%)	yes	204 (29.2)	35 (42.7)	6.252	0.012	0.036
	no	494 (70.8)	47 (57.3)			
Hypoechoic mass, n (%)	yes	549 (78.7)	70 (85.4)	2.018	0.155	0.277
	no	149 (21.3)	12 (14.6)			
Calcified foci, n (%)	yes	230 (33.0)	30 (36.6)	0.436	0.509	0.636
	no	468 (67.0)	52 (63.4)			
Doppler blood flow, n (%)	rich	152 (21.8)	20 (24.4)	0.163*	0.871	0.871
	little	376 (53.9)	41 (50.0)			
	none	170 (24.4)	21 (25.6)			

Continuous variables were expressed as mean ± standard deviation (M ±SD; normal distribution) or median (interquartile range (IQR); skewed distribution).

* Mann–Whitney U test. SLNM – skip lymph node metastasis; FDR – false discovery rate.

the included variables for univariate Cox regression. They all satisfied the proportional hazards assumption (Fig. 2). Among them, age and tumor size as continuous variables met the linearity assumption as well (Fig. 3). Univariate analyses showed that they were all associated with the development of SLNM (all $p < 0.05$) and were therefore included in the multivariate analysis. Multivariate Cox regression analysis revealed that older age, tumor in the upper pole, larger tumor size, and capsular invasion were the independent correlates of SLNM (all $p < 0.05$; Table 3).

Nomogram development

A nomogram was built based on the 4 independent predictors (age, tumor location, tumor size, and capsular invasion; Fig. 4). The estimated risk of SLNM was calculated by summing the points of each predictor, with the weight equal to the HR values. The risk range of SLNM was 20–60% in this nomogram.

Nomogram verification

To evaluate the accuracy of the nomogram, a high AUC was obtained (0.824 > 0.75) (95% CI: 0.891–0.964) after 1000 bootstrapping to adjust overfitting deviation in the ROC analysis, indicating a good discrimination (Fig. 5).

Evaluation of the calibration and clinical net benefit

The agreement between the probability of SLNM development predicted using the nomogram and the actual incidence was evaluated with the calibration curve and the H–L test. It showed good agreement with the actual incidence when the predicted probability was <60% ($\chi^2 = 5.263$, $p = 0.729$, H–L test; Fig. 6A). The DCA curve showed that the probability predicted using the nomogram obtained a net benefit when the probability was <60% (Fig. 6B). It indicated that the prediction model could reliably identify high-risk cN0 PTC patients with SLNM.

Table 2. Observed and expected counts of categorical variables in the SLNM and non-SLNM groups

Categorical variable		Count	Non-SLNM group (n = 698)	SLNM group (n = 82)
Gender, n	male	observed expected	228 227.3	26 26.7
	female	observed expected	470 470.7	56 55.3
Family history of thyroid cancer, n	yes	observed expected	78 76.1	7 8.9
	no	observed expected	620 621.9	75 73.1
History of Hashimoto's thyroiditis, n	yes	observed expected	138 133.3	11 15.7
	no	observed expected	560 564.7	71 66.3
Tumor location, n	upper pole	observed expected	204 216.6	38 25.4
	middle	observed expected	246 240.7	23 28.3
	lower pole	observed expected	248 240.7	21 28.3
Number of lesions, n	single	observed expected	402 412.5	59 48.5
	multiple	observed expected	296 285.5	23 33.5
Distribution of lesions, n	unilateral	observed expected	448 454.6	60 53.4
	bilateral	observed expected	250 243.4	22 28.6
Capsular invasion, n	yes	observed expected	280 299.8	55 35.2
	no	observed expected	418 398.2	27 46.8
Extraglandular invasion, n	yes	observed expected	204 213.9	35 25.1
	no	observed expected	494 484.1	47 56.9
Hypoechoic mass, n	yes	observed expected	549 553.9	70 65.1
	no	observed expected	149 144.1	12 16.9
Calcified foci, n	yes	observed expected	230 232.7	30 27.3
	no	observed expected	468 465.3	52 54.7

SLNM – skip lymph node metastasis.

Discussion

The SLNM in CLNM-negative cN0 patients affects the clinical stage and recurrence risk stratification. In this study, we revealed the independent correlates of the development of SLNM (age, tumor location, tumor size, and capsular invasion) by analyzing the clinical characteristics of cN+ patients without CLNM (typical SLNM) and cN0 patients with postoperative LLNM (occult SLNM). Based on these predictors, a nomogram was established to preoperatively predict the likelihood of SLNM

development in cN0 PTC patients who are at an increased risk of LNM, allowing for more individualized therapy.

The presence of SLNM is not detected with CLND. Sometimes, it is invisible for ultrasonography in an early stage due to atypical imaging features, leading to these patients being mistakenly classified as low-risk.¹⁰ Patients with occult SLNM are more likely to experience postoperative disease progression, which may lead to an unfavorable prognosis such as additional surgery.¹¹ The incidence of postoperative metastasis in cN0 PTC may be successfully lowered if these patients are identified prior

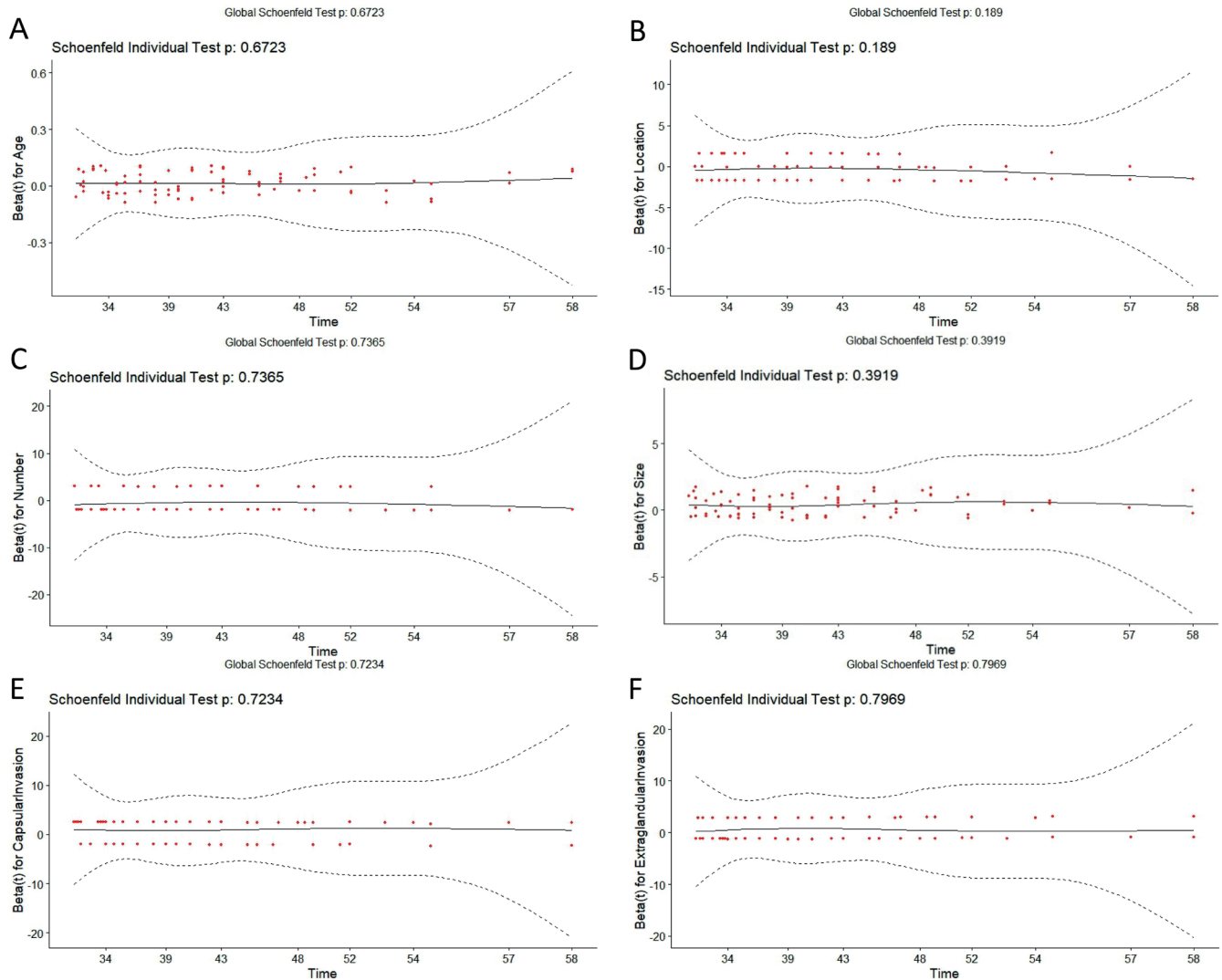


Fig. 2. Schoenfeld residuals plots for assessing the validity of proportional hazard assumption. The proportional hazards assumption is met for age (A), tumor location (B), number of lesions (C), tumor size (D), capsular invasion (E), and extraglandular invasion (F)

Table 3. Univariate and multivariate Cox regression analyses of the factors associated with SLNM in PTC patients

Variable		Univariate Cox regression			Multivariate Cox regression		
		p-value	HR	95% CI	p-value	HR	95% CI
Age		0.015	1.016	1.003–1.029	0.017	1.016	1.003–1.030
Tumor location	lower pole		reference			reference	
	middle	0.203	1.539	1.282–1.837		N/A	
	upper pole	0.001	2.287	1.419–3.685	0.017	1.801	1.111–2.917
Number of lesions	multiple		reference			reference	
	single	0.035	1.203	1.109–1.174	0.236	4.785	1.506–1.726
Tumor size		<0.001	1.549	1.289–1.861	<0.001	1.528	1.264–1.847
Capsular invasion	no		reference			reference	
	yes	<0.001	2.709	1.669–4.399	<0.001	2.941	1.789–4.835
Extraglandular invasion	no		reference			reference	
	yes	0.041	1.319	1.169–1.271	0.628	1.743	1.566–1.909

HR – hazard ratio; 95% CI – 95% confidence interval; N/A – not applicable; SLNM – skip lymph node metastasis; PTC – papillary thyroid cancer.

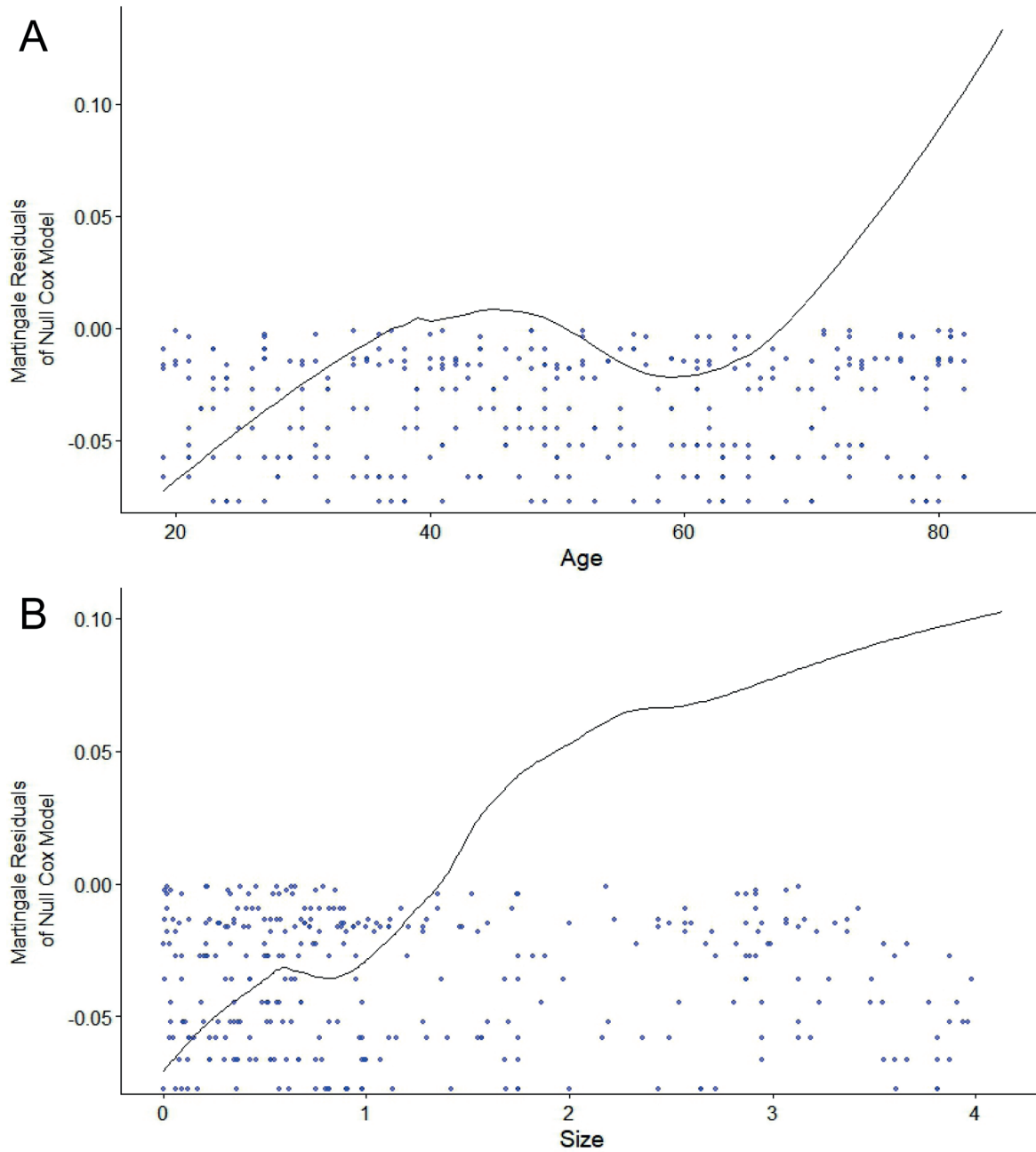


Fig. 3. Martingale residual plots for assessing the linearity assumption of continuous variables against survival time. Overall, there is a linear trend in age (A) and tumor size (B)

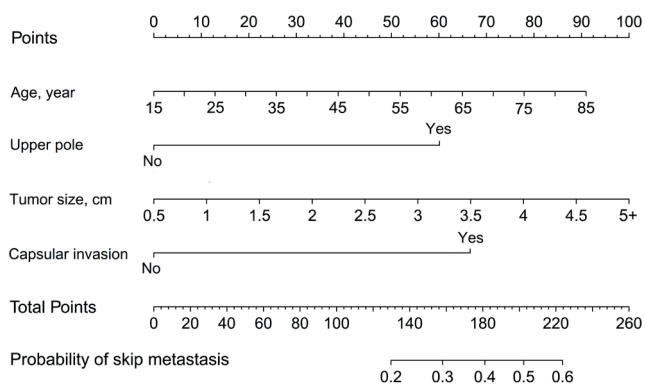


Fig. 4. Nomogram predicting the risk of SLNM in PTC patients. Each patient’s score is calculated from its predictors, and the total score corresponds to the probability of SLNM

SLNM – skip lymph node metastasis; PTC – papillary thyroid cancer.

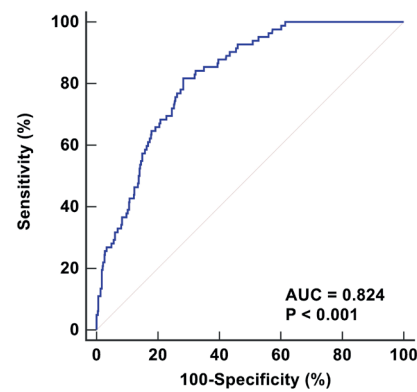


Fig. 5. Discrimination evaluation of the nomogram. The ROC curve reveals an AUC of 0.824, indicating good discrimination (>0.75)

ROC – receiver operating characteristic, AUC – area under the curve.

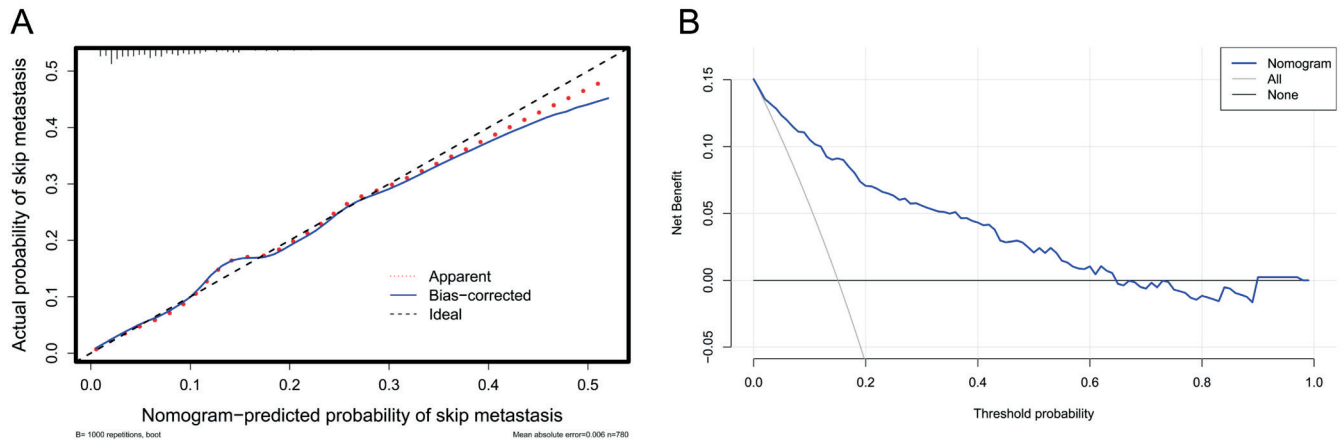


Fig. 6. Evaluation of the calibration and clinical net benefit of the nomogram. The calibration curve shows that the probability of SLNM predicted with the nomogram matches the actual incidence well when the probability is <60% (A). The DCA curve indicates that when the threshold probability is <60%, the nomogram yields clinical net benefit (B)

SLNM – skip lymph node metastasis; DCA – decision curve analysis.

to surgery, thus improving the prognosis.^{11,12} The majority of studies on SLNM analyzed the characteristics of cN+ patients compared to subjects without SLNM, while cN0 PTC patients were not enrolled.^{8,10,13} Despite the fact that Yang et al. included cN0 PTC patients in their study, they determined that cN0 PTC patients were all non-SLNM patients and did not conduct postoperative follow-up, ignoring the occult SLNM in cN0 PTC.¹⁴

Some of the possible reasons for postoperative LLNM in cN0 PTC patients are: 1) occult SLNM is present prior to surgery, and residual tumor cells in the LLN induce postoperative LLNM¹⁵; or 2) after CLND, tumor cells in the residual thyroid gland metastasize to the LLNs via the lymphatic pathway along the upper pole of thyroid vessels vasculatures because the lymphatic pathway to CLNs is blocked.¹⁶ Therefore, we believe that postoperative LLNM in cN0 PTC patients who received CLND is mostly SLNM. In this study, postoperative follow-up was performed to identify occult SLNM patients in order to investigate the risk factors of SLNM and establish a prediction model to estimate the risk of SLNM.

Multivariate Cox regression analysis in this study found that older age, larger tumor size, upper pole location, and capsular invasion were independent factors of the SLNM development. Older age is a risk factor for both PTC^{17–19} and LLNM.^{20,21} Wang et al. concluded that age ≥ 55 years was an independent risk factor for SLNM, which is consistent with the findings of this study.¹³ There is still controversy regarding the size and invasiveness of tumors in SLNM patients. Wang et al. and Lim et al. found that SLNM was more likely to develop in weakly invasive PTC, and that tumor size <1 cm was an independent risk factor.^{13,22} However, Yang et al. showed that tumor size >1 cm and capsular invasion were independent factors for SLNM.¹⁴ Our results support the idea of Yang et al.¹⁴ that large tumor size and capsular invasion are independent factors for the development of SLNM, and these factors are similar to the risk

factors for LLNM.^{23–25} One possible explanation is that a tumor with a larger diameter and capsular invasion may be closer to the lymphatic pathway along the upper pole of thyroid vessels, allowing tumor cells to directly metastasize to the LLN. In this study, tumors in the upper pole of the gland were found in 46.34% of SLNM patients, which was higher than in the non-SLNM group. It is in line with the studies by Yang et al.¹⁴ and Hou et al.²⁶ The possible explanation is that the lymph from the upper pole of the thyroid mainly enters the venous system through the lateral cervical lymph nodes along the lymphatic vessels accompanying the superior thyroid artery.^{16,27} Therefore, the tumor cells located in the upper pole of the thyroid are more susceptible to spread to the LLNs through the ascending lymphatic vessels, leading to SLNM.

To our knowledge, this is the first study to establish a nomogram for quantifying the likelihood of SLNM development in high-risk cN0 PTC patients before surgery. The model was confirmed to have good discrimination after resampling. When the predicted probability was <60%, the model agreed well with the actual incidence and could yield a net benefit. Clinicians can assess the likelihood of SLNM in each high-risk cN0 PTC patient before surgery by utilizing this nomogram. For example, when a 50-year-old patient with a 3-centimeter invasive tumor in the upper pole of the thyroid has a calculated score of approx. 220 points, it means that the likelihood that this patient will develop SLNM is more than 50%, and prophylactic lymph node dissection or closer nodal follow-up may be recommended.

Limitations

There are some limitations to this report. First, because it was a retrospective study with a limited sample, we did not have the opportunity to assess the angioinvasion of lymphatic vessels, or perform an external validation

to further evaluate the performance of the model. Second, limited follow-up time could result in missing patients with postoperative metastases due to occult SLNM. Finally, we were unable to analyze the occult SLNM in low-risk cN0 PTC patients because pathological results of their CLNs were not available. We plan to conduct a multi-center prospective study with a longer follow-up period in order to strengthen the prediction model.

Conclusions

We developed a nomogram which incorporated age, tumor location, tumor size, and capsular invasion, for preoperatively estimating the likelihood of SLNM development in cN0 PTC patients at an increased risk of LNM. If further validated, it will allow for personalized therapies to minimize the incidence of postoperative metastases in patients with cN0 PTC.

ORCID iDs

Fang Li  <https://orcid.org/0000-0003-4976-0783>
 Fang-Jian Zhou  <https://orcid.org/0000-0003-1811-3380>
 Tong-Wei Zhu  <https://orcid.org/0000-0002-5805-5552>
 Hua-Li Qiu  <https://orcid.org/0000-0003-3896-1475>
 Xiao-Ting Zhang  <https://orcid.org/0000-0003-0057-789X>
 Bo-Wen Ruan  <https://orcid.org/0000-0001-7098-2300>
 De-Yi Huang  <https://orcid.org/0000-0002-8060-1089>

References

- Liu X, Fu Q, Bian X, et al. Long non-coding RNA MAPK8IP2 inhibits lymphatic metastasis of thyroid cancer by activating hippo signaling via sponging miR-146b-3p. *Front Oncol.* 2021;10:600927. doi:10.3389/fonc.2020.600927
- Haugen BR, Alexander EK, Bible KC, et al. 2015 American Thyroid Association Management Guidelines for Adult Patients with Thyroid Nodules and Differentiated Thyroid Cancer: The American Thyroid Association Guidelines Task Force on Thyroid Nodules and Differentiated Thyroid Cancer. *Thyroid.* 2016;26(1):1–133. doi:10.1089/thy.2015.0020
- Shi L, Song H, Zhu H, Li D, Zhang N. Pattern, predictors and recurrence of cervical lymph node metastases in papillary thyroid cancer. *Contemp Oncol (Pozn).* 2013;6:504–509. doi:10.5114/wo.2013.38910
- Lei J, Zhong J, Jiang K, Li Z, Gong R, Zhu J. Skip lateral lymph node metastasis leaping over the central neck compartment in papillary thyroid carcinoma. *Oncotarget.* 2017;8(16):27022–27033. doi:10.18632/oncotarget.15388
- Mitchell AL, Gandhi A, Scott-Coombes D, Perros P. Management of thyroid cancer: United Kingdom National Multidisciplinary Guidelines. *J Laryngol Otol.* 2016;130(S2):S150–S160. doi:10.1017/S0022215116000578
- Hu D, Zhou J, He W, et al. Risk factors of lateral lymph node metastasis in cN0 papillary thyroid carcinoma. *World J Surg Onc.* 2018;16(1):30. doi:10.1186/s12957-018-1336-3
- Roh JL, Park JY, Rha KS, Park CI. Is central neck dissection necessary for the treatment of lateral cervical nodal recurrence of papillary thyroid carcinoma? *Head Neck.* 2007;29(10):901–906. doi:10.1002/hed.20606
- Attard A, Paladino NC, Lo Monte AI, et al. Skip metastases to lateral cervical lymph nodes in differentiated thyroid cancer: A systematic review. *BMC Surg.* 2019;18(Suppl 1):112. doi:10.1186/s12893-018-0435-y
- Jin WX, Jin YX, Ye DR, et al. Predictive factors of skip metastasis in papillary thyroid cancer. *Med Sci Monit.* 2018;24:2744–2749. doi:10.12659/MSM.907357
- Nie X, Tan Z, Ge M. Skip metastasis in papillary thyroid carcinoma is difficult to predict in clinical practice. *BMC Cancer.* 2017;17(1):702. doi:10.1186/s12885-017-3698-2
- Xu JJ, Yu E, McMullen C, et al. Patterns of regional recurrence in papillary thyroid cancer patients with lateral neck metastases undergoing neck dissection. *J Otolaryngol Head Neck Surg.* 2017;46(1):43. doi:10.1186/s40463-017-0221-3
- McNamara WF, Wang LY, Palmer FL, et al. Pattern of neck recurrence after lateral neck dissection for cervical metastases in papillary thyroid cancer. *Surgery.* 2016;159(6):1565–1571. doi:10.1016/j.surg.2016.02.005
- Wang W, Yang Z, Ouyang Q. A nomogram to predict skip metastasis in papillary thyroid cancer. *World J Surg Onc.* 2020;18(1):167. doi:10.1186/s12957-020-01948-y
- Yang Z, Heng Y, Zhao Q, et al. A specific predicting model for screening skip metastasis from patients with negative central lymph nodes metastasis in papillary thyroid cancer. *Front Endocrinol.* 2021;12:743900. doi:10.3389/fendo.2021.743900
- Kliseska E, Makovac I. Skip metastases in papillary thyroid cancer. *Coll Antropol.* 2012;36(Suppl 2):59–62. PMID:23397756
- Likhterov I, Reis LLD, Urken ML. Central compartment management in patients with papillary thyroid cancer presenting with metastatic disease to the lateral neck: Anatomic pathways of lymphatic spread. *Head Neck.* 2017;39(5):853–859. doi:10.1002/hed.24568
- Li X, Zhang H, Zhou Y, Cheng R. Risk factors for central lymph node metastasis in the cervical region in papillary thyroid carcinoma: A retrospective study. *World J Surg Onc.* 2021;19(1):138. doi:10.1186/s12957-021-02247-w
- Song L, Zhou J, Chen W, et al. Lymph node metastasis between the sternocleidomastoid and sternohyoid muscle in papillary thyroid carcinoma patients: A prospective study at multiple centers. *Asia J Surg.* 2021;44(8):1043–1049. doi:10.1016/j.asjsur.2021.01.005
- Dong Y, Wang D, Luo Y, et al. Comprehensive evaluation of risk factors for lymph node metastasis in patients with papillary thyroid carcinoma. *Oncol Lett.* 2021;21(3):188. doi:10.3892/ol.2021.12449
- Özden S, Çomçalı B, Ataş H, Er S, Tez M, Saylam B. A diagnostic dilemma: Skip metastasis in papillary thyroid cancer. *Am Surg.* 2020;86(3):245–249. PMID:32223805
- Chatchomchuan W, Thewjitcharoen Y, Karndumri K, et al. Recurrence factors and characteristic trends of papillary thyroid cancer over three decades. *Int J Endocrinol.* 2021;2021:9989757. doi:10.1155/2021/9989757
- Lim YC, Koo BS. Predictive factors of skip metastases to lateral neck compartment leaping central neck compartment in papillary thyroid carcinoma. *Oral Oncol.* 2012;48(3):262–265. doi:10.1016/j.oraloncology.2011.10.006
- Li X, Duan Y, Liu D, et al. Diagnostic model incorporating clinico-pathological characteristics of Delphian lymph node metastasis risk profiles in papillary thyroid cancer. *Front Endocrinol.* 2021;12:591015. doi:10.3389/fendo.2021.591015
- Zhu J, Huang R, Yu P, et al. Clinical implications of Delphian lymph node metastasis in papillary thyroid carcinoma. *Gland Surg.* 2021;10(1):73–82. doi:10.21037/gs-20-521
- Liu Z, Lei J, Liu Y, Fan Y, Wang X, Lu X. Preoperative predictors of lateral neck lymph node metastasis in papillary thyroid microcarcinoma. *Medicine (Baltimore).* 2017;96(10):e6240. doi:10.1097/MD.00000000000006240
- Hou J, Zhang Y, Fan Y, Wu B. Risk factors of skip lateral lymph node metastasis in papillary thyroid carcinoma. *Eur Arch Otorhinolaryngol.* 2021;278(2):493–498. doi:10.1007/s00405-020-06176-4
- Lee YS, Shin SC, Lim YS, et al. Tumor location-dependent skip lateral cervical lymph node metastasis in papillary thyroid cancer: Lateral metastasis in thyroid cancer. *Head Neck.* 2014;36(6):887–891. doi:10.1002/hed.23391

PIEZO2 promotes cell proliferation and metastasis in colon carcinoma through the *SLIT2/ROBO1/VEGFC* pathway

*Haotian Shang^C, *Aiguo Xu^{B,C}, Haicui Yan^B, Dandan Xu^{B,C}, Jingyu Zhang^{A,C,D,F}, Xinjian Fang^{E,F}

Department of Oncology, Lianyungang No. 2 People's Hospital, Lianyungang Clinical College of Bengbu Medical College, China

A – research concept and design; B – collection and/or assembly of data; C – data analysis and interpretation; D – writing the article; E – critical revision of the article; F – final approval of the article

Advances in Clinical and Experimental Medicine, ISSN 1899–5276 (print), ISSN 2451–2680 (online)

Adv Clin Exp Med. 2023;32(7):763–776

Address for correspondence

Jingyu Zhang
E-mail: lygzjy2013@outlook.com

Funding sources

This work was partially supported by grant No. LGY2020053 from Top-notch Talents of "Six One Projects" of high-level health talents in the 2020 project, grant No. TQ201903 from Growth Fund for young and middle-aged medical talents of Second People's Hospital of Lianyungang, and grant No. 2020byzd337 from the Science and Technology Project of Bengbu Medical College.

Conflict of interest

None declared

Acknowledgements

The authors would like to thank all individuals who participated in this study.

*Haotian Shang and Aiguo Xu contributed equally to this work.

Received on August 16, 2022

Reviewed on October 3, 2022

Accepted on December 15, 2022

Published online on February 8, 2023

Cite as

Shang H, Xu A, Yan H, Xu D, Zhang J, Fang X. *PIEZO2* promotes cell proliferation and metastasis in colon carcinoma through the *SLIT2/ROBO1/VEGFC* pathway. *Adv Clin Exp Med.* 2023;32(7):763–776. doi:10.17219/acem/157515

DOI

10.17219/acem/157515

Copyright

Copyright by Author(s)

This is an article distributed under the terms of the Creative Commons Attribution 3.0 Unported (CC BY 3.0) (<https://creativecommons.org/licenses/by/3.0/>)

Abstract

Background. The *PIEZO2* may be involved in the occurrence and development of tumors.

Objectives. To explore the potential mechanism and effect of *PIEZO2* on colon cancer.

Materials and methods. We assessed the expression and prognostic role of *PIEZO2* in patients with colon cancer. The role of *PIEZO2* in SW480 cell proliferation, migration and invasion in vitro was investigated using cell counting kit-8 (CCK-8), wound healing, and transwell and cell invasion assays, respectively. The effect of *PIEZO2* on SW480 cells in vivo was also explored. The potential mechanisms of *PIEZO2* in SW480 cells were detected using quantitative reverse-transcription polymerase chain reaction (qRT-PCR) and western blot.

Results. The *PIEZO2* was significantly increased in colon cancer tissues and the *PIEZO2* high expression group was associated with a lower overall survival (OS) rate. Furthermore, *PIEZO2* knockdown weakened the proliferation, migration and invasion of SW480 cells. The *PIEZO2* knockdown was related to a lower expression of *SLIT2*, *ROBO1*, *HIF-1a*, and *VEGFC*. Finally, the tumors in control SW480 cells grew faster and larger than those in mice inoculated with si-*PIEZO2* SW480 cells. Moreover, the si-*PIEZO2* SW480 cell group showed a reduced expression of *Ki67* and *VEGFC* and, at the same time, a significantly higher apoptosis index of tumor cells compared to the control group. The expression of *PIEZO2* was higher in cancer-associated fibroblasts (CAFs) of colon cancer.

Conclusions. The *PIEZO2* was increased in colon cancer tissues and was an unfavorable gene in patients with colon cancer, promoting colon cell proliferation, migration and invasion through the *SLIT2/ROBO1/VEGFC* pathway.

Key words: colon cancer, cancer-associated fibroblasts, *PIEZO2*, *SLIT2/ROBO1/VEGFC* pathway

Background

Because of its high mortality rate, colorectal cancer (CRC) has become a major health burden worldwide. Globally, there were more than 1.9 million new CRC cases and 935,000 deaths reported in 2020.¹ If the cancer is local, 90% of patients with CRC survive 5 years after the diagnosis. However, once the disease has distant metastases, this rate reduces dramatically to 10%.² The genetics of cancer cells is not a sole factor influencing tumor metastasis; additionally, the interaction between tumor cells and the surrounding microenvironment plays a pivotal role in tumor differentiation and progression.³ Mechanical stimulation including stiffness, shear stress, compression, and tensional forces from the surrounding microenvironment is frequent in tumor cells.⁴ Mechanotransduction, the conversion of physical stimuli into biochemical or electrical signals, plays a key role in biological processes in tumor cells, including development, proliferation, migration, and apoptosis.⁵

The *PIEZO* transmembrane proteins are conserved ion-channel proteins that sense external mechanical forces. The cell membrane pressure induced by external mechanical force can regulate changes in intracellular ions and exert physiological effects by changing the closure of the *PIEZO* transmembrane protein. The *PIEZO*s can regulate nociception and stem cell differentiation in *Drosophila*. The *PIEZO* transmembrane proteins mainly include 2 homologous proteins: *PIEZO1* and *PIEZO2*. Although these proteins are homologous, their roles reported in the literature are not consistent. The *PIEZO1* is mainly distributed in endothelial cells, red blood cells and hair cells in cochlea, as well as kidney, bladder and lung cancer cells. Under normal physiological conditions, *PIEZO1* is primarily responsible for the regulation of intravascular balance, blood pressure and axon growth. The *PIEZO2* is mainly distributed in the dorsal root nerve and trigeminal ganglion, which are responsible for regulating touch, proprioception of muscles and airway extension. It has been reported that *PIEZO*s are involved in the formation of human blood vessels.⁶ The *PIEZO* knockout can affect the growth and development of mice. Because of the important role of *PIEZO*s, the functions of the 2 homologous proteins have been increasingly studied.

In recent years, many studies have reported that *PIEZO*s may be involved in the occurrence and development of tumors, and may be related to angiogenesis. Gottlieb et al. reported that the reduction or deletion of *PIEZO1* played an important role in lung cancer metastasis,⁷ while Yang et al. indicated that the decrease in *PIEZO1* expression was related to the decrease in the gastric cancer metastasis.⁸ A study by Yang et al. showed that *PIEZO2* knockout can reduce angiogenesis, vascular permeability, endothelial cell proliferation, metastasis, and tubule formation in gliomas.⁹ Another study showed that the expression of *PIEZO1/2* was different in bladder cancer formation, suggesting

that *PIEZO1/2* plays a role in the proliferation and angiogenesis of bladder cancer cells.¹⁰ Chen et al. reported that the expression of *PIEZO1* was inversely proportional to the stage and prognosis of glioma.¹¹ The *PIEZO1* can regulate changes in the extracellular matrix and tissue hardness as well as promote tumor progression by activating the integrin focal adhesion kinase (*FAK*) signaling pathway; however, *PIEZO2* is not a prognostic factor. In a study by Pardo-Pastor et al., it was shown that *PIEZO1* mainly forms a mechanoreceptor ion pathway in breast cancer cells, whereas *PIEZO2* is involved in regulating RhoA, actin skeleton formation and cell movement.¹² However, the roles of *PIEZO*s in colon cancer and their underlying mechanisms remain unclear and need to be further elucidated.

Previous studies showed that the *SLIT/ROBO* signaling pathway inhibited the migration of nerve cells in the central nervous system, prevented the nerve axon at the suture from passing through the middle line of the nerve tube, and controlled the accurate localization of neurite in nervous system. Studies on the expression and function of *SLIT/ROBO* signaling in various cancers have been conducted.^{13–15} Recently, the molecular mechanism of *SLIT2/ROBO1* signaling in the regulation of colon cancer tumorigenesis has also been deeply studied. The *SLIT2* was highly expressed in colon cancer and its expression increased in pathological stages.¹⁶ At the same time, *SLIT2/ROBO1* signaling induced tumor metastasis in colon cancer partially through the activation of the transforming growth factor beta (*TGF-β*)/*Smads* pathway. Moreover, *SLIT2/ROBO1* signaling recruited *Src* to *E-cadherin* for tyrosine phosphorylation, leading to *E-cadherin* degradation and epithelial–mesenchymal transition in colon cancer.¹⁷ Accordingly, *SLIT2/ROBO1* signaling played an important role in the formation and metastasis of colon cancer.

Objectives

The above studies suggested *PIEZO2* played an important role in the occurrence and progression of tumors. However, the detailed mechanism was not clear in colon cancer. Therefore, this study was designed to explore the prognostic role of *PIEZO2* in colon cancer and whether the *SLIT2/ROBO1* pathway is responsible for *PIEZO2*-induced progression of colon cancer.

Materials and methods

Patient information

A total of 74 colon cancer tissue samples were collected from January 2015 to December 2016 from patients with colon cancer who received surgery at the Department

of Gastrointestinal Surgery, affiliated with Second People's Hospital of Lianyungang (Bengbu Medical College, China). In addition, we collected 30 colon cancer tumor tissues and matched normal tissues. Clinical data were complete and the last follow-up time was December 2021. Patients included in the study did not receive anticancer therapy such as radiotherapy, chemotherapy or biological therapy before surgery. This study was approved by the Animal Care and Use Ethics Committee of the Affiliated Lianyungang Hospital (Bengbu Medical College, China; approval No. 2020-013-02).

Cell culture

The human colorectal cell line SW480 was purchased from the cell bank of the Chinese Academy of Sciences (Shanghai, China). The cell line grew in Roswell Park Memorial Institute (RPMI) 1640 medium (cat. No. 21870076; Thermo Fisher Scientific, Waltham, USA) supplemented with 10% fetal bovine serum (FBS) (item code: 13011-8611; SolelyBio, Shanghai, China) and cultured in a humidified 5% CO₂ environment at 37°C.

Cell transfection

The SW480 cells were transfected with small interfering (si)RNA targeting *PIEZO2* (si-*PIEZO2*, 5'-GGATAGT-GAAGAGGAGGAAGA-3') and the corresponding negative control (NC) using Lipofectamine™ 2000 Transfection Reagent (1 µL/50 µL, cat. No. 12566014; Invitrogen, Carlsbad, USA). The transfection effect was evaluated using quantitative reverse-transcription polymerase chain reaction (qRT-PCR) and the positive cell line was used for the following experiments.

RT-qPCR assay

Total RNA was extracted using TRIzol reagent (cat. No. 15596026; Invitrogen) and synthesized into cDNA using a reverse transcriptase Moloney Murine Leukemia Virus (M-MLV) Kit (cat. No. 18057018; Invitrogen). The gene expression was detected with a SYBR® Premix Ex Taq™ (cat. No. 11780200; Thermo Fisher Scientific). The primers used in this study are presented in Table 1. The expression of *PIEZO2*, *HIF-1α*, *SLIT2*, *VEGFA*, *VEGFB*, *VEGFC*, *VEGFD*, and *ROBO1* was calculated using the 2^{-ΔΔC_q} method, and every value was measured thrice independently. The reaction conditions were as follows: 5 min at 95°C, followed by 40 cycles at 95°C for 30 s and 60°C for 45 s, and a final step at 72°C for 30 min.

Cell counting kit-8 assay

Cells (1×10⁴ cells) were plated in four 96-well plates. At every time point, we added 10 µL of cell counting kit-8 (CKK-8) solution (cat. No. C0037; Beyotime Biotechnology,

Table 1. Primer sequences used in the study

Gene symbol	Primer sequence (5'→3')
<i>PIEZO2</i>	forward: TTCCGATACAATGGGCTCTC
	reverse: GAGCTTCAAGGCTACCAAC
<i>HIF-1α</i>	forward: AGCACAGTTACAGTATTCCAGCAG
	reverse: AGTGGTGGCAGTGGTAGTGG
<i>SLIT2</i>	forward: TCCCCACAAATCTCCAGAG
	reverse: AGCGTAGTCCTGGAAAGCA
<i>VEGFA</i>	forward: GAGCGAGAAAGCATTGTTT
	reverse: GCAACGCGAGTCTGTGTGTTTT
<i>VEGFB</i>	forward: CAAGGCTGCCATCCAACAA
	reverse: AGGTGGTAAAATCTGAGTCGGG
<i>VEGFC</i>	forward: ACCAAACAAGGAGCTGGATG
	reverse: TCCCCACAAATCTCCAGAG
<i>VEGFD</i>	forward: TGTACAGACAGTGGGCAGTGGT
	reverse: AACCTGAAGCTGCCCTGATCT
<i>ROBO1</i>	forward: ACTCCTTACGCCACCACTCAG
	reverse: CCTGTGTCTGTGCTGATGATTGG
<i>h-actin</i>	forward: TGGACTTCGACAAGAGATG
	reverse: GAAGGAAGGCTGGAAGAGTG

Beijing, China) to each well and after the solution was incubated with cells at 37°C for 30 min, the absorbance at 450 nm was measured with a microplate reader. Every experiment was repeated thrice independently.

Wound healing assay

Cells (1×10⁵ cells) were seeded in 12-well plates. When cells reached 80% confluence, a 10-microliter sterile pipette tip was used to wound the cell monolayer. Then, a phase-contrast microscope (model IX71; Olympus Corp., Tokyo, Japan) was used to observe the cell migration at 0 h, 24 h and 48 h.

Transwell assay

Cells at a density of 6×10⁴ were plated in the upper layer (8 µm; Corning, Lowell, USA). The bottom chamber was filled with medium supplemented with 10% FBS. After 48 h, the cells in the lower chamber were fixed. Then, a crystal violet solution was used to stain cells for further analysis using the microscope (model IX71; Olympus Corp.). Twelve randomly chosen areas per sample were used to assess the number of penetrating cells.

Cell invasion assay

The 2×10⁵ cells were plated in the upper chamber of 24-well 8-micrometer pore well chambers (Corning). The cells were covered with diluted BD Matrigel™ (BD Biosciences, Franklin Lakes, USA) containing a complete

medium. The lower chamber was filled with a medium containing 10% FBS. After 24 h, cells on the lower layer were fixed with 4% paraformaldehyde solution and stained with 0.1% crystal violet solution. The total number of penetrating cells was calculated and pictures were taken with a light microscope (model CKX53; Olympus Corp.; $\times 200$ magnification).

Western blot

Total protein was extracted by means of a radioimmuno-precipitation assay (RIPA) buffer supplemented with a mixture of protease and phosphatase inhibitors. The protein concentration was determined with a bicinchoninic acid (BCA) protein assay. Protein samples were separated using 10% sodium dodecyl-sulfate polyacrylamide gel electrophoresis (SDS-PAGE) and transferred to a polyvinylidene fluoride (PVDF) membrane. After blocking with 10% fat-free milk, the membrane was incubated at 4°C overnight with the following primary antibodies: *HIF1 α* (1:6000, cat. No. 20960-1-AP), *ROBO1* (1:10000, cat. No. 20219-1-AP), *VEGFC* (1:1000, cat. No. 22601-1-AP), and *SLIT2* (1:600, cat. No. 20217-1-AP; all from ProteinTech Group). Next, the membrane was incubated with horseradish peroxidase (HRP) secondary antibody (1:3000, cat. No. HRP-60004; ProteinTech Group) for 1 h. Chemiluminescent HRP substrate and a suitable X-ray were used to detect the protein bands. Proteins were identified and quantified using the AlphaEaseFC software (Alpha Innotech, San Leandro, USA).

Animal experiments

Male athymic BALB/c mice (5–6 weeks, 16–18 g) were purchased from Nanjing University Animal Laboratory (Nanjing, China). The animals were provided with food and water ad libitum. All experiment conditions conformed to the 3R principles of animal experimentation. To evaluate the role of *PIEZO2* in vivo, the mice were injected with SW480 cell suspension (2×10^6) in 0.1 mL of culture medium subcutaneously into the right scapular region. The tumor size was measured every 7 days and calculated with the following formula: volume = tumor length \times (tumor width)² \times 0.5236. All data were recorded in millimeters. When the bearing tumors reached ~ 1 cm³, mice were killed and tumor samples were weighed and fixed in formalin followed by paraffin embedding.

Immunohistochemistry

In animal experiment, immunohistochemical *Ki-67* staining was used to evaluate the proliferative activity, and *VEGFC* expression was measured to evaluate the effect of *PIEZO2* on angiogenesis in tumor tissues. We also explored the expression of *PIEZO2* in colon cancer samples obtained from the patients of our hospital.

The anti-*Ki67* (cat. No. 27309-1-AP), anti-*PIEZO2* (cat. No. 26205-1-AP) and anti-*VEGFC* (cat. No. 22601-1-AP; all from ProteinTech Group) antibodies were diluted and used at 1:16000, 1:200 and 1:200, respectively. Goat anti-rabbit secondary antibodies were also diluted and used at 1:200, 1:500 and 1:500. The labelling indices were introduced to quantify the expression of *Ki-67* and *VEGFC*, calculated by the ratio of *Ki-67*- and *VEGFC*-positive cells/total cells and quantified using $\times 200$ magnification in 3 randomly selected areas in each tissue sample. We evaluated the *PIEZO2* expression in colon cancer tissues using the staining intensity and staining area of positive tumor cells in each section.¹⁸ The immunohistochemical score was used to assess the expression of *PIEZO2* referred to the protocol described by Tian et al.¹⁹ The median score was used as the split point. The group with values higher than or equal to the median was considered the high-expression group, and the the group with values lower than the median was considered the low-expression group.

TUNEL assay

Tumor tissues were cut into 5- μ m-thick slides and the slides were covered with the terminal deoxynucleotidyl transferase dUTP nick end labeling (TUNEL) reaction mixture (cat. No. PF00006; ProteinTech Group). After washing off the unbound enzyme conjugate, a substrate reaction was used to visualize the peroxidase (POD)-retained cells in the immune complex. Using a light microscope (model CKX53; Olympus Corp.) at $\times 200$ magnification, 3 different visual areas of each section were randomly selected and analyzed. The positive rate of apoptotic cells was defined as the density of apoptotic cells (the apoptosis index) using ImageJ software (National Institutes of Health, Bethesda, USA).

Statistical analyses

The relationship between *PIEZO2* expression and the clinical characteristics of gender or site of primary tumor in colon cancer patients was analyzed using Spearman's correlation analysis, and between *PIEZO2* protein expression and the remaining 6 variables using Kendall's tau-b correlation analysis. Comparison between the *PIEZO2* expression in tumor and paired normal tissue samples was performed using χ^2 test. The time from tumor resection to the patient's death or last follow-up was defined as the overall survival (OS) time. The impact of the prognostic role of clinical/pathological characteristics on OS was analyzed using the log-rank test and the Kaplan–Meier analysis. Subsequently, proportional hazard assumption was assessed using Schoenfeld residuals. The variables of N stage and *PIEZO2* did not meet the assumption. The univariate analysis was performed using Cox proportional

hazards regression model for variables that met the assumption. The time-dependent Cox regression model was used for variables that did not meet the assumption. The multivariate analysis was conducted using the time-dependent Cox regression model to exclude the influence of confounding factors. Since the data from the 2 groups met the assumption of normality, the differences between the 2 groups were evaluated using the Student’s t-test and expressed with mean ± standard deviation (M ±SD). Because the repeated measurement data from the 2 groups did not show normal distribution, the data of this part were analyzed using the Scheirer–Ray–Hare test and expressed as median ±range. The IBM SPSS v. 20.0 (IBM Corp., Armonk, USA), R v. 4.2.2 software (survminer package; R Foundation for Statistical Computing, Vienna, Austria) and GraphPad Prism v. 9 (GraphPad Software, San Diego, USA) were used in this study. The value of $p < 0.05$ was considered statistically significant.

Results

PIEZO2 expression was increased in colon cancer and associated with poor prognosis

A total of 30 colon cancer specimens with adjacent tissues were randomly selected from patients with colon cancer operated in Second People’s Hospital of Lianyungang. The expression of *PIEZO2* was analyzed using immunohistochemistry. The results indicated that *PIEZO2* was mainly located on the cell membrane and cytoplasm (Fig. 1A). The *PIEZO2* was highly expressed in colon cancer tissues compared with normal samples (18/30 compared to 9/30, $\chi^2 = 5.455$, $p = 0.020$; Fig. 1B). As shown in Table 2, high expression of *PIEZO2* was associated with tumor differentiation (Kendall’s tau-b = 0.360, $p = 0.002$), T stage (Kendall’s tau-b = 0.433, $p < 0.001$), N stage (Kendall’s tau-b = 0.453, $p < 0.001$), and clinical stage (Kendall’s tau-b = 0.322, $p = 0.006$). In addition, the prognostic data

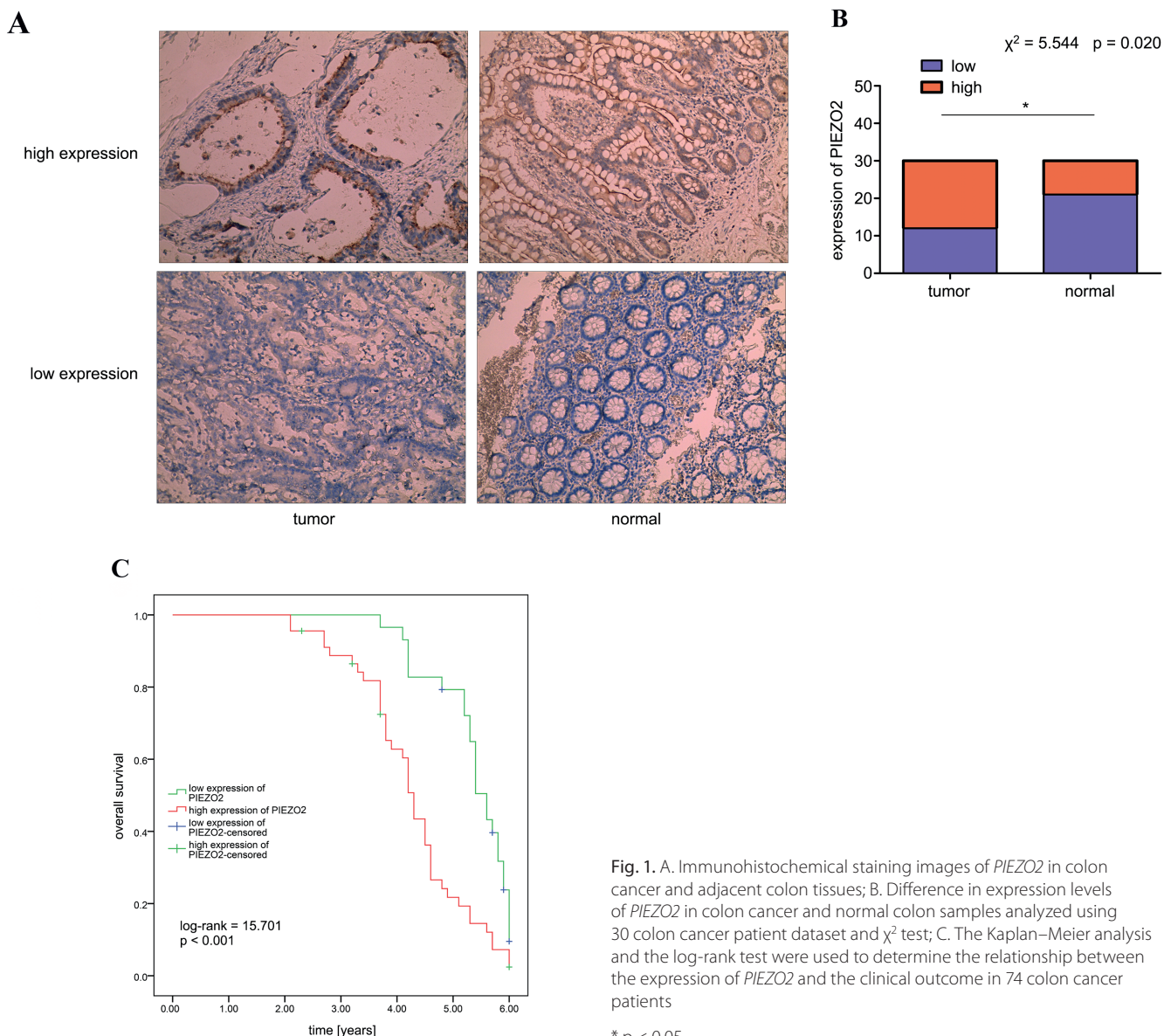


Fig. 1. A. Immunohistochemical staining images of *PIEZO2* in colon cancer and adjacent colon tissues; B. Difference in expression levels of *PIEZO2* in colon cancer and normal colon samples analyzed using 30 colon cancer patient dataset and χ^2 test; C. The Kaplan–Meier analysis and the log-rank test were used to determine the relationship between the expression of *PIEZO2* and the clinical outcome in 74 colon cancer patients

* $p < 0.05$.

showed that patients with high expression of *PIEZO2* had shorter OS (log-rank (Mantel–Cox) = 15.701, $p < 0.001$; Fig. 1C). Finally, we found that high expression of *PIEZO2* played an independent prognostic role for worsening OS in colon cancer, as shown with univariate and multivariate analyses ($p = 0.007$ and $p = 0.034$, respectively; Table 3).

Suppression of *PIEZO2* decreased the migration and invasion of colon cancer

To explore the potential role of *PIEZO2* in colon cancer, we identified 56 co-expressed genes (Fig. 2A) using the Coexpedia website (<http://www.coexpedia.org/index.php>). Gene Ontology (GO) function and pathway

enrichment analyses were performed using the DAVID database (<https://david.ncicrf.gov/>). As expected, the biological processes were primarily associated with extracellular matrix organization, cellular response to reactive oxygen species (ROS), positive regulation of transcription, templated DNA, and response to hypoxia (Fig. 2B). In terms of cellular components, these genes were also involved in the extracellular matrix (ECM), extracellular space, extracellular region, and receptor complexes (Fig. 2B). The following biological processes were included: ECM structural constituents, integrin binding, ECM binding, collagen binding, and proteoglycan binding (Fig. 2B). In addition, Kyoto Encyclopedia of Genes and Genomes (KEGG) pathway analysis indicated that the following

Table 2. The relationship between *PIEZO2* protein expression and clinical pathological features in colon cancer patients

Characteristic	Total, n	Expression level of <i>PIEZO2</i>		p-value
		high	low	
Age [years]	<65	30	18	0.907
	≥65	44	27	
Gender	male	44	25	0.401
	female	30	20	
Site of primary tumor	left	31	17	0.378
	right	43	28	
Differentiation	moderate and well	37	16	0.002
	poor	37	29	
T stage	T1+T2	29	10	<0.001
	T3+T4	45	35	
N stage	N0	26	8	<0.001
	N1+N2	48	37	
Clinical stage	I	20	12	0.006
	II+III	54	33	
CEA [ng/mL]	<6	19	9	0.931
	≥6	55	36	

CEA – carcinoembryonic antigen. Spearman's correlation analysis was used to analyze the relationship between the protein expression of *PIEZO2* and the clinical characteristics of gender or site of primary tumor. Kendall's tau-b correlation analysis was applied to explore the relationship between the protein expression of *PIEZO2* and the remaining 6 variables. The value of $p < 0.05$ was considered statistically significant.

Table 3. Univariate analysis and multivariate analysis of the overall survival (OS) in colon cancer patients

Characteristic	Univariate analysis			Multivariate analysis		
	HR	95% CI	p-value	HR	95% CI	p-value
Age	0.849	0.517–1.393	0.516	0.768	0.416–1.420	0.400
Gender	1.006	0.612–1.653	0.982	0.607	0.318–1.160	0.131
Tumor location	0.806	0.488–1.330	0.398	0.587	0.301–1.144	0.118
Differentiation	2.130	1.299–3.494	0.003	2.652	1.191–5.905	0.017
T stage	1.658	1.004–2.740	0.048	0.367	0.138–0.977	0.045
N stage (time-dependent variable)	3612.754	5.558–2348302.323	0.013	51.028	0.049–52836.422	0.267
Clinical stage	2.350	1.319–4.187	0.004	2.086	1.036–4.202	0.040
<i>PIEZO2</i> (time-dependent variable)	4261.402	9.758–1861054.007	0.007	1884.388	1.797–1976563.451	0.034
CEA	1.179	0.669–2.077	0.570	1.443	0.729–2.857	0.293

HR – hazard ratio; 95% CI – 95% confidence interval; CEA – carcinoembryonic antigen. Proportional hazard assumption was examined using Schoenfeld residuals. The variables of N stage and *PIEZO2* did not meet the assumption. Subsequently, the univariate analysis was performed using the Cox proportional hazards regression model for the variables that met the assumption. The time-dependent Cox regression model was used for variables that did not meet the assumption. At last, the multivariate analysis was conducted using the time-dependent Cox regression model to exclude the influence of confounding factors. The value of $p < 0.05$ was considered statistically significant.

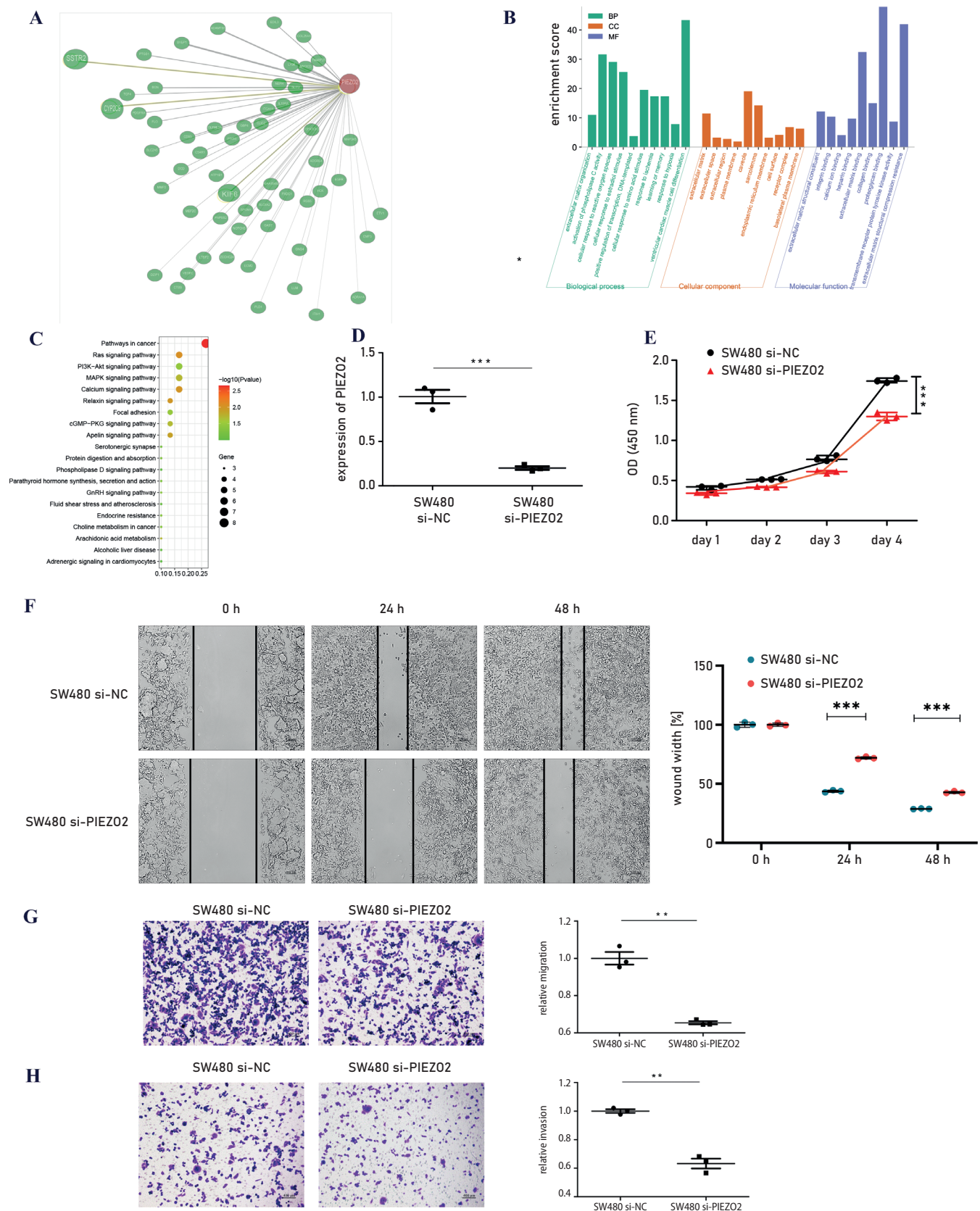


Fig. 2. Inhibition of *PIEZO2* suppresses the proliferation, migration and invasion in colon cancer cells. **A.** Fifty-six co-expressed genes of *PIEZO2* identified using the Coexpedia website; **B.** Enrichment analysis of co-expressed genes performed using the DAVID database; **C.** Kyoto Encyclopedia of Genes and Genomes (KEGG) pathway analysis of co-expressed genes conducted using the DAVID database; **D.** After the SW480 cells were transfected with small interfering (si)RNA targeting *PIEZO2*, the expression of *PIEZO2* in negative control (NC) and si-*PIEZO2* SW480 cells was tested using quantitative reverse-transcription polymerase chain reaction (qRT-PCR). The results were analyzed using the Student's t-test and expressed with mean \pm standard deviation ($M \pm SD$); **E.** Cell counting kit-8 (CCK-8) assay was performed to evaluate the cell viability of NC and si-*PIEZO2* SW480 cells. The results were analyzed using the Scheirer-Ray-Hare test and expressed as median (range); **F, G.** Wound healing and cell invasion assays were performed to evaluate the migration ability of NC and si-*PIEZO2* SW480 cells. The results were analyzed using the Student's t-test and expressed as $M \pm SD$; **H.** Matrigel™ invasion assay was performed to evaluate the invasion ability of NC and si-*PIEZO2* SW480 cells. The results were analyzed using the Student's t-test and expressed as $M \pm SD$. All experiment results were representative of 3 independent experiments

** $p < 0.01$; *** $p < 0.001$; OD – optical density.

pathways were enriched in cancer: Ras signaling, PI3K-Akt signaling, MAPK signaling, and calcium signaling pathways (Fig. 2C). As shown in Fig. 2D, a stable transfection with si-*PIEZO2* reduced the mRNA expression of *PIEZO2* in SW480 cells. Moreover, SW480 cells with si-*PIEZO2* showed weaker cell proliferation, migration and invasion functions (Fig. 2E–H).

PIEZO2 is linked to the *SLIT2/ROBO1/VEGFC* pathway

A previous study suggested that *PIEZO2* plays a pivotal role in tumor angiogenesis.⁹ We explored the mRNA expression of *VEGFA*, *VEGFB*, *VEGFC*, and *VEGFD* in control and transfected SW40 cells, and the results indicated that only the expression of *VEGFC* was significantly decreased in si-*PIEZO2* SW480 cells (Fig. 3A). A recent study indicated that *SLIT2/ROBO1* signaling participates

in angiogenesis in a pathological context.²⁰ We analyzed the relationship between *SLIT2*, *ROBO1*, *VEGFC*, *HIF-1 α* , and *PIEZO2* using the online website CBioPortal for Cancer Genomics (<http://www.cbioportal.org/>). The obtained results showed that the mRNA expression of *PIEZO2* is positively correlated with the expression of *VEGFC*, *SLIT2*, *ROBO1*, and *HIF-1 α* (Fig. 3B–E). Furthermore, we assessed the protein and mRNA expression of *VEGFC*, *SLIT2*, *ROBO1*, and *HIF-1 α* in control and transfected SW40 cells, and found that *VEGFC*, *SLIT2*, *ROBO1*, and *HIF-1 α* were expressed at lower levels in transfected SW40 cells compared to the control SW40 cells (Fig. 3F,G).

Suppression of *PIEZO2* inhibits the growth of colon cancer in vivo

To determine the function of *PIEZO2* in tumor growth, we injected control and transfected SW480 cells

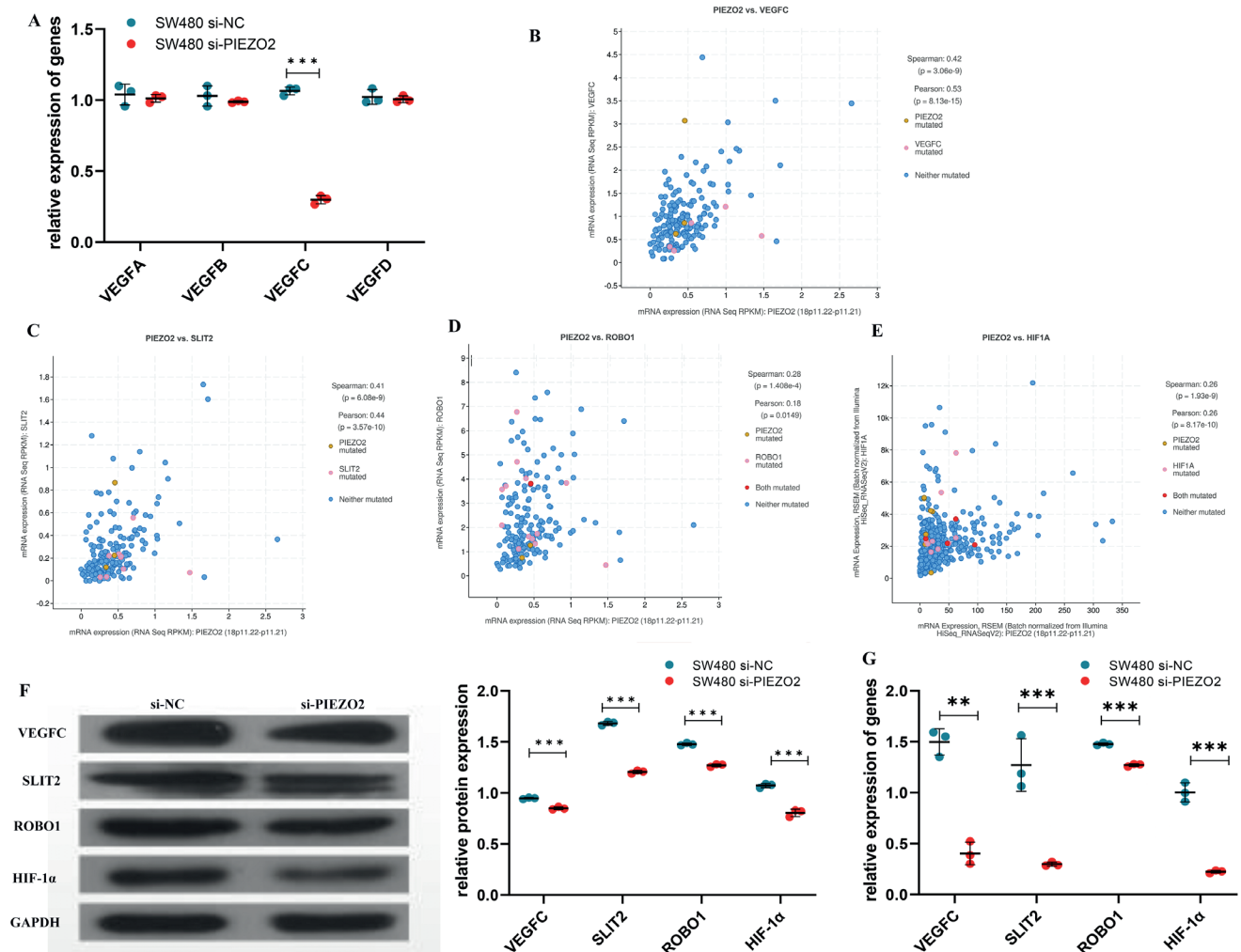


Fig. 3. *PIEZO2* is correlated with the *SLIT2/ROBO1/VEGFC* pathway. A. The expression of *VEGFA*, *VEGFB*, *VEGFC*, and *VEGFD* in negative control (NC) and si-*PIEZO2* SW480 cells was tested using quantitative reverse-transcription polymerase chain reaction (qRT-PCR). The differences were analyzed using the Student's t-test and expressed with mean \pm standard deviation ($M \pm SD$); B–E. Correlation between *PIEZO2* and *VEGFC*, *SLIT2*, *ROBO1*, and *HIF1A* was explored using the website CBioPortal for Cancer Genomics; F,G. The expression of *VEGFC*, *SLIT2*, *ROBO1*, and *HIF1A* in NC and si-*PIEZO2* SW480 cells were tested using western blot and qRT-PCR

** $p < 0.01$; *** $p < 0.001$.

subcutaneously into nude mice. As shown in Fig. 4A, tumors in control SW480 cell group grew faster and larger than those in transfected SW480 cell group. Consistent with the tumor volumes, the average tumor weight was clearly reduced (Fig. 4B). Moreover, the transfected SW480 cells showed a reduced expression of *Ki67* compared to the control group (Fig. 4C). Additionally, the group of transfected SW480 cells had a higher apoptosis index of tumor cells than the control group (Fig. 4D). Finally, we detected the expression of *VEGFC* in both groups. The results indicated that *VEGFC* expression in transfected SW480 cells was lower than in the control group (Fig. 4E).

Positive correlation exists between *PIEZO2* expression and cancer-associated fibroblasts

Recent studies have emphasized the role of cancer-associated fibroblasts (CAFs) in cancer progression and immune response. To explore the role of *PIEZO2* in CAFs, we analyzed the correlation between *PIEZO2* expression and CAFs using TIMER 2.0 (<http://timer.cistrome.org/>), and found that the expression of *PIEZO2* was positively correlated with CAFs in colon cancer (Fig. 5A). Then, we analyzed the expression markers of CAFs in colon cancer and discovered that *PIEZO2* expression was statistically associated with immune subtypes, including wound healing, interferon gamma (IFN- γ) dominant, inflammatory, lymphocyte depleted, and TGF- β dominant (Fig. 5B). Finally, we evaluated the role of *PIEZO2* in CAFs in the tumor immune single-cell hub (TISCH). The results indicated that the *PIEZO2* expression was positively correlated with CAFs in colon cancer (Fig. 5C).

Discussion

Our data provide evidence that *PIEZO2* expression increased in colon cancer and played a negative role in tumor survival. The results demonstrated that *PIEZO2* promoted the proliferation, migration and invasion of colon cancer cells, and the detailed mechanism may be related to the *SLIT2/ROBO1/VEGFC* pathway.

The *PIEZO* channels are a new class of mechanosensitive channels, mainly responsible for the induction to mechanical forces and the entry or exit of Ca^{2+} in cells.²¹ The *PIEZO* channels are large transmembrane proteins composed of more than 2500 amino acids and 24–36 putative transmembrane fragments, including *PIEZO1* and *PIEZO2* members. The *PIEZO* channels play an important physiological role in various mechanotransduction processes including touch, hearing and blood pressure perception in mammals. Recent evidence also suggested that *PIEZO1* was necessary for vascular development and function, and lineage choice of neural stem cells.²² The *PIEZO2* plays an essential role in sensory transmission

such as touch, mechanical proprioception, and gastrointestinal^{23,24} and respiratory physiology. Moreover, some studies reported that *PIEZO* family made paramount contributions to the skeletal system, mainly in bone formation and mechanically stimulated bone homeostasis.^{25,26}

Mechanosensitive channels are necessary for mechanotransduction and are frequently lodged on the cell surface. Our results also confirmed that *PIEZO2* is mainly expressed on the cell membranes of colon cells. The *PIEZO* channels play an important role in the pathogenesis of various diseases. Mechanical stress promoted stem cell differentiation by *PIEZO* channels in the adult *Drosophila* midgut, and this process was related to increased cytosolic Ca^{2+} levels caused by a direct mechanical stimulus.²⁷ In fibrotic tissues, mechanical signaling regulated the interactions between cells and the ECM through discoidin domain receptor 1.²⁸ However, several different cells sensed the stiffness of the surrounding substrate and responded to light by *PIEZO*s.²⁹ Stiffness may regulate the expression of matricellular protein *CCN1/CYR61* in endothelial cells after the tumor invasion, indicating that stiffness-induced changes are a potential target for impairing tumor metastasis.³⁰

Some studies have suggested that *PIEZO2* participates in the occurrence and development of malignant tumors. One study identified high expression of *PIEZO2* in breast cancer and revealed that patients with elevated expression of *PIEZO2* had a favorable prognosis in breast cancer.³¹ However, another study reported that the expression of *PIEZO2* was clearly reduced in non-small-cell lung cancer (NSCLC) tissue and high expression of *PIEZO2* correlated with better OS in NSCLC, especially in the adenocarcinoma subgroup.³² According to a recent study, *PIEZO2* significantly increased in bladder cancer tissue, indicating that *PIEZO2* dysfunction may contribute to the carcinogenesis of bladder cancer by causing proliferative changes and angiogenesis.¹⁰ Our results indicated that *PIEZO2* was highly expressed in colon cancer and correlated with poor prognosis, which is consistent with previous results.

As far as we know, when solid tumors grow beyond a certain size, they require angiogenesis to supply nutrients. In this process, some inflammatory and cell factors are involved.³³ Yang et al. reported that *PIEZO2* increased angiogenesis and vascular hyperpermeability in endothelial cells, and $Ca^{2+}/Wnt11/\beta$ -catenin signaling played an important role in this process.⁹ Another study suggested that intracellular Ca^{2+} signaling promoted angiogenesis and vasculogenesis by enhancing the functions of vascular endothelial cells (VECs) and endothelial colony-forming cells, which is linked to an increase in the expression of *PIEZO2*.³⁴ Therefore, these studies indicate that *PIEZO2* is involved in angiogenesis. In this study, we found that the expression of *VEGFC* was changing along with *PIEZO2* expression, which was verified by the level of mRNA, protein and in vivo studies. The *VEGFC* is a member of *VEGF* family and plays an important role in lymphangiogenesis. The *VEGFC* stimulates the formation of new lymph vessels and provides

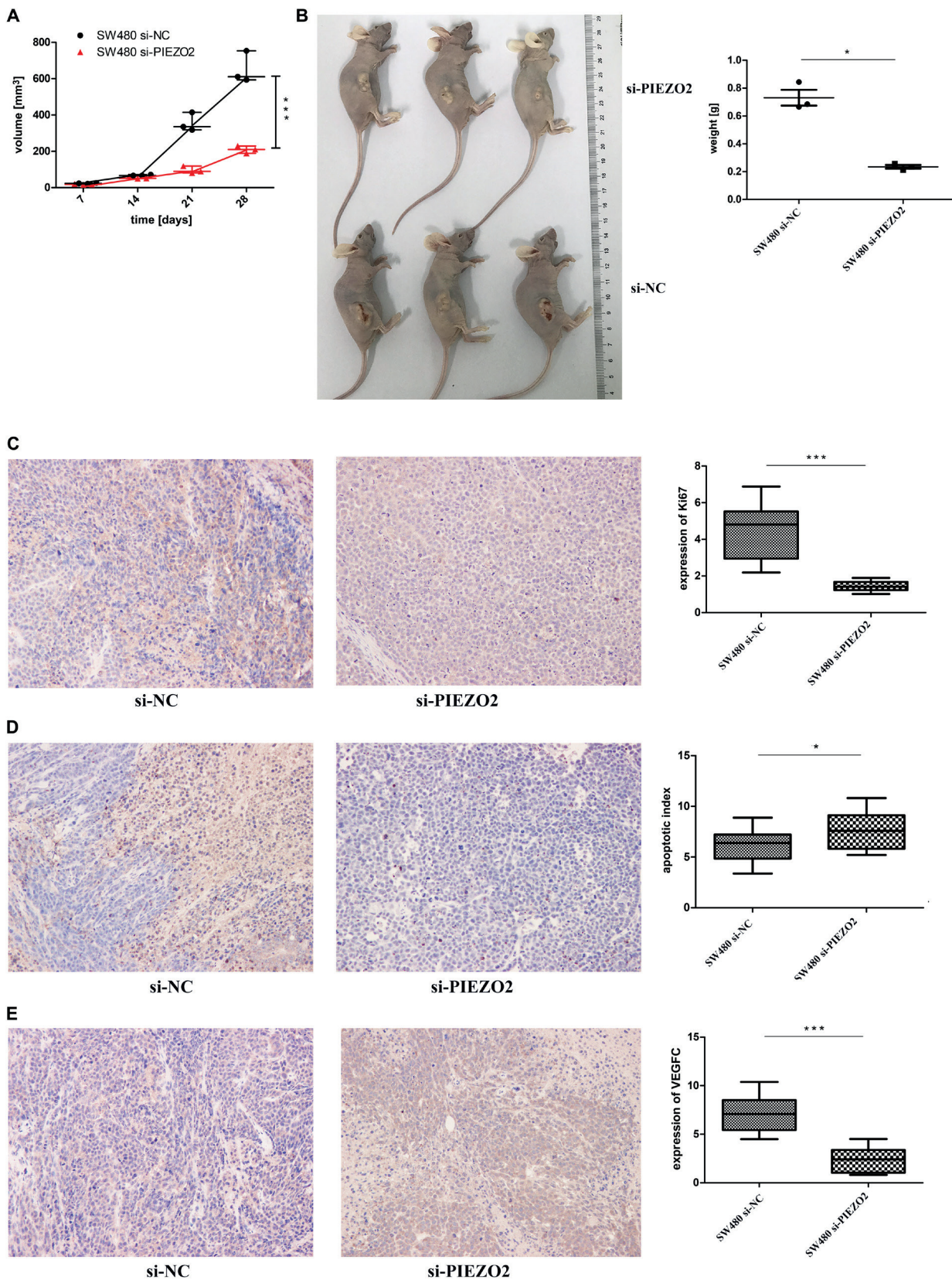


Fig. 4. Suppression of *PIEZO2* significantly inhibits the growth of colon cancer in vivo. The negative control (NC) or si-*PIEZO2* SW480 cells (2×10^6) in 0.1 mL of culture medium were injected subcutaneously into the right scapular region of nude mice to evaluate the antitumor activity of *PIEZO2* in vivo (3 mice per group). The tumor size was measured every 7 days using the formula $A \times B^2 \times 0.5236$, where A is the length and B is the width of the tumor; all measurements were recorded in millimeters. When the bearing tumors were approx. 1 cm³ in size, all mice were sacrificed, and tissue specimens were weighed and fixed in formalin for paraffin embedding. **A.** Tumor volumes were measured every 7 days using caliper measurements. The differences between the 2 groups were compared using the Scheirer–Ray–Hare test and expressed as median (range); **B.** The difference in tumor weight between the 2 groups was analyzed using the Student's t-test and expressed as mean \pm standard deviation ($M \pm SD$); **C.** Proliferation analysis of tumor tissues was performed using *Ki67* immunohistochemical staining, and the difference between the 2 groups was evaluated using the Student's t-test and expressed as $M \pm SD$; **D.** Apoptosis analysis of tumor tissues was performed using the terminal deoxynucleotidyl transferase dUTP nick end labeling (TUNEL) assay. The differences between the 2 groups were compared using the Student's t-test and expressed as $M \pm SD$; **E.** *VEGFC* expression was tested with immunohistochemical staining. The differences between the 2 groups were compared using the Student's t-test and expressed as $M \pm SD$

* $p < 0.05$; *** $p < 0.001$.

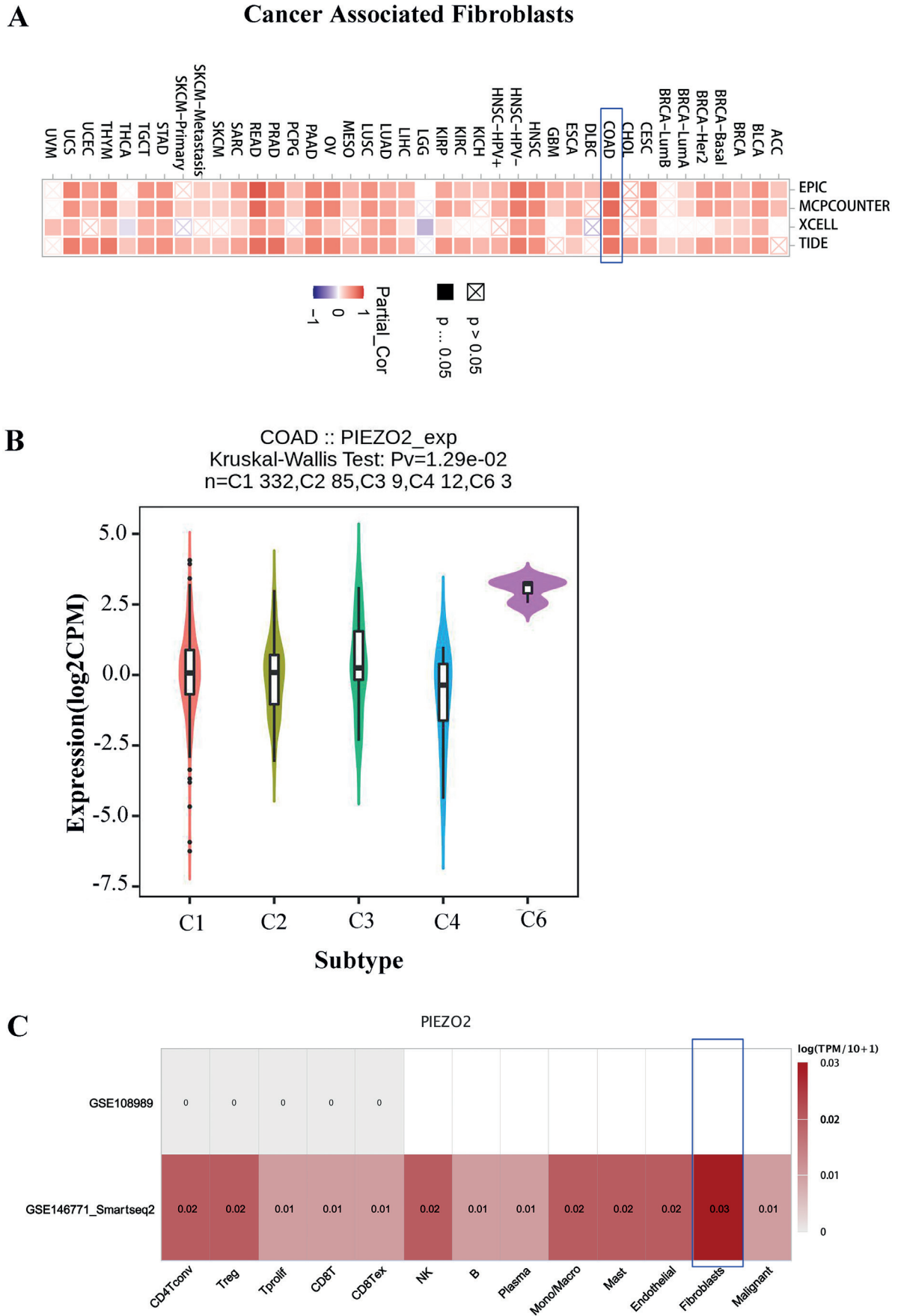


Fig. 5. Positive correlation between *PIEZO2* expression and cancer-associated fibroblasts (CAFs). A. *PIEZO2* expression level in immune subtypes in colon adenocarcinoma (COAD) based on tumor-immune system interactions database (TISIDB) (<http://cis.hku.hk/TISIDB/>); C. Correlation between *PIEZO2* expression in single-cell sequencing and CAFs using the tumor immune single-cell hub (TISCH)

a chance for detached cancer cells to metastasize to a distant site.³⁵ The *VEGFC* can promote the immune escape in colon cancer by activating *VEGFR3*, which results in tumor growth.³⁶ Moreover, our results suggest that *PIEZO2* is linked to the *SLIT2/ROBO1* pathway. Additionally, some studies reported that the *SLIT2/ROBO1* signaling participates in the process of angiogenesis.^{20,37} Overall, our results suggest that *PIEZO2* plays an antiangiogenic role through the *SLIT2/ROBO1/VEGFC* pathway. However, the detailed mechanism is needed to be explored further.

Currently, the tumor microenvironment (TME) is a trending topic in tumor research. Among numerous components of TME, CAFs play an important role in regulating tumorigenesis. Affo et al. found that a pan-CAF signature was significantly associated with poor survival in cholangiocarcinoma and tumor recurrence.³⁸ Another study found that when pancreatic cancer cells were co-cultured with CAFs, cancer stemness increased.³⁹ A recent study suggested that CAFs are the primary source of TIMP-1, and TIMP-1 production is enhanced through cancer–stromal interaction, which promotes cancer cell migration.⁴⁰ Regarding colon cancer, one study suggested that increased *RAB31* expression in CAFs may contribute to tumor progression by regulating hepatocyte growth factor (HGF) secretion in the tumor stoma.⁴¹ Our study showed that the expression of *PIEZO2* positively correlates with CAFs in colon cancer, indicating that *PIEZO2* is a prognostic factor of the disease. Recently, 6 immune subtypes were identified by immunogenomic data from 33 different types of cancer.⁴² This classification method can distinguish the beneficiaries of immune targeted therapy from multiple heterogeneous tumors. In this study, *PIEZO2* was significantly and aberrantly expressed in C1, C2, C3, C4, and C6 of colon cancer, suggesting that *PIEZO2* might have potential in cancer immune therapy. Moreover, the positive correlation between *PIEZO2* expression and CAFs was further validated using a single-cell sequencing dataset. However, the underlying mechanism of *PIEZO2* regulating CAFs requires further study.

Limitations

There are some shortcomings of our study that are worth considering. First, the sample size of clinical patients was relatively small. A large sample study would be needed to validate the results of our study. Second, the detailed mechanism of *PIEZO2* regulating *SLIT2/ROBO1/VEGFC* pathway had not been explored. This may be the direction of our further research.

Conclusions

The *PIEZO2* is highly expressed and is a poor prognostic factor in colon cancer. Moreover, *PIEZO2* can promote cell proliferation and mobility in colon carcinoma

through the *SLIT2/ROBO1/VEGFC* pathway. At the same time, *PIEZO2* is positively correlated with CAFs, indicating that it plays an important role in the CAF function. Therefore, *PIEZO2* may be a potential target for colon cancer treatment.

Supplementary data

The supplementary files are available at <https://doi.org/10.5281/zenodo.7428254>. The package contains the following files:

Supplementary Table 1. Results of χ^2 phi test for Fig. 1B.

Supplementary Table 2. Results of the log-rank test for Fig. 1C.

Supplementary Table 3. Results of the normality test for Fig. 2D.

Supplementary Table 4. Results of the Student's t-test for Fig. 2D.

Supplementary Table 5. Results of the normality test for Fig. 2E.

Supplementary Table 6. Results of the Scheirer–Ray–Hare test for Fig. 2E.

Supplementary Table 7. Results of the normality test for Fig. 2F.

Supplementary Table 8. Results of the Student's t-test for Fig. 2F.

Supplementary Table 9. Results of the normality test for Fig. 2G.

Supplementary Table 10. Results of the Student's t-test for Fig. 2G.

Supplementary Table 11. Results of the normality test for Fig. 2H.

Supplementary Table 12. Results of the Student's t-test for Fig. 2H.

Supplementary Table 13. Results of the normality test for Fig. 3A.

Supplementary Table 14. Results of the Student's t-test for Fig. 3A.

Supplementary Table 15. Results of the normality test for Fig. 3F.

Supplementary Table 16. Results of the Student's t-test for Fig. 3F.

Supplementary Table 17. Results of the normality test for Fig. 3G.

Supplementary Table 18. Results of the Student's t-test for Fig. 3G.

Supplementary Table 19. Results of the normality test for Fig. 4A.

Supplementary Table 20. Results of the Scheirer–Ray–Hare test Fig. 4A.

Supplementary Table 21. Results of the normality test for Fig. 4B.

Supplementary Table 22. Results of the Student's t-test for Fig. 4B.

Supplementary Table 23. Results of the normality test for Fig. 4C.

Supplementary Table 24. Results of the Student's t-test for Fig. 4C.

Supplementary Table 25. Results of the normality test for Fig. 4D.

Supplementary Table 26. Results of the Student's t-test for Fig. 4D.

Supplementary Table 27. Results of the normality test for Fig. 4E.

Supplementary Table 28. Results of the Student's t-test for Fig. 4E.

Supplementary Table 29. Results of Spearman's correlation analysis for Table 2.

Supplementary Table 30. Results of Kendall's tau-b correlation analysis for Table 2.

Supplementary Table 31. Results of Schoenfeld residuals for Table 3.

Supplementary Table 32. Results of the univariate analysis for Table 3.

Supplementary Table 33. Results of the multivariate analysis for Table 3.


ORCID iDs


Haotian Shang  <https://orcid.org/0000-0002-5057-5924>

Aiguo Xu  <https://orcid.org/0000-0002-1131-7391>

Haicui Yan  <https://orcid.org/0000-0002-4644-6628>

Dandan Xu  <https://orcid.org/0000-0002-2555-9279>

Jingyu Zhang  <https://orcid.org/0000-0002-8381-2973>

Xinjian Fang  <https://orcid.org/0000-0002-0366-5521>

References

- Sung H, Ferlay J, Siegel RL, et al. Global cancer statistics 2020: GLOBOCAN estimates of incidence and mortality worldwide for 36 cancers in 185 countries. *CA Cancer J Clin*. 2021;71(3):209–249. doi:10.3322/caac.21660
- Lee RM, Cardona K, Russell MC. Historical perspective: Two decades of progress in treating metastatic colorectal cancer. *J Surg Oncol*. 2019;119(5):549–563. doi:10.1002/jso.25431
- Willyard C. Cancer therapy: An evolved approach. *Nature*. 2016;532(7598):166–168. doi:10.1038/532166a
- De Felice D, Alaimo A. Mechanosensitive piezo channels in cancer: Focus on altered calcium signaling in cancer cells and in tumor progression. *Cancers (Basel)*. 2020;12(7):1780. doi:10.3390/cancers12071780
- Martino F, Perestrelo AR, Vinarský V, Pagliari S, Forte G. Cellular mechanotransduction: From tension to function. *Front Physiol*. 2018;9:824. doi:10.3389/fphys.2018.00824
- Coste B, Xiao B, Santos JS, et al. Piezo proteins are pore-forming subunits of mechanically activated channels. *Nature*. 2012;483(7388):176–181. doi:10.1038/nature10812
- Gottlieb PA, Bae C, Sachs F. Gating the mechanical channel Piezo1: A comparison between whole-cell and patch recording. *Channels*. 2012;6(4):282–289. doi:10.4161/chan.21064
- Yang XN, Lu YP, Liu JJ, et al. Piezo1 is as a novel trefoil factor family 1 binding protein that promotes gastric cancer cell mobility in vitro. *Dig Dis Sci*. 2014;59(7):1428–1435. doi:10.1007/s10620-014-3044-3
- Yang H, Liu C, Zhou RM, et al. Piezo2 protein: A novel regulator of tumor angiogenesis and hyperpermeability. *Oncotarget*. 2016;7(28):44630–44643. doi:10.18632/oncotarget.10134
- Etem E, Ceylan G, Özyayın S, Ceylan C, Özercan I, Kuloğlu T. The increased expression of Piezo1 and Piezo2 ion channels in human and mouse bladder carcinoma. *Adv Clin Exp Med*. 2018;27(8):1025–1031. doi:10.17219/acem/71080
- Chen X, Wanggou S, Bodalia A, et al. A feedforward mechanism mediated by mechanosensitive ion channel PIEZO1 and tissue mechanics promotes glioma aggression. *Neuron*. 2018;100(4):799.e7–815.e7. doi:10.1016/j.neuron.2018.09.046
- Pardo-Pastor C, Rubio-Moscardo F, Vogel-González M, et al. Piezo2 channel regulates RhoA and actin cytoskeleton to promote cell mechanobiological responses. *Proc Natl Acad Sci USA*. 2018;115(8):1925–1930. doi:10.1073/pnas.1718177115
- Mertsch S, Schmitz N, Jeibmann A, Geng JG, Paulus W, Senner V. Slit2 involvement in glioma cell migration is mediated by Robo1 receptor. *J Neurooncol*. 2008;87(1):1–7. doi:10.1007/s11060-007-9484-2
- Xia Y, Wang L, Xu Z, et al. Reduced USP33 expression in gastric cancer decreases inhibitory effects of Slit2-Robo1 signaling on cell migration and EMT. *Cell Prolif*. 2019;52(3):e12606. doi:10.1111/cpr.12606
- Ahirwar DK, Peng B, Charan M, et al. Slit2/Robo1 signaling inhibits small cell lung cancer by targeting β -catenin signaling in tumor cells and macrophages [published online as ahead of print on July 15, 2022]. *Mol Oncol*. 2022. doi:10.1002/1878-0261.13289
- Yao Y, Zhou Z, Li L, et al. Activation of Slit2/Robo1 signaling promotes tumor metastasis in colorectal carcinoma through activation of the TGF- β /Smads pathway. *Cells*. 2019;8(6):635. doi:10.3390/cells8060635
- Tan Q, Liang XJ, Lin SM, et al. Engagement of Robo1 by Slit2 induces formation of a trimeric complex consisting of Src-Robo1-E-cadherin for E-cadherin phosphorylation and epithelial-mesenchymal transition. *Biochem Biophys Res Commun*. 2020;522(3):757–762. doi:10.1016/j.bbrc.2019.11.150
- Gu Y, Li X, Bi Y, et al. CCL14 is a prognostic biomarker and correlates with immune infiltrates in hepatocellular carcinoma. *Aging*. 2020;12(1):784–807. doi:10.18632/aging.102656
- Tian Y, Zhou Y, Liu J, et al. Correlation of SIRT1 with poor prognosis and immune infiltration in patients with non-small cell lung cancer. *Int J Gen Med*. 2022;15:803–816. doi:10.2147/IJGM.S347171
- Liu J, Hou W, Guan T, et al. Slit2/Robo1 signaling is involved in angiogenesis of glomerular endothelial cells exposed to a diabetic-like environment. *Angiogenesis*. 2018;21(2):237–249. doi:10.1007/s10456-017-9592-3
- Xu XZS. Demystifying mechanosensitive piezo ion channels. *Neurosci Bull*. 2016;32(3):307–309. doi:10.1007/s12264-016-0033-x
- Qin L, He T, Chen S, et al. Roles of mechanosensitive channel Piezo1/2 proteins in skeleton and other tissues. *Bone Res*. 2021;9(1):44. doi:10.1038/s41413-021-00168-8
- Bai T, Li Y, Xia J, et al. Piezo2: A candidate biomarker for visceral hypersensitivity in irritable bowel syndrome? *J Neurogastroenterol Motil*. 2017;23(3):453–463. doi:10.5056/jnm16114
- Wang F, Knutson K, Alcaïno C, et al. Mechanosensitive ion channel Piezo2 is important for enterochromaffin cell response to mechanical forces: Piezo2 in EC cells. *J Physiol*. 2017;595(1):79–91. doi:10.1113/JP272718
- Zhou T, Gao B, Fan Y, et al. Piezo1/2 mediate mechanotransduction essential for bone formation through concerted activation of NFAT-YAP1- β -catenin. *eLife*. 2020;9:e52779. doi:10.7554/eLife.52779
- Wang L, You X, Lotinun S, Zhang L, Wu N, Zou W. Mechanical sensing protein PIEZO1 regulates bone homeostasis via osteoblast-osteoclast crosstalk. *Nat Commun*. 2020;11(1):282. doi:10.1038/s41467-019-14146-6
- He L, Si G, Huang J, Samuel ADT, Perrimon N. Mechanical regulation of stem-cell differentiation by the stretch-activated Piezo channel. *Nature*. 2018;555(7694):103–106. doi:10.1038/nature25744
- Coelho NM, McCulloch CA. Mechanical signaling through the discoidin domain receptor 1 plays a central role in tissue fibrosis. *Cell Adh Migr*. 2018;12(4):348–362. doi:10.1080/19336918.2018.1448353
- Gottlieb PA. A tour de force: The discovery, properties and function of piezo channels. *Curr Top Membr*. 2017;79:1–36. doi:10.1016/bs.ctm.2016.11.007
- Reid SE, Kay EJ, Neilson LJ, et al. Tumor matrix stiffness promotes metastatic cancer cell interaction with the endothelium. *EMBO J*. 2017;36(16):2373–2389. doi:10.15252/embj.201694912
- Lou W, Liu J, Ding B, et al. Five miRNAs-mediated PIEZO2 down-regulation, accompanied with activation of Hedgehog signaling pathway, predicts poor prognosis of breast cancer. *Aging*. 2019;11(9):2628–2652. doi:10.18632/aging.101934
- Huang Z, Sun Z, Zhang X, et al. Loss of stretch-activated channels, PIEZO2, accelerates non-small cell lung cancer progression and cell migration. *Biosci Rep*. 2019;39(3):BSR20181679. doi:10.1042/BSR20181679
- Carmeliet P, Jain RK. Molecular mechanisms and clinical applications of angiogenesis. *Nature*. 2011;473(7347):298–307. doi:10.1038/nature10144

34. Moccia F. Endothelial Ca²⁺ signaling and the resistance to anticancer treatments: Partners in crime. *Int J Mol Sci.* 2018;19(1):217. doi:10.3390/ijms19010217
35. Ellis LM, Hicklin DJ. VEGF-targeted therapy: Mechanisms of anti-tumour activity. *Nat Rev Cancer.* 2008;8(8):579–591. doi:10.1038/nrc2403
36. Tacconi C, Ungaro F, Correale C, et al. Activation of the VEGFC/VEGFR3 pathway induces tumor immune escape in colorectal cancer. *Cancer Res.* 2019;79(16):4196–4210. doi:10.1158/0008-5472.CAN-18-3657
37. Romano E, Manetti M, Rosa I, et al. Slit2/Robo4 axis may contribute to endothelial cell dysfunction and angiogenesis disturbance in systemic sclerosis. *Ann Rheum Dis.* 2018;77(11):1665–1674. doi:10.1136/annrheumdis-2018-213239
38. Affo S, Nair A, Brundu F, et al. Promotion of cholangiocarcinoma growth by diverse cancer-associated fibroblast subpopulations. *Cancer Cell.* 2021;39(6):883. doi:10.1016/j.ccell.2021.03.012
39. Nallasamy P, Nimmakayala RK, Karmakar S, et al. Pancreatic tumor microenvironment factor promotes cancer stemness via SPP1–CD44 axis. *Gastroenterology.* 2021;161(6):1998.e7–2013.e7. doi:10.1053/j.gastro.2021.08.023
40. Nakai N, Hara M, Takahashi H, et al. Cancer cell-induced tissue inhibitor of metalloproteinase-1 secretion by cancer-associated fibroblasts promotes cancer cell migration. *Oncol Rep.* 2022;47(6):112. doi:10.3892/or.2022.8323
41. Yang T, Zhiheng H, Zhanhui W, et al. Increased RAB31 expression in cancer-associated fibroblasts promotes colon cancer progression through HGF-MET signaling. *Front Oncol.* 2020;10:1747. doi:10.3389/fonc.2020.01747
42. Thorsson V, Gibbs DL, Brown SD, et al. The immune landscape of cancer. *Immunity.* 2018;48(4):812.e14–830.e14. doi:10.1016/j.immuni.2018.03.023

A novel mutation in collagen transport protein, *MIA3* gene, detected in a patient with clinical symptoms of Ehlers–Danlos hypermobile syndrome

Anna Junkiert-Czarnecka^{A,C,D}, Maria Pilarska-Deltow^{B,C}, Aneta Bąk^{B,C}, Marta Heise^{B,C}, Olga Haus^{D–F}

Department of Clinical Genetics Nicolaus Copernicus University, Toruń, Poland

A – research concept and design; B – collection and/or assembly of data; C – data analysis and interpretation; D – writing the article; E – critical revision of the article; F – final approval of the article

Advances in Clinical and Experimental Medicine, ISSN 1899–5276 (print), ISSN 2451–2680 (online)

Adv Clin Exp Med. 2023;32(7):777–781

Address for correspondence

Anna Junkiert-Czarnecka
E-mail: ajczarnecka@cm.umk.pl

Funding sources

This investigation was supported by a grant from National Science Centre, Poland (grant No. 2018/29/N/NZ5/00345).

Conflict of interest

None declared

Acknowledgements

We would like to thank all patients tested in this investigation.

Received on October 25, 2022

Reviewed on November 8, 2022

Accepted on December 21, 2022

Published online on January 5, 2023

Abstract

Background. Collagen, the most abundant human protein, is a significant component of the extracellular matrix (ECM) in tissues and organs like skin, bone, ligaments, and tendons. Collagen secretion is a complex, multistage process involving many molecules. A protein playing one of the main functions in this process is TANGO1 encoded by *MIA3* gene. In the hypermobile type of Ehlers–Danlos syndrome (hEDS), one of the most common collagenopathies with no known genetic background, disrupted secretion of many molecules (including collagen) was observed.

Objectives. The aim of this study was the evaluation of the *MIA3* gene role in hEDS patients.

Materials and methods. One hundred patients with clinically diagnosed hEDS and negative next-generation sequencing (NGS) testing for connective tissue disorder (e.g. Ehlers–Danlos syndrome, osteogenesis imperfect (OI), Marfan syndrome, and others) were tested for molecular changes in the *MIA3* gene.

Results. Among the 100 tested patients, 14 single structural changes in the *MIA3* gene were detected. Thirteen were missense benign or likely benign, while 1 variant (c.567dup, p.Leu1880ThrfsTer6) was truncating the TANGO1 protein.

Conclusions. We suppose that the presence of truncating variant (c.567dup) in the *MIA3* gene and disrupted secretion of connective tissue protein may be one of the pathogenic mechanisms of clinical symptoms present in the tested patient, but these findings require a more comprehensive multidimensional investigation.

Key words: NGS, hypermobility, Ehlers–Danlos syndrome, *MIA3*, TANGO1

Cite as

Junkiert-Czarnecka A, Pilarska-Deltow M, Bąk A, Heise M, Haus O. A novel mutation in collagen transport protein, *MIA3* gene, detected in a patient with clinical symptoms of Ehlers–Danlos hypermobile syndrome. *Adv Clin Exp Med.* 2023;32(7):777–781. doi:10.17219/acem/158028

DOI

10.17219/acem/158028

Copyright

Copyright by Author(s)

This is an article distributed under the terms of the Creative Commons Attribution 3.0 Unported (CC BY 3.0) (<https://creativecommons.org/licenses/by/3.0/>)

Background

Collagen, the most abundant human protein, is a major component of the extracellular matrix (ECM) in tissues and organs like skin, bone, ligaments, tendons, arteries, veins, as well as the gastrointestinal and respiratory systems. All human proteins, including collagen, require proper protein folding, maturation and secretion processes. Collagen biosynthesis is a complex, multistage process involving many molecules. It takes place in the rough endoplasmic reticulum (rER). In the lumen of the rER, collagen molecule undergoes a series of post-translational modifications, e.g., hydroxylation and glycosylation. Then, the collagen molecule is transported via the Golgi apparatus to the extracellular space.¹

Efficient transport of procollagen molecules from the rER to the Golgi apparatus involves a special protein transport complex. Procollagen folded in the rER has ~300 nm in length, which is too large to fit conventional coat protein complex II (COPII) vesicles (vesicles have approx. 60–80 nm in diameter).¹ For the secretion of large molecules, another trafficking system is required. Saito et al. showed that transmembrane protein transport and Golgi organization (TANGO1; NP_940953.2), encoded by *MIA3* (NM_198551.4) gene, facilitates the entrance of collagen into COPII vesicles at the rER exit site.² TANGO1 is a protein of 1907 amino acids composed of the SH3 domain (N-terminus) that binds collagen molecules, 2 coiled-coil domains (CC1 and CC2), and the proline-rich domain (PRD), which all assist in the formation of collagen-like COPII vesicles (C-terminus) and play a significant role in interactions between the endoplasmic reticulum and the COPII components (Sec23/Sec24). Shortening of this TANGO1 domain may disrupt vesicle formation and result in a reduction of the capability of collagen and other ECM protein transport.^{2–4}

The potential function of the TANGO1 molecule was assessed by Wilson et al. in a study on knockout mice. Their analysis revealed that secretion of numerous collagens, including collagen type I, II, III, IV, VII, and IX, from fibroblasts to the ECM was disrupted, most likely because of the defective export of these molecules from the endoplasmic reticulum.⁵ The major role of TANGO1 in collagen molecule transport was also confirmed by Raote et al. and Ishikawa et al.^{4,6}

Ehlers–Danlos syndrome (EDS) is a heterogeneous group of heritable connective tissue disorders. The 2017 international classification of EDS recognizes 13 subtypes that are caused by pathogenic variants in 19 different genes, encoding different types of collagen or protein involved in collagen metabolism or functioning. For all types of EDS, the genetic background was determined, except the hypermobile type of EDS (hEDS), which is one of the most common connective tissue disorders.⁷ Despite intensive investigation, genes related to hEDS have not been identified yet.

Studying hEDS patients, Chiarelli et al. assessed the presence of some ECM proteins inside and outside fibroblasts. The study showed that ECM proteins, especially collagen type I, III and V, as well as fibrillin, tenascin and fibronectin, were detected only in the cell cytoplasm of hEDS patients, while in the intercellular space they were either not visible or only a few thin, sparse fibrils were present. Contrarily, in the healthy control group, these proteins were visible inside and outside cells.⁸ Abnormality in ECM transport protein may be one of the components of the molecular background of clinical symptoms of hEDS. The cause of dysfunction of ECM protein transport from cytoplasm to the intracellular space in hEDS patients is unknown. In the ECM protein transport pathway, many molecules are involved, and one of them may be the TANGO1 protein.

Objectives

The aim of this study was the evaluation of the role of *MIA3* gene role in hEDS patients.

Materials and methods

The study group included 100 hEDS patients of Polish origin, 84 women and 16 men, aged 17–63 years (median: 31 years). Patients were enrolled in the study by experienced clinical geneticists, according to the 2017 international classification of the EDS diagnostic criteria.⁷ Joint hypermobility was evaluated on the Beighton scale. Patients were not related. The control group consisted of 100 volunteers from the general Polish population matched by age and sex with the investigated group, healthy (including lack of EDS) at the time of the investigation and without a history of EDS in the family. Enrollment in the control group was based on volunteers' medical history.

All hEDS patients or their parents provided informed consent to participate in the study. Consent to publish clinical/genetics data has been obtained from the patients.

The study was approved by the Ethics Committee of the Collegium Medicum in Bydgoszcz, Nicolaus Copernicus University, Toruń, Poland (approval No. KB485/2013).

The analysis was performed on genomic DNA (gDNA) which was extracted from leukocytes (fibroblasts were not available) with QIAamp DNA Mini Kit (Qiagen, Hilden, Germany) using standard procedures. In all patients, other types of EDS or other connective tissue disorders were excluded by testing them with NGS technology (Illumina, San Diego, USA). The connective tissue congenital defects panel included *COL5A1*, *COL5A2*, *COL3A1*, *COL1A1*, *COL1A2*, *HSP47*, *TNXB*, *ADAMTS2*, *PLOD1*, *FKBP14*, *ZNF469*, *PRDM5*, *B4GALT7*, *B3GALT6*, *SLC39A13*, *CHST14*, *DSE*, *COL12A1*, *C1R*, *C1S*, *SEC23A*, *SEC24D*, *COL6A1*, *COL6A2*, *COL6A3*, *COL9A1*, *COL9A2*, *FBN1*,

FBN2, *FLNA*, *FLNB*, *ELN*, *NOTCH1*, *MYH11*, *MYLK*, *TGFB2*, *TGFB3*, and *TGFBR1*. Copy number variations (CNV) analysis was also performed.

Molecular analysis of all exons of the *MIA3* gene was performed with Sanger sequencing according to standard procedure (primer sequences available upon request). The pathogenicity of detected variants was assessed according to the ACMG guideline released by VarSome.^{9,10}

Results

All patients were tested using NGS multi-gene panel for connective tissue disorders, EDS, osteogenesis imperfect (OI), Marfan syndrome, and others. In any of them, no pathogenic or likely pathogenic variants were detected. Copy number variations were also not detected. The next step of the investigation was the sequencing of the *MIA3* gene using Sanger sequencing. In 14 patients among 100, 5 variants in *MIA3* were detected. Four of 5 alterations were missense variants (benign or likely benign) and 1 was a frameshift variant assessed as a likely pathogenic (class 4 according to ACMG) (Table 1). All found alterations were heterozygotes. The variants were not detected in the control group.

Frameshift variant c.5637dup, which results in termination of transcription (p.Leu1880ThrfsTer6), was found in a 49-year-old woman. She presented with hypermobility of joints (7/9 Beighton score), recurrent dislocations, arachnodactyly, chronic severe joints and spinal pain since childhood, fatigue, soft, mild, hyperextensible and easy bruising skin, stretch marks, brain aneurysm, astigmatism, blue sclerae, hyperopia, dry eyes, many food products intolerances, and a positive family history. Her 14-year-old

daughter suffered from hypermobility (9/9 Beighton score), chronic joint pain, scoliosis, soft and mild hyperextensible skin, and blue sclerae. The first symptoms occurred earlier (at about 10 years of age) and in a more severe form than in her mother. She was also a carrier of the c.5637dup *MIA3* variant.

The proband and her daughter were first clinically diagnosed with rheumatoid arthritis. Later on, the disorder was excluded. Both were of normal height (mother 174 cm, daughter 165 cm), and both also had a normal bone density. Proband's parents were not tested (they did not consent to participate in the study). However, proband indicated that her mother had symptoms similar to her own but in a milder form and with onset in older age (Fig. 1).

Discussion

MIA3 gene encodes a transmembrane protein which plays an important role in the transport of different proteins from fibroblasts and chondrocytes to extracellular space. In an investigation by Wilson et al., mice lacking TANGO1 protein displayed neonatal lethality with a chondrodysplasia, lack of bone mineralization, dwarfism, and defective secretion of numerous collagens (including collagen type I, II, III, IV, VII, and IX).⁵ Recently, Lekszas et al. identified a homozygous synonymous variant in *MIA3* (c.3621A>G, p.Arg1207=) that leads to exon 8 skipping, which results in truncating of TANGO1 protein. The affected patient presented with various skeletal abnormalities including short stature, scoliosis, osteopenia, brachydactyly and clinodactyly, dentinogenesis imperfecta, and mild intellectual disability. Another observation was a drastic reduction of collagen I secretion from

Table 1. Variants detected in the *MIA3* gene

No.	Patient assigned lab number	Nucleotide	Amino acid	ExAC frequency
1.	46	c.1099A>T	p.(Thr367Ser)	T = 0.78%
2.	148	c.1099A>T	p.(Thr367Ser)	T = 0.78%
3.	61	c.1099A>T	p.(Thr367Ser)	T = 0.78%
4.	62	c.1099A>T	p.(Thr367Ser)	T = 0.78%
5.	63	c.1099A>T	p.(Thr367Ser)	T = 0.78%
6.	68	c.1099A>T	p.(Thr367Ser)	T = 0.78%
7.	80	c.1099A>T	p.(Thr367Ser)	T = 0.78%
8.	140	c.1099A>T	p.(Thr367Ser)	T = 0.78%
9.	85	c.2566G>A	p.(Asp856Asn)	A = 0.01%
10.	24	c.2637C>A	p.(Asp879Glu)	A = 0.1%
11.	25	c.2637C>A	p.(Asp879Glu)	A = 0.1%
12.	26	c.2637C>A	p.(Asp879Glu)	A = 0.1%
13.	139	c.2687C>T	p.(Aln896Val)	T = 0.09%
14.	90	c.5637dup	p.Leu1880ThrfsTer6	dup = 0.001%

Conclusions

The role of *MIA3* or other genes involved in connective tissue protein secretion should be taken into account as potential etiological factors in connective tissue hereditary diseases, including hEDS; however, their role in the process requires much wider investigation.

ORCID iDs

Anna Junkiert-Czarnecka  <https://orcid.org/0000-0002-0067-2072>

Maria Pilarska-Deltow  <https://orcid.org/0000-0002-3171-8408>

Aneta Bąk  <https://orcid.org/0000-0001-8879-2521>

Marta Heise  <https://orcid.org/0000-0002-2201-6148>

Olga Haus  <https://orcid.org/0000-0002-5206-0553>

References

- Bonfanti L, Mironov AA, Martínez-Menárguez JA, et al. Procollagen traverses the Golgi stack without leaving the lumen of cisternae. *Cell*. 1998;95(7):993–1003. doi:10.1016/S0092-8674(00)81723-7
- Saito K, Chen M, Bard F, et al. TANGO1 facilitates cargo loading at endoplasmic reticulum exit sites. *Cell*. 2009;136(5):891–902. doi:10.1016/j.cell.2008.12.025
- Reynolds HM, Zhang L, Tran DT, Ten Hagen KG. Tango1 coordinates the formation of endoplasmic reticulum/Golgi docking sites to mediate secretory granule formation. *J Biol Chem*. 2019;294(51):19498–19510. doi:10.1074/jbc.RA119.011063
- Raote I, Ortega Bellido M, Pirozzi M, et al. TANGO1 assembles into rings around COPII coats at ER exit sites. *J Cell Biol*. 2017;216(4):901–909. doi:10.1083/jcb.201608080
- Wilson DG, Phamluong K, Li L, et al. Global defects in collagen secretion in a *Mia3/TANGO1* knockout mouse. *J Cell Biol*. 2011;193(5):935–951. doi:10.1083/jcb.201007162
- Ishikawa Y, Ito S, Nagata K, Sakai LY, Bächinger HP. Intracellular mechanisms of molecular recognition and sorting for transport of large extracellular matrix molecules. *Proc Natl Acad Sci U S A*. 2016;113(41):E6036–E6044. doi:10.1073/pnas.1609571113
- Malfait F, Francomano C, Byers P, et al. The 2017 international classification of the Ehlers–Danlos syndromes. *Am J Med Genet*. 2017;175(1):8–26. doi:10.1002/ajmg.c.31552
- Chiarelli N, Carini G, Zoppi N, et al. Transcriptome-wide expression profiling in skin fibroblasts of patients with joint hypermobility syndrome/Ehlers–Danlos syndrome hypermobility type. *PLoS One*. 2016;11(8):e0161347. doi:10.1371/journal.pone.0161347
- Kopanos C, Tsiolkas V, Kouris A, et al. VarSome: The human genomic variant search engine. *Bioinformatics*. 2019;35(11):1978–1980. doi:10.1093/bioinformatics/bty897
- Richards S, Aziz N, Bale S, et al. Standards and guidelines for the interpretation of sequence variants: A joint consensus recommendation of the American College of Medical Genetics and Genomics and the Association for Molecular Pathology. *Genet Med*. 2015;17(5):405–424. doi:10.1038/gim.2015.30
- Lekszas C, Foresti O, Raote I, et al. Biallelic TANGO1 mutations cause a novel syndromal disease due to hampered cellular collagen secretion. *eLife*. 2020;9:e51319. doi:10.7554/eLife.51319
- Guillemyn B, Nampoothiri S, Syx D, Malfait F, Symoens S. Loss of TANGO1 leads to absence of bone mineralization. *JBMR Plus*. 2021;5(3):e10451. doi:10.1002/jbm4.10451
- Clark EM, Link BA. Complementary and divergent functions of zebrafish Tango1 and Ctage5 in tissue development and homeostasis. *Mol Biol Cell*. 2021;32(5):391–401. doi:10.1091/mbc.E20-11-0745

Increased GPR35 expression in human colorectal and pancreatic cancer samples: A preliminary clinical validation of a new biomarker

Tomasz Mackiewicz^{1,4,A–D,F}, Jakub Włodarczyk^{1,2,B,C,F}, Marta Zielińska^{1,B,E,F}, Marcin Włodarczyk^{2,5,B,F}, Adam Durczyński^{3,B,F}, Piotr Hogendorf^{3,B,F}, Łukasz Dżiki^{2,5,B,F}, Jakub Fichna^{1,A,C,E,F}

¹ Department of Biochemistry, Faculty of Medicine, Medical University of Łódź, Poland

² Central Veterans' University Hospital, Clinic of General and Colorectal Surgery, Łódź, Poland

³ Norbert Barlicki Memorial Teaching Hospital No. 1, Clinic of General and Transplantation Surgery, Łódź, Poland

⁴ Roche Polska Sp. z o.o., Warsaw, Poland

⁵ Department of General and Oncological Surgery, Medical University of Łódź, Poland

A – research concept and design; B – collection and/or assembly of data; C – data analysis and interpretation;

D – writing the article; E – critical revision of the article; F – final approval of the article

Advances in Clinical and Experimental Medicine, ISSN 1899–5276 (print), ISSN 2451–2680 (online)

Adv Clin Exp Med. 2023;32(7):783–789

Address for correspondence

Jakub Fichna

E-mail: jakub.fichna@umed.lodz.pl

Funding sources

This research was funded by the Medical University of Lodz, Poland (grant No. #503/1-156-04/503-11-001-19 to JF).

Conflict of interest

None declared

Acknowledgements

TM participates in the program "Doktorat wdrożeniowy" of the Polish Ministry of Science and Education.

Received on June 24, 2022

Reviewed on July 8, 2022

Accepted on December 9, 2022

Published online on January 13, 2023

Cite as

Mackiewicz T, Włodarczyk J, Zielińska M, et al. Increased GPR35 expression in human colorectal and pancreatic cancer samples: A preliminary clinical validation of a new biomarker.

Adv Clin Exp Med. 2023;32(7):783–789.

doi:10.17219/acem/157291

DOI

10.17219/acem/157291

Copyright

Copyright by Author(s)

This is an article distributed under the terms of the Creative Commons Attribution 3.0 Unported (CC BY 3.0)

(<https://creativecommons.org/licenses/by/3.0/>)

Abstract

Background. G protein-coupled receptor 35 (GPR35) is involved in carcinogenesis; however, limited experimental data are available on its actual expression in patients with colorectal cancer (CRC) and pancreatic adenocarcinoma (PDAC).

Objectives. We aimed to measure the relative expression of GPR35 in samples from patients with CRC or PDAC.

Materials and methods. Using real-time polymerase chain reaction (RT-PCR), we have examined GPR35 expression in surgery samples from 40 CRC and 17 PDAC patients, and performed analysis of the results.

Results. The analysis of GPR35 expression in patients with CRC revealed correlations between relative GPR35 mRNA expression and several tumor characteristics, with statistical significance for higher American Joint Committee on Cancer (AJCC) stages, T stages and histological grades. GPR35 expression was significantly higher in tumor samples compared to the paired healthy samples collected from the same patient. Similar, although not statistically significant trends were found in PDAC tumor samples for sex (lower expression in women) and for samples with no nodal involvement (lower expression). Samples with higher tumor T stages and higher histological grades or considered inoperable had higher GPR35 expression.

Conclusions. We have identified correlations which confirm our expectation of high GPR35 expression in CRC and PDAC. Our findings suggest the prognostic value of GPR35 testing in patients with an increased risk of CRC or PDAC development, and warrant further clinical confirmation.

Key words: colorectal cancer, biomarker, pancreatic adenocarcinoma, GPR35, G protein-coupled receptor 35

Background

Due to late diagnosis and limited effective treatment options, colorectal cancer (CRC) and pancreatic ductal adenocarcinoma (PDAC) are cancers with poor prognosis and low overall survival (OS); this remains especially critical for PDAC, which is metastasizing early.

Colorectal cancer is the 3rd most commonly diagnosed cancer and 2nd cause of death from cancer worldwide. The 2020 incidence of CRC was 1,931,590 and mortality was 935,173; these trends are increasing as there were 1,850,000 cases and 880,000 deaths cases in 2018.¹ The overall 5-year survival rate in CRC is 65%; however, rates vary between 91% for localized and 15% for metastatic stage.²

The peak incidence of PDAC is in patients between 60 and 80 years of age, and there were 495,773 new PDAC cases and 466,003 deaths in 2020,^{1,3} with trends also increasing. Approximately 80–85% diagnoses are made as locally advanced (laPDAC) or distant metastatic disease (mPDAC) with limited therapeutic options, and only a minority of patients (15–20%) are eligible for surgical resection.^{4,5}

The current surveillance for CRC includes colonoscopies and histological testing of biopsied mucosa, whereas an endoscopic ultrasound (EUS) with fine-needle aspiration biopsy is the recommended diagnostic method for PDAC. We need less invasive methods for early diagnosis, and an extensive research for easily accessible biomarkers is ongoing worldwide; however, no clinically relevant biomarkers for detection of CRC or PDAC have been established so far.

G protein-coupled receptors (GPCRs) and corresponding kinases play a key role in many human diseases and the GPCR family has been proven strongly associated with tumor growth and metastasis.^{6,7} There is an increasing evidence of the role of GPR35, a GPCR family member, in carcinogenesis, facilitating cancer growth and metastasis, and GPR35 expression has already been linked to various cancers (gastric, breast, colon or non-small cell lung),^{8–11} indicating a role of GPR35 as a clinical tumor biomarker. Based on the literature research and The Cancer Genome Atlas (TCGA) database, the relationship between the GPR35 expression pattern and OS or disease-specific survival (DSS) in patients with CRC was examined. The performed analysis showed a negative association between positive GPR35 expression Z-score and OS in males, which remains statistically significant in advanced stages of CRC, suggesting the prognostic value of early testing of GPR35 in male patients with an increased risk of CRC development.¹²

Objectives

Based on these initial findings for CRC, and reports on the role of GPR35 in carcinogenesis of PDAC,^{11,13} we aimed to obtain further clinical confirmation. We have performed

laboratory analyses of GPR35 mRNA relative expression in human CRC and PDAC samples, all obtained with patient's permission, during routine surgery which the patients underwent for primary diagnosis of CRC or PDAC. Our objective was to confirm the increased expression of GPR35 in tissues collected from patients with CRC or PDAC, which we planned to be the first step in assessing the potential role of GPR35 as a biomarker for CRC or PDAC.

Materials and methods

Dataset and patient characteristics

Patients recruited to the study were admitted for CRC surgery at the Clinic of General and Colorectal Surgery of the Central Veterans' University Hospital in Łódź and for PDAC surgery at the Clinic of General and Transplantation Surgery, Norbert Barlicki Memorial Teaching Hospital No. 1 in Łódź, both being the hospitals of the Medical University of Łódź, Poland. The project was approved by the Bioethical Committee at the Medical University of Łódź (approval No. RNN/171119/KE) and all patients provided written informed consent.

Tumor samples were resected with a safety margin during the routine surgeries from the relevant parts of the affected organs for biochemical and histological assessment. In 30 patients with CRC, additional small samples were collected from nearby healthy bowel tissue with a macroscopic margin of approx. 4–5 cm from the tumor. The samples were kept on ice and transferred to the Department of Biochemistry, Medical University of Łódź, where they were stored at –80°C until further analyses. We managed to recruit 57 patients altogether – 40 with CRC and 17 with PDAC.

Detailed characteristics of the study groups are provided in Table 1 for CRC and in Table 2 for PDAC.

RNA isolation and GPR35 analysis with RT-PCR

RNA isolation

The RNA isolation from the colonic tissue samples has been performed with the use of Total RNA Mini Plus kit delivered by A&A Biotechnology (Gdańsk, Poland), and the purity and quantity of the isolated RNA were measured using a Colibri Microvolume Spectrometer (Titertek Berthold; Colibri, Frankfurt am Main, Germany). Total RNA was eluted using diethyl-pyrocyanate-treated water.

Reverse transcription

The cDNA synthesis was performed with the RevertAid First Strand cDNA Synthesis Kit (Fermentas Canada Inc., Burlington, Canada) in accordance with the manufacturer's

Table 1. CRC study group characteristics (n = 40)

Characteristics	Variable	Value
Sex	male	n = 24
	female	n = 16
Age [years]		54.73 ± 8.85
Tumor localization	rectum	n = 13
	sigmoid	n = 10
	descending colon	n = 3
	transverse colon	n = 4
	ascending colon	n = 10
AJCC stage	II	n = 21
	III	n = 13
	IV	n = 6
Lymph nodes	N0 (no regional involvement)	n = 21
	Nx (regional involvement)	n = 19
Tumor stage	T2	n = 9
	T3	n = 24
	T4	n = 7
Histological grade	1	n = 11
	2	n = 18
	3	n = 11

CRC – colorectal cancer; AJCC – American Joint Committee on Cancer.

Table 2. Pancreatic adenocarcinoma (PDAC) study group characteristics (n = 17)

Characteristics	Variable	Value
Sex	male	n = 10
	female	n = 7
Age [years]		65.05 ± 12.4
Lymph nodes	N0 (no regional involvement)	n = 5
	Nx (regional involvement)	n = 12
Tumor stage	T1	n = 1
	T2	n = 4
	T4	n = 12
Histological grade	1	n = 4
	2	n = 9
	3	n = 4
Qualification for surgery	operable	n = 5
	inoperable	n = 12

protocol. Total RNA (300 ng) was used in the reverse transcription reaction in a total volume of 20 µL, with the following 4-step incubation: 25°C for 10 min, 50°C for 15 min, 85°C for 5 min, and 4°C for 10 min.

Quantitative real-time RT-PCR

For the quantification of mRNA expression, we applied the real-time fluorescence detection polymerase chain reaction (RT-PCR) method with FAM dye-labeled TaqMan

probes of GPR35 (Hs00271114_s1; Thermo Fisher Scientific, Waltham, USA). Values obtained for studied genes were normalized to the expression of the hypoxanthine phosphoribosyltransferase 1 (*HPRT1*) gene (Hs02800695_m1; Thermo Fisher Scientific) as an endogenous control. The real-time reaction mixture was prepared in a total volume of 20 µL and consisted of 1.0 µL cDNA, 10 µL TaqMan Gene Expression Master Mix, 1.0 µL TaqMan Gene Expression Assays, and 8 µL RNA-free water; this was performed in duplicate. Cycle parameters were as follows: initial denaturation at 95°C for 10 min, followed by 40 cycles of sequential incubations at 95°C for 15 s and at 60°C for 1 min. The initial amount of the template was evaluated as a Ct parameter. The relative expression level normalized to *HPRT1* was calculated as $2^{-\Delta Ct}$. The number of cycles linearly correlates with the logarithmic value of RNA quantity.

Statistical analyses

The data were analyzed using Statistica v. 13.1 (StatSoft Inc., Tulsa, USA). A Shapiro–Wilk test was used to determine a normality of distribution; continuous variables were expressed as mean ± standard deviation (M ± SD). The comparisons of the study groups were performed with the Mann–Whitney U test and Kruskal–Wallis test. Multiple groups comparisons were followed by post hoc tests (Dunn’s test). Pearson correlation coefficient was used in the correlation analysis. A value of $p < 0.05$ was considered statistically significant.

Results

GPR35 expression in patients with CRC

We found a correlation between relative GPR35 expression and diverse patient and tumor characteristics.

The median expression of GPR35 was the highest in samples with AJCC stage IV and the difference was statistically significant (Fig. 1A). The median expression of GPR35 was higher in samples with higher T stage, with statistically significant relation between T stage 2 and 3 (Fig. 1B). We have also found a similar statistically significant correlation with relative GPR35 expression between tumor histological grade 1 and grade 3 (Fig. 1C). A paired comparison of healthy and tumor samples obtained from CRC patients revealed significantly higher relative mRNA expression of GPR35 in the latter (Fig. 1D).

Analyzing results from CRC samples, we did not find any significant differences in GPR35 expression between women and men (GPR35 relative mRNA expression in CRC tissue regarding to the patient’s sex was 14.61 ± 32.04 for male sex and 10.31 ± 24.61 for female sex; $p = 0.943$; Mann–Whitney U test). No significant correlation between

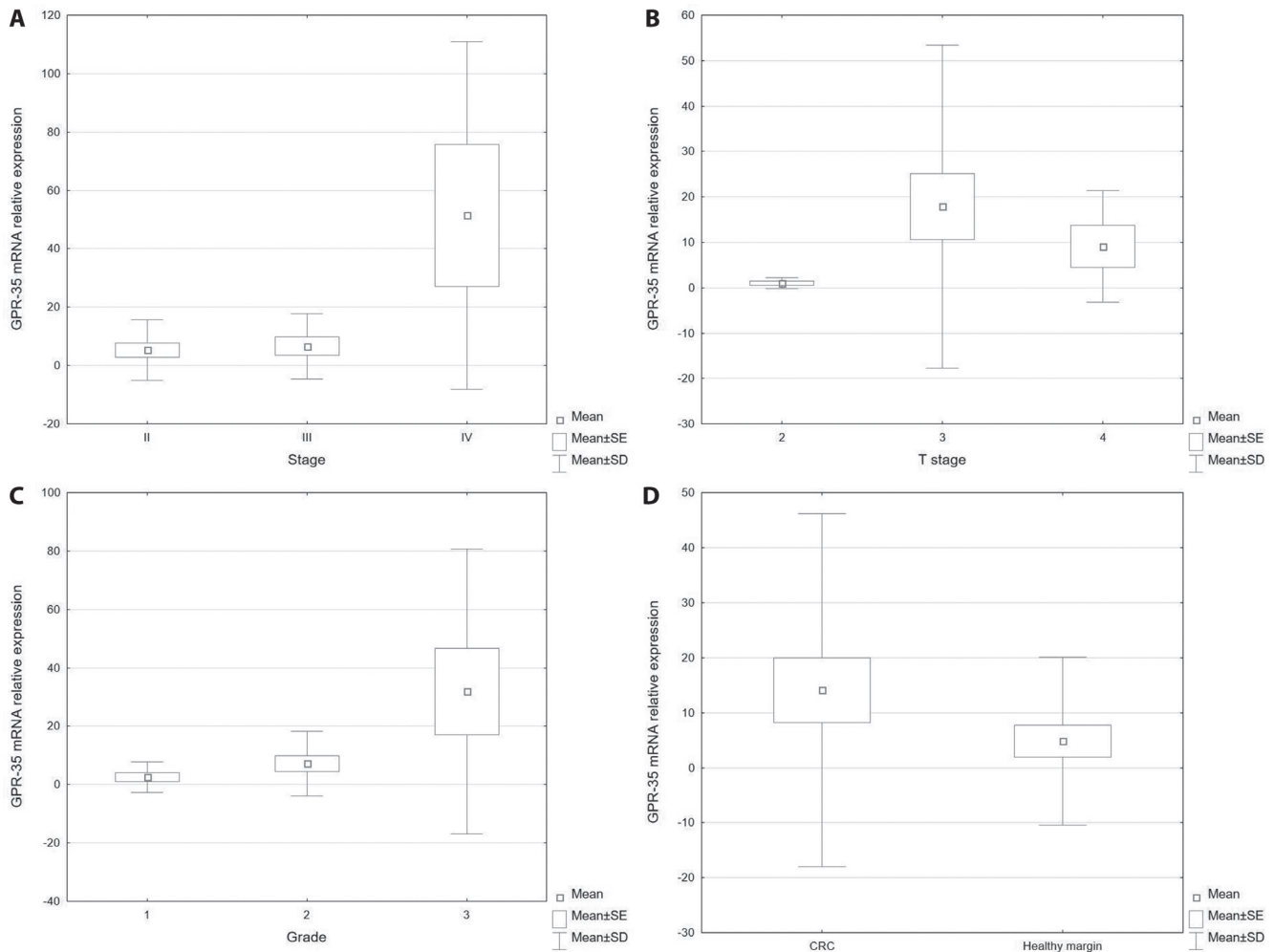


Fig. 1. A. GPR35 mRNA expression in colorectal cancer (CRC) in relation to American Joint Committee on Cancer (AJCC) stage (II: 5.3 ± 10.44 ; III: 6.64 ± 11.17 ; IV: 51.44 ± 59.5 ; $p = 0.01$; Kruskal–Wallis test followed by Dunn’s post hoc test; II compared to IV – $p = 0.007$; III compared to IV – $p = 0.044$), $n = 40$; B. GPR35 mRNA expression in CRC in relation to T stage (T2: 1.02 ± 1.15 ; T3: 17.89 ± 35.57 ; T4: 9.09 ± 12.33 ; $p = 0.017$; Kruskal–Wallis test followed by Dunn’s post hoc test; T2 compared to T3 – $p = 0.014$), $n = 40$; C. GPR35 mRNA expression in CRC in relation to tumor grade (G1: 2.52 ± 5.28 ; G2: 7.21 ± 11.13 ; G3: 31.89 ± 48.87 ; $p = 0.013$; Kruskal–Wallis test followed by Dunn’s post hoc test; G1 compared to G3 – $p = 0.01$), $n = 40$; D. Expression of GPR35 in healthy margin of colon tissue and in CRC sample (healthy margin: 4.82 ± 15.32 ; CRC: 14.1 ± 32.1 ; $p = 0.008$; Mann–Whitney test), $n = 57$.

SD – standard deviation; SE – standard error.

GPR35 mRNA relative expression level and patients’ age was found either ($r = 0.0277$; $p = 0.867$). We did not find any correlation in relative GPR35 mRNA expression level neither regarding the CRC tumor size ($r = -0.1385$; $p = 0.4$) nor the status of nodal involvement (Nx: 15.29 ± 34.22 compared to N0: 10.28 ± 22.79 ; $p = 0.527$; Mann–Whitney U test).

GPR35 expression in patients with PDAC

We have found a trend in difference in GPR35 mRNA relative expression levels between women and men, with lower GPR35 expression in women (Fig. 2A). GPR35 expression was lower in samples obtained from patients with PDAC and no regional nodes involvement (Fig. 2B). Other analyzed features included tumor T stage, with higher GPR35 expression in T4 (Fig. 2C), and tumor histological grade, where grades 2 and 3 had higher GPR35 expression

than grade 1 (Fig. 2D). However, all these differences were not statistically significant.

Another interesting trend observed in GPR35 expression regarded inoperable and operable tumors; however, it was not statistically significant either (Fig. 3). Moreover, we have not found any significant differences in GPR35 expression related to patients’ age ($r = 0.343$; $p = 0.178$), PDAC tumor size ($r = 0.094$; $p = 0.721$) or CA 19-9 level ($r = -0.201$; $p = 0.439$).

Discussion

Despite progress in developing diagnostic tools and treatment, the overall 5-year survival rate in PDAC remains below 10%.¹⁴ The current biomarkers used for diagnosis or monitoring treatment progress, such as carbohydrate antigen 19-9 (CA19-9) and carcinoembryonic

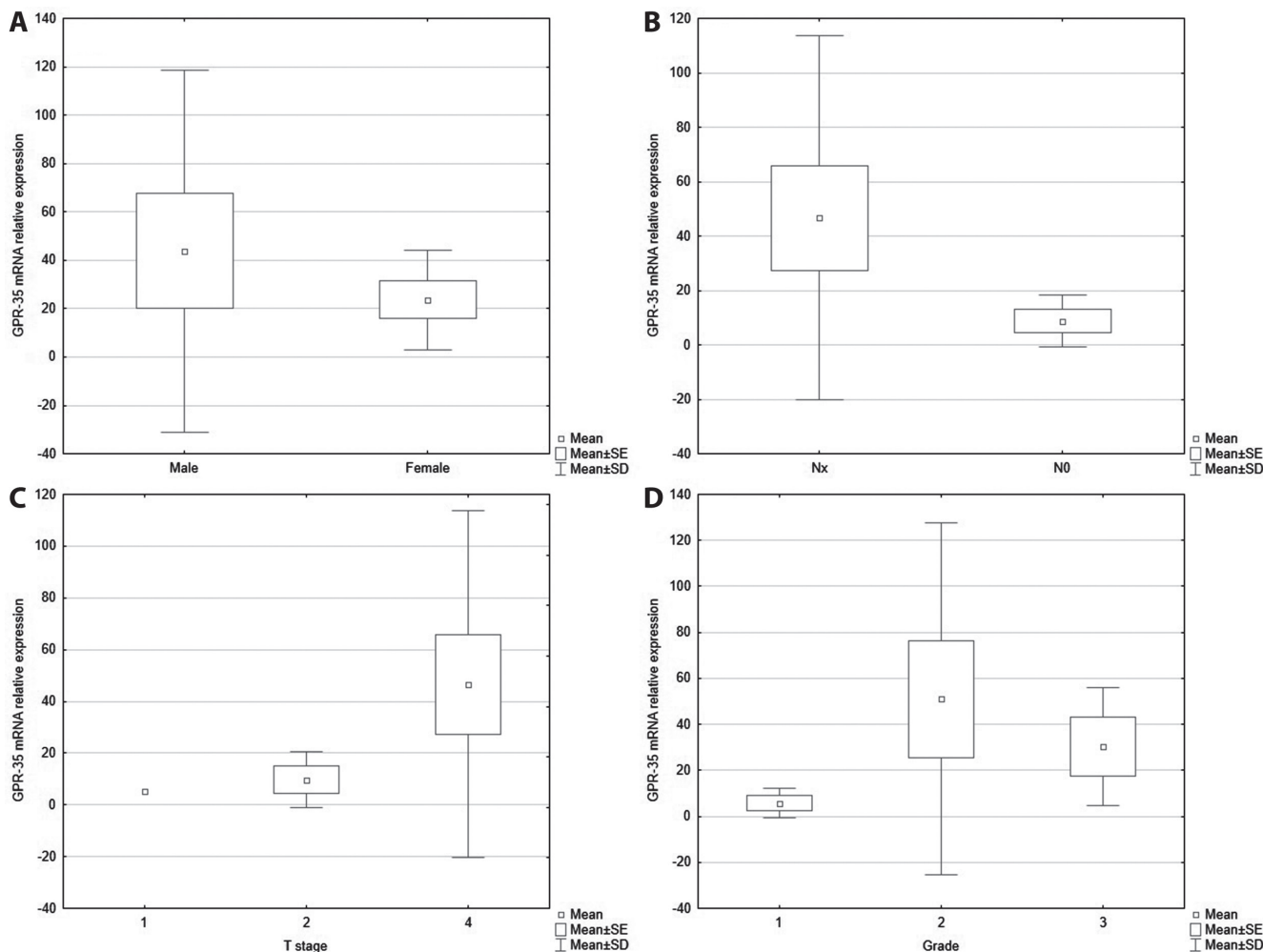


Fig. 2. A. GPR35 mRNA expression in pancreatic tissue in relation to the patient’s sex (male: 43.83 ± 74.83 compared to female: 23.65 ± 20.67 ; $p = 0.464$; Mann–Whitney U test), $n = 17$; B. GPR35 mRNA expression in pancreatic tissue in relation to the nodal metastases status (Nx: 46.65 ± 66.89 compared to N0: 8.81 ± 9.63 ; $p = 0.126$; Mann–Whitney U test), $n = 17$; C. GPR35 mRNA expression in pancreatic tissue in relation to T stage (T1: 5.05 ; T2: 9.75 ± 10.85 ; T4: 46.65 ± 66.89 ; $p = 0.260$; Kruskal–Wallis test followed by Dunn’s post hoc test), $n = 17$; D. GPR35 mRNA expression in pancreatic tissue in relation to tumor grade (G1: 5.75 ± 6.46 ; G2: 51.04 ± 76.43 ; G3: 30.38 ± 25.56 ; $p = 0.124$; Kruskal–Wallis test followed by Dunn’s post hoc test), $n = 17$.

SD – standard deviation; SE – standard error.

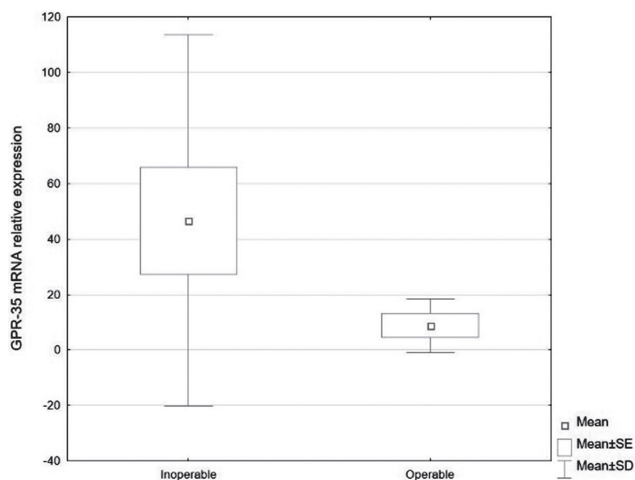


Fig. 3. GPR35 mRNA expression in pancreatic tissue in relation to surgery outcome (inoperable: 46.65 ± 66.89 compared to operable: 8.81 ± 9.63 ; $p = 0.126$; Mann–Whitney U test), $n = 17$.

SD – standard deviation; SE – standard error.

antigen (CEA), are neither sensitive nor specific enough for detection of PDAC, so biomarkers for early diagnosis are needed. The OS in CRC is around 65%; however, the more advanced the cancer, the lower the survival,¹⁵ so early diagnosis remains crucial.

Several studies confirmed that various tumor cells, including lung, prostate, colon, pancreas, and mesenchyma, express GPCRs in an abnormal manner, including those GPCRs that participate in cell proliferation, migration, invasiveness, and angiogenesis.¹⁶ Consequently, multiple genes, positively correlated with the expression of GPR35 belonging to the signaling pathways involved in CRC pathogenesis, were found using the Kyoto Encyclopedia of Genes and Genomes (KEGG) pathway analysis tool. These included ribosome and metabolic pathways, glycerophospholipid metabolism, vascular endothelial growth factor (VEGF) or mTOR signaling pathways.¹² GPR35 plays also a role in PDAC pathogenesis, regulating

the anti-proliferation, survival, apoptosis, and autophagy mechanisms, especially via the AKT, ERK and HIF1- α pathways.¹³

Importantly, the relative GPR35 expression can already be found in the publicly available databases, such as the TCGA PanCancerAtlas, and there are reports available about statistically significant shorter OS in patients with positive GPR35 Z-score based on these data – the recent concerning males with CRC and PDAC.¹²

To confirm the correlation between GPR35 mRNA relative expression and development of PDAC or CRC, we performed laboratory investigation of tumor samples from patients with advanced PDAC or CRC who were undergoing surgery for their primary diagnosis. From a group of patients with CRC, we also collected healthy samples. These assessments of GPR35 expression were our first steps to confirm the relevance of GPR35 in the carcinogenesis of both CRC and PDAC.

Here, we found correlations between a relative GPR35 expression at mRNA level and different tumor characteristics; of note, we observed statistical significance in CRC samples only. In general, the more advanced the tumor, the higher the median GPR35 expression. In CRC, this was confirmed for AJCC stage IV, T stage and histological grade, and also by a higher relative GPR35 expression in tumor samples than in the healthy paired samples collected from the same patient. All these correlations were statistically significant. Correlations regarding patient's sex (lower GPR35 expression in women), age, tumor size, or nodal involvement were not statistically significant.

In PDAC tumor samples, we found similar trends in GPR35 mRNA relative expression levels regarding sex (lower expression in women) and involvement of regional lymph nodes (less involved or not involved at all). Samples with tumor T stage 4 had much higher GPR35 expression than stages 2 or 3; similarly, higher tumor histological grades (2 and 3) had higher GPR35 expression than grade 1. A clear trend was seen between tumors considered inoperable when compared to operable, with much lower GPR35 expression in the latter. Interestingly, there was no correlation in GPR35 expression level regarding CA 19-9 level, which, if paired with GPR35, could play a role in PDAC diagnostics.

GPR35 expression levels are increased in CRC and PDAC tumors, and should be investigated further on larger groups of patients, including patients from the risk groups, to enable conclusions about the role GPR35 could play as a biomarker. In case of CRC, the patients have higher risk if: 1) they suffer from inflammatory bowel disease (IBD), such as Crohn's disease or ulcerative colitis; and/or 2) have a personal or family history of CRC or colorectal polyps, familial adenomatous polyposis (FAP) or Lynch syndrome.¹⁷ GPR35 expression could be measured in them for early CRC diagnosis. Such measurement could be included during screening procedures for CRC, which

is usually performed in patients 40–45 years old, and repeated regularly later, especially in those with lifestyle risk factors, such as lack of physical activity, inappropriate diet, overweight or obesity, alcohol consumption, and tobacco use. Confirmation of increased GPR35 expression in samples collected during colonoscopy could suggest increased risk of CRC development and encourage targeted diagnostic procedures.

The assessment of GPR35 expression could have similar importance in early PDAC diagnosis in high-risk populations before they develop the symptoms. These could be patients with genetic conditions (including hereditary breast and ovarian cancer syndrome, Lynch syndrome, familial adenomatous polyposis, Peutz–Jeghers syndrome, familial atypical multiple mole melanoma syndrome, hereditary pancreatitis, cystic fibrosis, and ataxia–teleangiectasia), chronic pancreatitis or those with diabetes mellitus, or patients with modifiable risk factors such as tobacco or alcohol use, diet or obesity.¹⁸ Assessments of GPR35 expression from pancreatic tissues will have to be performed on pancreas samples collected during EUS, which is less reliable than colonoscopy for this purpose.

In summary, our results show the correlation between relative GPR35 mRNA expression and advanced development of CRC or PDAC, and confirm the role of GPR35 in carcinogenesis. Further clinical investigations are needed to confirm whether GPR35 could play a role as an early biomarker for CRC or PDAC.








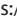
Limitations

Our analysis has some limitations, related especially to small sample size of our study, which provided us with restricted number of samples from patients with CRC and especially with PDAC. It needs to be underlined that this is only a preliminary study; however, we hope that our encouraging results will motivate researchers to continue investigations on bigger populations, including patients at risk.

Conclusions

Our results suggest the role of GPR35 as a potential biomarker for CRC or PDAC; however, more clinical data from patients at risk to develop these cancers are needed to confirm the suitability of GPR35 as an early biomarker.

ORCID iDs

Tomasz Mackiewicz  <https://orcid.org/0000-0001-7505-8141>
Jakub Włodarczyk  <https://orcid.org/0000-0003-2010-5136>
Marta Zielińska  <https://orcid.org/0000-0001-5939-791X>
Marcin Włodarczyk  <https://orcid.org/0000-0001-9118-4623>
Adam Durczyński  <https://orcid.org/0000-0003-2999-5454>
Piotr Hogendorf  <https://orcid.org/0000-0002-4458-0145>
Łukasz Dżiki  <https://orcid.org/0000-0002-0390-0827>
Jakub Fichna  <https://orcid.org/0000-0002-8443-4417>

References

1. Sung H, Ferlay J, Siegel RL, et al. Global cancer statistics 2020: GLOBOCAN estimates of incidence and mortality worldwide for 36 cancers in 185 countries. *CA A Cancer J Clin.* 2021;71(3):209–249. doi:10.3322/caac.21660
2. Siegel RL, Miller KD, Goding Sauer A, et al. Colorectal cancer statistics, 2020. *CA A Cancer J Clin.* 2020;70(3):145–164. doi:10.3322/caac.21601
3. Ushio J, Kanno A, Ikeda E, et al. Pancreatic ductal adenocarcinoma: Epidemiology and risk factors. *Diagnostics (Basel).* 2021;11(3):562. doi:10.3390/diagnostics11030562
4. Shinde RS, Bhandare M, Chaudhari V, Shrikhande SV. Cutting-edge strategies for borderline resectable pancreatic cancer. *Ann Gastroenterol Surg.* 2019;3(4):368–372. doi:10.1002/ags3.12254
5. Principe DR, Underwood PW, Korc M, Trevino JG, Munshi HG, Rana A. The current treatment paradigm for pancreatic ductal adenocarcinoma and barriers to therapeutic efficacy. *Front Oncol.* 2021;11:688377. doi:10.3389/fonc.2021.688377
6. Pronin AN, Morris AJ, Surguchov A, Benovic JL. Synucleins are a novel class of substrates for G protein-coupled receptor kinases. *J Biol Chem.* 2000;275(34):26515–26522. doi:10.1074/jbc.M003542200
7. Dorsam RT, Gutkind JS. G-protein-coupled receptors and cancer. *Nat Rev Cancer.* 2007;7(2):79–94. doi:10.1038/nrc2069
8. Okumura S, Baba H, Kumada T, et al. Cloning of a G-protein-coupled receptor that shows an activity to transform NIH3T3 cells and is expressed in gastric cancer cells. *Cancer Sci.* 2004;95(2):131–135. doi:10.1111/j.1349-7006.2004.tb03193.x
9. Quon T, Lin LC, Ganguly A, Tobin AB, Milligan G. Therapeutic opportunities and challenges in targeting the orphan G protein-coupled receptor GPR35. *ACS Pharmacol Transl Sci.* 2020;3(5):801–812. doi:10.1021/acspstsci.0c00079
10. Ali H, AbdelMageed M, Olsson L, et al. Utility of G protein-coupled receptor 35 expression for predicting outcome in colon cancer. *Tumour Biol.* 2019;41(6):101042831985888. doi:10.1177/1010428319858885
11. Cerami E, Gao J, Dogrusoz U, et al. The cBio cancer genomics portal: An open platform for exploring multidimensional cancer genomics data. *Cancer Discov.* 2012;2(5):401–404. doi:10.1158/2159-8290.CD-12-0095
12. Mackiewicz T, Jacenik D, Talar M, Fichna J. The GPR35 expression pattern is associated with overall survival in male patients with colorectal cancer. *Pharmacol Rep.* 2022;74(4):709–717. doi:10.1007/s43440-022-00371-2
13. Kim M. The role of G protein-coupled receptor 35 in pancreatic cancer [doctoral thesis]. Perth, Australia; Curtin University; 2020. <http://hdl.handle.net/20.500.11937/84527>. Accessed June 3, 2022.
14. Stark AP, Sacks GD, Rochefort MM, et al. Long-term survival in patients with pancreatic ductal adenocarcinoma. *Surgery.* 2016;159(6):1520–1527. doi:10.1016/j.surg.2015.12.024
15. van den Berg I, Coebergh van den Braak RRRJ, van Vugt JLA, Ijzermans JNM, Buettner S. Actual survival after resection of primary colorectal cancer: Results from a prospective multicenter study. *World J Surg Onc.* 2021;19(1):96. doi:10.1186/s12957-021-02207-4
16. Chaudhary PK, Kim S. An insight into GPCR and G-proteins as cancer drivers. *Cells.* 2021;10(12):3288. doi:10.3390/cells10123288
17. Johnson CM, Wei C, Ensor JE, et al. Meta-analyses of colorectal cancer risk factors. *Cancer Causes Control.* 2013;24(6):1207–1222. doi:10.1007/s10552-013-0201-5
18. Bekkali N, Oppong K. Pancreatic ductal adenocarcinoma epidemiology and risk assessment: Could we prevent? Possibility for an early diagnosis. *Endosc Ultrasound.* 2017;6(9):S58–S61. doi:10.4103/eus.eus_60_17

ATPIF1 alleviates oxygen glucose deprivation/reoxygenation-induced astrocyte injury in vitro: A rat model of ischemic brain injury

Zhijie Wei^{1,2,A–D,F}, Rui Wu^{2,A–C,F}, Li Zhang^{2,A–C,F}, Ping Xu^{2,A,C,E,F}

¹ Department of Neurology, Soochow University, China

² Department of Neurology, Affiliated Hospital of Zunyi Medical University, China

A – research concept and design; B – collection and/or assembly of data; C – data analysis and interpretation; D – writing the article; E – critical revision of the article; F – final approval of the article

Advances in Clinical and Experimental Medicine, ISSN 1899–5276 (print), ISSN 2451–2680 (online)

Adv Clin Exp Med. 2023;32(7):791–802

Address for correspondence

Ping Xu

E-mail: xuping5272021@126.com

Funding sources

The study was supported by Science and Technology Foundation of Guizhou Provincial Health Commission (grant No. Gzwbkj2021-025).

Conflict of interest

None declared

Acknowledgements

The authors would like to acknowledge the funder for the financial support.

Received on March 22, 2022

Reviewed on September 1, 2022

Accepted on December 14, 2022

Published online on March 7, 2023

Cite as

Wei Z, Wu R, Zhang L, Xu P. ATPIF1 alleviates oxygen glucose deprivation/reoxygenation-induced astrocyte injury in vitro: A rat model of ischemic brain injury. *Adv Clin Exp Med.* 2023;32(7):791–802. doi:10.17219/acem/157477

DOI

10.17219/acem/157477

Copyright

Copyright by Author(s)

This is an article distributed under the terms of the Creative Commons Attribution 3.0 Unported (CC BY 3.0) (<https://creativecommons.org/licenses/by/3.0/>)

Abstract

Background. The role of ATPIF1 in ischemic brain injury is rarely reported.

Objectives. This study explored the effect of ATPIF1 on astrocyte activity under oxygen glucose deprivation/reoxygenation (OGD/R).

Materials and methods. The study sample was randomly allocated into: 1) control group (blank control); 2) OGD/R group (hypoxia for 6 h/reoxygenation for 1 h); 3) siRNA negative control (NC) group (OGD/R model+siRNA NC); and 4) siRNA-ATPIF1 group (OGD/R model+siRNA-ATPIF1). The OGD/R cell model was established from Sprague Dawley (SD) rats to simulate ischemia/reperfusion injury. Cells in the siRNA-ATPIF1 group were treated with siATPIF1. Ultrastructural changes in the mitochondria were observed using transmission electron microscopy (TEM). Apoptosis, cell cycle, reactive oxygen species (ROS), and mitochondrial membrane potential (MMP) were detected with flow cytometry. The protein expression levels of nuclear factor kappa B (NF- κ B), B-cell lymphoma 2 (Bcl-2), Bcl-2-associated X (Bax), and caspase-3 were detected with western blot.

Results. In the model group, the cell structure and the ridge structure were destroyed, and mitochondria edema, outer membrane damage and vacuole-like lesions were observed. Compared with the control group, the OGD/R group had considerably increased apoptosis, G0/G1 phase, ROS content, MMP, and Bax, caspase-3 and NF- κ B protein expression, as well as markedly decreased S phase and Bcl-2 protein expression. Compared with the OGD/R group, the siRNA-ATPIF1 group had considerably decreased apoptosis, G0/G1 phase, ROS content, MMP, and Bax, caspase-3 and NF- κ B protein expression, as well as remarkably increased S phase and Bcl-2 protein expression.

Conclusions. The inhibition of ATPIF1 may alleviate OGD/R-induced astrocyte injury by regulating the NF- κ B signaling pathway, inhibiting apoptosis, and reducing the ROS content and MMP in the rat brain ischemic model.

Key words: apoptosis, NF- κ B signaling pathway, OGD/R, astrocytes, ATPIF1

Background

Ischemic cerebrovascular disease has been the leading cause of disability and mortality globally.^{1,2} A variety of biochemical mechanisms are involved in the pathophysiological process of the disease, including brain energy metabolism disorder, reactive oxygen species (ROS) production, inflammation, acidosis, and apoptosis.³ As the most widely distributed and numerous cells in the brain, astrocytes are very important for maintaining neuronal structure and function.^{4,5} When ischemic injury occurs, astrocytes can fill the damaged area, maintain the stability of the environment in the central nervous system, provide nutrients for neurons, and protect neurons; thus, they are crucial for the repair of an ischemic area and to avoid the secondary injury of neurons.⁶

All cell activities are inseparable from adenosine triphosphate (ATP) consumption; hence, ATP synthesis and decomposition in astrocytes are of great importance after the ischemic injury. Mitochondrial ATPase inhibitor, ATP1F1, is a nuclear coding protein that can interact with ATP synthase.⁷ The ATP1F1 is the most characteristic regulator of F1Fo-ATP synthase. It combines with enzymes inhibiting its hydrolytic activity to protect cells from ATP consumption.⁸ The ATP1F1 has been associated with a variety of diseases, such as diabetic nephropathy, breast cancer and anemia.^{9–12} The ATP1F1 can aggravate the development of diabetic nephropathy by inducing mitochondrial damage.⁹ The inhibition of ATP1F1 can improve the severe decrease in electron transport chain activity in mitochondrial pathology.¹⁰ However, the role of ATP1F1 in ischemic brain injury is rarely reported.

In biological systems, the mitochondria are the main place for cells to generate energy. They are also the key intracellular targets for initiating the intrinsic pathway of apoptosis.¹³ The ATP1F1 abnormality causes a series of chain reactions in the mitochondria. The mitochondria are the main part of ROS production in tissues. Increased ROS levels can induce apoptosis through endogenous and exogenous pathways.¹⁴ Nuclear factor kappa B (NF- κ B) is a traditional transcription factor. It regulates the apoptosis program through its downstream target genes under different stimuli, such as ROS accumulation and inflammatory factors.¹⁵ However, the role of ATP1F1 in astrocyte apoptosis mediated by oxygen glucose deprivation/reoxygenation (OGD/R) remains unknown.

Objectives

The aim of this study was to explore the effect of ATP1F1 on astrocyte activity in Sprague Dawley (SD) rats under OGD/R. We hypothesized that siATP1F1 has a protective effect on the astrocyte activity in OGD/R-induced astrocyte injury. The findings of this study may help develop a feasible approach to treating ischemic cerebrovascular disease.

Materials and methods

Ethics declarations

The Animal Care and Use Committee of the Affiliated Hospital of Zunyi Medical University, China, has given the approval to the experiments and protocol used in this study (approval No. 2020041501).

Experimental animals

Specific pathogen-free SD rats (female, 3 months old; male, 9 months old; license No. SCXK (Xiang) 2019-0014) were obtained from Changsha Tianqin Biotechnology Co., Ltd. (Hunan, China) and raised under 30–70% humidity, 20–26°C and 12 h/12 h light/dark cycle. The rats were allowed food and water ad libitum.

Primary cell isolation and identification

The rats were caged together with a male–female ratio of 1:2, and the neonatal rats were used for further experiments. No gender requirement was set for the neonatal rats. A total of 4 litters with about 12 neonatal rats in each litter were used. The neonatal rats were given sodium pentobarbital (45 mg/kg; MilliporeSigma, Burlington, USA). The brains of the rats were removed following cervical dislocation after immersion and disinfection with 75% ethanol for 1 min. The pia mater covered on the surface of the brain tissue was stripped, and the rat cerebral cortex was separated and washed repeatedly with D-Hank's solution (Beijing Solarbio Science & Technology Co., Ltd., Beijing, China). The washed cortex was repeatedly ground and sieved (220 mesh screen). The screen was repeatedly washed and the cell suspension was transferred to a 15-milliliter clean tube. The pooled samples were centrifuged at 4°C (1500 rpm) for 5 min. The supernatant was discarded, the precipitate was resuspended in Dulbecco's modified Eagle's medium (DMEM; Gibco, Thermo Fisher Scientific, Waltham, USA) containing 10% fetal bovine serum (FBS; Beijing Solarbio Science & Technology Co., Ltd.), and the cells were cultured in 5% CO₂ at 37°C. The medium was replaced with a fresh medium every 3 days. When the cells reached 90% confluence, they were placed in a 37°C shaker incubator for 4–6 h. Then, the microglia supernatant was removed.

The cell climbing sheets were washed with 0.1 M phosphate-buffered saline (PBS), fixed with 4% paraformaldehyde (Beijing Solarbio Science & Technology Co., Ltd.) at room temperature (RT) for 15 min, and blocked for 40 min with 3% goat serum (Beijing Solarbio Science & Technology Co., Ltd.) and 0.1% Triton X-100 (MilliporeSigma). The cells were incubated with rabbit anti-gial fibrillary acidic protein (anti-GFAP) primary antibody (1:200, AB53554; Abcam, Cambridge, UK) at 4°C overnight and IgG/Cy3 fluorescent secondary antibody (1:200,

A0502; Beyotime Biotechnology Inc., Shanghai, China) at RT for 60 min. Then, 4',6-diamidino-2-phenylindole (DAPI; Jiangsu KeyGen Biotech Corp., Ltd., Jiangsu, China) was applied and incubated for 3 min. The cells were mounted with 95% glycerol and observed using a fluorescence microscope (model CX41; Olympus Corp., Tokyo, Japan).

OGD/R cell model

Third-generation astrocytes with good growth condition were selected and 0.125% trypsin (Beijing Solarbio Science & Technology Co., Ltd.) was added for digestion. The cells were centrifuged at 1500 rpm for 5 min and the precipitation was resuspended. The cells were seeded in a 6-well culture plate (1×10^5 /well) and cultured in sugar-free DMEM with 94% N₂, 5% CO₂ and 1% O₂ at 37°C for 24 h. The cells were collected and detected at 1, 3, 6, and 24 h.

Cell transfection

The cells were cultured in a 6-well plate. Cell transfection was performed when they reached 70% confluence. Lipofectamine 3000 kit (Invitrogen, Thermo Fisher Scientific, Waltham, USA) was used. A 12.5 µL small interfering RNA (siRNA) was mixed with 125 µL of Opti-MEM (Gibco) and 5 µL of Lipofectamine 3000 was mixed with 125 µL of Opti-MEM. Both mixtures were separately incubated at RT for 5 min, then mixed, incubated for 15 min at RT, and added to the cells cultured in the 6-well plate for 4 h. The cells were cultured in DMEM/F-12 complete medium (Gibco) containing 20% FBS (BBI Life Sciences Corp., Shanghai, China).

The transcription sequences were obtained from the National Center for Biotechnology Information (NCBI;

<https://www.ncbi.nlm.nih.gov/>). The target gene sequences were handed over to General Biol Co., Ltd. (Anhui, China), which directly provided the siRNA. The siRNA sequences are shown in Table 1.

Experimental grouping

The experimental grouping was randomly divided into:

- 1) control group (blank control);
- 2) OGD/R group (hypoxia for 6 h/reoxygenation for 1 h);
- 3) siRNA negative control (NC) group (OGD/R model +siRNA NC);
- 4) siRNA-ATPIF1 group (OGD/R model+siRNA-ATPIF1).

The investigators performing the subsequent experiments were blinded to the group allocation.

Quantitative real-time polymerase chain reaction

The cells were collected and Trizol reagent (CW BIO, Jiangsu, China) was used for the total RNA extraction. Reverse transcription to cDNA was performed with a HiFiScript cDNA Synthesis Kit (Vazyme Biotech, Jiangsu, China) according to the kit instructions. Quantitative PCR was conducted with a quantitative real-time polymerase chain reaction (qPCR) system (CFX Connect; Bio-Rad, Hercules, USA). The reaction system and reaction steps are presented in Table 2. The primers are shown in Table 3. The β-actin (Sino Biological Inc., Beijing, China) served as the internal control. The relative ATPIF1 mRNA expression was determined based on the $2^{-\Delta\Delta Ct}$ method.

Table 2. Reaction system and reaction steps of quantitative real-time polymerase chain reaction (qPCR) system

Reagent	Volume	
RNase free dH ₂ O	9.5 µL	
cDNA	1 µL	
Forward primer	1 µL	
Reverse primer	1 µL	
2× SYBR Green PCR Master Mix	12.5 µL	
Step	Temperature	Time
Pre-denaturation	95°C	10 min
Denaturation	95°C	10 s
Annealing	58°C	30 s
Extension	72°C	30 s
Number of cycles	40	

Table 1. siRNA sequences

siRNA	siRNA sequence
siATPIF1-1	CGGCAUAAGAAGAAGAUUATT UAAUCUUCUUCUUAUGCCGTT
siATPIF1-2	AGAGAAGGCCUGAAGAGGAUTT AUCCUCUUCAGCCUUCUCUTT
siATPIF1-3	GCACCAUGAAGAUGAGAUUUTT AAUCUCAUCUUCUUAUGGUGCTT
NC	UUCUCCGAACGUGUCACGUTT ACGUGACACGUUCGGAGAATT

NC – negative control.

Table 3. Primers of quantitative real-time polymerase chain reaction (qPCR)

Primer	Sequence	Length [nt]	Product length [bp]	Annealing temperature [°C]
ATPIF1 F	CTCGGTGCTGGGGTATGA	19	252	56.81
ATPIF1 R	ATGCCGTTTCGATCTGTTTT	19		
β-actin F	GCCATGTACGTAGCCATCCA	20	375	59.5
β-actin R	GAACCGCTCATTGCCGATAG	20		

Western blot

The cells were lysed in the radioimmunoprecipitation (RIPA) buffer (Applygen Technologies Inc., Beijing, China) at 4°C for 30 min and then centrifuged at 12,000 rpm for 10 min. For total protein determination, the supernatant was carefully extracted, and determination was conducted according to the Bradford method (Beijing Solarbio Science & Technology Co., Ltd.). This step was followed by protein denaturation and sample loading. Sodium dodecyl sulfate-polyacrylamide gel electrophoresis (SDS-PAGE; Xilong Scientific Co., Ltd., Guangdong, China) was performed for 2 h before transferring to polyvinylidene fluoride membrane (PVDF; MilliporeSigma) at 300 mA. The primary antibodies used included mouse monoclonal anti-glyceraldehyde 3-phosphate dehydrogenase (anti-GAPDH; 1:2000, cat. No. TA-08; ZSGB-BIO, Beijing, China), mouse anti-ATPIF1 (1:1000, ab110277; Abcam), mouse anti-B-cell lymphoma 2 (anti-Bcl-2; 1:1000, cat. No. 60178-1-Ig; Proteintech, Rosemont, USA), rabbit anti-Bcl-2-associated X (anti-Bax; 1:1000, cat. No. 50599-2-Ig; Proteintech), rabbit anti-nuclear factor-kappa B (anti-NF- κ B; 1:1000, 10745-1-AP; Proteintech), and rabbit anti-caspase-3 (1:1000, cat. No. YT0656; ImmunoWay Biotechnology Co., Plano, USA). The primary antibodies were added and incubated at 4°C overnight. Then, the secondary antibodies were added and incubated at RT for 2 h. The secondary antibodies used included goat anti-rabbit IgG antibody (H+L, horseradish peroxidase (HRP)-conjugated, 1:2000, cat. No. ZB-2301) and goat anti-mouse IgG antibody (H+L, HRP-conjugated, 1:2000, cat. No. ZB-2305; ZSGB-BIO). The chemiluminescent substrate was added, and the membrane was examined using a gel imaging system (ChemiDoc XRS+; Bio-Rad). The blot was analyzed using Quantity One software v. 4.62 (Bio-Rad) with GAPDH as the internal reference, using the equation: relative protein expression = (target protein integral optical density (IOD) / internal reference protein IOD).

Detection with flow cytometry

Apoptosis

The cells (1×10^6 – 3×10^6) were collected. An Annexin V-Propidium Iodide (PI) Analysis Kit (MultiSciences (Lianke) Biotech Co., Ltd., Hangzhou, China) was used for apoptosis detection based on the manufacturer's instructions. The cells were washed 3 times with pre-cooled PBS, resuspended with 300 μ L of $\times 1$ binding buffer, added with 3 μ L of Annexin V-fluorescein isothiocyanate (FITC) and 5 μ L of PI-phycoerythrin solution, and mixed gently. Then, the cells were incubated in the dark at RT (20–25°C) for 10–20 min and placed in an ice bath. The detection was performed on a NovoCyte™ flow cytometer (NovoCyte 2060R; ACEA Bio (Hangzhou) Co., Ltd., Hangzhou, China).

Cell cycle

The cells were collected, washed with PBS, 1 mL of DNA staining solution and 10 μ L of PI solution were added, and the cells were mixed. Then, they were incubated in the dark at RT for 30 min. The cell cycle was determined with flow cytometry.

ROS

The cells were harvested and a final concentration of 10 μ M 2',7'-dichlorofluorescein diacetate (DCFH-DA) solution (Reactive Oxygen Species Assay Kit; Jiangsu KeyGEN BioTECH Co., Ltd.) was obtained with 1:1000 dilution of DCFH-DA in serum-free medium. The cell culture medium was replaced with the diluted DCFH-DA. The cells were incubated at 37°C for 20 min and then washed 3 times with serum-free medium and 3 times with PBS. The ROS levels were determined with flow cytometry.

Membrane potential

The cells were collected, washed with PBS and centrifuged at 2000 rpm for 5 min. Next, the cells were resuspended with 500 μ L of JC-1 solution (BestBio, Shanghai, China) and cultured at 37°C with 5% CO₂ for 15–20 min. Then, they were centrifuged at 2000 rpm for 5 min, washed twice with $\times 1$ incubation buffer, resuspended with 500 μ L of $\times 1$ incubation buffer, and analyzed with flow cytometry.

Statistical analyses

Data analysis was performed with GraphPad Prism 7 software (GraphPad Software, San Diego, USA). The comparisons between groups were performed using one-way analysis of variance (ANOVA) with Bonferroni post hoc test. The value of $p < 0.05$ was considered statistically significant.

Outcome measures

The outcome measures were the effects of siATPIF1 on the mitochondrial structure, apoptosis, cell cycle, ROS production, mitochondrial membrane potential (MMP), apoptosis-related genes, and the NF- κ B pathway in the OGD/R model.

Results

Isolation and identification of astrocytes

The isolated and purified cells were star-shaped, and many long and branched processes were separated from the cell body. The GFAP is a marker for astrocytes. Immunofluorescence results showed that the nuclei of astrocytes were stained blue and the cells were stained red (GFAP). The purity of astrocytes was more than 95% (Fig. 1).

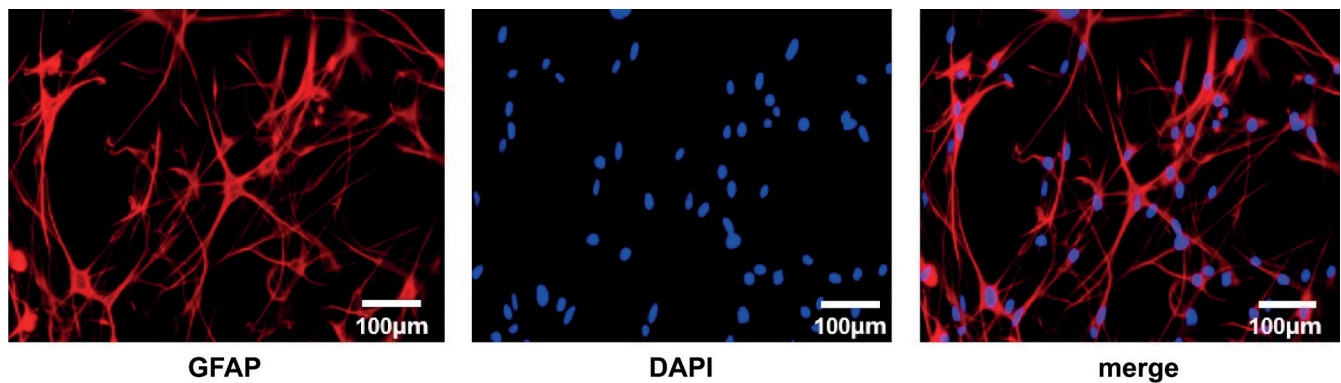


Fig. 1. Astrocyte identification

DAPI – 4',6-diamidino-2-phenylindole; GFAP – glial fibrillary acidic protein.

Selection of OGD/R model conditions

As shown in Fig. 2A, the apoptosis rate was the highest at 1 h of reperfusion compared with the control group. Many cells were irregular and had mitochondrial edema, outer membrane damage, vacuole-like lesions, or damaged ridge structure at 1 h of reperfusion (Fig. 2B). Moreover, the mitochondria were irregular, some mitochondria were swollen, and the cristae disappeared at 3 h after reperfusion. Finally, the mitochondrial ridge structure was destroyed and became a vacuole-like lesion at 24 h after reperfusion. Figure 2C shows that ATPIF1 protein expression increased remarkably at 1 h of reperfusion. Therefore, the model was established at 1 h of reperfusion in subsequent experiments.

ATPIF1 siRNA transfection efficiency verification

As shown in Fig. 3, the ATPIF1 mRNA expression levels in the siRNA groups (particularly the siATPIF1-2 group) were considerably lower than those in the control and siRNA NC groups. The ATPIF1 protein expression levels in the siRNA-2 and siRNA-3 groups were remarkably lower than in the control and siRNA NC groups. Therefore, siRNA-2 was selected for subsequent experiments.

Effect of siATPIF1 on mitochondrial structure in the OGD/R model

The mitochondrial morphological changes were examined using transmission electron microscopy (TEM). As shown in Fig. 4, the cell morphology in the control group was normal and the ridge structure was complete; the cell and ridge structures in the OGD/R group were destroyed, and mitochondria edema, outer membrane damage or vacuole-like lesions were noted; the cells in the siRNA NC group were irregular, some mitochondria were swollen and cristae disappeared; the cell and mitochondrial membrane

structures in the siRNA-ATPIF1 group were complete, and most of the ridge structures were normal.

Effects of siATPIF1 on apoptosis and cell cycle in the OGD/R model

The apoptosis rate in the OGD/R group was considerably higher than in the control group, whereas the apoptosis rate in the siRNA-ATPIF1 group was substantially lower than in the OGD/R group (Fig. 5A). The OGD/R group had a remarkably increased G0/G1 and a remarkably decreased S phase compared with the control group. Moreover, the siRNA-ATPIF1 group had a considerably decreased G0/G1 phase and substantially increased S phase compared with the OGD/R group (Fig. 5B).

Effects of siATPIF1 on ROS and MMP in the OGD/R model

The ROS levels in the OGD/R group were significantly increased compared with the control group; the ROS levels in the siRNA-ATPIF1 group were significantly decreased compared with the OGD/R group (Fig. 6A). The MMP in the OGD/R group was considerably increased compared with the control group, and the MMP in the siRNA-ATPIF1 group was remarkably decreased compared with the OGD/R group (Fig. 6B).

Effects of siATPIF1 on apoptosis-related genes and NF- κ B pathway in the OGD/R model

The western blot results are shown in Fig. 7. The OGD/R group had substantially increased Bax, caspase-3 and NF- κ B protein expression, and remarkably decreased Bcl-2 protein expression compared with the control group. The siRNA-ATPIF1 group had remarkably decreased Bax, caspase-3 and NF- κ B protein expression levels, and increased Bcl-2 protein expression compared with the OGD/R group.

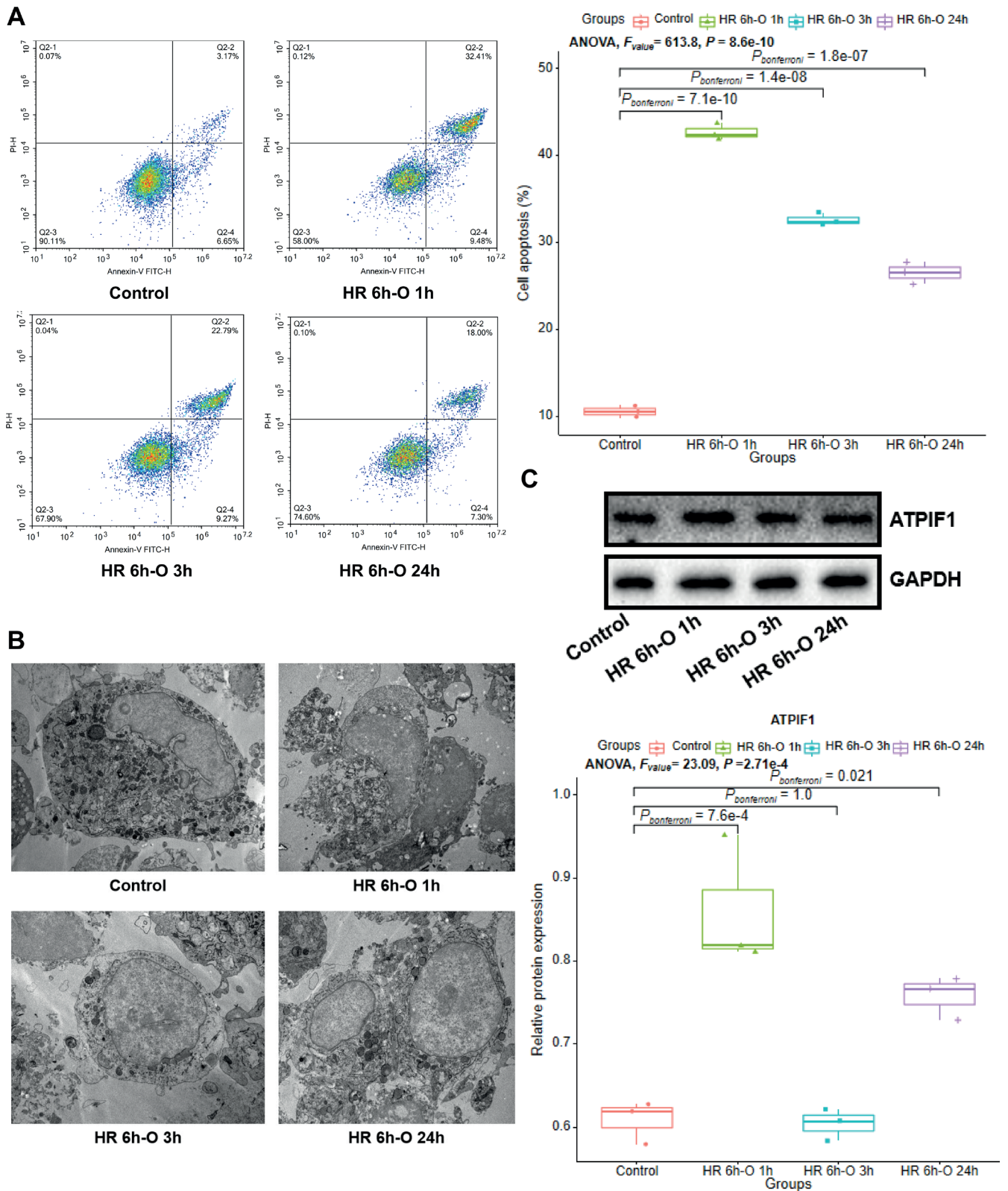


Fig. 2. Selection of oxygen glucose deprivation/reoxygenation (OGD/R) model. A. Scatter plots of cell apoptosis (analysis of variance (ANOVA), $F = 613.8$, $p = 8.6e-10$); Hypoxia reoxygenation (HR) 6h-O 1h compared to controls, $p_{bonferroni} = 7.1E-10$; HR 6h-O 3h compared to controls, $p_{bonferroni} = 1.4E-08$; HR 6h-O 24h compared to controls, $p_{bonferroni} = 1.8E-07$; B. Ultrastructural changes in the mitochondria determined using transmission electron microscopy (TEM); C. ATP1F1 protein expression (ANOVA, $F = 23.09$, $p = 0.000271$); HR 6h-O 1h compared to controls, $p_{bonferroni} = 7.6E-04$; HR 6h-O 3h compared to controls, $P_{bonferroni} = 1.0000$; HR 6h-O 24h compared to controls, $p_{bonferroni} = 0.0213$). The data analysis results are presented in Supplementary Table 1

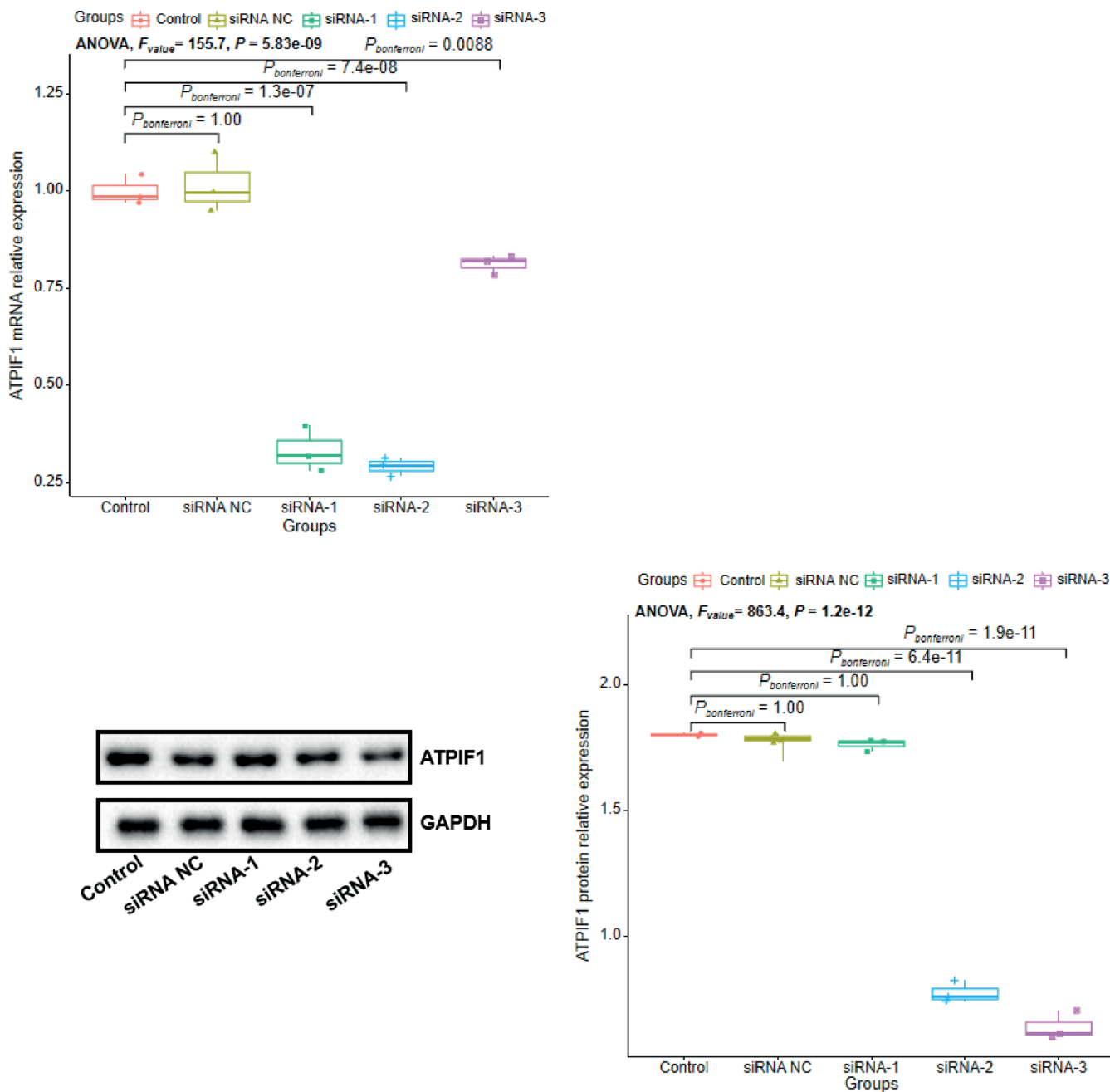


Fig. 3. The ATPIF1 siRNA transfection efficiency in each group. ATPIF1 mRNA relative expression: analysis of variance (ANOVA), $F = 155.7, p = 5.83e-09$; siRNA-1 compared to controls, $p_{bonferroni} = 1.3E-07$, compared to siRNA NC, $p_{bonferroni} = 1.0E-07$; siRNA-2 compared to controls, $p_{bonferroni} = 7.4E-08$, compared to siRNA NC, $p_{bonferroni} = 6.0E-08$; siRNA-3 compared to controls, $p_{bonferroni} = 0.0088$, compared to siRNA NC, $p_{bonferroni} = 0.005$. The ATPIF1 protein relative expression: ANOVA, $F = 863.4, p = 1.2e-12$; siRNA-1 compared to controls, $p_{bonferroni} = 1.0000$, compared to siRNA NC, $p_{bonferroni} = 1.0000$; siRNA-2 compared to controls, $p_{bonferroni} = 6.4E-11$, compared to siRNA NC, $p_{bonferroni} = 7.4E-11$; siRNA-3 compared to controls, $p_{bonferroni} = 1.9E-11$, compared to siRNA NC, $p_{bonferroni} = 2.1E-11$. The data analysis results are presented in Supplementary Table 1

Discussion

Evidence of the relationship between ischemic brain injury and increased astrocyte injury has been found in previous research.¹⁶ Astrocytes are the most abundant cell type in the central nervous system.¹⁷ They communicate with neurons, oligodendrocytes and endothelial cells, and participate in maintaining normal brain function.¹⁸ Therefore, astrocytes have become the neuroprotective target

in ischemic brain injury.¹⁹ The ATPIF1 is a mitochondrion-localized protein encoded by nuclear DNA. The ATPIF1 can inhibit ATP hydrolysis through ATP synthase when bound to F1 complexes α and β .²⁰ The ATPIF1 regulates mitochondrial morphology and cell survival.²¹ Our study demonstrated that siRNA-ATPIF1 may protect astrocytes from OGD/R-induced apoptosis and necrosis by maintaining mitochondrial anti-apoptosis (Bcl-2 upregulation) and bioenergetic function.

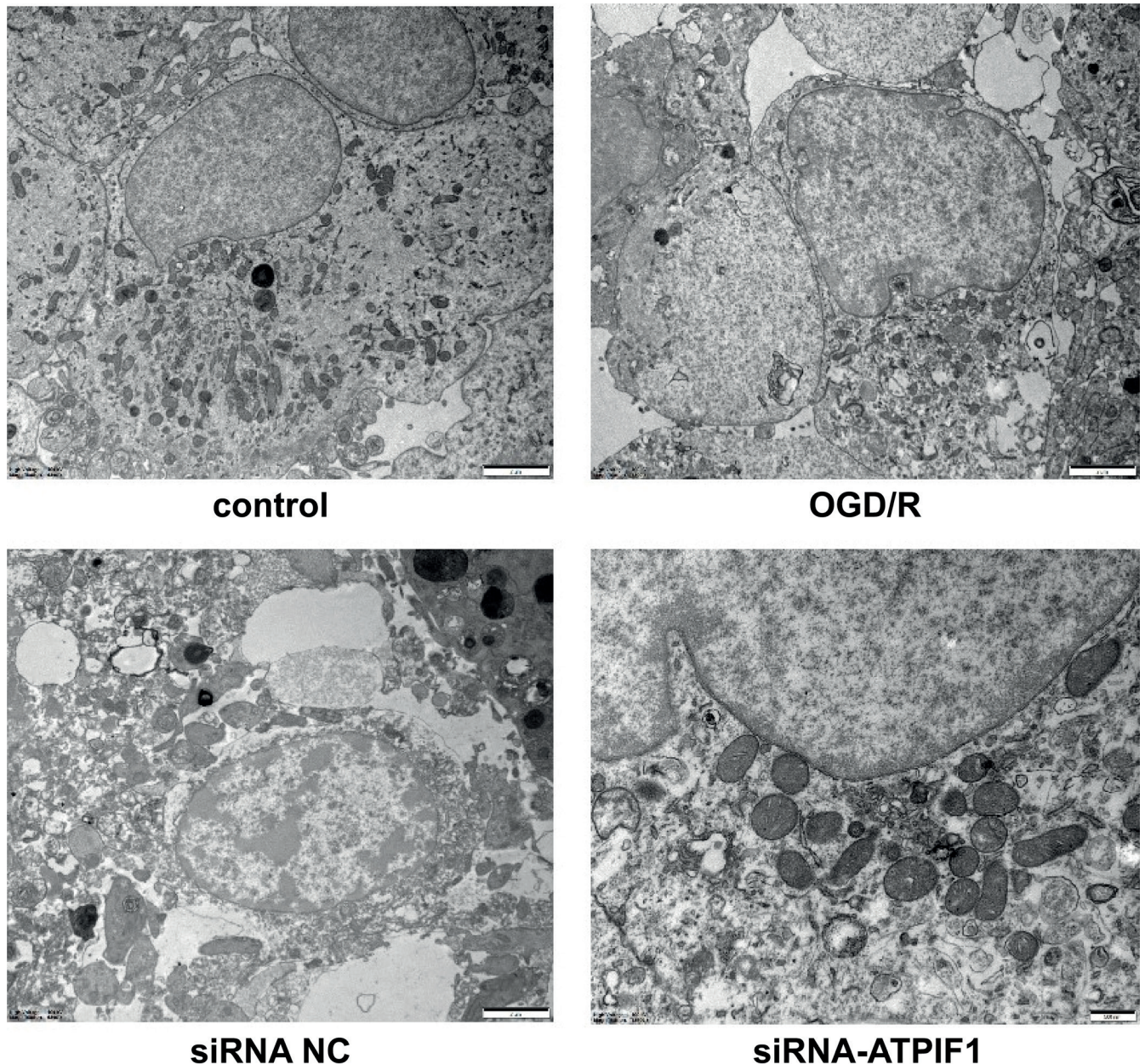


Fig. 4. Morphological changes in the mitochondria in each group
OGD/R – oxygen glucose deprivation/reoxygenation.

Apoptosis can be induced by extrinsic (death receptor) and intrinsic (mitochondrial) pathways.²² Mitochondrial morphology changes in the mitochondria-mediated pathway. The increase in mitochondrial membrane permeability causes the activation of downstream effector caspases, such as caspase-3, and eventually induces apoptosis.²³ Xu et al. demonstrated that ATPIF1 plays a key role in regulating cleaved caspase-3 expression in the microglia.²⁴ The Bcl-2 family proteins, such as Bax and Bcl-2, mediate the intrinsic pathway by altering the outer membrane permeability of the mitochondria.²⁵ The Bax protein is a common channel of the mitochondria-mediated apoptosis pathway.²⁶ We found

that siRNA-ATPIF1 could inhibit Bax and increase Bcl-2 protein expression in astrocytes. The OGD/R-induced astrocytes had increased MMP and abnormal mitochondrial morphology, and siRNA-ATPIF1 inhibited these processes. Cleaved caspase-3 expression decreased in the OGD/R cells treated with siRNA-ATPIF1. The results showed that siRNA-ATPIF1 could effectively inhibit mitochondria-mediated apoptosis in astrocytes after the OGD/R treatment.

The NF- κ B plays an active role in apoptosis.²⁷ In a non-stimulated state, NF- κ B and I κ B form a complex in the cytoplasm, but they are not activated. The I κ B is rapidly phosphorylated after cell stimulation and further degraded

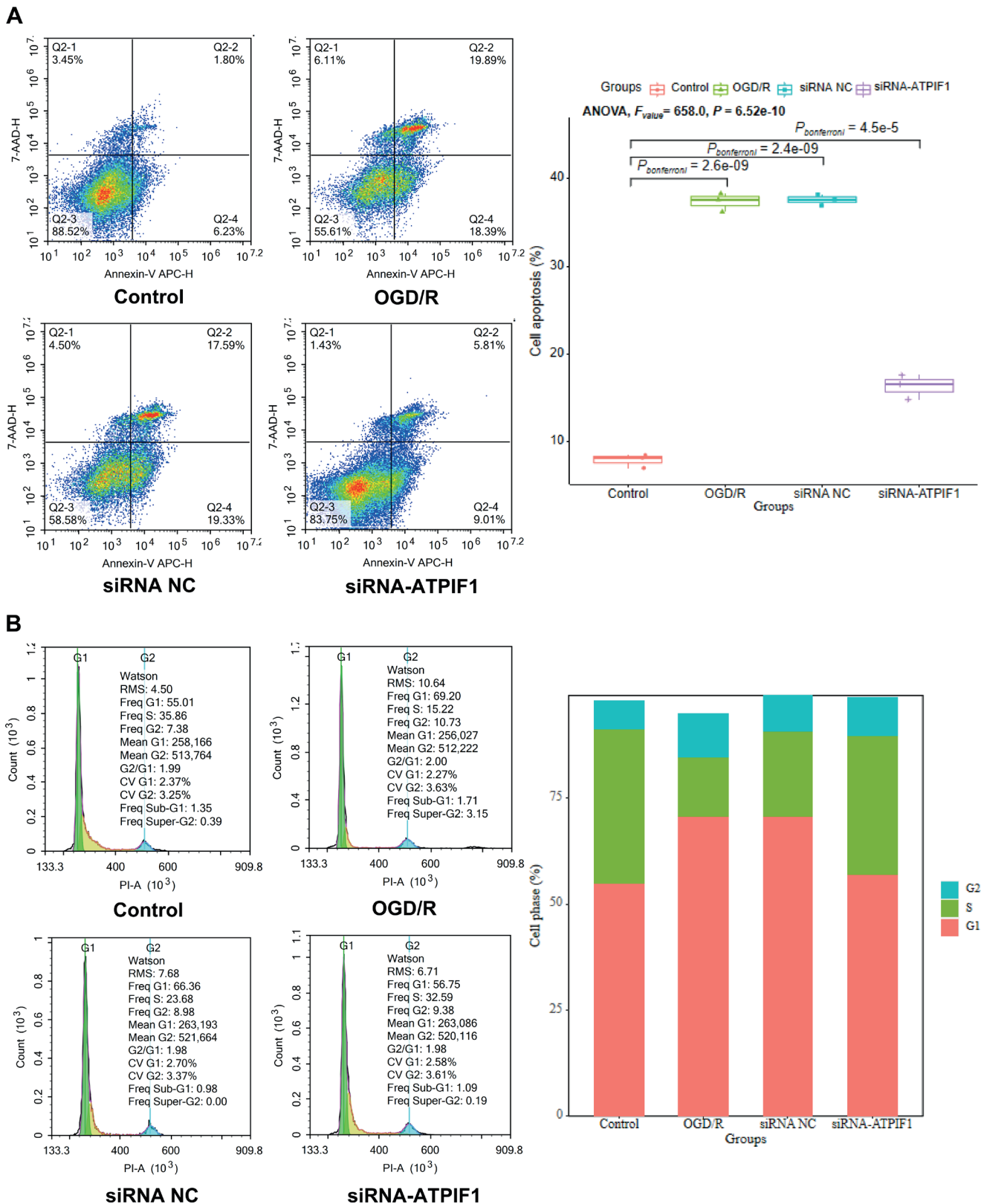


Fig. 5. Apoptosis and cell cycle detected using flow cytometry. A. Scatter plots of cell apoptosis (analysis of variance (ANOVA), $F = 658.0$, $p = 6.52e-10$; oxygen glucose deprivation/reoxygenation (OGD/R) compared to controls, $p_{\text{bonferroni}} = 2.6E-09$; siRNA-ATPIF1 compared to OGD/R, $p_{\text{bonferroni}} = 0.000000037$); B. Cell cycle. The data analysis results are presented in Supplementary Table 1

by ubiquitinase or protease.²⁸ After $\text{I}\kappa\text{B}$ degradation is complete, $\text{NF-}\kappa\text{B}$ is rapidly activated and then translocated into the nucleus to react with the downstream

targets.²⁹ The $\text{NF-}\kappa\text{B}$ can respond to ROS accumulation signals and initiate the pro-apoptotic pathway activation.³⁰ The present study found that astrocytes produce

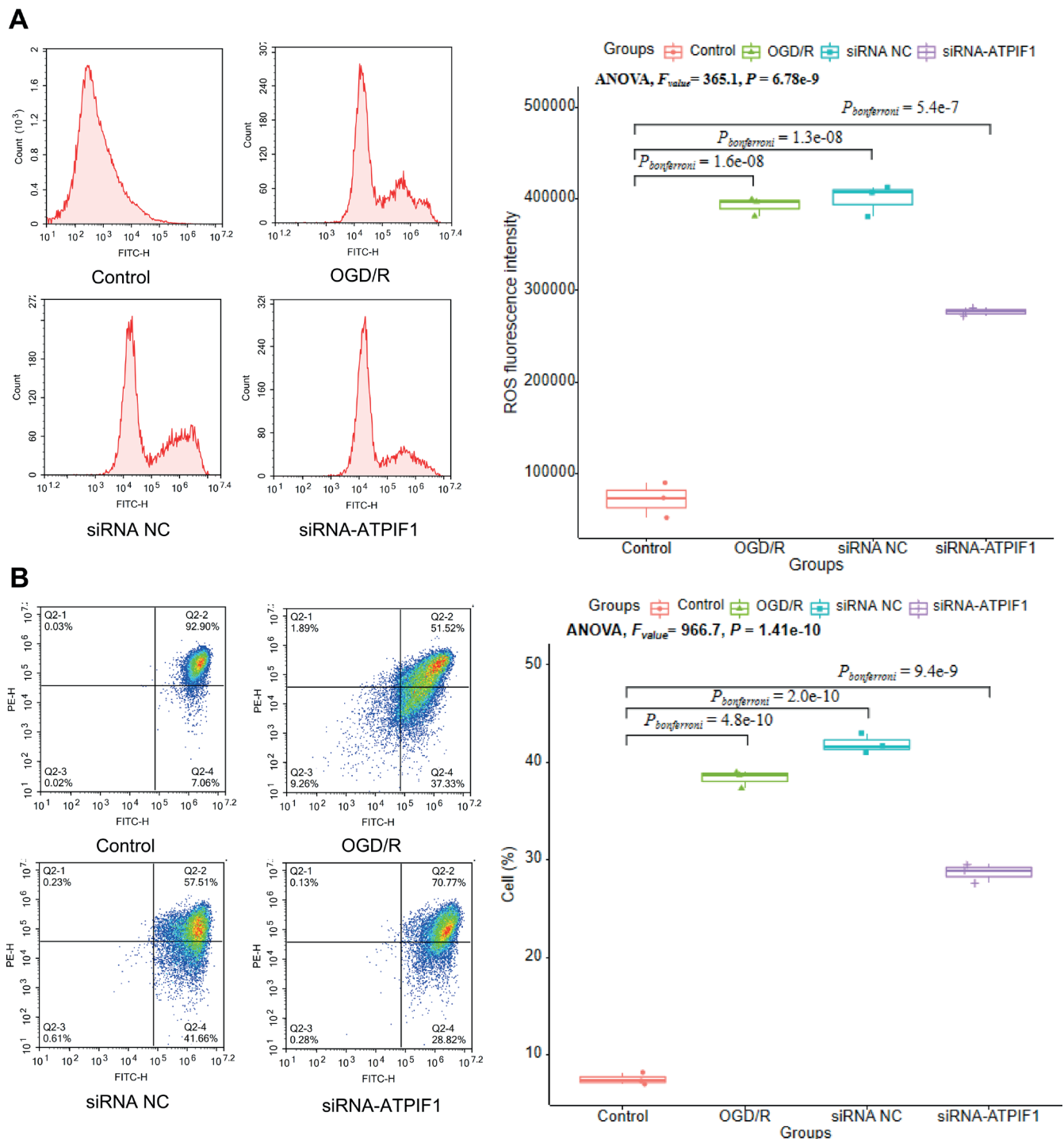


Fig. 6. Reactive oxygen species (ROS) and membrane potential detected using flow cytometry. A. ROS level (analysis of variance (ANOVA), $F = 365.1$, $p = 6.78e-09$; oxygen glucose deprivation/reoxygenation (OGD/R) compared to controls, $p = 0.000000016$; siRNA-ATPIF1 compared to OGD/R, $p_{bonferroni} = 4.3E-05$); B. Membrane potential (ANOVA, $F = 966.7$, $p = 1.41e-10$; OGD/R compared to controls, $p_{bonferroni} = 4.8E-10$; siRNA-ATPIF1 compared to OGD/R, $p_{bonferroni} = 4.6E-06$). The data analysis results are presented in Supplementary Table 1

a large amount of ROS after OGD/R. Therefore, we investigated whether NF- κ B is involved in ATP1F1-mediated mitochondrial apoptosis. Western blot results showed that ATP1F1 knockdown could reduce NF- κ B expression, indicating that the NF- κ B signaling pathway may be involved in ATP1F1-induced mitochondrial apoptosis in astrocytes.

Limitations

Although this study has clarified the effect of ATP1F1 on astrocyte apoptosis, some studies have pointed out that pH changes also have a remarkable effect on ATP1F1 activity.³¹ However, this factor was not taken into account in our experiments. The effect of hypoxia on pH value in vivo and

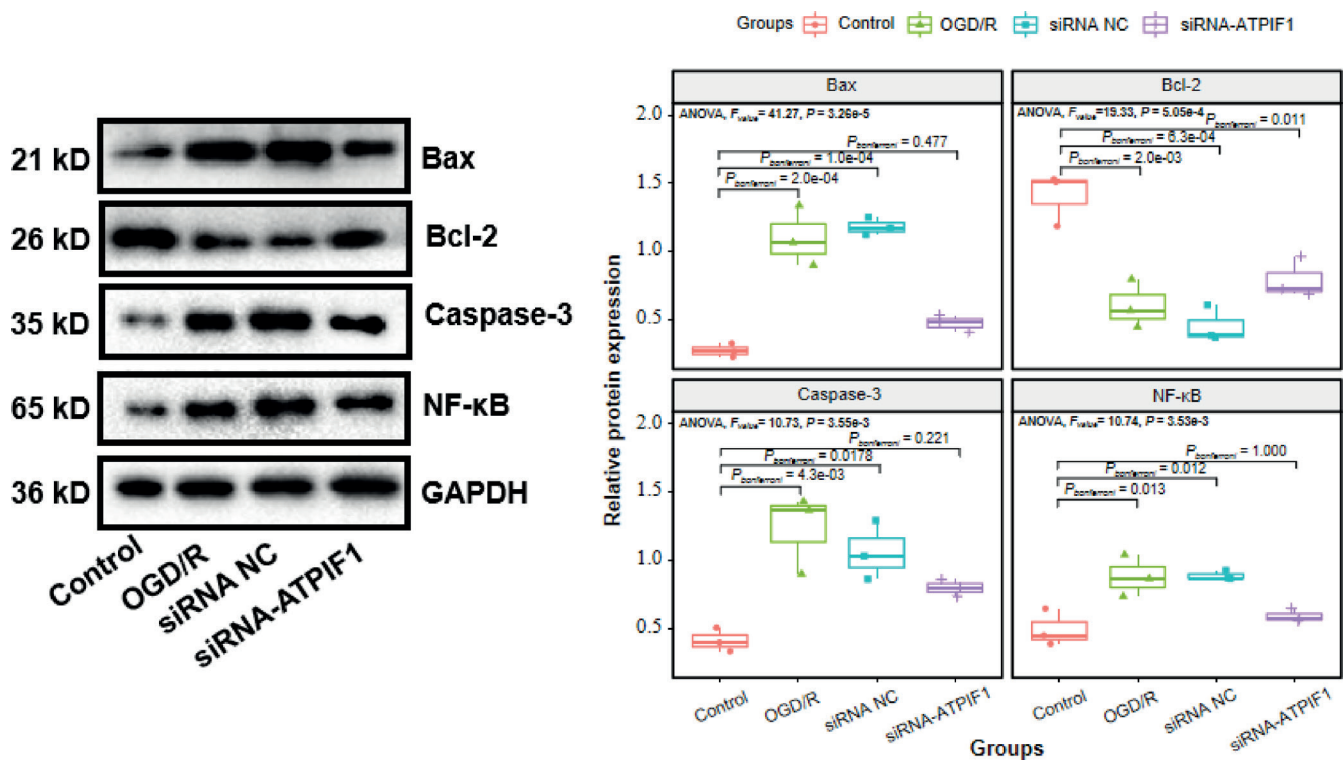


Fig. 7. Bcl-2-associated X (Bax), B-cell lymphoma 2 (Bcl-2), caspase-3, and nuclear factor kappa B (NF-κB) protein expression. Bax: analysis of variance (ANOVA), $F = 41.27$, $p = 3.26 \times 10^{-5}$; oxygen glucose deprivation/reoxygenation (OGD/R) compared to controls, $p_{\text{bonferroni}} = 2.0 \times 10^{-4}$; siRNA-ATPIF1 compared to OGD/R, $p_{\text{bonferroni}} = 0.001$. Bcl-2: ANOVA, $F = 19.33$, $p = 0.000505$; OGD/R compared to controls, $p_{\text{bonferroni}} = 2.0 \times 10^{-3}$; siRNA-ATPIF1 compared to controls, $p_{\text{bonferroni}} = 0.011$, compared to OGD/R, $p_{\text{bonferroni}} = 1.000$. Caspase-3: ANOVA, $F = 10.73$, $p = 0.00355$; OGD/R compared to controls, $p_{\text{bonferroni}} = 0.0043$; siRNA-ATPIF1 compared to controls, $p_{\text{bonferroni}} = 0.221$, compared to OGD/R, $p_{\text{bonferroni}} = 0.135$. NF-κB: ANOVA, $F = 10.74$, $p = 0.00353$; OGD/R compared to controls, $p_{\text{bonferroni}} = 0.013$, siRNA-ATPIF1 compared to controls, $p_{\text{bonferroni}} = 1.000$, compared to OGD/R, $p_{\text{bonferroni}} = 0.061$. The data analysis results are presented in Supplementary Table 1

then on ATPIF1, particularly in animals and even in humans, will also be a direction of our subsequent studies.

Recently, the application of ATPIF1 gene-silenced T cells in the preparation of antitumor drugs has also been described, which provides a new direction for the research and development of adoptive immunotherapy for tumors. We believe that cell therapy by *ATPIF1* gene knockout can have a broad development prospect in the treatment of cerebral ischemia injury.

Conclusions

This study is the first to report that during ischemic brain injury, ATPIF1 regulation of mitochondria-mediated apoptosis is associated with the promotion of NF-κB activation. The ATPIF1 knockdown can improve the mitochondrial morphology, inhibit MMP, massive ROS accumulation and NF-κB activation, reduce Bax expression, increase Bcl-2 protein expression, and maintain astrocyte viability in OGD/R-induced injury.

Generalizability/translation

The findings of this study may be generalized to other species or experimental conditions, including human biology.

Data availability statement

Data will be made available by the corresponding author upon reasonable request.

Supplementary files

The supplementary files are available at <https://doi.org/10.5281/zenodo.7454344>. The package contains the following files:

Supplementary Table 1. Data analysis for Fig. 2,3,5,6,7.

ORCID iDs

Zhijie Wei <https://orcid.org/0000-0001-9593-5084>
 Rui Wu <https://orcid.org/0000-0003-3921-456X>
 Li Zhang <https://orcid.org/0000-0001-7958-4720>
 Ping Xu <https://orcid.org/0000-0002-5166-4080>

References

- Radak D, Katsiki N, Resanovic I, et al. Apoptosis and acute brain ischemia in ischemic stroke. *Curr Vasc Pharmacol.* 2017;15(2):115–122. doi:10.2174/1570161115666161104095522
- Feigin VL, Krishnamurthi RV, Parmar P, et al. Update on the global burden of ischemic and hemorrhagic stroke in 1990–2013: The GBD 2013 Study. *Neuroepidemiology.* 2015;45(3):161–176. doi:10.1159/000441085
- Avan A, Hachinski V. Stroke and dementia, leading causes of neurological disability and death, potential for prevention. *Alzheimers Dementia.* 2021;17(6):1072–1076. doi:10.1002/alz.12340

4. Wang J, Sareddy GR, Lu Y, et al. Astrocyte-derived estrogen regulates reactive astrogliosis and is neuroprotective following ischemic brain injury. *J Neurosci*. 2020;40(50):9751–9771. doi:10.1523/JNEUROSCI.0888-20.2020
5. Rossi DJ, Brady JD, Mohr C. Astrocyte metabolism and signaling during brain ischemia. *Nat Neurosci*. 2007;10(11):1377–1386. doi:10.1038/nn2004
6. van Putten MJAM, Fahlke C, Kafitz KW, Hofmeijer J, Rose CR. Dysregulation of astrocyte ion homeostasis and its relevance for stroke-induced brain damage. *Int J Mol Sci*. 2021;22(11):5679. doi:10.3390/ijms22115679
7. Kandul NP, Zhang T, Hay BA, Guo M. Selective removal of deletion-bearing mitochondrial DNA in heteroplasmic *Drosophila*. *Nat Commun*. 2016;7(1):13100. doi:10.1038/ncomms13100
8. Martín-Jiménez R, Faccenda D, Allen E, et al. Reduction of the ATPase inhibitory factor 1 (IF₁) leads to visual impairment in vertebrates. *Cell Death Dis*. 2018;9(6):669. doi:10.1038/s41419-018-0578-x
9. Li J, Sun YBY, Chen W, et al. Smad4 promotes diabetic nephropathy by modulating glycolysis and OXPHOS. *EMBO Rep*. 2020;21(2):e48781. doi:10.15252/embr.201948781
10. Chen WW, Birsoy K, Mihaylova MM, et al. Inhibition of ATP1F1 ameliorates severe mitochondrial respiratory chain dysfunction in mammalian cells. *Cell Rep*. 2014;7(1):27–34. doi:10.1016/j.celrep.2014.02.046
11. Kurbasic E, Sjöström M, Krogh M, et al. Changes in glycoprotein expression between primary breast tumour and synchronous lymph node metastases or asynchronous distant metastases. *Clin Proteom*. 2015;12(1):13. doi:10.1186/s12014-015-9084-7
12. Shah DI, Takahashi-Makise N, Cooney JD, et al. Mitochondrial Atp1f1 regulates haem synthesis in developing erythroblasts. *Nature*. 2012;491(7425):608–612. doi:10.1038/nature11536
13. Mu W, Cheng X, Zhang X, et al. Hinokiflavone induces apoptosis via activating mitochondrial ROS/JNK/caspase pathway and inhibiting NF- κ B activity in hepatocellular carcinoma. *J Cell Mol Med*. 2020;24(14):8151–8165. doi:10.1111/jcmm.15474
14. Wang X, Lu X, Zhu R, et al. Betulinic acid induces apoptosis in differentiated PC12 cells via ROS-mediated mitochondrial pathway. *Neurochem Res*. 2017;42(4):1130–1140. doi:10.1007/s11064-016-2147-y
15. Zhang T, Zhao G, Zhu X, et al. Sodium selenite induces apoptosis via ROS-mediated NF- κ B signaling and activation of the Bax–caspase-9–caspase-3 axis in 4T1 cells. *J Cell Physiol*. 2019;234(3):2511–2522. doi:10.1002/jcp.26783
16. Yamagata K. Astrocyte-induced synapse formation and ischemic stroke. *J Neurosci Res*. 2021;99(5):1401–1413. doi:10.1002/jnr.24807
17. Santello M, Toni N, Volterra A. Astrocyte function from information processing to cognition and cognitive impairment. *Nat Neurosci*. 2019;22(2):154–166. doi:10.1038/s41593-018-0325-8
18. Bayraktar OA, Bartels T, Holmqvist S, et al. Astrocyte layers in the mammalian cerebral cortex revealed by a single-cell in situ transcriptomic map. *Nat Neurosci*. 2020;23(4):500–509. doi:10.1038/s41593-020-0602-1
19. Zamboni M, Llorens-Bobadilla E, Magnusson JP, Frisén J. A widespread neurogenic potential of neocortical astrocytes is induced by injury. *Cell Stem Cell*. 2020;27(4):605–617.e5. doi:10.1016/j.stem.2020.07.006
20. Wang K, Chen H, Zhou Z, Zhang H, Zhou HJ, Min W. ATP1F1 maintains normal mitochondrial structure which is impaired by CCM3 deficiency in endothelial cells. *Cell Biosci*. 2021;11(1):11. doi:10.1186/s13578-020-00514-z
21. Faccenda D, Tan CH, Seraphim A, Duchen MR, Campanella M. IF1 limits the apoptotic-signalling cascade by preventing mitochondrial remodelling. *Cell Death Differ*. 2013;20(5):686–697. doi:10.1038/cdd.2012.163
22. Uzdensky AB. Apoptosis regulation in the penumbra after ischemic stroke: Expression of pro- and antiapoptotic proteins. *Apoptosis*. 2019;24(9–10):687–702. doi:10.1007/s10495-019-01556-6
23. Li M, Tan J, Miao Y, Lei P, Zhang Q. The dual role of autophagy under hypoxia-involvement of interaction between autophagy and apoptosis. *Apoptosis*. 2015;20(6):769–777. doi:10.1007/s10495-015-1110-8
24. Xu Y, Gao G, Sun X, Liu Q, Li C. ATPase inhibitory factor 1 is critical for regulating sevoflurane-induced microglial inflammatory responses and caspase-3 activation. *Front Cell Neurosci*. 2021;15:770666. doi:10.3389/fncel.2021.770666
25. Clavier A, Rincheval-Arnold A, Colin J, Mignotte B, Guéna I. Apoptosis in *Drosophila*: Which role for mitochondria? *Apoptosis*. 2016;21(3):239–251. doi:10.1007/s10495-015-1209-y
26. Soond SM, Kozhevnikova MV, Savvateeva LV, Townsend PA, Zamyatnin AA. Intrinsically connected: Therapeutically targeting the cathepsin proteases and the Bcl-2 family of protein substrates as co-regulators of apoptosis. *Int J Mol Sci*. 2021;22(9):4669. doi:10.3390/ijms22094669
27. Khan H, Ullah H, Castilho PCMF, et al. Targeting NF- κ B signaling pathway in cancer by dietary polyphenols. *Crit Rev Food Sci Nutr*. 2020;60(16):2790–2800. doi:10.1080/10408398.2019.1661827
28. Soleimani A, Rahmani F, Ferns GA, Ryzhikov M, Avan A, Hassanian SM. Role of the NF- κ B signaling pathway in the pathogenesis of colorectal cancer. *Gene*. 2020;726:144132. doi:10.1016/j.gene.2019.144132
29. Kandasamy M. NF- κ B signalling as a pharmacological target in COVID-19: Potential roles for IKK β inhibitors. *Naunyn Schmiedeberg's Arch Pharmacol*. 2021;394(3):561–567. doi:10.1007/s00210-020-02035-5
30. Shen M, Hu Y, Yang Y, et al. Betulinic acid induces ROS-dependent apoptosis and S-phase arrest by inhibiting the NF- κ B pathway in human multiple myeloma. *Oxid Med Cell Longev*. 2019;2019:5083158. doi:10.1155/2019/5083158
31. Cabezón E, Butler PJG, Runswick MJ, Carbajo RJ, Walker JE. Homologous and heterologous inhibitory effects of ATPase inhibitor proteins on F-ATPases. *J Biol Chem*. 2002;277(44):41334–41341. doi:10.1074/jbc.M207169200

hsa_circ_0017842 acts as a competing endogenous RNA to enhance the malignancy of gastric cancer

*Xigang Wen^{1,A,D,F}, *Wenling Han^{2,B–D,F}, Chao Liu^{1,E,F}

¹ Department of Gastrointestinal Surgery, Third People's Hospital of Hubei Province, Wuhan, China

² Department of Hospital Infection, Third People's Hospital of Hubei Province, Wuhan, China

A – research concept and design; B – collection and/or assembly of data; C – data analysis and interpretation; D – writing the article; E – critical revision of the article; F – final approval of the article

Advances in Clinical and Experimental Medicine, ISSN 1899–5276 (print), ISSN 2451–2680 (online)

Adv Clin Exp Med. 2023;32(7):803–812

Address for correspondence

Chao Liu
E-mail: ChaoLiu53@163.com

Funding sources

None declared

Conflict of interest

None declared

* Xigang Wen and Wenling Han contributed equally to this work.

Received on June 21, 2022

Reviewed on June 29, 2022

Accepted on December 23, 2022

Published online on March 30, 2023

Abstract

Background. Circular RNAs (circRNAs) have been shown to act as competing endogenous RNAs (ceRNAs) participating in the progression of gastric cancer (GC).

Objectives. Our study aimed to investigate whether hsa_circ_0017842 can affect the malignancy of GC in a ceRNA manner.

Materials and methods. Gene expression microarrays from GEO DataSets database, quantitative real-time polymerase chain reaction (qPCR) and western blotting were used to identify the expression levels of hsa_circ_0017842, miR-1294, and secreted protein, acidic and rich in cysteine (SPARC) in GC. The function of hsa_circ_0017842/miR-1294/SPARC axis in GC cells was confirmed using gain- and loss-of-function assays. In addition, luciferase and RNA pulldown assays were performed to demonstrate the ceRNA mechanism of hsa_circ_0017842 involving miR-1294 and SPARC.

Results. The upregulation of hsa_circ_0017842 and SPARC, and downregulation of miR-1294 were observed in GC. Upregulating hsa_circ_0017842 in GC cells led to an increase in their proliferation, migration and invasion, and hsa_circ_0017842 knockdown showed the opposite effects on GC cells. Moreover, hsa_circ_0017842 was shown to be a sponge for miR-1294, thereby regulating SPARC expression. Due to the targeting relationship among hsa_circ_0017842, miR-1294 and SPARC, SPARC knockdown could relieve the effect of hsa_circ_0017842 overexpression on GC cells.

Conclusions. Overall, this study confirmed that hsa_circ_0017842 acted as a ceRNA to promote the malignancy of GC cells through regulating the miR-1294/SPARC axis. Our findings might help better elucidate the molecular mechanism of GC tumorigenesis, and as a result improve the overall survival of GC patients.

Key words: SPARC, ceRNA, gastric cancer, hsa_circ_0017842, miR-1294

Cite as

Wen X, Han W, Liu C. hsa_circ_0017842 acts as a competing endogenous RNA to enhance the malignancy of gastric cancer. *Adv Clin Exp Med.* 2023;32(7):803–812. doi:10.17219/acem/158484

DOI

10.17219/acem/158484

Copyright

Copyright by Author(s)

This is an article distributed under the terms of the Creative Commons Attribution 3.0 Unported (CC BY 3.0) (<https://creativecommons.org/licenses/by/3.0/>)

Background

Gastric cancer (GC), with high incidence and mortality, ranks among the top 5 malignant tumors and is the 3rd leading cause of cancer-related deaths worldwide.^{1,2} According to the latest data from the World Health Organization (WHO) from 2020, the number of new GC cases in China was almost 480,000.³ Although the incidence and mortality of GC decrease with the improvements in diagnosis and therapy, overall survival (OS) is poor in most countries due to the heterogeneity and complex regulatory mechanism of this disease.^{4–6} Hence, exploring the molecular mechanism of GC tumorigenesis is an urgent need for improving the therapy of GC.

Circular RNAs (circRNAs) belong to the non-coding RNA family and exhibit a covalently closed-loop structure by direct back-splicing or exon skipping.^{7,8} By means of high-throughput sequencing and bioinformatic analysis, circRNAs were confirmed to be abnormally expressed and participate in various diseases.^{9–11} In GC, circRNAs have been shown to act as competing endogenous RNAs (ceRNAs) by regulating the expression of microRNAs (miRNAs) to release the target genes of miRNAs, thereby regulating GC progression.^{12–14} The hsa_circ_0005556 acts as a ceRNA to sponge miR-4270-enhanced MMP19 expression, thereby accelerating GC progression.¹⁵ The circRNA ITCH as a ceRNA could suppress the metastasis of GC cells by sponging miR-199a-5p/Klotho axis.¹⁶ In the present study, we found the abnormal expression of hsa_circ_0017842 in GC samples using a circRNA expression microarray. To our knowledge, the function of hsa_circ_0017842 has not been reported. As a result of bioinformatic analysis, we predicted that hsa_circ_0017842 might sponge miR-1294. In GC, the inhibitory effect of miR-1294 on GC cells has been identified.^{17–19} However, the circRNA as upstream of miR-1294 in GC is still unknown.

Secreted protein, acidic and rich in cysteine (SPARC), a matricellular glycoprotein, is expressed in embryonic tissues, bone and endothelial cells, and has been shown to play a key role in the development and differentiation of chondrocytes and megakaryocytes.^{20,21} Clinically, SPARC was found to be overexpressed in GC tissues, and its overexpression was correlated with the poor survival rate of GC patients with tumor-node-metastasis (TNM) stages I, II and III.²² In *in vitro* studies, knocking down SPARC reduced the number of invasive GC cells, suggesting its promotive function in GC development.²³ Bioinformatic analysis in our study predicted that SPARC was a target gene of miR-1294. Furthermore, the interaction between miR-1294 and SPARC has not been explored in any diseases.

Objectives

By means of a literature review and bioinformatic analysis, we aimed to investigate whether hsa_circ_0017842 acts as a crucial circRNA to regulate GC progression by targeting the miR-1294/SPARC pathway. Our findings could contribute to elucidating the molecular mechanism of GC tumorigenesis to improve the overall survival of GC patients.

Materials and methods

Bioinformatic analysis

GSE93541 from a public database (GEO DataSets; <https://www.ncbi.nlm.nih.gov/gds>) was used to identify the expression of hsa_circ_0017842 in GC samples and normal samples from the same patients. Then, starBase (<https://starbase.sysu.edu.cn/panCancer.php>) and circInteractome database (<https://starbase.sysu.edu.cn/panCancer.php>) were applied to predict the downstream miRNAs of hsa_circ_0017842, whereas TargetScan database (<https://starbase.sysu.edu.cn/panCancer.php>) was used to predict the downstream mRNAs of the predicted miRNAs. Besides, we also used 2 gene expression microarrays (GSE103236 and GSE79973) from GEO DataSets to confirm the upregulated genes in GC with adjusted $p < 0.05$ and $\log_2FC > 1$. STRING tool (<https://cn.string-db.org/>) was used to construct protein-protein interaction (PPI) networks for the screened genes.

Clinical samples and cell lines

The GC samples and corresponding adjacent non-tumor samples were collected from 34 patients who were diagnosed with GC in the Third People's Hospital of Hubei Province (Wuhan, China) between January 2021 and January 2022. Our study was approved by the Ethics Committee of the Third People's Hospital of Hubei Province (2021 Ethic Audit Section No. 16) and adheres to the ethical standards of the Declaration of Helsinki. Every patient enrolled in this study gave written informed consent.

Table 1 displays the clinical characteristics of 34 GC patients. All cell lines were purchased from Procell (Wuhan, China), including 2 GC cell lines (AGS, cat. No. CL-0022; MKN-7 and cat No. CL-0574) and human gastric mucosa cell line GES-1 (cat. No. CL-0563). The AGS cells were kept in Ham's F-12 medium (cat No. PM150810; Procell) at 37°C and 5% CO₂, whereas GES-1 and MKN-7 cells were kept in RPMI-1640 medium (cat. No. PM150110; Procell) at 37°C and 5% CO₂. All media were supplemented with 10% fetal bovine serum (FBS; cat. No. 164210-50; Procell) and 1% penicillin/streptomycin (cat. No. PB180120; Procell).

Table 1. Clinical characteristics of the gastric cancer patients

Characteristics		Numbers of cases (%)
Age [years]	≥60	19 (55.9)
	<60	15 (44.1)
Gender	male	22 (64.7)
	female	12 (35.3)
Tumor size	<3 cm	14 (41.2)
	≥3cm	20 (58.8)
TNM stage	I + II	9 (26.5)
	III + IV	25 (73.5)
Grade	well	5 (14.7)
	moderately	20 (58.8)
	poor	9 (26.5)

TNM – tumor-node-metastasis.

qPCR and RNase R treatment

TRIzol Total RNA isolation kit (cat. No. KGA1201; Key-Gen Biotech, Nanjing, China) was used for RNA extraction from tissues and cells. Then, cDNA synthesis and quantitative real-time polymerase chain reaction (qPCR) were carried out using a PrimeScript Reverse Transcription Kit (Takara, Shiga, Japan) and SYBR Green Master Mix Kit (Takara), respectively. The $2^{-\Delta\Delta Ct}$ method was applied for identifying the relative expression of circRNA, miRNA and mRNA using GAPDH or U6 as an endogenous control. Table 2 includes all the primer sequences used in this study.

For RNase R treatment, 2 µg of isolated RNA from GC cells were treated with or without 3 U/mg RNase R (Sigma-Aldrich, St. Louis, USA). After incubation for 60 min at 37°C, the expression of hsa_circ_0017842 and its linear gene *FAM188A* was measured with qPCR to demonstrate the stability of hsa_circ_0017842.

Table 2. Primer sequences in this study

Gene		Primer sequence
hsa_circ_0017842	forward	5'-TGATCCTAGTTGATGGCCCTAA-3'
	reverse	5'-GAGAGCCACTTGACAGAGACC-3'
hsa-miR-1270	forward	5'-CTGGAGATATGGAAGAGCTGTGT-3'
	reverse	5'-TGCAAAGAGCCACATAGAAGAT-3'
hsa-miR-620	forward	5'-GCCGAGATGGAGATAGATAT-3'
	reverse	5'-CTCAACTGGTGTCTGTGGA-3'
hsa-miR-1294	forward	5'-CTTAGTTGCGTTACACCCCTTCTTG-3'
	reverse	5'-CTGTCACCTTACCCTTCCAGTTT-3'
hsa-miR-1286	forward	5'-GCCGAGTGCAGGACCAAGATG-3'
	reverse	5'-CTCAACTGGTGTCTGTGGA-3'
SPARC	forward	5'-CGAAGAGGAGGTGGTGGCGGAAA-3'
	reverse	5'-GGTGTGTTCCTCATCCCTCTCATA-3'
GAPDH	forward	5'-CTCTCTGCTCCTCTGTTCGACAG-3'
	reverse	5'-AGGGGTCTTACTCCTTGGAGGCCA-3'
U6	forward	5'-CTCGCTTCGGCAGCACA-3'
	reverse	5'-AACGCTTCACGAATTTGCGT-3'

Cell transfection

All vectors used for cell transfection were purchased from Ke Lei Biological Technology Co., Ltd. (Shanghai, China). The pcDNA3.1-circ vector was used to construct hsa_circ_0017842 expression vectors (circ-OE), and the empty vector was used as a negative control (NC). The siRNAs targeting hsa_circ_0017842 (si-circ) and *SPARC* (si-SPARC) were used to knock down hsa_circ_0017842 and *SPARC*, respectively, with si-NC as NC. The miR-1294 mimic was designed to overexpress miR-1294 and mimic-NC was used as NC. For cell transfections, the mentioned vectors were applied to the GC cells at 50 nM concentration using Lipofectamine 3000 (Invitrogen, Carlsbad, USA). The qPCR was carried out to identify the transfection efficiency of vectors 48 h after transfection.

EdU assay

EdU-647 cell proliferation kit (Beyotime Biotechnology, Beijing, China) was used to assess cell proliferation. After transfection, 1×10^4 GC cells were seeded into a 96-well plate for incubation overnight. After incubation, 10 µM EdU was applied to cells for 2 h at 37°C. Then, the cells were fixed with 4% paraformaldehyde, treated with 0.1% Triton X-100, rinsed with phosphate-buffered saline (PBS), and incubated with 100 µL click reaction cocktail. Next, the cells were incubated in 5 µg/mL Hoechst 33342 to stain cell nuclei. Finally, the cells were observed and imaged using a fluorescence microscope (model TE2000; Nikon Corp., Tokyo, Japan).

Transwell assay

Transwell assays were performed to assess the change in cell migration and invasion. In cell migration detection, 1×10^4 transfected GC cells suspended in 200 µL of serum-free medium were added into the upper chamber; at the same time, 500 µL of medium with 10% FBS was added into the bottom chamber. After 48 h, the cells that remained on the lower surface were fixed with methanol, stained with crystal violet and observed under an inverted microscope (model TS2; Nikon Corp.). In cell invasion detection, the membrane in the upper chamber was coated with Matrigel (BD Biosciences, Franklin Lakes, USA) before adding the cells. The following procedure was the same as cell migration.

RNA pulldown assay

A biotinylated RNA pulldown assay was used to identify the interaction between circRNA and miRNA, as described in a previous study.²⁴ Briefly, 1×10^7 GC cells were collected, lysed, and incubated with hsa_circ_0017842 probe-coated beads at 4°C overnight. After washing, the RNA was isolated to perform qPCR.

Luciferase assay

Wild-type hsa_circ_0017842 (WT-circ) or SPARC (SPARC-WT) containing binding sites for miR-1294 were constructed by Beijing Qualityard Biotechnology Co., Ltd. (Beijing, China) using a pGL3 vector (Promega, Madison, USA). Mutant hsa_circ_0017842 (MUT-circ) or SPARC (SPARC-MUT) without binding sites for miR-1294 were also constructed by Beijing Qualityard Biotechnology Co., Ltd. using a pGL3 vector. The aforementioned vectors were co-transfected into GC cells with miR-1294 mimic or mimic-NC. Luciferase activity was detected 48 h after transfection with the aid of a dual-luciferase report analysis system (Promega).

Western blotting

Protein concentrations, isolated using Radioimmuno-precipitation Assay (RIPA) Lysis Buffer (cat. No. KGP702; KeyGen Biotech), were quantified with BCA Protein Assay Kit (Tiangen Biotech, Beijing, China). Protein samples were separated using 12% sodium dodecyl-sulfate polyacrylamide gel electrophoresis (SDS-PAGE) gel, then transferred to polyvinylidene difluoride (PVDF) membranes and blocked with 5% skimmed milk for 3 h at 22°C. The membranes were incubated overnight at 4°C with primary antibodies, including anti-SPARC (1:1000; cat. No. ab207743; Abcam, Cambridge, USA) and anti-GAPDH (1:1000; cat. No. ab9485; Abcam). Next, the membranes were probed with fluorescent rabbit secondary antibodies (cat.

No. 18-4517-32; Rockland Immunochemicals, Rockland, USA) at 22°C for 2 h. Finally, the protein blots were visualized using Odyssey 3.2 (LI-COR Biosciences, Lincoln, USA).

Statistical analyses

Independent experiments were performed in triplicate. The data were analyzed using GraphPad Prism v. 8.0 (GraphPad Software, San Diego, USA) and expressed as the mean \pm standard deviation ($M \pm SD$). Each independent experiment included at least 3 samples. Shapiro–Wilk test was used to confirm the normal distribution of all data, and F test/Brown–Forsythe test was used to confirm the homogeneity of variances. Student's t-test was applied for statistical differences between the 2 groups, whereas Kruskal–Wallis test with Dunn's post hoc test or Mann–Whitney U test was applied for statistical differences if the number of samples was ≤ 9 . A value of $p < 0.05$ denotes statistical significance.

Results

The upregulation of hsa_circ_0017842 in GC

According to a circRNA expression microarray GSE93541, hsa_circ_0017842 was overexpressed in GC samples compared to normal non-tumor samples (Fig. 1A). In our collected clinical samples, hsa_circ_0017842 was

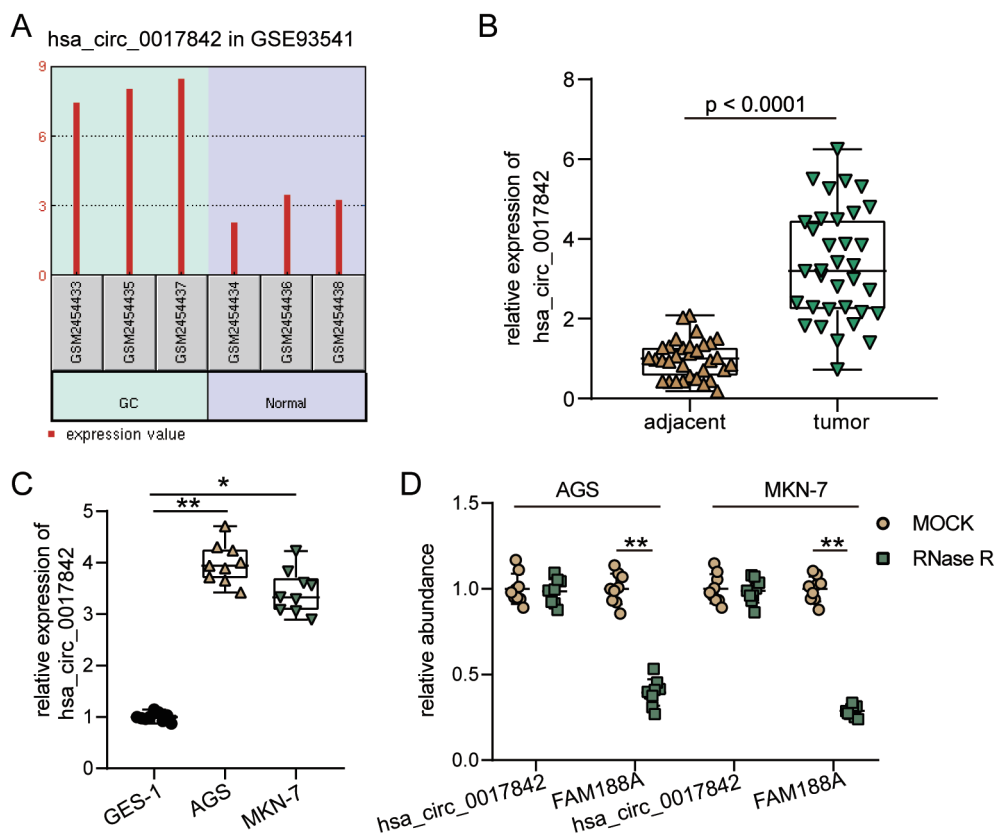


Fig. 1. The upregulation of hsa_circ_0017842 in gastric cancer (GC). A. A circular RNA (circRNA) expression microarray GSE93541 identified the upregulation of hsa_circ_0017842 in GC samples; B. hsa_circ_0017842 overexpression in GC tissues was detected using quantitative real-time polymerase chain reaction (qPCR) (paired Student's t-test, $n = 34$); C. hsa_circ_0017842 overexpression in GC cells (AGS and MKN-7) was detected using qPCR ($*p < 0.05$, $**p < 0.01$; Kruskal–Wallis test; $n = 9$); D. RNase R treatment confirmed the stable structure of hsa_circ_0017842 ($**p < 0.01$; Mann–Whitney U test; $n = 9$). All experiments were performed in triplicate.

also upregulated in GC samples compared to adjacent normal samples (Fig. 1B). In GC cells (AGS and MKN-7), hsa_circ_0017842 expression was significantly elevated (Fig. 1C). RNase R treatment did not produce any change in hsa_circ_0017842 expression, suggesting that the structure of hsa_circ_0017842 was stable (Fig. 1D). To summarize, hsa_circ_0017842 exhibited a stable structure and was overexpressed in GC.

The positive effect of hsa_circ_0017842 on GC cells

To explore the effect of hsa_circ_0017842 on GC cells, we transfected circ-OE vectors and si-circ to overexpress and knock down hsa_circ_0017842 in GC cells, respectively. Figure 2A displays the increase of hsa_circ_0017842 expression by more than 6-fold in GC cells after transfection with circ-OE vectors, whereas its expression decreased by more than 70% in GC cells after transfection with si-circ. The EdU assays revealed that circ-OE elevated EDU

positive rate, but si-circ caused a decline of EDU positive rate, suggesting the positive effect of hsa_circ_0017842 on cell proliferation (Fig. 2B). The transwell assay identified an increase in the number of migration cells and invasion cells after the GC cells were transfected with circ-OE, but showed a decrease after the GC cells were transfected with si-circ (Fig. 2C,D). All data suggested that hsa_circ_0017842 contributed to the proliferation, migration and invasion of GC cells.

hsa_circ_0017842 as a ceRNA to target miR-1294

To identify the miRNAs that bind to hsa_circ_0017842, 2 online databases (starBase and TargetScan) were used and 4 miRNAs were identified (miR-620, miR-1270, miR-1294, and miR-1286; Fig. 3A). RNA pulldown assays confirmed that only miR-1294 could be pulled down from GC cell samples with the hsa_circ_0017842 probe (Fig. 3B). Hence, we chose miR-1294 for further investigation. The binding

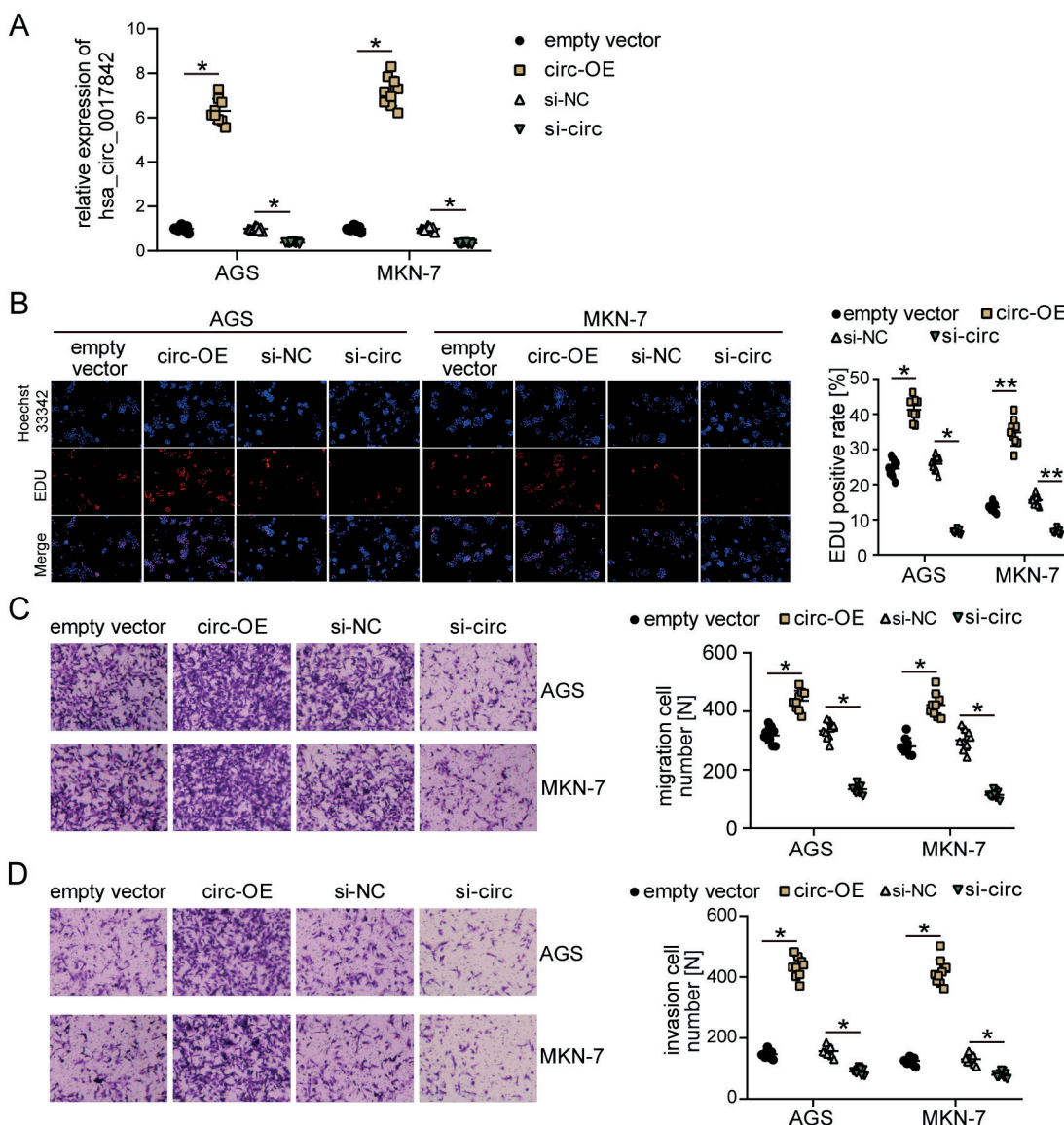


Fig. 2. The positive effect of hsa_circ_0017842 on gastric cancer (GC) cells. A. High transfection efficiency of the hsa_circ_0017842 overexpression vector (circ-OE) and siRNA of hsa_circ_0017842 (si-circ) was confirmed using quantitative real-time polymerase chain reaction (qPCR); B. The positive effect of hsa_circ_0017842 on cell proliferation in GC cells was detected using EdU assay; C,D. Transwell assay showed that hsa_circ_0017842 promoted cell migration (C) and cell invasion (D)

*p < 0.05, **p < 0.01; Kruskal–Wallis test; n = 9. All experiments were performed in triplicate.

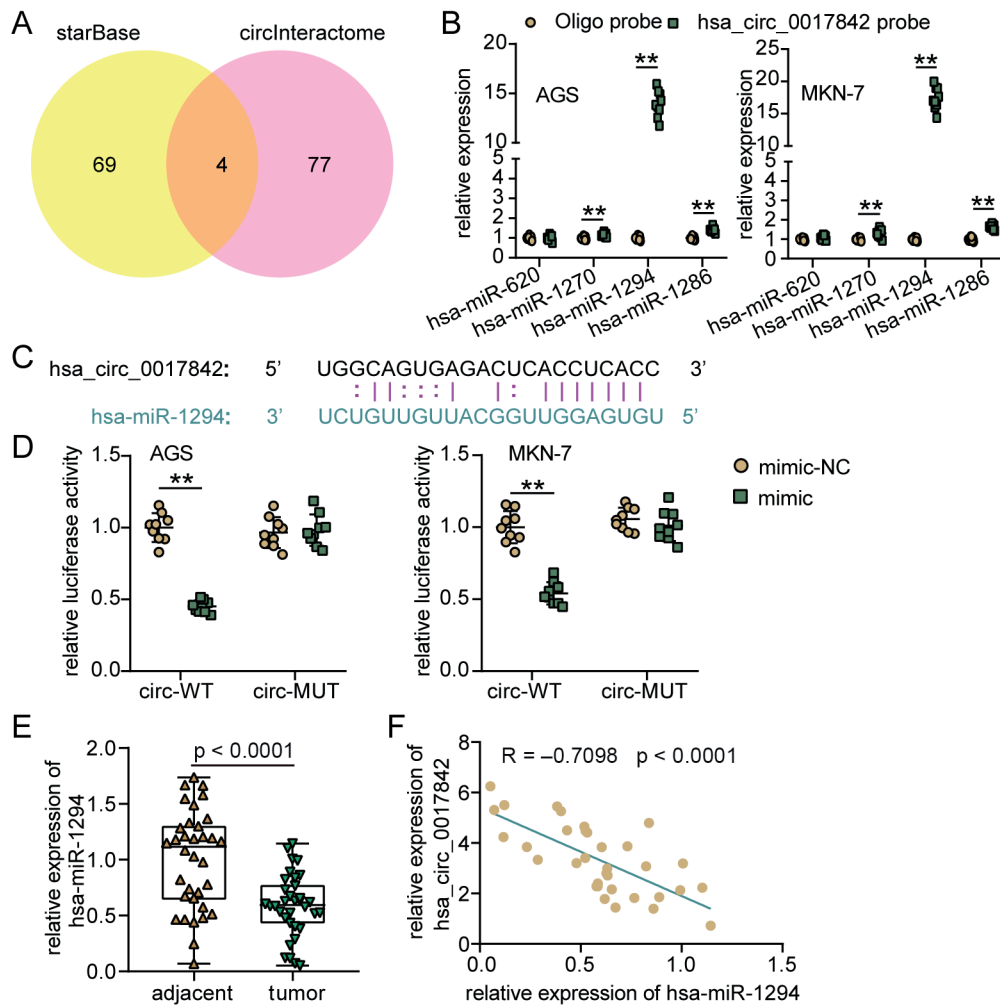


Fig. 3. hsa_circ_0017842 as a ceRNA to target miR-1294. A. starBase and circInteractome predicted miRNAs binding to hsa_circ_0017842; B. The interaction between hsa_circ_0017842 and miR-1294 was confirmed using RNA pull-down assay (** $p < 0.01$; Mann-Whitney U test; $n = 9$); C. The binding sites between hsa_circ_0017842 and miR-1294; D. The binding sites between hsa_circ_0017842 and miR-1294 were confirmed with luciferase assay (** $p < 0.01$; Kruskal-Wallis test; $n = 9$); E. The downregulation of miR-1294 in GC tissues was detected using quantitative real-time polymerase chain reaction (qPCR) (paired Student's t-test; $n = 34$); F. The negative correlation between hsa_circ_0017842 and miR-1294 was analyzed with Pearson's correlation analysis. All experiments were performed in triplicate

sites between hsa_circ_0017842 and miR-1294 are shown in Fig. 3C. According to the binding sites, the circ-WT with binding sites and circ-MUT without binding sites were designed to perform a luciferase assay. The miR-1294 mimic reduced the luciferase activity in the circ-WT group but not in the circ-MUT group, suggesting that miR-1294 could bind to hsa_circ_0017842 (Fig. 3D). Compared with adjacent normal tissues, miR-1294 expression was significantly downregulated in GC tissues ($p < 0.0001$, Fig. 3E). After Pearson's correlation analysis, hsa_circ_0017842 expression and miR-1294 expression in GC samples displayed a negative correlation (Fig. 3F). In conclusion, miR-1294 is downregulated in GC samples and could be sponged by hsa_circ_0017842.

SPARC as a target gene of miR-1294

To predict the target genes of miR-1294, TargetScan database was used. At the same time, GSE103236 and GSE79973 mRNA microarrays were performed using GC samples and adjacent normal samples to identify the up-regulated genes. Finally, 21 genes were screened from TargetScan, GSE103236 and GSE79973 (Fig. 4A). The PPI network of the 21 screened genes was constructed using

the STRING tool (Fig. 4B) because SPARC connected the most genes in network. Therefore, SPARC was selected as the key gene to be explored. Figure 4C displays the binding sites between SPARC and miR-1294. After performing a luciferase assay, it was found that luciferase activity was reduced in the SPARC-WT group only when GC cells were transfected with miR-1294 mimic (Fig. 4D). The SPARC expression was upregulated almost 3-fold in GC samples (Fig. 4E), and its expression was negatively related to miR-1294 expression in GC samples (Fig. 4F). These results confirmed that SPARC was overexpressed in GC samples and is a target of miR-1294.

Silencing SPARC reversed the positive role of hsa_circ_0017842 overexpression in GC cells

To identify whether the effect of hsa_circ_0017842 on GC cells could be regulated by SPARC, we transfected si-SPARC and circ-OE into GC cells to perform the following experiments. Western blotting showed that circ-OE induced a >1.5-fold increase in the expression of SPARC protein, whereas si-SPARC decreased the expression of SPARC protein by approx. 50% (Fig. 5A). However,

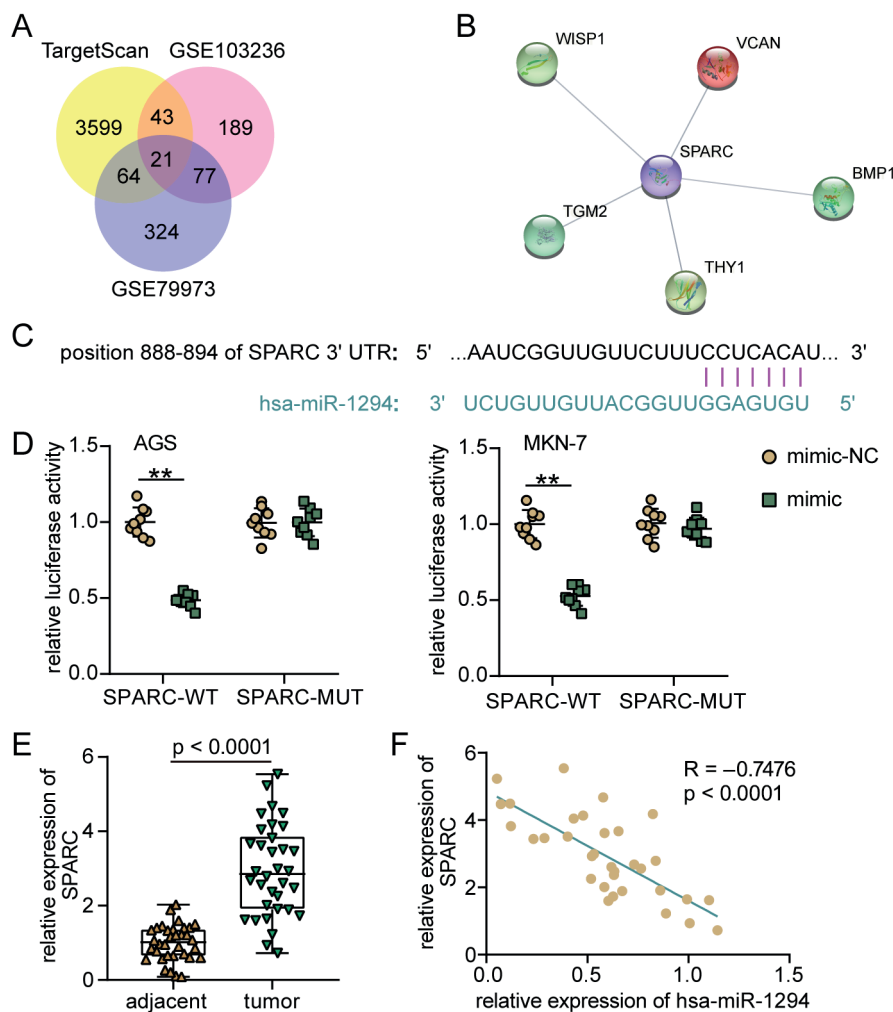


Fig. 4. *SPARC* as a target gene of miR-1294. A. 21 genes were screened from TargetScan, GSE103236, and GSE79973. TargetScan was used to predict the target genes of miR-1294. GSE103236 and GSE79973 are 2 mRNA microarrays used to screen for upregulated genes that satisfy the criteria: adjusted $p < 0.05$ and $\log_2FC > 1$; B. *SPARC* was the center of the PPI network constructed using STRING tool; C. The binding sites between *SPARC* and miR-1294; D. The binding sites between *SPARC* and miR-1294 were confirmed with luciferase assay (** $p < 0.01$; Kruskal–Wallis test; $n = 9$); E. *SPARC* overexpression in GC tissues was detected using quantitative real-time polymerase chain reaction (qPCR) (paired Student’s t-test; $n = 34$); F. Negative correlation between *SPARC* and miR-1294 was analyzed using Pearson’s correlation analysis. All experiments were performed in triplicate

co-transfection of si-*SPARC* and circ-OE did not change the expression of *SPARC* protein compared with empty vector or si-NC groups (Fig. 5A). The results of EdU assay suggested that si-*SPARC* suppressed cell proliferation and reversed the circ-OE-induced increase in cell proliferation (Fig. 5B). Likewise, si-*SPARC* resulted in less cell migration, and it reversed the enhancement of cell migration caused by circ-OE (Fig. 5C). A consistent result was reproduced in cell invasion, showing that silencing *SPARC* reduced the number of invasive cells and attenuated the circ-OE-mediated enhancement of cell invasion (Fig. 5D). Taken together, we showed that the positive role of hsa_circ_0017842 overexpression in GC cells was reversed through silencing *SPARC*.

Discussion

The circRNAs are considered to play crucial roles in GC progression through a ceRNA mechanism.^{12,25,26} In the present study, we found that hsa_circ_0017842 was overexpressed in GC and enhanced the proliferation, migration and invasion of GC cells. Moreover, hsa_circ_0017842 acted as a ceRNA to regulate the miR-1294/*SPARC* axis in GC

cells. Due to the interactions between hsa_circ_0017842, miR-1294 and *SPARC*, *SPARC* knockdown could reverse the positive effect of hsa_circ_0017842 on GC progression.

The abnormal expression of circRNAs was detected in GC, and different circRNAs were found to play different roles in GC.^{27,28} For instance, high expression of circ-SHKBP1 was related to advanced TNM stage and poor prognosis in GC, and its overexpression promoted cell metastasis and angiogenesis of GC cells.²⁹ Another circRNA located in the nucleus, circ-HuR, could attenuate tumor growth and metastasis of GC cells in vivo.³⁰ Here, we used a circRNA microarray of GC from GEO DataSets and qPCR to identify the upregulation of hsa_circ_0017842 in GC samples. By a series of gain-or-loss experiments, hsa_circ_0017842 was confirmed to be an oncogenic circRNA in GC which promotes proliferation, migration and invasion of GC cells.

In recent years, increasing evidence has demonstrated that circRNAs acting as ceRNAs participate in GC progression by sponging miRNAs to regulate target genes of miRNAs.^{31–33} Zhang et al. reported that circ_HN1, miR-628-5p and Ecto-5’-nucleotidase could construct a ceRNA network to regulate GC development.³³ The circ-ITCH as a ceRNA regulated the miR-199a-5p/Klotho axis,

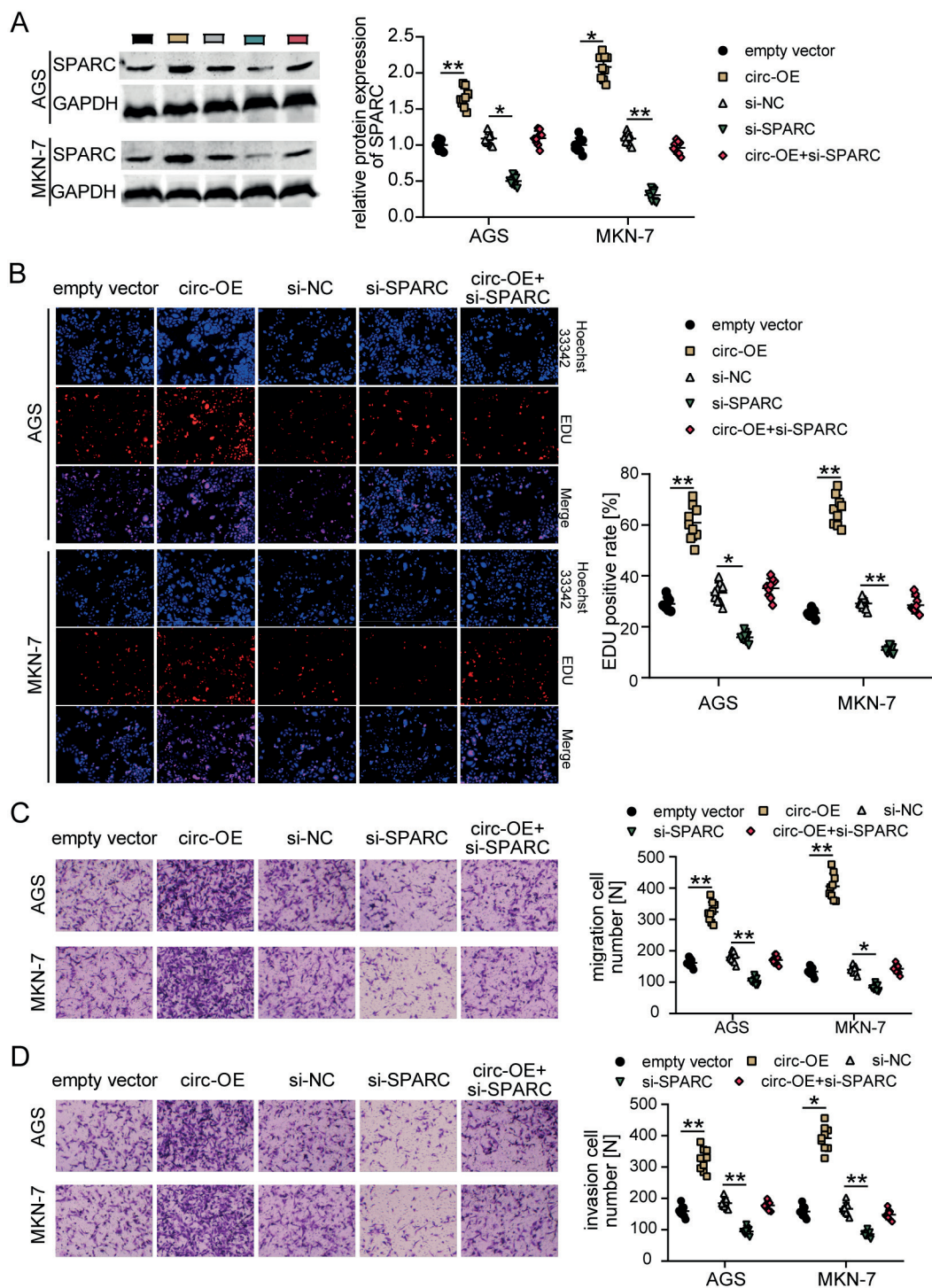


Fig. 5. Silencing *SPARC* diminished the positive effect of hsa_circ_0017842 overexpression on GC cells. **A.** Western blotting detected the expression of *SPARC* in transfected GC cells; **B.** The positive effect of hsa_circ_0017842 overexpression on cell proliferation was reversed by silencing *SPARC*; **C,D.** Silencing *SPARC* recovered the effect of hsa_circ_0017842 overexpression on cell migration (**C**) and cell invasion (**D**)

* $p < 0.05$, ** $p < 0.01$; Kruskal-Wallis test; $n = 9$. All experiments were performed in triplicate.

thereby inhibiting metastasis of GC cells.¹⁶ However, no study identified a ceRNA network of hsa_circ_0017842. Innovatively, we used bioinformatic analysis and in vitro experiments to demonstrate that hsa_circ_0017842 could be a ceRNA that sponges miR-1294, thereby enhancing *SPARC* expression in GC cells. This means that we constructed a novel ceRNA network on hsa_circ_0017842 to participate in GC progression, which enriched the regulatory network of GC.

The function of *SPARC* in GC has been explored in several studies. Clinically, *SPARC* was found to be upregulated

in GC tissues, and its overexpression predicted a poor survival rate of GC.²² In vitro, *SPARC* knockdown in GC cells reduced cell invasion and enhanced cell apoptosis, suggesting the oncogenic function of *SPARC* in GC cells.²³ Consistent with previous studies, we also observed the upregulation of *SPARC* in GC tissues and cells, while silencing *SPARC* suppressed the proliferation, migration and invasion of GC cells. However, whether circRNA could regulate *SPARC* by ceRNA network in GC has not been confirmed yet. In this study, we have revealed for the first time that hsa_circ_0017842 is upstream of *SPARC*

by sponging miR-1294 to upregulate *SPARC* expression, thereby eliminating the inhibitory effect of *SPARC* knock-down on GC cells.

Limitations


Our study revealed the function and mechanism of hsa_circ_0017842 in GC development. However, whether hsa_circ_0017842 can affect the malignancy of GC cells in vivo has not been investigated. Lymph node metastasis has been found to be associated with tumor development^{34,35}; therefore, we will explore the relationship between hsa_circ_0017842 and lymph node metastasis in GC samples in the future. Furthermore, the role of hsa_circ_0017842 in GC in a clinical setting, such as GC prognosis, chemotherapy resistance, as a drug target, etc., is still not explored. In our further research, we will focus on these areas.

Conclusions

Our study demonstrated that hsa_circ_0017842 acted as a competing endogenous RNA to enhance the malignancy of GC by sponging miR-1294 to upregulate *SPARC*. The function of hsa_circ_0017842 in GC is identified, which may provide a novel target for GC therapy in the years to come.

ORCID iDs

Xigang Wen  <https://orcid.org/0000-0002-8509-9323>

Wenling Han  <https://orcid.org/0000-0003-4240-6319>

Chao Liu  <https://orcid.org/0000-0001-9355-3146>

References

- Sung H, Ferlay J, Siegel RL, et al. Global cancer statistics 2020: GLOBOCAN estimates of incidence and mortality worldwide for 36 cancers in 185 countries. *CA A Cancer J Clin*. 2021;71(3):209–249. doi:10.3322/caac.21660
- Etemadi A, Safiri S, Sepanlou SG, et al. The global, regional, and national burden of stomach cancer in 195 countries, 1990–2017: A systematic analysis for the Global Burden of Disease study 2017. *Lancet Gastroenterol Hepatol*. 2020;5(1):42–54. doi:10.1016/S2468-1253(19)30328-0
- Li K, Zhang A, Li X, Zhang H, Zhao L. Advances in clinical immunotherapy for gastric cancer. *Biochim Biophys Acta Rev Cancer*. 2021;1876(2):188615. doi:10.1016/j.bbcan.2021.188615
- Allemani C, Weir HK, Carreira H, et al. Global surveillance of cancer survival 1995–2009: Analysis of individual data for 25,676,887 patients from 279 population-based registries in 67 countries (CONCORD-2). *Lancet*. 2015;385(9972):977–1010. doi:10.1016/S0140-6736(14)62038-9
- Tan P, Yeoh KG. Genetics and molecular pathogenesis of gastric adenocarcinoma. *Gastroenterology*. 2015;149(5):1153–1162.e3. doi:10.1053/j.gastro.2015.05.059
- Nakamura J. Methylation-mediated gene silencing as biomarkers of gastric cancer: A review. *World J Gastroenterol*. 2014;20(34):11991–12006. doi:10.3748/wjg.v20.i34.11991
- Qu S, Yang X, Li X, et al. Circular RNA: A new star of noncoding RNAs. *Cancer Lett*. 2015;365(2):141–148. doi:10.1016/j.canlet.2015.06.003
- Memczak S, Jens M, Elefsinioti A, et al. Circular RNAs are a large class of animal RNAs with regulatory potency. *Nature*. 2013;495(7441):333–338. doi:10.1038/nature11928
- Li J, Sun D, Pu W, Wang J, Peng Y. Circular RNAs in cancer: Biogenesis, function, and clinical significance. *Trends Cancer*. 2020;6(4):319–336. doi:10.1016/j.trecan.2020.01.012
- Jia N, Li J. Role of circular RNAs in preeclampsia. *Dis Markers*. 2019;2019:7237495. doi:10.1155/2019/7237495
- Gu W, Sun Y, Zheng X, et al. Identification of gastric cancer-related circular RNA through microarray analysis and bioinformatics analysis. *Biomed Res Int*. 2018;2018:2381680. doi:10.1155/2018/2381680
- Guan YJ, Ma JY, Song W. Identification of circRNA–miRNA–mRNA regulatory network in gastric cancer by analysis of microarray data. *Cancer Cell Int*. 2019;19(1):183. doi:10.1186/s12935-019-0905-z
- Luo Z, Rong Z, Zhang J, et al. Circular RNA circCCDC9 acts as a miR-6792-3p sponge to suppress the progression of gastric cancer through regulating CAV1 expression. *Mol Cancer*. 2020;19(1):86. doi:10.1186/s12943-020-01203-8
- Guo LL. Competing endogenous RNA networks and gastric cancer. *World J Gastroenterol*. 2015;21(41):11680–11687. doi:10.3748/wjg.v21.i41.11680
- Shen D, Zhao H, Zeng P, et al. Circular RNA hsa_circ_0005556 accelerates gastric cancer progression by sponging miR-4270 to increase MMP19 expression. *J Gastric Cancer*. 2020;20(3):300–312. doi:10.5230/jgc.2020.20.e28
- Wang Y, Wang H, Zheng R, et al. Circular RNA ITCH suppresses metastasis of gastric cancer via regulating miR-199a-5p/Klotho axis. *Cell Cycle*. 2021;20(5–6):522–536. doi:10.1080/15384101.2021.1878327
- Wang Y, Liu G, Sun S, Qin J. miR-1294 alleviates epithelial–mesenchymal transition by repressing FOXC1 in gastric cancer. *Genes Genom*. 2020;42(2):217–224. doi:10.1007/s13258-019-00899-3
- Wu D, Li H, Wang J, et al. LncRNA NEAT1 promotes gastric cancer progression via miR-1294/AKT1 axis. *Open Med*. 2020;15(1):1028–1038. doi:10.1515/med-2020-0218
- Shi YX, Ye BL, Hu BR, Ruan XJ. Expression of miR-1294 is downregulated and predicts a poor prognosis in gastric cancer. *Eur Rev Med Pharmacol Sci*. 2018;22(17):5525–5530. doi:10.26355/eurrev_201809_15813
- Podhajcer OL, Benedetti LG, Girotti MR, Prada F, Salvatierra E, Llera AS. The role of the matricellular protein SPARC in the dynamic interaction between the tumor and the host. *Cancer Metastasis Rev*. 2008;27(4):691–705. doi:10.1007/s10555-008-9146-7
- Yan Q, Sage EH. SPARC, a matricellular glycoprotein with important biological functions. *J Histochem Cytochem*. 1999;47(12):1495–1505. doi:10.1177/002215549904701201
- Zhao ZS, Wang YY, Chu YQ, Ye ZY, Tao HQ. SPARC is associated with gastric cancer progression and poor survival of patients. *Clin Cancer Res*. 2010;16(1):260–268. doi:10.1158/1078-0432.CCR-09-1247
- Yin J, Chen G, Liu Y, et al. Downregulation of SPARC expression decreases gastric cancer cellular invasion and survival. *J Exp Clin Cancer Res*. 2010;29(1):59. doi:10.1186/1756-9966-29-59
- Wang K, Long B, Liu F, et al. A circular RNA protects the heart from pathological hypertrophy and heart failure by targeting miR-223. *Eur Heart J*. 2016;37(33):2602–2611. doi:10.1093/eurheartj/ehv713
- Zhang X, Wang S, Wang H, et al. Circular RNA circNRIP1 acts as a microRNA-149-5p sponge to promote gastric cancer progression via the AKT1/mTOR pathway. *Mol Cancer*. 2019;18(1):20. doi:10.1186/s12943-018-0935-5
- Peng L, Sang H, Wei S, et al. circCUL2 regulates gastric cancer malignant transformation and cisplatin resistance by modulating autophagy activation via miR-142-3p/ROCK2. *Mol Cancer*. 2020;19(1):156. doi:10.1186/s12943-020-01270-x
- Ghafouri-Fard S, Honarmand Tamizkar K, Jamali E, Taheri M, Ayatollahi SA. Contribution of circRNAs in gastric cancer. *Pathol Res Pract*. 2021;227:153640. doi:10.1016/j.prp.2021.153640
- Fang X, Wen J, Sun M, Yuan Y, Xu Q. CircRNAs and its relationship with gastric cancer. *J Cancer*. 2019;10(24):6105–6113. doi:10.7150/jca.32927
- Xie M, Yu T, Jing X, et al. Exosomal circSHKBP1 promotes gastric cancer progression via regulating the miR-582-3p/HUR/VEGF axis and suppressing HSP90 degradation. *Mol Cancer*. 2020;19(1):112. doi:10.1186/s12943-020-01208-3
- Yang F, Hu A, Li D, et al. Circ-HuR suppresses HuR expression and gastric cancer progression by inhibiting CNBP transactivation. *Mol Cancer*. 2019;18(1):158. doi:10.1186/s12943-019-1094-z

31. Li X, Li Z, Liu P, et al. Novel circRNAs in hub ceRNA axis regulate gastric cancer prognosis and microenvironment. *Front Med (Lausanne)*. 2021;8:771206. doi:10.3389/fmed.2021.771206
32. Xia T, Pan Z, Zhang J. CircPDZD8 promotes gastric cancer progression by regulating CHD9 via sponging miR-197-5p. *Aging (Albany NY)*. 2020;12(19):19352–19364. doi:10.18632/aging.103805
33. Zhang J, Wang F, Zhang H, Cao M. A novel circular RNA circ_HN1/miR-628-5p/Ecto-5'-nucleotidase competing endogenous RNA network regulates gastric cancer development. *Bioengineered*. 2021;12(2): 9739–9752. doi:10.1080/21655979.2021.1989259
34. Isik A, Soran A, Grasi A, Barry N, Sezgin E. Lymphedema after sentinel lymph node biopsy: Who is at risk? *Lymph Res Biol*. 2022;20(2): 160–163. doi:10.1089/lrb.2020.0093
35. Işık A, Fırat D, Peker K, İnal A, Yılmaz İ, Çelebi F. Breast skin necrosis after methylene blue dye injection: Breast image. *Sakarya Med J*. 2018;8(1):153–156. doi:10.31832/smj.376329

A systematic review of clinical trials using single or combination therapy of oral or topical finasteride for women in reproductive age and postmenopausal women with hormonal and nonhormonal androgenetic alopecia

*Niloufar Najar Nobari^{1,A,D–F}, Masoumeh Roohaninasab^{1,A,B,D–F}, Afsaneh Sadeghzadeh-Bazargan^{1,B,E,F}, Azadeh Goodarzi^{1,D–F}, Elham Behrangi^{1,B,C,E,F}, Farahnaz Nikkha^{2,E,F}, *Mohammadreza Ghassemi^{1,B–F}

¹ Department of Dermatology, Rasool Akram Medical Complex Clinical Research Development Center, School of Medicine, Iran University of Medical Sciences, Tehran, Iran

² Rasool Akram Medical Complex, Iran University of Medical Sciences, Tehran, Iran

A – research concept and design; B – collection and/or assembly of data; C – data analysis and interpretation;

D – writing the article; E – critical revision of the article; F – final approval of the article

Advances in Clinical and Experimental Medicine, ISSN 1899–5276 (print), ISSN 2451–2680 (online)

Adv Clin Exp Med. 2023;32(7):813–823

Address for correspondence

Azadeh Goodarzi

E-mail: azadeh_goodarzi1984@yahoo.com

Funding sources

None declared

Conflict of interest

None declared

Acknowledgements

The authors would like to thank the Rasool Akram Medical Complex Clinical Research Development Centre (RCRDC) for its technical and editorial assistance.

* Niloufar Najar Nobari and Mohammadreza Ghassemi contributed equally to this work.

Received on December 8, 2021

Reviewed on June 20, 2022

Accepted on December 20, 2022

Published online on March 10, 2023

Cite as

Nobari NN, Roohaninasab M, Sadeghzadeh-Bazargan A, et al. A systematic review of clinical trials using single or combination therapy of oral or topical finasteride for women in reproductive age and postmenopausal women with hormonal and nonhormonal androgenetic alopecia. *Adv Clin Exp Med.* 2023;32(7):813–823.

doi:10.17219/acem/157990

doi:10.17219/acem/157990

DOI

10.17219/acem/157990

Copyright

Copyright by Author(s)

This is an article distributed under the terms of the Creative Commons Attribution 3.0 Unported (CC BY 3.0) (<https://creativecommons.org/licenses/by/3.0/>)

Abstract

Female pattern hair loss (FPHL) is a hereditary form of hair loss in women and the most common patterned progressive hair loss in female patients with androgenetic alopecia (AGA). One of the best methods for treating hair loss in women is the finasteride treatment. This systematic review includes a summary of the pharmacology of finasteride and the effect of the drug on women, especially those in the menopausal age group, and is aimed at elucidating methods of preventing systematic side effects. A search of all published literature from 1999 to 2020 has been conducted with the use of PubMed/MEDLINE, Embase, PsycINFO, TRIP Cochrane, as well as Cochrane Skin databases. A total of 380 articles were found, of which 260 articles were removed and 87 review studies were excluded. Lastly, full texts of 33 original articles were reviewed and 14 articles that met the inclusion criteria were selected. Ten out of the 14 articles reported a high rate of alopecia recovery in women taking finasteride. Based on the results, it can be stated that 5 mg of oral finasteride per day could be an effective and safe treatment in normoandrogenic women with FPHL, especially when used in combination with other drugs, such as topical estradiol and minoxidil. We also found that topical finasteride is more effective than other topical formulas for treating hair loss.

Key words: oral, FPHL, finasteride, topical, female pattern hair loss

Introduction

Hair loss is a part of the natural hair growth cycle. When the balance between new hair growth and old hair loss is disturbed, excessive hair loss occurs. A medical term for excessive hair loss is alopecia.¹ Female pattern hair loss (FPHL) or androgenetic alopecia (AGA), is the most common cause of hair loss in women, which could be genetic or inherited.^{2–6} Androgenetic alopecia becomes more severe during menopause due to decreased estrogen levels. In less than 50% of women who reach the age of 65, their normal volume of hair remains unchanged, and the rest of women experience this form of hair loss.^{7,8} Androgenetic alopecia causes regional baldness in men and a decrease in the overall density and thickness of the hair in women.

In women, AGA usually has 3 stages: 1) reduction of hair density on both sides of the vertex; 2) expansion of low-density areas; 3) specific baldness in the vertex and a decrease in hair density in lateral parts. At different stages, pattern hair loss could be graded using the Savin scale.^{9,10} Pattern hair loss begins with widening of the central part of the hair and thinning of the hairs at the top and crown of the head.¹¹ Female pattern hair loss is characterized by the miniaturization of hair follicles, resulting in shorter, thinner and more brittle hairs, and eventually in halted hair production, reducing the total number of hair follicles on the head. In female, unlike male pattern baldness, the hairline is preserved and does not regress, and hair loss rarely leads to complete baldness.¹² Underlying diseases and tumors could cause female pattern baldness. Moreover, smoking can increase incidence or severity of the disease. Most people with AGA experience significant hair loss between the ages of 40 and 50.¹³

Regarding the mechanism of hair loss in women, molecular changes cause follicular damage, in which the role of androgen hormones is very prominent.¹⁴ The role of genetic and other influencing factors (described below) has not yet been fully elucidated; however, they play an important role in the pathogenesis of FPHL.¹⁵ In women who do not have high androgen levels, genetic predisposition is more likely to cause hair loss. Genetic susceptibility affects the increase in circulating androgen levels and hormones involved in developing FPHL through binding to follicular target cells, particularly intracellular androgen receptors.¹⁶ Studies on genome have shown that genetic defects play a role in the severity of hair loss.^{17–20}

One of the most important medicines used in the treatment of hair loss is finasteride. The drug was approved by the Food and Drug Administration (FDA) in 1997.²¹ Finasteride with the chemical formula of $C_{23}H_{36}N_2O_2$ is insoluble in water but soluble in dilute solutions.^{22,23} It is well absorbed in the gastrointestinal tract and food does not affect its absorption. The drug is metabolized in the liver and converted to inactive compounds that are excreted in the bile.²⁴

Finasteride prevents the body from converting testosterone to dihydrotestosterone (DHT); moreover, it crosses the blood–brain barrier, albeit in small amounts.²⁵ Finasteride is used to treat male and female PHL as well as the symptoms of benign prostatic hyperplasia in male patients with an enlarged prostate. However, later studies showed that finasteride could be used to treat hair loss.²⁶ The drug suppresses scalp DHT levels by up to 43% in 28 days and up to 65% in 42 days,²⁷ and selectively inhibits the activity of 5 α -reductase type II. This enzyme is required for the activity of some androgen hormones, hair follicles and sebaceous glands in the skin; also, it is sensitive to androgen hormones.²⁸ Along with finasteride, minoxidil is the mainstay of treatment for FPHL, which is often used as a treatment for different types of hair loss.^{26–28}

Objectives

Regarding its effective form and efficacy on different age groups of women, as well as considering its effect on hereditary hormonal diseases, finasteride has its supporters and opponents. To the best of our knowledge, no complete summary about finasteride treatment in postmenopausal women and the optimal conditions for greater effectiveness of the drug has yet been presented. Therefore, in this systematic review, we tried to evaluate the effect of finasteride treatment, administered orally or topically, in women with FPHL in different age groups and with different underlying conditions (hormonal or nonhormonal). For this purpose, we reviewed relevant clinical trials available in the scientific databases.

Materials and methods

The present systematic review is comprehensively evaluates single or combination therapy involving oral or topical treatment with finasteride for hormonal and nonhormonal hair loss in women from 1999 to 2020. The finasteride therapy was studied by examining the dosage used and the side effects. A comprehensive search of the PubMed/MEDLINE, Embase, PsycINFO, TRIP Cochrane, and Cochrane Skin databases was performed, according to pre-determined clinical endpoints.

The clinical examination of the topical and oral use of finasteride in women with alopecia and hair loss constituted the main body of the selected articles. The articles that were used for this systematic review included clinical trials, retrospective, prospective, double-blind, and randomized studies.

Inclusion criteria were at least 1 group treated with finasteride, the coverage of results related to the effectiveness of finasteride, and the use of in vivo therapy only. Exclusion criteria were articles written in the language other than

English, articles that were designed as nonoriginal or that were not trials, or studies on finasteride that did not concern the treatment of alopecia in women.

To collect information regarding finasteride treatment, the following key words were searched in the desired databases: “hormonal and nonhormonal hair loss”, “single therapy”, “combination”, “oral finasteride treatment”, “topical hair loss”, etc. Electronic search was conducted on 380 articles. Of these, 260 articles were removed after reviewing the title or abstract, since they were unrelated to the topic of the research, and 87 review studies were excluded. Finally, the full texts of 33 original articles were reviewed and 14 clinical trials that met the inclusion criteria were selected. Figure 1 depicts the Preferred Reporting Items for Systematic Reviews and Meta-Analyses (PRISMA) chart of evaluated studies.

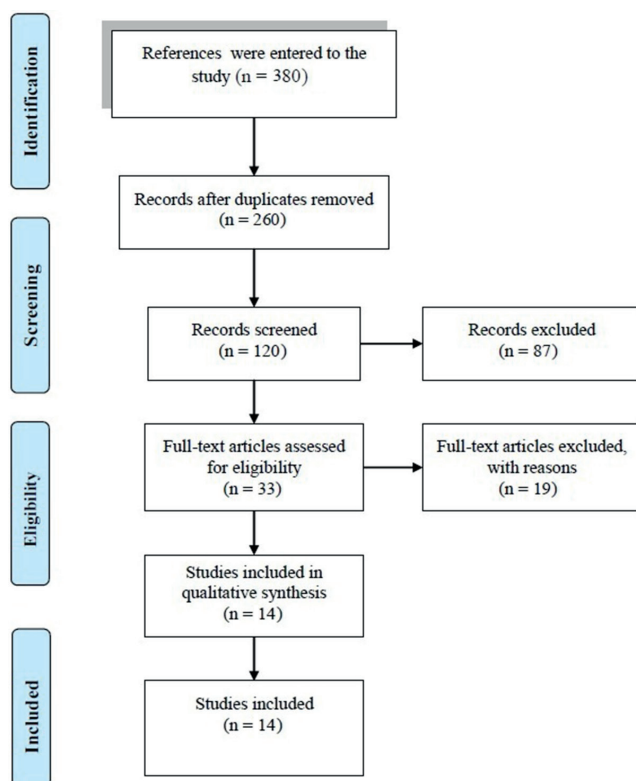


Fig. 1. Preferred Reporting Items for Systematic Reviews and Meta-Analyses (PRISMA) flowchart of studies evaluated for this systematic review

Screening and data extraction

Two authors trained in performing systematic reviews and database searching conducted the search strategy. In the first stage, the titles and abstracts of the articles were reviewed; in the next stage, two authors independently reviewed the full text of the articles. After preparing a list of titles and summaries of studies, articles were evaluated in terms of various methodological aspects, including sampling methods, reliability of the tools used and the objectives of the study. Finally, a set of articles appropriate in terms of topic coverage and content structure was included in the article.

Results and discussion

Out of 33 reviewed articles, 14 articles were included in the study based on the inclusion/exclusion criteria. A summary of the results of the 14 original trials that were reviewed is given in Table 1.

Among the selected articles, 4 were randomized control, 5 were uncontrolled prospective, 4 were retrospective studies, and 1 was a case report.

The quality of the articles was assessed using the Cochrane Risk of Bias 2 tool (<https://methods.cochrane.org/risk-bias-2>). According to this tool, only 1 study had a risk of bias in 5 areas, 2 studies had a risk of bias in 3 areas, and 1 had a risk of bias in 2 areas. Other studies had unclear risk of bias in 4 areas, namely selection bias, performance, reporting, and types of bias.

Out of the 14 chosen articles, 10 (3 randomized control, 3 uncontrolled prospective and 4 retrospective studies) reported a high rate of alopecia recovery in women taking finasteride. In 2 prospective articles and 1 retrospective article included, the rate of improvement after the treatment period was high. Two articles reported a reduced rate of recovery after the treatment.

The criteria for reviewing the results of articles were as follows: articles in which the improvement rate or the percentage of patients reporting improvement was more than 50% were considered articles with high recovery, articles with an improvement rate of less than 50% were considered articles with great improvement, and articles in which there was no significant difference between the treated group and the control group were considered articles with a decrease in recovery.

In this study, data on 735 postmenopausal patients with FPHL aged 21–65 years and treated with finasteride were analyzed. After reviewing the articles, it was concluded that in 50% of cases treated with finasteride, significant and high efficacy were observed, in 25% of them partial to moderate efficacy was seen, and in 25% no efficacy was observed; also, only in one of the 14 articles, no improvement in hair thickness and growth was observed. In 25% of the articles, in addition to finasteride, other medications such as estradiol and minoxidil were used to enhance the efficacy of the treatment. The lowest dose of finasteride was 1 mg/day and the maximum dose was 5 mg/day. The minimum duration of treatment was 3.5 months and the maximum duration was 12 months.

Based on the results of 4 clinical trials included in Table 1, the treatment with 5 mg oral finasteride per day can be considered an effective and safe therapy for normoandrogenic women with FPHL.^{29–31}

Overall, the reviewed articles showed that hair loss and hair growth problems were reduced after the topical administration of finasteride. The use of topical finasteride gives promising results.

Other studies provide similar data. In a systematic study, Lee et al. showed that topical finasteride treatment

Table 1. Findings of studies related to single or combination therapy with oral or topical finasteride

Author, year and study type	Title	Population/age	Dosage/method/duration of use	Results
Price et al. ² 2000 RCT	Lack of efficacy of finasteride in postmenopausal women with AGA	137 postmenopausal women with AGA 41–60 years	1 mg of finasteride or placebo daily; the effectiveness was evaluated by counting the scalp hairs, evaluating the photos taken by an expert panel and by histological analysis of the scalp biopsy specimens	after 1 year of treatment, there was no significant difference in hair number change between finasteride and placebo groups; both treatment groups had a significant reduction in the number of hairs in the anterior/anterior (anterior/middle) area of the scalp during the 1-year study period; the evaluations showed no improvement in the process of hair thinning, increased hair growth, or improved hair appearance in people treated with finasteride compared to the placebo group; in postmenopausal women with AGA, taking 1 mg of finasteride per day for 12 months does not increase hair growth and does not slow the progression of hair thinning
Carmina and Lobo ¹³ 2003 RCT	Treatment of hyperandrogenic alopecia in women: Fertility and sterility	48 hyperandrogenic premenopausal women with FPHL 25 ± 2 years Ludwig scores I–III	finasteride 5 mg/day vs CPA with EE vs flutamide 250 mg/day vs none; the experiment period was 12 months	flutamide significantly decreased Ludwig scores; no significant changes in Ludwig scores and clinical evaluation in finasteride group
Oliveira-Soares et al. ²⁹ 2013 uncontrolled prospective	Finasteride 5 mg/day treatment of patterned hair loss in normoandrogenetic postmenopausal women	40 postmenopausal women with normal menopause and AGA	5 mg of oral finasteride daily for 18 months; the effectiveness was assessed by patient satisfaction and global photo evaluation	after 6 months, 22 patients showed significant improvement, 12 showed moderate improvement and 6 did not show any improvement; according to the evaluation of the photos, 8 patients did not show improvement, 16 cases showed moderate improvement and 16 cases showed significant improvement in the 6 th month; slight improvements were observed over time from 6 to 12–18 months; decreased libido was observed in 4 patients and an increase in liver enzymes was observed in 1 patient; older patients showed less positive response
Yeon et al. ³¹ 2011 uncontrolled prospective	5 mg/day finasteride treatment for normoandrogenic Asian women with FPHL	87 women with FPHL during pre- and postmenopause	5 mg of oral finasteride daily for 12 months	after 12 months, 70 patients (81.4%) had recovered, 10 patients showed moderate and 4 patients showed significant improvement; 13 patients (15.1%) stayed unchanged and 3 patients (3.3%) had a low exacerbation; 4 patients (4.6%) had mild side effects that disappeared quickly
Suchonwanit et al. ³³ 2019 RCT	Efficacy of topical combination of 0.25% finasteride and 3% minoxidil versus 3% minoxidil solution in FPHL	30 postmenopausal women with FPHL	each participant was randomly administered 0.25% topical finasteride with 3% topical minoxidil or 3% topical minoxidil solution for 24 weeks	after 24 weeks, hair density and diameter had increased in both groups, and finasteride/minoxidil was significantly superior to minoxidil solution in terms of hair diameter; no systemic side effects have been reported; serum dihydrotestosterone levels in the finasteride/minoxidil group decreased significantly from the beginning; topical combination of 0.25% finasteride and 3% minoxidil may be a promising option in the treatment of FPHL with an additional benefit in increasing hair diameter; it may be absorbed through the skin, thus it should be used only in postmenopausal women
Iorizzo et al. ³⁵ 2006 uncontrolled prospective	Finasteride treatment of FPHL	38 women with FPHL 21–48 years	2.5 mg of finasteride daily and 3 mg of oral contraceptive drug, containing drospirenone and 30 µg of ethinylestradiol; the experiment period was 12 months	62% of patients showed improvement after taking 2.5 mg of finasteride daily while taking contraceptives; further studies are needed to understand which hair loss pattern responds best to this treatment

Table 1. Findings of studies related to single or combination therapy with oral or topical finasteride – cont.

Author, year and study type	Title	Population/age	Dosage/method/duration of use	Results
Kohler et al. ³⁹ 2007 retrospective	Effect of finasteride 5 mg (Proscar) on acne and alopecia in female patients with normal serum levels of free testosterone	12 women (6 with acne and 6 with alopecia)	5 mg of oral finasteride daily for 12 months	9 out of 12 patients who received treatment had significantly reduced symptoms and an improved mental state than before receiving finasteride; the other 3 patients did not receive finasteride at all and did not report any change in acne/alopecia; further evaluation is needed to clarify more accurate indications for prescribing finasteride in women with acne and alopecia
Verdonschot et al. ⁴⁰ 2014 retrospective	The effectiveness of finasteride and dutasteride used for 3 years in women with AGA	120 women with FPHL 16–84 years	finasteride 1.25 mg/day or dutasteride 0.15 mg/day; the experiment period was 3 years	improved hair thickness in 81.7% of patients in finasteride group and in 83.3% of patients in dutasteride group; improved hair density from GPA in 68.9% of patients in finasteride group compared to 65.6% of patients in dutasteride group
Won et al. ⁴¹ 2018 retrospective	Clinical efficacy of oral administration of finasteride at a dose of 2.5 mg/day in women with FPHL	112 women in the pre- and postmenopausal period with FPHL 25–65 years	finasteride 2.5 mg/day; the duration of the review period was 12 months	using global photographs, it was found that 33 cases (29.5%) of the 112 studied patients showed a slight improvement, 73 cases (65.2%) showed a significant improvement, while in 6 cases (5.4%) no changes were recorded; finasteride has a better effect on hair growth when patients have lower Ludwig scores and are of older age
Rossi et al. ⁴⁴ 2020 retrospective and single-blind	Efficacy of topical finasteride 0.5% vs 17 α -estradiol 0.05% in the treatment of postmenopausal FPHL	119 women	subjects were divided into 2 groups: the 1 st group consisted of 69 women treated with 0.5% finasteride and 2% minoxidil; in the 2 nd group, 50 women were treated with 0.17% estradiol and 2% minoxidil	the efficacy of finasteride and 17 α -estradiol was statistically significant at the 6, 12 and 18 months; the effect of topical finasteride was significantly greater than the 17 α -estradiol solution in the 6-, 12- and 18-month studies; the highest improvement after 12–18 months was observed with the topical application of finasteride; topical 0.5% finasteride in combination with 2% minoxidil could be a valid treatment option for menopausal FPHL, which shows higher efficacy than topical 17 α -estradiol with 2% minoxidil at 6, 12 and 18 months of follow-up
Camacho-Martinez ⁵⁸ 2009 RCT	Finasteride for hair loss in women	137 postmenopausal women with normal serum testosterone 41–60 years	patients were divided into 2 groups and received 5 mg of finasteride (67 people) or placebo (70 people) for 12 months	doses used are 5 mg/week to 5 mg/day, for periods of 6 months to more than 2 years; finasteride at different doses was well tolerated with the side effects of the treatment; finasteride could cause changes in male fetuses and it is important to control consumption in pregnant women
Boychenko et al. ⁵⁹ 2012 case report	Finasteride in the treatment of female pattern (androgenic) alopecia	one 44-year-old woman with androgenic alopecia	1.25 mg of oral finasteride daily for 3.5 months	hair loss has been significantly reduced and excess hair growth has been reported without side effects
Trüeb ⁶⁰ 2004 uncontrolled prospective	Finasteride treatment of patterned hair loss in normoandrogenic postmenopausal women	5 postmenopausal women without clinical symptoms or high blood pressure	2.5 or 5.5 mg of oral finasteride daily; the effectiveness was evaluated at 6, 12 and 18 months	oral finasteride at a dose of 2.5 mg/day or more may be effective in treating hair loss in postmenopausal women in the absence of clinical or laboratory symptoms; finasteride treatment with all evaluation methods, improved scalp hair
Kim et al. ⁶² 2012 uncontrolled prospective	Efficacy of finasteride 1.25 mg on FPHL	18 postmenopausal women with normal androgen, iron, ferritin levels, and thyroid function tests at baseline	the study was performed for 28 weeks with a minimum dose of 1.25 mg of finasteride daily	after 28 weeks of treatment, phototrichogram evaluation showed a 5.87% increase in hair density and an 11.8% mean increase in hair thickness that was not statistically significant; 1.25 mg daily dose of finasteride administered for 28 weeks showed measurable efficacy in FPHL patients but did not show objective clinical efficacy; a dose higher than 1.25 mg/day, more patients and longer duration of treatment are required to confirm the effect of this clinical trial on normoandrogenic FPHL

RCT – randomized controlled trial; FPHL – female pattern hair loss; AGA – androgenetic alopecia; CPA – cyproterone acetate; EE – ethinyl estradiol; GPA – global photographic assessment.

significantly reduced hair loss and hair growth problems. The authors stated that the initial results regarding the use of topical finasteride are limited but safe and promising. However, continued research on drug delivery, ideal topical concentrations and frequency of use, side effects, and use for other alopecia helps to elucidate the full extent of the topical use of finasteride.³²

Systemic pharmacodynamic evaluation of oral finasteride

Experts have been studying the effects of finasteride on FPHL for many years. In 2000, Price et al. in a 1-year study on the effectiveness of finasteride (1 mg/day) in 137 postmenopausal female patients with AGA concluded that taking 1 mg of finasteride per day had low efficacy and did not increase hair growth and diameter. Further research should be performed in this regard.²

There is a lot of clinical evidence regarding the therapeutic effects of finasteride and its important and effective role in the treatment of female pattern baldness.^{2,33,34} However, a small percentage of studies have reported lack of efficacy of finasteride treatment; for instance, a 1-year study showed that finasteride had no significant effect on the treatment of postmenopausal women with alopecia.¹³

In a 2006 study of finasteride doses, Iorizzo et al. stated that it was unclear whether the achieved success was due to higher doses of finasteride (2.5 mg instead of 1 mg) or its association with oral contraceptives containing drospirenone (with antiandrogenic properties). Further studies are necessary to understand which hair loss pattern responds best to this treatment.³⁵ Two-thirds of women treated with finasteride experience hair regrowth. Finasteride is aimed at controlling hair loss, not at its definitive treatment, thus a continuous administration of the drug is indicated for better results.³⁴ In men, however, better therapeutic responses have been seen.^{36,37} One study has shown that finasteride has a positive effect in 90% of men with male pattern baldness. After 5 years of treatment, 48% of men showed increased hair growth, 42% did not show any hair loss, and the remaining 10% experienced hair loss. In contrast, 6% of men treated with placebo reported increased hair growth and 19% did not report any new hair loss, while the remaining 75% continued to lose hair.³⁸

In parallel with the Iorizzo study, Kohler et al. conducted a retrospective study with the use of questionnaire on 12 female patients in 2007.³⁹ In patients who received the treatment, the symptoms significantly decreased and they reported an improved mental state. However, further evaluation is needed to elucidate more accurate indications for the administration of finasteride in women with acne and alopecia.³⁹

Another study on oral finasteride in 87 normoandrogenic women with FPHL was conducted in 2011 by Yeon et al. In this study, in order to evaluate the clinical effect

of 5 mg of oral finasteride in normoandrogenic Asian women with FPHL, 87 women were enrolled and followed up for 12 months. On initial visits, the average hair density was $90 \pm 22 \text{ cm}^2$ and the average hair thickness was $64 \pm 11 \mu\text{m}$. After 12 months of treatment with finasteride, hair density increased significantly to $107 \pm 23 \text{ cm}^2$ and hair thickness increased significantly to $70 \pm 9 \mu\text{m}$. In 70 cases (80.4%), an improvement was noticed. Thirteen (15.1%) patients did not notice any changes and 3 patients (3.3%) had a slight exacerbation. Four patients (4.6%) reported side effects, such as headache, menstrual irregularities, dizziness, and increased body hair growth. However, these side effects were mild and quickly disappeared. The results of the study indicated that the treatment with 5 mg of oral finasteride per day could be effective and safe for normoandrogenic women with FPHL.³¹

Two years later, Oliveira-Soares et al. conducted a study in 40 normoandrogenic postmenopausal women with AGA. The study was performed for 18 months, and patients were given 5 mg of oral finasteride daily. After 6 months, 22 patients noticed a significant improvement, 12 showed a moderate improvement and 6 did not show any improvement. According to the evaluation of the photos, 8 patients did not show any improvement, 16 patients showed a moderate improvement and 16 cases showed a significant improvement after 6 months. A decrease in libido was reported by 4 female patients and an increase in liver enzymes was observed in 1 patient. Finally, it was shown that taking 5 mg of oral finasteride per day is very effective and can improve hair loss pattern in postmenopausal women.^{29,40}

Five years later, a study was conducted by Won et al. in 112 pre- and postmenopausal women. A dose of 2.5 mg of oral finasteride per day was prescribed. The follow-up period of this study was 3 months and the patients who received other FPHL treatments, including topical minoxidil, were excluded from the study. Using photos taken at the end of the finasteride course, 33 cases (29.5%) showed a slight improvement, 73 cases (65.2%) showed a significant improvement, while in 6 cases (5.4%) no change was recorded. From these data, it was concluded that finasteride at a dose of 2.5 mg/day could be effective for the treatment of patients with FPHL and it is more effective for patients with lower Ludwig scores and older age.⁴¹ Knowing more about promising treatments of AGA and its probable associations with metabolic syndrome and other dermatologic disorders^{42,43} helps manage the disorder better, especially in challenging cases.

Present studies on the topical administration of finasteride in the treatment of AGA are limited to a small number of randomized controlled trials, prospective studies and retrospective medical records; thus, more extensive research is needed in this regard. General data from the studies evaluating the efficacy and safety of topical finasteride treatment in AGA show promising results compared to systemic subjects.

Comparative evaluation of systemic pharmacodynamics of finasteride with other substances

Numerous studies have been performed to compare the performance of finasteride with other substances in improving hair loss pattern in women. For instance, in a double-blind randomized controlled trial by Suchonwanit et al. in 2019, the efficacy of a topical combination of 0.25% finasteride and 3% minoxidil compared to 3% minoxidil solution in hair loss in 30 postmenopausal women was examined. To determine the efficacy of the treatment, hair density and diameter were measured, and evaluations were performed at 1, 8, 16, and 24 weeks; side effects and serum DHT levels were also assessed. Finally, it was concluded that hair density and diameter increased in both groups, and finasteride/minoxidil was significantly superior to minoxidil solution in terms of improving hair diameter. No systemic side effects were reported. However, serum DHT levels in the finasteride/minoxidil group decreased significantly from those reported at baseline.³³

Additionally, in a study by Rossi et al., 0.5% topical finasteride showed a significantly higher efficacy in the treatment of FPHL in postmenopausal women compared to 17 α -estradiol 0.05%.⁴⁴ In that study, 119 postmenopausal female patients were examined. The patients were divided into 2 groups; the 1st group consisted of 69 women treated with 0.5% finasteride and 2% minoxidil, and the 2nd group of 50 women were treated with 17 α -estradiol 0.17% and 2% minoxidil. Photographs were taken at the beginning and at 6-, 12- and 18-month follow-ups. Improvement was statistically significant at 6 and 12–18 months for both finasteride and 17 α -estradiol groups. The efficacy of topical finasteride was significantly higher than that of the 17 α -estradiol solution in the first 6 months and at 12–18 months of follow-up. In general, the highest improvement rate was observed after 12–18 months of topical finasteride treatment.⁴⁰

Mechanism of action of finasteride

Finasteride stimulates the growth of fresh hair at the molecular level. It is a synthetic azasteroid with high potency as a noncompetitive and selective inhibitor that irreversibly inhibits the activity of an enzyme that converts the male sex hormone (testosterone) to its active form in the hair follicle.⁴⁴ Testosterone affects the skin, hair follicles, prostate gland, and skin sebaceous glands.³⁹ Hair follicle tissues are sensitive to a special form of testosterone called DHT. Testosterone is converted to DHT by an enzyme called 5 α -reductase. Finasteride inhibits the action of this enzyme and prevents the conversion of testosterone to DHT. The α -reductase includes 2 types, namely type 1 and type 2. Type 1 is more common in adipose tissue, and type 2 is more common in hair follicles and prostate

tissue.⁴⁵ People with normal or high levels of type 2 enzyme have high levels of normal DHT and are more likely to loose hair. Finasteride inhibits type 2 of this enzyme, lowers DHT levels and reduces the risk of male PHL.⁴⁶ The plasma half-life of this drug is 8 h and its biological effects last longer.²¹

Although preliminary results regarding the use of topical finasteride are limited, studies have shown that it may be safe for use in patients wishing to prevent systemic side effects.³⁹

Finasteride significantly reduces the DHT levels in the blood and scalp, which is thought to be the effect of the drug. Taking 1 mg of finasteride per day reduces blood DHT levels by up to 70% and increases blood testosterone levels by about 10%, which is within the normal range. Patients who used this drug regularly experienced hair growth and thickening of their hair strands, resulting in a high hair density.³⁹ In various studies, doses of 2–5 mg finasteride demonstrated a positive effect on the treatment process.^{29,30,35,41} The results showed that taking finasteride in the form of a 5-milligram tablet per day, with food or alone, had good efficacy.³¹ Finasteride should be taken regularly to achieve the desired result, and taking more than the desired dose does not increase the effect of the drug and could cause side effects.²⁹

It is important to note that finasteride only controls the complication and could not be used as a short-term treatment. If finasteride administration is stopped, the DHT hormone, which causes hair loss, returns to a high level after a while. Therefore, to maintain low DHT levels, daily administration of finasteride should be continued.⁴⁰

Finasteride and 5 α -reductase

In various studies, the α -reductase has been mentioned as an effective enzyme in the process of hair loss. The 5 α -reductase is an enzyme that converts testosterone into a more active form, DHT. If the level of this enzyme increases, more testosterone is converted to DHT and as a result, more hair loss occurs. The 5 α -reductase enzyme has 2 types; type 1 is found mostly in the sebaceous glands, which naturally make the skin slippery and sticky, and type 2 is more common in the genitourinary tract and hair follicles. Type 2 of enzyme is more important in hair loss.⁴⁵ Finasteride is a selective inhibitor of the 2nd type of 5 α -reductase. It appears to act on the 5 α -reductase enzyme in hair follicles and inhibit the production of DHT.³⁷

Testosterone is also involved in reducing adipose tissue. High levels of testosterone may reduce the scalp's ability to regulate follicular acidity. It has been shown that older women respond less positively to finasteride treatment.³³ This is because, in young people, the follicles inside the scalp are covered with a layer of fat. Young skin can also retain water better. When this water is lost, the scalp compresses the follicles, causing them to shrink. As the follicles try to maintain their state, excess enzyme activity

occurs in that area. Converting more testosterone to DHT increases erosion and causes hair loss. More DHT production and male pattern hair loss may one day lead scientists to finally succeed in discovering male pattern baldness treatment.⁴⁶

New generation of 5 α -reductase inhibitors

In addition to finasteride, another new drug called dutasteride has been discussed in several studies. It is a new generation of 5 α -reductase inhibitors (5-ARIs). It inhibits both types I- and II- α -reductase isoenzymes, and is 3 times more potent than finasteride in inhibiting type I enzymes and 100 times more potent in inhibiting type II enzymes.⁴⁷ Dutasteride is not currently approved by FDA for females, but it can be used as an adjunctive therapeutic agent.⁴⁸ A study in 416 men with AGA reported that taking 2.5 mg of dutasteride per day was much more effective than 5 mg of finasteride in increasing hair growth and improving the appearance of skin.⁴⁹ In a single-case study of a 46-year-old woman with FPHL who had a low response to minoxidil and finasteride, a clinical improvement was reported after 6 months of 0.5-mg daily dutasteride treatment.⁵⁰ These data support the efficacy of dutasteride; however, broader studies are needed and certain situations like pregnancy planning, contraception, normal basic laboratory data, etc. should be considered.

Follow-up time

Dihydrofinasteride reduces testosterone in the scalp by 64% and serum by 68%. After 12 months of administration, the number of full and thick hairs on the scalp increases and the number of thin hairs decreases. Finasteride could effectively stop the hair miniaturization and initiate hair regrowth. The finasteride pill is taken daily and its effects appear within 4–6 months. Usually, after 24 months, the maximum effect occurs. The efficacy of finasteride lasts as long as the drug is administered. Finasteride can be taken with food or on an empty stomach.⁵¹ The administration for at least 12–18 months has a positive effect on hair loss²⁹ and 1 year of treatment or more (about 2 years) showed better results.¹⁴ However, during the first 6 months, the existing hairs become a little thinner. Sometimes the reason for this is that hair loss is progressing and the effect of finasteride has not yet begun, while in some cases it is due to the loss of a series of miniature hairs, which leave space for new and healthy hair growth. Therefore, short and thin hairs will be lost, and thick and healthy hairs will replace them.⁴⁴

Side effects

Finasteride, like all drugs, is associated with possible risks and side effects. Studies by Oliveira-Soares et al. showed that side effects such as decreased libido

in 4 patients and increased liver enzymes in 1 patient were observed.²⁹ Another study showed that 4 female patients (4.6%) experienced side effects (headache, menstrual irregularities, dizziness, and increased body hair growth). However, these side effects were mild and disappeared after a while.³¹ In another study, finasteride was well tolerated at different doses, although some side effects were observed. This study states that finasteride can alter and increase female characteristics in male fetuses by affecting fetal hormones. Therefore, finasteride should be eliminated before pregnancy, and women in childbearing age should employ safety precautions when taking finasteride.³⁰

In another study on women with a pattern of hair loss, the findings showed that treatment with finasteride had acceptable results, hair loss was significantly reduced and excess hair growth was reported without any side effects.²⁵ In men, the findings show that very few men face side effects while taking the drug; about 2% experience decreased sexual potency or ejaculation problems, decreased semen volume, and erection problems. Unfortunately, some individuals have also experienced aggression and mild depression.⁵²

The findings of studies related to single or combination therapy with oral or topical finasteride have been summarized in Table 1.

There are some other emerging and promising systemic drugs for male and female pattern AGA; one of them is oral minoxidil. In an original study with 30 cases of male pattern AGA who were treated with oral minoxidil 5 mg/day, total hair counts were significantly increased at weeks 12 and 24. Vertex area revealed 100% improvement with a 43% of excellent response. The frontal area also exhibited significant improvement; however, it was less pronounced than that in the vertex area. Safety profile was acceptable and the most common side effects were hypertrichosis (93%) and pedal edema (10%). Case selection is of extreme importance in this treatment, and patients with cardiovascular problems or significant hypertension may not be good candidates for this therapy.⁵³ In another 6-month trial, the authors suggested that 1.25 mg daily low dose of oral minoxidil can be considered an effective therapeutic option for male pattern AGA with an acceptable safety profile, and higher doses (2.5–5 mg/day) may be beneficial in resistant cases.⁵⁴ In another study in 148 women with FPHL, oral minoxidil was used at the dosage of 0.25–2 mg/day (median: 1 mg/day) for a mean duration of 9 months, and 85% of patients received oral minoxidil in combination with other drugs. About 80% of patients experienced a clinical improvement (in 65% of cases this improvement was slight), and patients with more advanced stages of alopecia experienced a more visible clinical improvement. There was no statistically significant difference in the effectiveness or safety of the drug in terms of dosage or age.⁵⁵

In a systematic review that evaluated the efficacy of oral minoxidil on nonscarring alopecia (including AGA and alopecia areata), the authors found that oral minoxidil

usually has been used in the range of 0.25–5 mg/daily/twice daily. Acceptable clinical improvement has been shown in 61–100% and 18–82.4% of patients with AGA and alopecia areata, respectively. This therapy also had promising results in FPHL, chronic telogen effluvium, monilethrix, and permanent post-chemotherapy alopecia. Although this regimen has been considered safe, hypertrichosis and postural hypotension were among the most common side effects. In addition to efficacy and safety, oral minoxidil resulted in better compliance than the topical form.⁵⁶ In a review study encompassing 634 cases, oral minoxidil has been used as the primary treatment for hair loss. The most common condition among studied patients was AGA, but alopecia areata, telogen effluvium, permanent chemotherapy-induced alopecia, lichen planopilaris, loose anagen syndrome, and monilethrix were other conditions that required treatment. There are not enough high-level evidence studies using standardized objective measurements which compare the efficacy and safety of different doses of treatment. Finasteride and dutasteride are usually used when there is a difficulty with the topical formula.⁵⁷

It is of great importance to compare finasteride with oral minoxidil in future trials and review studies.

Limitations

There are less trial studies on the use of finasteride in women than in men, and there are a few well-designed prospective clinical trials concerning the use of topical finasteride. Moreover, in this systematic review, we only included trial studies, the number of which is limited. There is a need for further trial studies in this field.

Conclusions

Various drugs, including topical minoxidil, oral finasteride and oral antiandrogens, are widely used for treating FPHL. Studies have shown that different doses of finasteride are effective in controlling FPHL in postmenopausal women and in the women in reproductive age. Administration of the drug should be continued for at least a year until the hair density reaches the desired level. To increase the effectiveness of the drug, the usage of higher doses, such as 5 mg/day, provided that there is resistance in patients or side effects, is recommended. As it is not very effective in women over 70 years of age, this drug can be recommended for younger age groups. Dutasteride, a new generation of 5 α -reductase inhibitors, is also being discussed for treatment, and the use of this drug could be considered in certain situations. The current systematic review has shown that finasteride can be a very effective treatment for FPHL. In the reviewed articles, the effectiveness of the drug reported for topical and oral use was between 15% and 65.2%. In all reviewed articles, side effects


were either not reported, observed in a low percentage (4.6%) of female patients or tolerable for them. The use of combination drugs such as topical estradiol and minoxidil could increase the effectiveness of the drug. It was also found that topical finasteride is more effective than other topical formulas used.

The FDA has not yet approved the use of finasteride in the treatment of hair loss in women due to its effect on female hormones and the growth of external genitalia in male fetuses. However, due to its low side effects, the present findings recommend it for nonpregnant women, considering the specific conditions and risk factors such as pregnancy and hormonal diseases.


It is recommended that future studies maximize therapeutic trials and evaluate the efficacy and side effects of this treatment in patients with FPHL.


ORCID iDs


Niloufar Najar Nobari  <http://orcid.org/0000-0002-4245-1980>


Masoumeh Roohaninasab  <https://orcid.org/0000-0002-2862-6422>

Afsaneh Sadeghzadeh-Bazargan

 <https://orcid.org/0000-0003-1102-6241>

Azadeh Goodarzi  <https://orcid.org/0000-0002-1249-4429>

Elham Behrangi  <https://orcid.org/0000-0002-6545-3460>

Farahnaz Nikkhhah  <https://orcid.org/0000-0002-6137-5696>

Mohammadreza Ghassemi  <https://orcid.org/0000-0002-0706-554X>

References

- Ramos PM, Miot HA. Female pattern hair loss: A clinical and pathophysiological review. *An Bras Dermatol*. 2015;90(4):529–543. doi:10.1590/abd1806-4841.20153370
- Price VH, Roberts JL, Hordinsky M, et al. Lack of efficacy of finasteride in postmenopausal women with androgenetic alopecia. *J Am Acad Dermatol*. 2000;43(5):768–776. doi:10.1067/mjd.2000.107953
- Soheila N, Behzad I, Mehdi G, Fahimeh A, Niloufar N. The influence of osteopontin on the pathogenesis of alopecia areata and its association with disease severity. *Iran J Dermatol*. 2018;21(2):43–47. doi:10.22034/ijd.2018.98350
- Lajevardi V, Ghodsi SZ, Goodarzi A, Hejazi P, Azizpour A, Beygi S. Comparison of systemic mycophenolate mofetil with topical clobetasol in lichen planopilaris: A parallel-group, assessor- and analyst-blinded, randomized controlled trial. *Am J Clin Dermatol*. 2015;16(4):303–311. doi:10.1007/s40257-015-0122-z
- Roohaninasab M, Goodarzi A, Ghassemi M, Sadeghzadeh-Bazargan A, Behrangi E, Najar Nobari N. Systematic review of platelet-rich plasma in treating alopecia: Focusing on efficacy, safety, and therapeutic durability. *Dermatol Ther*. 2021;34(2):e14768. doi:10.1111/dth.14768
- Mohammad A, Baba A, Ghassemi M. Comparison between serum levels of vitamin D and zinc in women with diffuse non-scarring hair loss (telogen effluvium) and healthy women. *Pak J Med Health Scis*. 2020;14(3):1400–1404. <https://pjmhsonline.com/2020/july-sep/1400.pdf>
- Rogers NE, Avram MR. Medical treatments for male and female pattern hair loss. *J Am Acad Dermatol*. 2008;59(4):547–566. doi:10.1016/j.jaad.2008.07.001
- Torabi P, Behrangi E, Goodarzi A, Roohaninasab M. A systematic review of the effect of platelet-rich plasma on androgenetic alopecia of women. *Dermatol Ther*. 2020;33(6):e13835. doi:10.1111/dth.13835
- Hung PK, Chu TW, Tsai RY, Kung CW, Lin SJ, Chen CM. Quantitative assessment of female pattern hair loss. *Dermatol Sin*. 2015;33(3):142–145. doi:10.1016/j.dsi.2015.01.002
- Olsen EA, Messenger AG, Shapiro J, et al. Evaluation and treatment of male and female pattern hair loss. *J Am Acad Dermatol*. 2005;52(2):301–311. doi:10.1016/j.jaad.2004.04.008
- Brzezińska-Wcisło L. Assessment of efficacy of Diane-35 in androgenetic feminine alopecia [in Polish]. *Wiad Lek*. 2003;56(3–4):202–205. PMID:12923971.

12. Burke BM, Cunliffe WJ. Oral spironolactone therapy for female patients with acne, hirsutism or androgenic alopecia. *Br J Dermatol*. 1985; 112(1):124–125. doi:10.1111/j.1365-2133.1985.tb02305.x
13. Carmina E, Lobo RA. Treatment of hyperandrogenic alopecia in women. *Fertil Steril*. 2003;79(1):91–95. doi:10.1016/S0015-0282(02)04551-X
14. Fabbrocini G, Cantelli M, Masarà A, Annunziata MC, Marasca C, Cacciapuoti S. Female pattern hair loss: A clinical, pathophysiologic, and therapeutic review. *Int J Womens Dermatol*. 2018;4(4):203–211. doi:10.1016/j.ijwd.2018.05.001
15. Redler S, Messenger AG, Betz RC. Genetics and other factors in the aetiology of female pattern hair loss. *Exp Dermatol*. 2017;26(6):510–517. doi:10.1111/exd.13373
16. Orme S, Cullen DR, Messenger AG. Diffuse female hair loss: Are androgens necessary? *Br J Dermatol*. 1999;141(3):521–523. doi:10.1046/j.1365-2133.1999.03049.x
17. Carey AH, Chan KL, Short F, White D, Williamson R, Franks S. Evidence for a single gene effect causing polycystic ovaries and male pattern baldness. *Clin Endocrinol*. 1993;38(6):653–658. doi:10.1111/j.1365-2265.1993.tb02150.x
18. Stefanato CM. Histopathology of alopecia: A clinicopathological approach to diagnosis. *Histopathology*. 2010;56(1):24–38. doi:10.1111/j.1365-2559.2009.03439.x
19. Hillmer AM, Flaquer A, Hanneken S, et al. Genome-wide scan and fine-mapping linkage study of androgenetic alopecia reveals a locus on chromosome 3q26. *Am J Hum Genet*. 2008;82(3):737–743. doi:10.1016/j.ajhg.2007.11.014
20. Randall VA. Androgens and hair growth. *Dermatol Ther*. 2008;21(5):314–328. doi:10.1111/j.1529-8019.2008.00214.x
21. Cash TF, Price VH, Savin RC. Psychological effects of androgenetic alopecia on women: Comparisons with balding men and with female control subjects. *J Am Acad Dermatol*. 1993;29(4):568–575. doi:10.1016/0190-9622(93)70223-G
22. Sinclair RD, Dawber RPR. Androgenetic alopecia in men and women. *Clin Dermatol*. 2001;19(2):167–178. doi:10.1016/S0738-081X(00)00128-0
23. Cash TF. The psychology of hair loss and its implications for patient care. *Clin Dermatol*. 2001;19(2):161–166. doi:10.1016/S0738-081X(00)00127-9
24. Dinh QQ, Sinclair R. Female pattern hair loss: Current treatment concepts. *Clin Interv Aging*. 2007;2(2):189–199. PMID:18044135.
25. Deplewski D, Rosenfield RL. Role of hormones in pilosebaceous unit development. *Endocrine Rev*. 2000;21(4):363–392. doi:10.1210/edrv.21.4.0404
26. DeVillez RL, Jacobs JP, Szpunar CA, Warner ML. Androgenetic alopecia in the female: Treatment with 2% topical minoxidil solution. *Arch Dermatol*. 1994;130(3):303–307. PMID:8129407.
27. Suchonwanit P, Rojhirunsakool S, Khunkhet S. A randomized, investigator-blinded, controlled, split-scalp study of the efficacy and safety of a 1550-nm fractional erbium-glass laser, used in combination with topical 5% minoxidil versus 5% minoxidil alone, for the treatment of androgenetic alopecia. *Lasers Med Sci*. 2019;34(9):1857–1864. doi:10.1007/s10103-019-02783-8
28. Lee GY, Lee SJ, Kim WS. The effect of a 1550 nm fractional erbium-glass laser in female pattern hair loss: Fractional photothermolysis laser treatment of female pattern hair loss. *J Eur Acad Dermatol Venereol*. 2011;25(12):1450–1454. doi:10.1111/j.1468-3083.2011.04183.x
29. Oliveira-Soares R, Silva JM, Correia MP, André M. Finasteride 5 mg/day treatment of patterned hair loss in normo-androgenetic postmenopausal women. *Int J Trichol*. 2013;5(1):22–25. doi:10.4103/0974-7753.114709
30. Li R. More new tricks with old drugs: Finasteride for hair loss in women. British Columbia Drug and Poison Information Centre (BC DPIC). 2009. <http://www.dpic.org/article/professional/finasteride-hair-loss-women>
31. Yeon J, Jung J, Choi J, et al. 5 mg/day finasteride treatment for normoandrogenic Asian women with female pattern hair loss. *J Eur Acad Dermatol Venereol*. 2011;25(2):211–214. doi:10.1111/j.1468-3083.2010.03758.x
32. Lee SW, Juhasz M, Mobasher P, Ekelem C, Mesinkovska NA. A systematic review of topical finasteride in the treatment of androgenetic alopecia in men and women. *J Drugs Dermatol*. 2018;17(4):457–463. PMID:29601622.
33. Suchonwanit P, Iamsung W, Rojhirunsakool S. Efficacy of topical combination of 0.25% finasteride and 3% minoxidil versus 3% minoxidil solution in female pattern hair loss: A randomized, double-blind, controlled study. *Am J Clin Dermatol*. 2019;20(1):147–153. doi:10.1007/s40257-018-0387-0
34. Gentile P. Autologous cellular method using micrografts of human adipose tissue derived follicle stem cells in androgenic alopecia. *Int J Mol Sci*. 2019;20(14):3446. doi:10.3390/ijms20143446
35. Iorizzo M, Vincenzi C, Voudouris S, Piraccini BM, Tosti A. Finasteride treatment of female pattern hair loss. *Arch Dermatol*. 2006;142(3):298–302. doi:10.1001/archderm.142.3.298
36. Gentile P, Cole J, Cole M, et al. Evaluation of not-activated and activated PRP in hair loss treatment: Role of growth factor and cytokine concentrations obtained by different collection systems. *Int J Mol Sci*. 2017;18(2):408. doi:10.3390/ijms18020408
37. Ghassemi M, Ghaffarpour G, Ghods S. The effect of GGC and CAG repeat polymorphisms on the androgen receptor gene in response to finasteride therapy in men with androgenetic alopecia. *J Res Med Sci*. 2019;24(1):104. doi:10.4103/jrms.JRMS_27_19
38. Ohtawa M, Takayama F, Saitoh K, Yoshinaga T, Nakashima M. Pharmacokinetics and biochemical efficacy after single and multiple oral administration of losartan, an orally active nonpeptide angiotensin II receptor antagonist, in humans. *Br J Clin Pharmacol*. 1993;35(3):290–297. doi:10.1111/j.1365-2125.1993.tb05696.x
39. Kohler C, Tschumi K, Bodmer C, Schneiter M, Birkhaeuser M. Effect of finasteride 5 mg (Proscar) on acne and alopecia in female patients with normal serum levels of free testosterone. *Gynecol Endocrinol*. 2007;23(3):142–145. doi:10.1080/09513590701214463
40. Verdonchot E, Boersma I, Oranje A, Grimalt R, Iorizzo M, Piraccini B. The effectiveness of finasteride and dutasteride used for 3 years in women with androgenetic alopecia. *Indian J Dermatol Venereol Leprol*. 2014;80(6):521–525. doi:10.4103/0378-6323.144162
41. Won Y, Lew B, Sim W. Clinical efficacy of oral administration of finasteride at a dose of 2.5 mg/day in women with female pattern hair loss. *Dermatol Ther*. 2018;31(2):e12588. doi:10.1111/dth.12588
42. Elham B, Somayeh S, Afsaneh SB, et al. The effect of metformin in the treatment of intractable and late onset acne: A comparison with oral isotretinoin. *Iran J Dermatol*. 2019;22(2):47–52. doi:10.22034/ijd.2019.98371
43. Ehsani AH, Mortazavi H, Balighi K, et al. Changes in body mass index and lipid profile in psoriatic patients after treatment with standard protocol of infliximab. *Acta Med Iran*. 2016;54(9):570–575. PMID:27832688.
44. Rossi A, Magri F, D'Arino A, et al. Efficacy of topical finasteride 0.5% vs 17 α -estradiol 0.05% in the treatment of postmenopausal female pattern hair loss: A retrospective, single-blind study of 119 patients. *Dermatol Pract Concept*. 2020;10(2):e2020039. doi:10.5826/dpc.1002a39
45. Mazzarella G, Loconsole G, Cammisa G, Mastrolonardo G, Vena G. Topical finasteride in the treatment of androgenic alopecia: Preliminary evaluations after a 16-month therapy course. *J Dermatolog Treat*. 1997;8(3):189–192. doi:10.3109/09546639709160517
46. Rojhirunsakool S, Suchonwanit P. Parietal scalp is another affected area in female pattern hair loss: An analysis of hair density and hair diameter. *Clin Cosmet Investig Dermatol*. 2017;11:7–12. doi:10.2147/CCID.S153768
47. Clark RV, Hermann DJ, Cunningham GR, Wilson TH, Morrill BB, Hobbs S. Marked suppression of dihydrotestosterone in men with benign prostatic hyperplasia by dutasteride, a dual 5 α -reductase inhibitor. *J Clin Endocrinol Metab*. 2004;89(5):2179–2184. doi:10.1210/jc.2003-030330
48. Olsen EA, Hordinsky M, Whiting D, et al. The importance of dual 5 α -reductase inhibition in the treatment of male pattern hair loss: Results of a randomized placebo-controlled study of dutasteride versus finasteride. *J Am Acad Dermatol*. 2006;55(6):1014–1023. doi:10.1016/j.jaad.2006.05.007
49. Gupta AK, Charrette A. The efficacy and safety of 5 α -reductase inhibitors in androgenetic alopecia: A network meta-analysis and benefit-risk assessment of finasteride and dutasteride. *J Dermatolog Treat*. 2014;25(2):156–161. doi:10.3109/09546634.2013.813011
50. Olszewska M, Rudnicka L. Effective treatment of female androgenic alopecia with dutasteride. *J Drugs Dermatol*. 2005;4(5):637–640. PMID:16167423.

51. Hugh Rushton D, Norris MJ, Van Neste D. Hair regrowth in male and female pattern hair loss does not involve the conversion of vellus hair to terminal hair. *Exp Dermatol*. 2016;25(6):482–484. doi:10.1111/exd.12945
52. Suchonwanit P, Srisuwanwattana P, Chalermroj N, Khunkhet S. A randomized, double-blind controlled study of the efficacy and safety of topical solution of 0.25% finasteride admixed with 3% minoxidil vs. 3% minoxidil solution in the treatment of male androgenetic alopecia. *J Eur Acad Dermatol Venereol*. 2018;32(12):2257–2263. doi:10.1111/jdv.15171
53. Panchaprateep R, Lueangarun S. Efficacy and safety of oral minoxidil 5 mg once daily in the treatment of male patients with androgenetic alopecia: An open-label and global photographic assessment. *Dermatol Ther (Heidelb)*. 2020;10(6):1345–1357. doi:10.1007/s13555-020-00448-x
54. Pirmez R, Salas-Callo CI. Very-low-dose oral minoxidil in male androgenetic alopecia: A study with quantitative trichoscopic documentation. *J Am Acad Dermatol*. 2020;82(1):e21–e22. doi:10.1016/j.jaad.2019.08.084
55. Rodrigues-Barata R, Moreno-Arrones OM, Saceda-Corralo D, et al. Low-dose oral minoxidil for female pattern hair loss: A unicenter descriptive study of 148 women. *Skin Appendage Disord*. 2020;6(3):175–176. doi:10.1159/000505820
56. Sharma AN, Michelle L, Juhasz M, Muller Ramos P, Atanaskova Mesinkovska N. Low-dose oral minoxidil as treatment for non-scarring alopecia: A systematic review. *Int J Dermatol*. 2020;59(8):1013–1019. doi:10.1111/ijd.14933
57. Randolph M, Tosti A. Oral minoxidil treatment for hair loss: A review of efficacy and safety. *J Am Acad Dermatol*. 2021;84(3):737–746. doi:10.1016/j.jaad.2020.06.1009
58. Camacho-Martínez FM. Hair loss in women. *Semin Cutan Med Surg*. 2009;28(1):19–32. doi:10.1016/j.sder.2009.01.001
59. Boychenko O, Bernstein RM, Schweiger ES. Finasteride in the treatment of female pattern (androgenic) alopecia: A case report and review of the literature. *Cutis*. 2012;90(2):73–76. PMID:22988650.
60. Trüeb RM. Finasteride treatment of patterned hair loss in normoandrogenic postmenopausal women. *Dermatology*. 2004;209(3):202–207. doi:10.1159/000079890
61. Zhao J, Harada N, Okajima K. Dihydrotestosterone inhibits hair growth in mice by inhibiting insulin-like growth factor-I production in dermal papillae. *Growth Horm IGF Res*. 2011;21(5):260–267. doi:10.1016/j.ghir.2011.07.003
62. Kim WJ, Song M, Ko HC, Kim BS, Kim MB. Efficacy of finasteride 1.25 mg on female pattern hair loss: A pilot study. *Ann Dermatol*. 2012;24(3):370–372. doi:10.5021/ad.2012.24.3.370
63. Tang L, Bernardo O, Bolduc C, Lui H, Madani S, Shapiro J. The expression of insulin-like growth factor 1 in follicular dermal papillae correlates with therapeutic efficacy of finasteride in androgenetic alopecia. *J Am Acad Dermatol*. 2003;49(2):229–233. doi:10.1067/S0190-9622(03)00777-1

